Volume 2 Issue 1 (2016) · ISSN 2424-7723

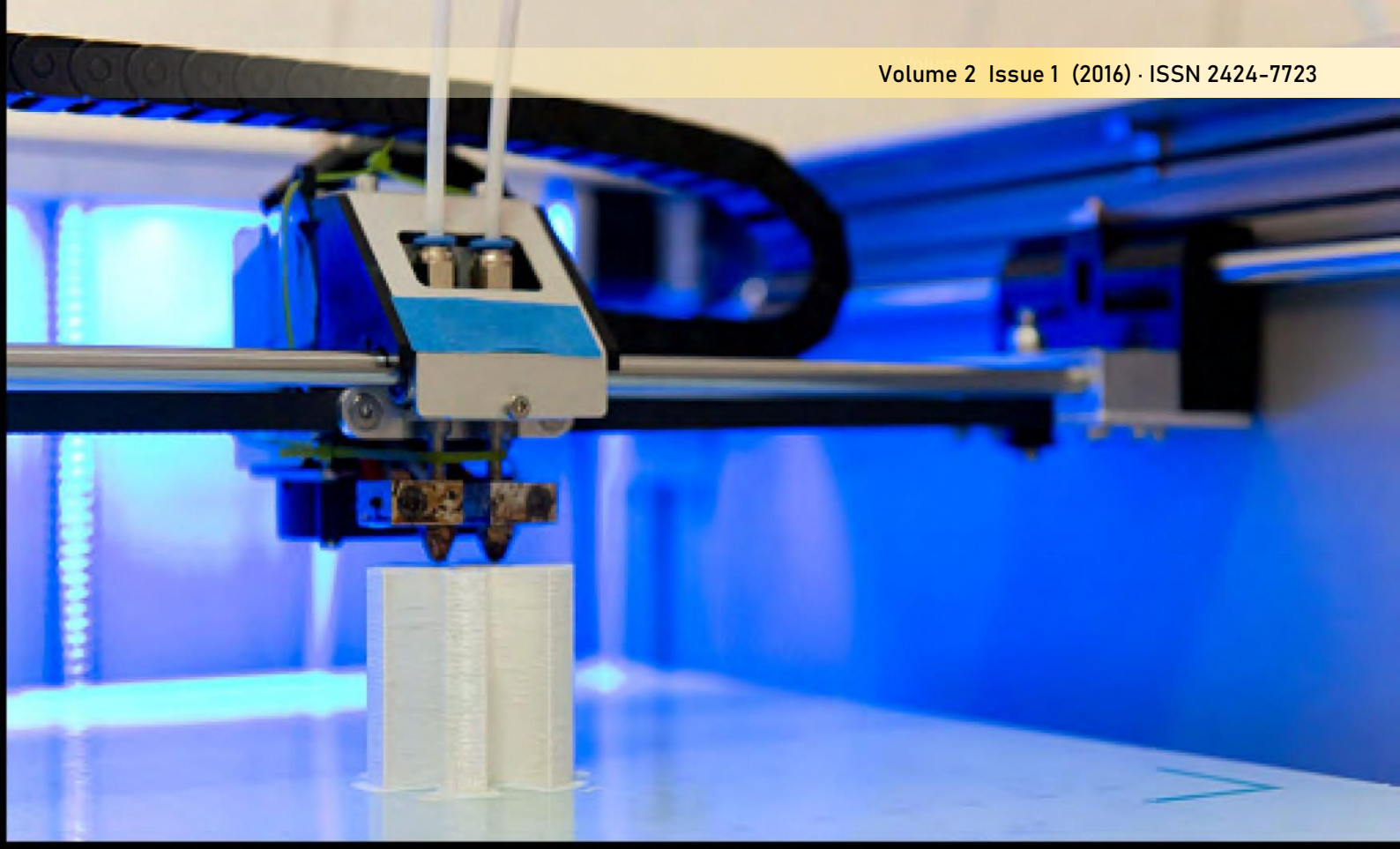

INTERNATIONAL JOURNAL OF BIOPRINTING

WHIOCE PUBLISHING PTE. LTD.
PROVIDING
FIRST-CLASS SCIENTIFIC INFORMATION
FOR TOP SCHOLARS

Editorial Board

Volume 2 Issue 1 • 2016
ISSN 2424-7723 (print) ISSN 2424-8002 (online)

INTERNATIONAL JOURNAL OF BIOPRINTING

Editor-in-Chief
Chee Kai Chua
Nanyang Technological University, Singapore

WHIOCE PUBLISHING PTE. LTD.

Volume 2 | Issue 1 | 2016 | Page 1 – 102 |

International Journal of Bioprinting

https://ijb.whioce.com/index.php/int-j-bioprinting

CONTENTS

EDITORIAL

A Foreword from the Editor

Editor-in-Chief: Chee Kai CHUA

Executive Director, Singapore Centre for 3D Printing
Professor, Manufacturing & Industrial Engineering Cluster
School of Mechanical & Aerospace Engineering, College of Engineering
Nanyang Technological University

http://dx.doi.org/10.18063/IJB.2016.01.011.

Welcome to the year of 2016!

Since last July when the first issue of *International Journal of Bioprinting* (IJB) was successfully launched, five new international editorial board members have joined us, including Dr. Aleksandr Ovsiankikov (Vienna University of Technology, Austria), Dr. Giovanni Vozzi (University of Pisa, Italy), Dr. Boris N. Chickkov (Laser Zentrum Hannover e.V., Germany), Dr. Peter Dubruel (Universiteit Gent, Belgium) and Dr. Ali Khademhosseini (Harvard Medical School, USA). The total number of board members has increased to 24 (see Figure 1) in half a year, but I hope that this great team will continue to grow to 30 or more within this year.

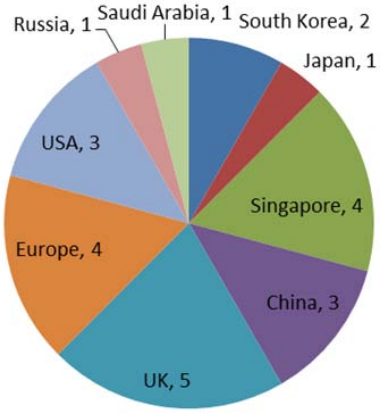

Figure 1. Number of editorial board members by country/region.

International Bioprinting Congress (IBC) is an annual international conference event focusing on the latest status and development of bioprinting. Singapore has hosted the first and second IBC in the past two years. This year, IBC will change its name to "Bioprinting and 3D Printing in the Life Sciences", to reflect an increased coverage of scope, such as biomedical engineering and tissue engineering. The new conference will be held in Singapore on 21–22 July, 2016. For details and registration, please go to the website shown in brackets (http://selectbiosciences.com/conferences/index.aspx?conf=BIO3D). We welcome all to come to Singapore to join our discussions on bioprinting and 3D printing in the life sciences.

Last but not least, I am pleased to present the second issue of IJB. This second issue includes one perspective, two reviews, six original research articles and one project report. In the first article, An *et al*. discussed the early forms of 4D bioprinting and proposed a definition to unify distinct approaches[1]. Mehrban *et al*. reviewed the role of bioprinting in tissue engineering, with a special focus on bioprinting of stem cell-laden hydrogels[2]. Sánchez-Salcedo *et al*. reviewed and analysed the issue of bacterial adhesion in bioprinted 3D scaffolds[3]. In research, Tse *et al*. reported a wax-based inkjet printing method which could guide cells to grow into complex patterns[4]. Koudan *et al*. studied how tissue spheroids patterns responded to a nanofibrous substrate[5]. Ng *et al*. developed a new hydrogel system for bioprinting a better skin tissue[6]. Wang *et al*. reported an interesting bioprinting method to generate fibrous scaffolds with extremely complex geometries[7]. Boehm *et al*. reported a bioprinted microneedle system for an easy and quick detection of fluid samples from histamine-con-

taminated tuna[8]. Leong *et al*. reported a simple and efficient method for making 3D nanofibrous scaffolds[9]. Finally, Bibb *et al*. presented a detailed report on the European ArtiVasc 3D project and discussed the successes and lessons that had been learnt[10].

References

1. An J, Chua K C and Mironov V, 2016, A perspective on 4D bioprinting. *International Journal of Bioprinting*, vol.2(1): 3–5. http://dx.doi.org/10.18063/IJB.2016.01.003
2. Mehrban N, Teoh G Z and Birchall M A, 2016, 3D bioprinting for tissue engineering: Stem cells in hydrogels. *International Journal of Bioprinting*, vol.2(1): 6–19. http://dx.doi.org/10.18063/IJB.2016.01.006
3. Sánchez-Salcedo S, Colilla M, Izquierdo-Barba I, *et al*., 2016, Preventing bacterial adhesion on scaffolds for bone tissue engineering. *International Journal of Bioprinting*, vol.2(1): 20–34. http://dx.doi.org/10.18063/IJB.2016.01.008
4. Tse C W C, Ng S S, Stringer J, *et al*., 2016, Utilising inkjet printed paraffin wax for cell patterning applications. *International Journal of Bioprinting*, vol.2(1): 35–44. http://dx.doi.org/10.18063/IJB.2016.01.001
5. Koudan E V, Bulanova E A, Pereira F D A S, *et al*., 2016, Patterning of tissue spheroids biofabricated from human fibroblasts on the surface of electrospun polyurethane matrix using 3D bioprinter. *International Journal of Bioprinting*, vol.2(1): 45–52. http://dx.doi.org/10.18063/IJB.2016.01.007
6. Ng W L, Yeong W Y and Naing M W, 2016, Polyelectrolyte gelatin-chitosan hydrogel optimized for 3D bioprinting in skin tissue engineering. *International Journal of Bioprinting*, vol.2(1): 53–62. http://dx.doi.org/10.18063/IJB.2016.01.009
7. Wang H, Vijayavenkataraman S, Wu Y, *et al*., 2016, Investigation of process parameters of electrohydrodynamic jetting for 3D printed PCL fibrous scaffolds with complex geometries. *International Journal of Bioprinting*, vol.2(1): 63–71. http://dx.doi.org/10.18063/IJB.2016.01.005
8. Boehm R D, Jaipan P, Yang K-H, *et al*., 2016, Microstereolithography-fabricated microneedles for fluid sampling of histamine-contaminated tuna. *International Journal of Bioprinting*, vol.2(1): 72–80. http://dx.doi.org/10.18063/IJB.2016.01.010
9. Leong W S, Wu S C, Ng K W, *et al*., 2016, Electrospun 3D multi-scale fibrous scaffold for enhanced human dermal fibroblasts infiltration. *International Journal of Bioprinting*, vol.2(1): 81–92. http://dx.doi.org/10.18063/IJB.2016.01.002
10. Bibb R, Nottrodt N and Gillner A, 2016, Artificial vascularized scaffolds for 3D-tissue regeneration — a report of the ArtiVasc 3D Project. *International Journal of Bioprinting*, vol.2(1): 93–102. http://dx.doi.org/10.18063/IJB.2016.01.004

PERSPECTIVE

A perspective on 4D bioprinting

Jia An[1], Chee Kai Chua[1] and Vladimir Mironov[2,3]

[1] Singapore Centre for 3D Printing, School of Mechanical and Aerospace Engineering, Nanyang Technological University, Singapore

[2] Renato Archer Information Technology Center, Campinas, Sao Paulo, Brazil

[3] The Laboratory of Biotechnological Research, 3D Bioprinting Solutions, Kashirskoe Roadway, 68/2, Moscow, Russian Federation

Abstract: 3D bioprinting has been invented for more than a decade. A disruptive progress is still lacking for the field to significantly move forward. Recently, the invention of 4D printing technology may point a way and hence the birth of 4D bioprinting. However, 4D bioprinting is not well defined and appear to have a few distinct early forms. In this article, a personal perspective on the early forms of 4D bioprinting is presented and a definition for 4D bioprinting is proposed.

Keywords: 4D printing, bioprinting, additive manufacturing, rapid prototyping, tissue engineering.

*Correspondence to: Jia An, Singapore Centre for 3D Printing, School of Mechanical and Aerospace Engineering, Nanyang Technological University, Singapore; Email: anjia@ntu.edu.sg

Received: October 22, 2015; **Accepted:** November 2, 2015; **Published Online:** November 5, 2015

Citation: An J, Chua K C and Mironov V, 2016, A perspective on 4D bioprinting. *International Journal of Bioprinting*, vol.2(1): 3–5. http://dx.doi.org/10.18063/IJB.2016.01.003.

1. Introduction

The technology of 3D bioprinting has been invented for more than a decade[1]. A disruptive progress is still lacking for the field to significantly move forward. Recently, the invention of 4D printing technology may point a way. 4D printing technology is invented by Massachusetts Institute of Technology (MIT) and the fourth dimension refers to time[2]. The main difference from 3D printing is that it involves a programmed shape change over the post-printing time. 4D bioprinting is believed to be an extension of 4D printing into biomedical science and engineering. However, in the current literature, there is hardly a report on applying MIT's 4D printing technology to biomedical applications. Indeed, the phrase of "4D bioprinting" can be found in a few recent reviews[3–5], but all briefly mention it without giving further detailed information. At the time of writing, 4D bioprinting is still more of a thing-to-be rather than a well-established matter of fact. Therefore in this paper we would only be able to discuss some early forms of 4D bioprinting and based on which we propose a definition that unifies them.

2. Approaches and Definition

Figure 1 shows three current approaches in 4D bioprinting. They are distinct from each other. The first approach strictly follows MIT's concept of 4D printing, in which a substrate material (e.g., smart biopolymer or responsive hydrogel), upon stimulus, folds into a pre-defined 3D configuration, and the printed cell or tissue materials simply follow the folding of the substrate and form into a desired shape[6]. The second approach is kind of "*in vivo* 4D bioprinting". A 3D printed polymer medical device is implanted first and then accommodates the growth of tissue or organ over the postsurgical period[7]. When the tissue or organ becomes stronger and stronger, the medical device gradually breaks and is absorbed by the body. In this approach, the growth of the tissue could be seen as the stimulation. The third approach involves on-demand

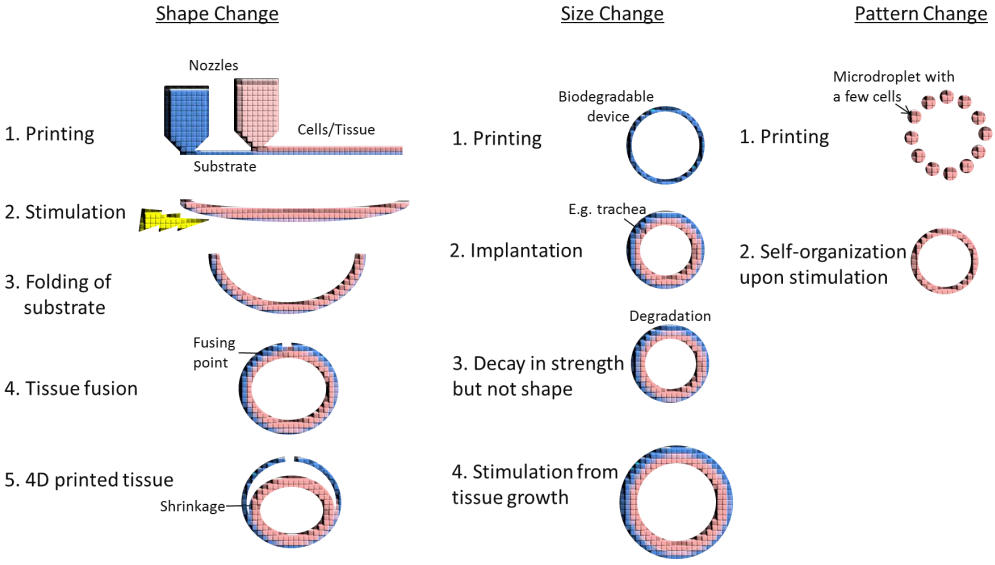

Figure 1. Three approaches in 4D bioprinting.

self-assembly or self-organization. Micro-droplets of cells are precisely deposited into a certain pattern, and then the pattern changes over time due to cell communication and self-organization[8]. In this approach, self-assembly is stimulated to occur, but what could stimulate the pattern to change is not clear yet. It is difficult to compare these three approaches and conclude what is better and what is not, since all are supported by limited study at the current stage. Nonetheless, every approach is interesting and worth further exploration in future.

Since current approaches are different from each other and there is no consensus on the exact form of 4D bioprinting, we would like to propose the following definition for 4D bioprinting to accommodate all current studies and perhaps future studies as well.

4D bioprinting refers to groups of programmable self-assembly, self-folding or self-accommodating technologies which include three main defining or essential components: (i) man-made and not nature-made programmable design, (ii) 2D or 3D bioprinting process, and (iii) post-printing programmable evolving of bioprinted constructs which could be driven by cells or biomaterials and triggered by external signals.

This definition of 4D bioprinting has several features. Firstly, 4D bioprinting is not defined as a single technology. Similar to additive manufacturing, it is defined as a family of technologies based on different principles.

Secondly, there must be a man-made programmable design for self-assembly, self-folding and self-accommodating processes. The process design could be stepwise, relating the type and degree of stimulation to the type and degree of change. The process may or may not be reversible, but it is preferable to have the process being reversible in the design.

Thirdly, the programmable design must be printable by existing bioprinting processes. It could be printing in 2D and then folding into 3D or printing in 3D and then changing into another 3D configuration.

Lastly and most importantly, the self-assembly or self-organization must not occur naturally, but instead it must be driven by cells or biomaterials and triggered by external stimulation, otherwise it does not suit our definition of 4D bioprinting. In 4D bioprinting, the post-printing path in the fourth dimension needs to be manually manipulated. Therefore, fusion of 3D printed tissue spheroids into certain shape is not considered as 4D bioprinting, because tissue fusion process is natural, unless the printed spheroids can hold its as-printed state and start to fuse upon external stimulation. Furthermore, in some reported cases[9], cell contraction and cell migration for cell-driven self-folding and self-assembly is actually also a natural biological process. The folding of the cell origami is not a programmed design, also because the sequence of the folding planes is totally random, neither controlled nor repeatable.

3. Conclusion

In summary, there are clear differences between 3D bioprinting and 4D bioprinting. The major diffe-

rentiating factor is whether there is a stimulation to trigger the as-printed tissue/organ preforms to change over time in a predefined path. In this sense, the combination of 3D bioprinting and bioreactor could be a form of 4D bioprinting, provided the change in tissues/organ can be pre-defined. The future forms of 4D bioprinting would be really unpredictable. However, the differences between 3D bioprinting and 4D bioprinting will continue to widen when more and more research results are available. The early forms of 4D bioprinting may be just the tip of an iceberg; in addition to shape, size and pattern, there could be more other forms of changes in future, such as microstructure, property or even functionality. The era of 4D bioprinting is on its way.

Conflict of Interest and Funding

No conflict of interest was reported by the authors. The authors thank the Singapore National Research Foundation for funding Singapore Centre for 3D Printing.

Acknowledgements

The authors thank Dr. Fabien Guillemot for his discussion at the 2nd International Bioprinting Congress in Singapore (9–10 July 2015).

Reference

1. Chua C K and Yeong W Y, 2015, Yeong, *Bioprinting: Principles and Applications*, World Scientific Publishing Company Incorporated, Singapore.
2. Tibbits S, 2014, 4D printing: Multi-material shape change. *Architectural Design*, vol.84(1): 116–121. http://dx.doi.org/10.1002/ad.1710
3. Dababneh A B and Ozbolat I T, 2014, Bioprinting technology: A current state-of-the-art review. *Journal of Manufacturing Science and Engineering*, vol.136(6): 061016. http://dx.doi.org/10.1115/1.4028512
4. Khoo Z X, Teoh E M J, Liu Y, *et al*. 2015, 3D printing of smart materials: A review on recent progresses in 4D printing. *Virtual and Physical Prototyping*, vol.10(3): 103–122. http://dx.doi.org/10.1080/17452759.2015.1097054
5. Wang S, Lee J M and Yeong W Y, 2015, Smart hydrogels for 3D bioprinting. *International Journal of Bioprinting*, vol.1(1): 3–14. http://dx.doi.org/10.18063/IJB.2015.01.005
6. Mironov V, 2014, *Proceedings of the 1st International Bioprinting Congress, July 24–25, 2014*: *4D Bioprinting: Biofabrication of rod-like and tubular tissue engineered constructs using programmable self-folding bioprinted biomaterials*.
7. Morrison R J, Hollister S J, Niedner M F, *et al*. 2015, Mitigation of tracheobronchomalacia with 3D-printed personalized medical devices in pediatric patients. *Science Translational Medicine*, vol.7(285): 285ra64. http://dx.doi.org/10.1126/scitranslmed.3010825
8. Guillemot F, 2015, *Proceedings of the 2nd International Bioprinting Congress, July 9–10, 2015: 4D bioprinting: A new paradigm for engineering complex tissues*.
9. Kuribayashi-Shigetomi K, Onoe H and Takeuchi S, 2012, Cell origami: Self-folding of three-dimensional cell-laden microstructures driven by cell traction force, *PLOS ONE*, vol.7(12): e51085. http://dx.doi.org/10.1371/journal.pone.0051085

REVIEW ARTICLE

3D bioprinting for tissue engineering: Stem cells in hydrogels

Nazia Mehrban[1], Gui Zhen Teoh[1] and Martin Anthony Birchall[2*]

[1] Department of General Surgery, University College London, London, WC1E 6BT, United Kingdom
[2] Ear Institute, University College London, London, WC1X 8DA, United Kingdom

Abstract: Surgical limitations require alternative methods of repairing and replacing diseased and damaged tissue. Regenerative medicine is a growing area of research with engineered tissues already being used successfully in patients. However, the demand for such tissues greatly outweighs the supply and a fast and accurate method of production is still required.

3D bioprinting offers precision control as well as the ability to incorporate biological cues and cells directly into the material as it is being fabricated. Having precise control over scaffold morphology and chemistry is a significant step towards controlling cellular behaviour, particularly where undifferentiated cells, i.e., stem cells, are used. This level of control in the early stages of tissue development is crucial in building more complex systems that morphologically and functionally mimic *in vivo* tissue.

Here we review 3D printing hydrogel materials for tissue engineering purposes and the incorporation of cells within them. Hydrogels are ideal materials for cell culture. They are structurally similar to native extracellular matrix, have a high nutrient retention capacity, allow cells to migrate and can be formed under mild conditions. The techniques used to produce these materials, as well as their benefits and limitations, are outlined.

Keywords: 3D bioprinting, hydrogels, stem cells, polymers, tissue engineering

*Correspondence to: Martin Anthony Birchall, Ear Institute, University College London, London, WC1X 8DA, United Kingdom; Email: m.birchall@ucl.ac.uk

Received: September 17, 2015; **Accepted:** November 27, 2015; **Published Online:** December 9, 2015

Citation: Mehrban N, Teoh G Z and Birchall M A, 2016, 3D bioprinting for tissue engineering: Stem cells in hydrogels. *International Journal of Bioprinting*, vol.2(1): 6–19. http://dx.doi.org/10.18063/IJB.2016.01.006.

1. Introduction

Whilst 2D printing has had a big influence on everyday living, the advent of additive processing technology in 1986[1] has seen an explosion in innovative ways of producing 3D structures, such as electronic devices[2], aircraft parts[3], medical devices[4] and tissue mimics[5–7]. For clinical applications, early designs based on creating sacrificial moulds as templates for the biomaterials[8] were quickly superseded by aqueous systems that could directly print biological materials[9–11]. Today, the focus is no longer just on providing a suitable platform for cell growth but combining engineering, materials science and cell biology to create a bespoke material of specific dimensions. That material must then integrate well with the patient's healthy tissue and restore functionality to an acceptable level. In the pursuit of developing materials that meet such criteria, manufacturing techniques have also become more complex.

3D bioprinting is the spatial control of the original scaffold preparation techniques with integration of chemical cues and living cells[12]. Printing sensitive biological materials presents new challenges, such as maintaining cell viability throughout the manufacturing process and preventing denaturation of proteins.

In this review we introduce some of the materials used for bioprinting, how stem cells are currently incorporated into the materials and the advantages and limitations of the techniques used to achieve this. Here the focus is to review 3D bioprinting techniques currently employed to create implantable tissue. However, the same techniques may also be employed to create models for studying 3D cell behaviour, diseases and modes of repair.

2. Techniques for 3D Bioprinting

The main approaches to 3D bioprinting are: biomimicry (taking inspiration from nature to develop novel materials), autonomous self-assembly (using cellular organisation to guide the development of bioprinted tissues) and mini-tissue building blocks (identifying and recreating the building blocks of tissues to produce complex systems)[13]. For any one of these strategies, there are a number of techniques that can be employed for their fabrication.

2.1 Inkjet Bioprinting

Based on 2D ink-printing technology, inkjet printing is still the most popular printing method for 3D biological tissues analogues. The first modifications of the technology replaced the ink reservoir with bioink and the paper-feed tray with an *x-y-z* controllable stage[14]. Inkjet printers use thermal or acoustic methods to deliver controlled volumes of the bioink to previously defined locations[15] and build the structure layer-by-layer. Thermal methods generate heat at the print head which forces ink out of the nozzle through pressure pulses. Although temperatures can reach 200–300°C during thermal inkjet printing, this lasts a few microseconds, resulting in an overall temperature rise of 4–10°C for aqueous systems, which has been shown not to have a detrimental effect on cell viability[16]. This method of printing is fast, cheap and readily available. However, although temperature effects on cells has been shown to be minimal, other factors such as print-head clogging, mechanical stress and unreliability in bioink dispensing, present the biggest disadvantages.

Acoustic inkjet printing technology is based on generating pressure in the nozzle by applying a voltage to a piezoelectric crystal which changes the crystal's conformation. Controlling this process precisely allows the bioink to be deposited as droplets[17]. A modification of this process uses ultrasound to create an acoustic radiation field and form droplets from an air-liquid interface. Control of droplet size and rate of deposition comes from ultrasound pulse, duration and amplitude[18]. The acoustic methods can be modified so that they are not reliant on nozzles[19]. This reduces the risk of clogging and shear stress on cells. There are also no changes in temperature during droplet formation. However, there is a risk of causing cell lysis and membrane damage from the frequencies used to change the piezoelectric crystal shape.

One of the main drawbacks of using either thermal or piezoelectric-based inkjet printing methods is that only liquids with low viscosities are easily printable. This introduces further problems in creating a solid structure once the bioink has been deposited onto the stage[20]. Methods of addressing this issue are outlined in Section 3. Similarly, only low cell numbers can be printed to avoid the nozzle from clogging and to reduce shear stress on the cells[13]. However, once these issues are addressed, inkjet methods offer fast, cheap and high resolution bioprinting with the ability to change drop size and density, thereby the ability to create gradients. When this is coupled with multiple nozzles, it is clear why inkjet printing techniques are so attractive to tissue engineers[21,22].

2.2 Laser-Induced Forward Transfer Bioprinting (LIFT)

Laser-induced forward transfer (LIFT) technology uses pulses of laser focused on a 'ribbon' upon which the biological material is layered as a solution. The pulse creates a high-pressure bubble which forces the biological material off the ribbon and onto a collector. The technology is not as popular as inkjet and microextrusion for bioprinting but is increasingly being used[23,24]. The component set-up for LIFT is entirely different to inkjet and microextrusion technologies and as such the printing resolution and speed is dependent on factors including laser energy, material wettability and surface tension, the spacing between the ribbon and the substrate and material viscosity[25].

The benefits of LIFT are that it is a nozzleless system and so clogging of the print head is no longer an issue, a range of viscosities can be printed without causing a detrimental effect on cell viability[26] and high cell numbers can be printed[27]. These are all advantageous over conventional bioprinting systems.

However, the complexity of LIFT is its biggest downfall. Individual ribbons are required for depositing different bioinks which can be time-consuming

and expensive when printing multiple materials or cell types. Furthermore, the ribbon coating method does not lend itself to distributing cells accurately and metal contaminants are present in the final printed construct; as metal coating is used to create a laser energy absorbing layer on the ribbon.

Even so, as the price for 3D printing is decreasing and LIFT technology is becoming more accessible, several researchers have used it to fabricate clinically relevant constructs, both acellular[28] and cellular[29,30]. As component parts are modified to suit bioprinting for the purpose of tissue engineering, the interest in this technology is likely to grow substantially.

2.3 Microextrusion Bioprinting

Microextrusion printing is one of the most popular and cheapest methods of non-biological printing[31]. The technique uses force to extrude material via a microextrusion head onto a stage, both of which can usually be controlled along the *x*, *y* and *z* axes[32]. For bioprinting, materials can be extruded mechanically or pneumatically[33]. Pneumatic systems are ideal for printing materials that have higher viscosities[34] as they are limited only by the system's air-pressure capabilities and nozzle diameter. The mechanism is simple but delays caused by the compressed gas which controls material flow can affect the printing resolution. Mechanical motor-based microextruders are more complex and provide better spatial resolution but are limited by the forces they can generate and therefore struggle to extrude materials with high viscosities[35].

The temperature of the stage and print head of a microextrusion system can be controlled, which allows a range of materials to be printed[13]. Furthermore, as force is used to extrude the material, high cell densities can be printed, although, as with inkjet methods, the forces generated can affect cell viability. As microextrusion uses higher forces than inkjet printing methods, the cell viability can be as low as 40%[36] or even lower if higher pressures are used. This impact on cell viability can be reduced by lowering the extrusion pressure and printing through nozzles with a large gauge size, although this in turn affects the printing resolution and speed. Nevertheless as microextrusion technology can print high cell densities and can be fitted with multiple extrusion heads, allowing for multi-material or multi-cell printing[37], it remains the most popular method for self-assembly cell printing; through which cells are deposited as spheroids without a secondary support material[38]. Microextrusion printing has already been used to produce aortic valves[39] and pharmokinetic[40] and disease[41] models. Furthermore, there is room for improvement as the technology is capable of printing non-biological materials at high resolution.

2.4 Stereolithography and Projection Pattern Bioprinting

Stereolithography is traditionally used to fabricate solid structures from photocurable polymer or resin using a laser and an *x*-*y*-*z*-controlled stage[42]. The technique is based on solid freeform fabrication with polymerised layers printed bottom-up, although top- down stereolithography approaches also exist. The printing resolution is dependent on laser energy and focus. Although traditionally the technique has been used to produce acellular scaffolds, researchers have incorporated photopolymerisable proteins and cell-guiding cues into the scaffolds using stereolithography[43].

Projection stereolithography, also known as digital micromirror device microfabrication, is a modification of the original system which uses micromirrors to create a reflective photomask for fabricating the scaffold layer by layer[44]. Further advancements in the technology have led to the development of a more complex system which allows the entire 3D structure to be polymerised at the same time[45]. Such a system can dramatically reduce the printing speed.

The main drawback with using traditional stereolithography to print scaffolds is that it is not easy to incorporate cells into the structure and maintain viability as it is being fabricated, unless the set-up is modified first[46]. Typically the scaffold is formed first and cells are seeded post-fabrication.

3. Selecting Suitable Materials for 3D Bioprinting

The main challenge in engineering tissues is replicating the *in vivo* environment chemically, mechanically and morphologically. Therefore, the scaffold material on which the cells will be cultured is one of the most important initial choices to be made. The source of these materials may be natural or synthetic (Figure 1). Both types of materials have been used for tissue engineering in equal measure[47–49]. Natural materials are biocompatible while synthetic materials can be modified

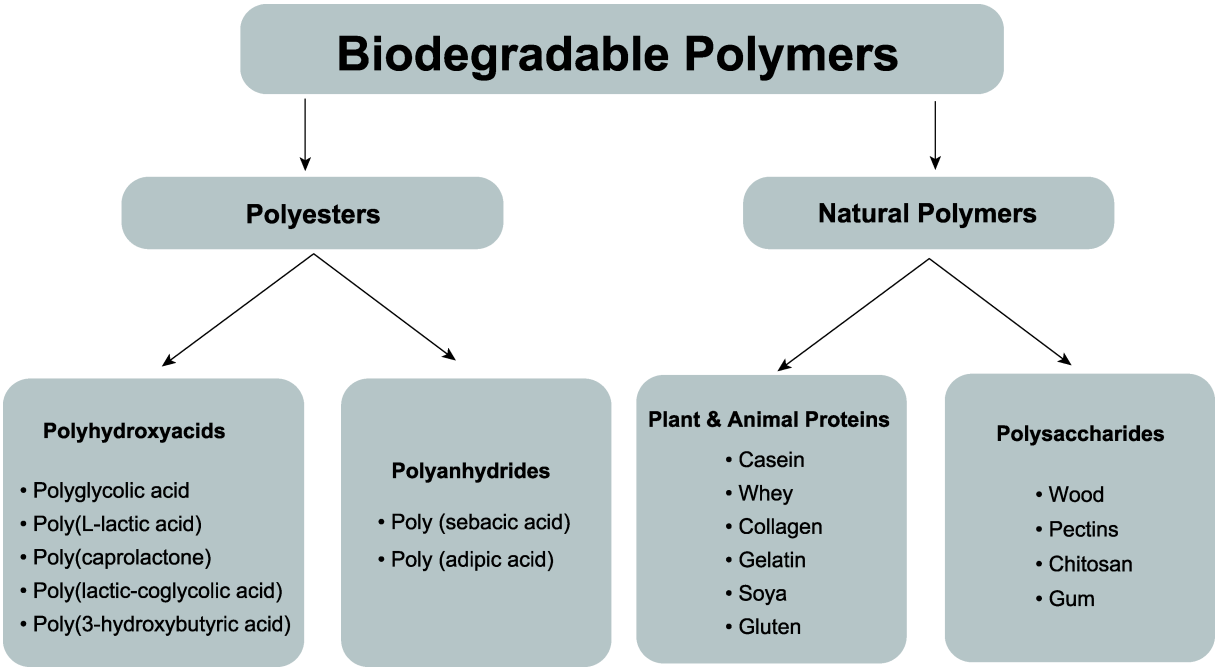

Figure 1. Biodegradable polymers used for bioprinting applications.

easily and are therefore easier to handle during manufacture. However, natural materials often lack the mechanical integrity required whilst synthetic materials are often not biocompatible[50]. Some researchers have sought to overcome these issues by combining favourable elements from both categories to create hybrid materials[51,52]. Even so, not all of these materials are suited to 3D printing. While the high temperatures and solvents used in the initial 3D printing techniques are not employed for bioprinting, there are still certain criteria, which need to be met when selecting suitable bioprinting materials.

3.1 Printability

It is important to be able to both deposit the material accurately and retain spatial resolution in order to control the overall scaffold geometry. Some bioprinting techniques cannot print viscous materials (such as inkjet methods) while others shear-thin the material and therefore affect its formation (such as microextrusion). Temporal resolution is another aspect which needs to be addressed, as materials that take too long to 'set' will affect the spatial resolution of the scaffold, whilst materials that set too quickly will be in danger of blocking the nozzle. Other factors to consider are whether the cells or biomolecules will encounter shear stress or high temperatures during printing. Current cell-printing technologies report a high variation in cell viabilities; typically between 40% and 90%.

3.2 Biocompatibility

Original expectations of material biocompatibility centered on minimising inflammation and creating materials that would not produce cytotoxic side-effects. Today, however, biocompatibility can include the incorporation of biochemical functionality, i.e. growth factors or growth factor mimics, and nanoscale scaffold morphology to improve and enhance the interaction of cells with the scaffold, and therefore engineered tissue with the *in vivo* environment[13]. It is vital to select a material which can be modified through the printing process such that there is the option of building complexity into the system.

3.3 Degradation

Degradation of a material into smaller chemical units due to material chemistry, oxidising agents, enzymes or ionising radiation and ultrasound occurs via two mechanisms: surface (materials loss layer by layer) or bulk (fragmentation of the whole material)[53]. Figure 2 shows both mechanisms.

The main indicators of degradation are reduction in sample mass, loss of mechanical strength and changes in chemical bonds and groups. Controlled degradation is vital as material loss and a reduction in mechanical integrity of the overall scaffold[54] can alter the

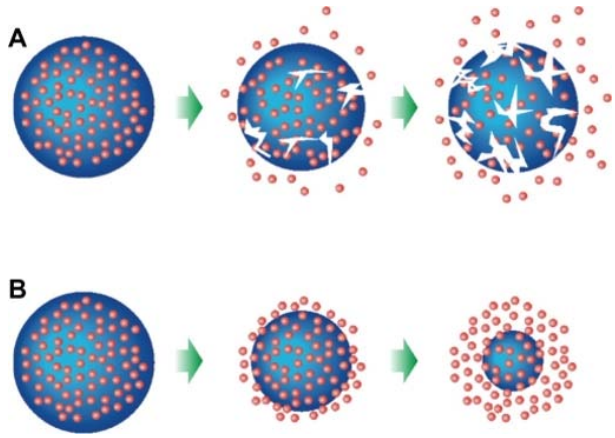

Figure 2. Mechanisms of degradation: bulk (A) and surface (B) degradation.

cellular response to the material. For example, during bulk degradation scaffolds can become more porous, which in turn will have a profound effect on cell migration behaviour and nutrient uptake.

When selecting a bioprintable material which has a suitable degradation profile, it is necessary to also consider whether the cells will contract the scaffold in any way and change its dimensions or whether the material's swelling behaviour will be altered and the effect any by-products from degradation may have on surrounding tissue. A relatively inert and printable material or combination of materials that maintain the correct dimensions could still produce by-products that are toxic or not readily removed by the body[55] and therefore present new challenges *in vivo*.

In order to assess the degradation behaviour of a material, factors such as chemical composition, thermal properties, surface area to volume ratio and stereochemistry must also be taken into consideration.

3.4 Mechanical Strength and Structural Integrity

As stated in Section 2.3, maintaining structural integrity at the same rate as cell growth is highly challenging but necessary. Not only does it provide cells with a physical support, studies have also shown that a mechanical strength which matches *in vivo* conditions can strongly influence cell proliferation and differentiation[56–58]. Several researchers have used a hybrid material approach to create a mechanically suitable environment[59,60]. However, the printability, from changes in viscosities and a mismatch in the most suitable printing technique for the materials, must be assessed and thus further adds to the complexity of the issue. These problems are not insurmountable and several researchers have created 3D printed hybrid scaffolds (see Section 4.3).

4. Using Hydrogels for 3D Bioprinting

Hydrogels are an ideal tissue engineering material which can be sourced naturally, created synthetically or used in combination with other materials[61–64]. Hydrogel networks are comprised of polymer or peptide chains. They have a high content of water, ideal for absorbing high levels of nutrients and oxygen[65], allowing cells to migrate within the scaffold[66] and the waste to diffuse out[67].

Synthesised materials, such as those based on polyethylene glycol and polyacrylamide, offer more control over modification than naturally derived materials such as alginate, collagen, fibrin and hyaluronic acid[62,64].

4.1 Synthetic Materials

Having control over gelation time and mechanical strength are two of the most important elements in hydrogel bioprinting. If the gelation time is too long, the spatial resolution is lost and layers cannot be printed with accuracy. To control the setting time the gelation mechanism can be manipulated by chemically modifying the material, introducing crosslinking agents or varying the polymer content[68]. Müller *et al.*[69] were able to control the printability of Pluronic, a block-copolymer, by mixing acrylated with unmodified Pluronic F127 and stabilising the structure through ultraviolet (UV) crosslinking while Barry *et al.*[70] used direct-write assembly and UV photopolymerisation to produce poly(acrylamide)-based gels for fibroblast culture. With any of the techniques the process of printing a new layer should not disrupt or dissolve the previously deposited material.

Hydrogels as a whole have a high water content which is ideal for maintaining cell viability. However, the material provides low structural support[71]. By using chemical or physical crosslinking methods this can also be improved and therefore solve two major issues using one modification technique. Being able to control scaffold formation in this way would suggest that for bioprinting, synthetic materials, owing to their customisability, are superior to naturally-derived materials. However, cellular interactions and biocompatibility are almost always better on natural materials than synthetic[72]. To improve the biocompatibility of synthetic materials, functional sequences, such as peptide adhesion motifs, can be covalently attached to the material. The drawback of this approach is introducing

even more complexity to an already modified system.

4.2 Natural Materials

In contrast, natural materials, although inferior to synthetic hydrogels in terms of controlling gelation kinetics and mechanical strength, are able to chemically and physically mimic native extracellular matrix (ECM). Collagen is the most abundant component of ECM[73]. It is widely used in tissue engineering applications and contains cell-guiding chemical cues, such as the cell adhesion peptide sequence arginine-glycine-aspartic acid (RGD)[74]. However, although it is widely used as a bioprinting material, collagen is an unlikely gold-standard candidate as it contracts and does not retain its original shape.

Hyaluronic acid (HA), is also a naturally derived material which does retain its shape and is already used clinically[75]. HA forms very soft gels but can be modified and crosslinked using a variety of methods including the UV method described in Section 4.1[76] and thiol-modified HA using gold nanoparticles[77] to increase its stiffness. Similarly, fibrin is already used in surgery as a haemostatic agent and sealant[78,79]. The added complexity with fibrin is that it crosslinks through the addition of thrombin. However, it can produce mechanically stable hydrogels and has been blended with other gels for bioprinting purposes[80].

Some natural gels are difficult to print, not because they form soft gels as described in the earlier examples, but because their gelation properties are undesirable. Gelatin is one such material. It forms a gel easily by temperature control but has a melting temperature of 30–35°C[81], which is below the standard physiological temperature of 37°C. Similarly, alginate produces gels easily through cation crosslinking, but unless it is modified with motifs that can guide cells to adhere, proliferate and differentiate, it is relatively inert[82].

4.3 Hybrid Materials

An alternative approach to producing scaffolds with desirable properties is to create a hybrid. A study on methacrylated hyaluronic acid combined with methacrylated gelatin showed that not only could cell viability be maintained but by varying the concentrations of the two materials, the stiffness and viscosity of the hybrid could be controlled[83]. Other researchers have used a similar approach to bioprint scaffolds for a range of uses, including cartilage engineering[84] and to tune material properties for a range of scaffolds[85].

The main issue in using this approach is matching the printable properties of the separate materials or selecting a bioprinting technique which would allow both materials to be printed simultaneously under different conditions. Although the latter adds another level of complexity to printing 3D biocompatible scaffolds, it is a branch of bioprinting that is currently being explored[86].

5. Cell Encapsulation in Hydrogels for Printable Bioinks

The choice of cells for 3D bioprinting is often based on the type of tissue being created. However, as tissues and organs are composed of multiple cell types which have a range of specific functions, it is likely that the bioprinting requirement will be for a mixture of cells. Current methods predominantly involve printing individual cell types in specific patterns, designed to mimic native tissue cell distribution[87]. Although cells have been printed in single drops, with each drop containing one or two cells[88], it is currently not possible to print individual cells reliably. This is not an issue as long as large cell agglomerates (clusters of cells large enough to cause cell death at the centre of the cell mass) can be avoided and cell-to-cell contact can be maintained. The size of these agglomerates will depend on the type of cells used and the ease with which nutrient and waste exchange can occur at the centre of the mass.

For a more efficient system, resembling a native 3D environment, a material-cell composite ink would be more suitable. The ability to encapsulate cells within the material as it is being printed allows researchers to create a more tissue-like environment compared with creating a 2D construct first onto which cells are then seeded[89]. With hydrogels this has been attempted with some success[90], creating cell-laden constructs that contain microvascular networks[91] and are able to integrate well with native tissue[22]. Combining cells with hydrogels is a delicate balance of maintaining high cell viability whilst ensuring that there are not too many cells in the gel to cause hyperplasia or apoptosis, either by optimising the number of cells added at the loading stage of the process or by controlling the rate of cell proliferation post-printing[13].

When using hydrogels with cells, there are a number of factors which could cause cell death. One of the most obvious causes is the method selected for gelation. During crosslinking or temperature-based gelation the cell viability could be substantially affected[92].

The introduction of cytotoxic crosslinking agents should be avoided and as cells are only able to survive in a narrow temperature range, the list of gel candidates is substantially reduced. However, by combining materials, the list of printable gels could once again be expanded.

Furthermore, the time required for gelation is of importance. The longer it takes for the material to be printed and form the structure, the more likely the layers printed at the start of the process will lose viability, thus limiting the use of the construct. Other factors include the introduction of stress on cells through changes in the viscosity of the gel. While control of viscosity would make the gel more printable, slight changes could lead to low cell viability rates. Stress could also be introduced by methods of extruding the bioink[36] and changes in temperature during the printing process, although the latter is dependent on how long high temperatures are maintained. In their study, Cui *et al.*[16] reported a rise in temperature during printing from 22°C to 46°C. However, as the drops produced cooled within seconds, no significant apoptosis was observed.

6. Using Stem Cells for 3D Bioprinting

The ideal cell type for bioprinting is dependent on the accessibility and availability of the cells, the self-renewal and expansion capacity, differentiation profile and cellular tumorigenicity as well as viability following encapsulation and printing. Stem cells are a particularly attractive cell type as they are pluripotent and able to differentiate into other cell types upon exposure to the correct physical and chemical guidance cues[93]. Within the human body, there are a number of viable sources of stem cells, such as the bone marrow, periosteum and adipose tissue[94–96].

6.1 Stem Cells Selection

Stem cell differentiation can be guided through the incorporation of tissue-specific chemical signals in the scaffold, although some researchers suggest that this may not be necessary to promote differentiation and subsequent tissue regeneration[97]. While the advantages of using pluripotent cells in bioprinting are clear, there are ethical considerations which must be taken into account when using stem cells. Furthermore, the generation of pluripotent stem cells from adult cells (induced pluripotent stem cells, iPSC) pose the risk of tumorigenicity which must also be considered[98]. Ethical issues aside, there are three main categories of stem cells which can be considered for 3D bioprinting: embryonic, somatic and iPSC.

***6.1.1** Embryonic Stem Cells (ESCs)*

With the ability to form any cell type and indefinite self-renewal[99], embryonic stem cells (ESCs) are the ideal cell type for tissue engineering. One of the challenges in using ESCs for regenerating or repairing tissue is identifying the conditions needed to drive the cells towards a specific lineage. As cell differentiation is influenced by both chemical and physical cues, the identification of ideal culture conditions adds another level of complexity to an already difficult task.

The biggest drawback of using ESCs is that they are derived from a blastocyst. In some countries, ESCs research is prohibited or severely restricted due to the ethical issues this raises. Furthermore, where research in the field is allowed, the number of cells derived from an embryonic source is low and, unless expanded significantly *in vitro*, is unlikely to meet clinical demand.

***6.1.2** Adult Stem Cells*

Adult stem cells cover any postnatal somatic cell that is undifferentiated and can self-renew[100]. These cells can be derived from a number of sources including brain, liver and bone marrow[101]. Mesenchymal stem cells (MSCs) are readily available from bone marrow, adipose tissue, amniotic fluid, the synovium and periosteum and are known to be less tumorigenic than their embryonic or fetal counterparts[98]. MSCs are non-haematopoietic, are relatively straightforward to obtain via bone marrow harvesting methods[102] and interact well with a range of materials that may be used for cellular encapsulation to produce viable bioinks. Table 1 features the types of adult MSCs which have been used for bioprinting applications.

Although MSCs can be harvested from the patient's own tissue, and therefore reduce the risk of rejection, only 0.001%–0.01% of total nucleated cells in bone marrow are MSCs[102]. A possible alternative source which could be used is adipose derived MSCs (ADMSCs). Adipose tissue is abundant and many researchers have used ADMSCs successfully towards tissue engineering[94,103,104].

***6.1.3** Induced Pluripotent Stem Cells (iPSC)*

The discovery that stem cells can be generated directly from adult cells by the introduction of four transcription factors has revolutionised biomedical research[105–108]. By using the patient's own cells, the ethical issues related to stem cell research and the concern surrounding tissue rejection can be avoided. Furthermore,

Table 1. Examples of human mesenchymal stem cells used in bioprinting and their performance

No.	Human Cell Type	Scaffold Materials	Regenerated Tissue	Bioprinting Technologies	References
1	Amniotic-derived mesenchymal stem cells	Fibrin-collagen Hydrogel	Skin	Inkjet	Skardal *et al*. 2012[21]
	(a) Evidence of re-epithelialisation on skin wound in mice with an increase in microvessel density and capillary diameter over 14 days. However, cells did not fully integrate with native tissue.				
2	Adipose-derived mesenchymal stem cells	Alginate	Adipose	Laser-assisted	(a) Gruene *et al*. 2011[119]
	(a) Adipogenic lineage pathway maintained for 10 days with expression of adipogenic markers similar to those expressed in native adipose tissue.				
3	Bone marrow-derived mesenchymal stem cells	(a) acrylated peptides and acrylated poly(ethylene glycol) (b) poly L-lysine coated carbon nanotubes and acetylated collagen	Bone and Cartilage	Inkjet	(a) Gao *et al*. 2015[120] (b) Holmes and Zhang 2013[121]
	(a) High cell viability (87.9 ± 5.3%) and good differentiation, evidenced by mineral and cartilage matrix deposition. (b) Biomimetic poly L-lysine coated carbon nanotubes and acetylated collagen can induce proliferation of MSCs.				

as the iPSCs can be derived from any somatic cell, the yield is high.

However, as a relatively recent discovery, there is still a lot of research to be done on how the cells behave long term. Furthermore, genetic manipulation of cells poses a risk of tumorigenicity[98], introducing new problems in their clinical use. For this reason, some researchers have sought to find alternative routes for generating iPSCs, for example via protein reprogramming[109].

6.2 Stem Cell Bioprinting

When selecting cells for bioprinting, an important factor to consider is the robustness of the cells. Many of the 3D bioprinting technologies outlined in Section 2 can affect cell viability, some of which are discussed in Section 5, and with a limited supply of stem cells, it is essential that this is taken into consideration. While selecting the appropriate bioprinting technique, it is important to ensure that the stem cells retain their pluripotency. If the printing method affects the differentiation potential, primarily through creating a microenvironment to which the stem cells are sensitive[110–112], then a complex scaffold, irrespective of whether it contains cell-guiding functional motifs, is unlikely to produce the desired tissue. Using laser-based printing, Gruene *et al.*[113] showed that this is possible. Furthermore, early consideration of the interaction between stem cells, the encapsulating material and other cell types used during the bioprinting process could also increase overall viability and help maintain pluripotency[114–116].

As stem cells are sensitive to topography, the scaffold design could strongly influence cell morphology, proliferation and differentiation without the need for additional biological cues[117,118]. Eliminating the addition of growth factors or growth factor-like cues, to reduce bioink complexity, could help improve bioprinting resolution and the overall quality of the product. With the right combination of stem cells, bioprinting technology and scaffold materials, engineering a functional tissue suitable for clinical applications becomes a very real possibility.

7. Future Directions

With the progression in complexity of bioprinted structures, it is clear that the future of clinically relevant 3D printed materials lies in replicating complex and heterogeneous tissues. In this review we have described how technological advancement has occurred in parallel to hybrid material development. Bioprinting is no longer confined to a process for combining one cell type with one material; the emphasis today is to use a variety of material types to create bespoke scaffolds onto which chemical cues can be tethered and multiple cell types can be printed with precision.

Popularity in the use of this technology has led to cheaper systems being made available and therefore more accessible. However, the speed at which the scaffolds are produced is still an area of exploration. This progress is necessary, not only to maintain high cell viability rates but also to scale up the process and fabricate enough scaffolds to meet clinical demands. Kolesky *et al.*[91] estimate that to print an adult human liver using a single nozzle with a 200 µm diameter, it would take 3 days. However, by switching to a 64-nozzle system under the same conditions this could be reduced to 1 hour. Such a difference in production speeds could result in scaffolds being produced to meet individual needs quickly whilst reducing the sur-

gical demand for bespoke solutions.

Material compatibility with such advanced systems must also be assessed. A physiologically relevant scaffold must be able to support and guide cell growth and differentiation both chemically and physically. As well as creating complex blends of bioinks, this would require heterogeneous material fabrication and precision-printing to create organized gradients or complex patterns of cells and functional motifs which mimic native ECM more closely. One approach currently being explored to meet these requirements is the use of smart materials, i.e., materials that are able to change their shape, mechanical strength and permeability in response to external or physiological stimuli[117]. Smart hydrogels can respond to changes in pH[122], temperature[123] and electric and magnetic fields[124,125]. These materials are particularly attractive as the scaffold could mould itself as the cells mature.

An alternative approach is to print decellularised ECM directly to provide the structural and chemical cues the cells require. It is believed by some researchers that no matter how complex the hydrogel-based scaffolds become, decellularised ECM is still the closest representation of an *in vivo* environment[126] and therefore the future of bioprinting tissues. The downside with this method is harvesting the ECM first but if tissue-specific ECM can be derived with ease, then this method may help resolve some of the cell functionality issues currently experienced when using other, more conventional scaffolds.

Through the various examples cited in this review, it is clear that bioprinting itself has been successfully used to maintain cell viability and incorporate cell-guiding cues into complex scaffold materials. The main challenge facing researchers in this field today is fine-tuning the technique to mirror native tissue complexity. The goal in tissue engineering is always to improve the patient's quality of life and by creating bespoke materials that are able to regenerate or guide tissue development in a cheap and fast way, 3D bioprinting has become a powerful and highly flexible tool for achieving this. Furthermore, as knowledge on technologies and materials advances, it is entirely plausible that in the future *in situ* bioprinting systems could be developed to both scan the patient's wound site and print the cell-laden scaffold directly into the wound, all without leaving the operating theatre. Significant progress in this area has already been made towards skin[21] and cartilage repair[22].

Author Contributions

All authors contributed towards the writing of this review paper. We thank Dr. James Bowen for his insights and discussions.

Conflict of Interest and Funding

No conflict of interest was reported by all authors. This work was supported by the Medical Research Council (MR/K026453/1, MAB and NM) and the Engineering and Physical Sciences Research Council (EP/K504610/1, GZT).

References

1. Hull C W, 1986, Apparatus for production of three-dimensional objects by stereolithography. US 4575330 A, Google Patents.
http://dx.doi.org/10.1007/s11427-015-4850-3
2. Leigh S J, Bradley R J, Purssell C P, *et al.*, 2012, A simple, low-cost conductive composite material for 3D printing of electronic sensors. *PLoS ONE*, vol.7: e49365.
http://dx.doi.org/10.1371/journal.pone.0049365
3. Berman B, 2012, 3-D printing: The new industrial revolution. *Business Horizons*, vol.55(2): 155–162.
http://dx.doi.org/10.1016/j.bushor.2011.11.003
4. Rengier F, Mehndiratta A, von Tengg-Kobligk H, *et al.*, 2010, 3D printing based on imaging data: Review of medical applications. *International Journal of Computer Assisted Radiology and Surgery*, vol.5(4): 335–341.
http://dx.doi.org/10.1007/s11548-010-0476-x
5. Mehrban N, Bowen J, Vorndran E, *et al.*, 2013, Structural changes to resorbable calcium phosphate bioceramic aged *in vitro*. *Colloids and Surfaces B: Biointerfaces*, vol.111: 469–478.
http://dx.doi.org/10.1016/j.colsurfb.2013.06.020
6. Mehrban N, Paxton J Z, Bowen J, *et al*., 2011, Comparing physichochemical properties of printed and hand cast biocements designed for ligament replacement. *Advances in Applied Ceramics*, vol.110(3): 162–167.
http://dx.doi.org/10.1179/1743676110Y.0000000012
7. Ricci J L, Clark E A, Murriky A, *et al*., 2012, Three-dimensional printing of bone repair and replacement materials: Impact on craniofacial surgery. *Journal of Craniofacial Surgery*, vol.23(1): 304–308.
http://dx.doi.org/10.1097/SCS.0b013e318241dc6e
8. Tsang V L and Bhatia S N, 2004, Three-dimensional tissue fabrication. *Advanced Drug Delivery Reviews*, vol.56(11): 1635–1647.
http://dx.doi.org/10.1016/j.addr.2004.05.001
9. Mironov V, Boland T, Trusk T, *et al*. 2003, Organ printing: Computer-aided jet-based 3D tissue engineering. *Trends in Biotechnology*, vol.21(4): 157–161.

http://dx.doi.org/10.1016/S0167-7799(03)00033-7

10. Hollister S J, 2005, Porous scaffold design for tissue engineering. *Nature Materials*, vol.4: 518–524. http://dx.doi.org/10.1038/nmat1421
11. Seitz H, Rieder W, Irsen S, *et al.*, 2005, Three-dimensional printing of porous ceramic scaffolds for bone tissue engineering. *Journal of Biomedical Materials Research Part B: Applied Biomaterials*, vol.74B(2): 782–788. http://dx.doi.org/10.1002/jbm.b.30291
12. Khademhosseini A, Langer R, Borenstein J, *et al.*, 2006, Microscale technologies for tissue engineering and biology. *Proceedings of the National Academy of Sciences of the United States of Americ*a, vol.103(8): 2480–2487. http://dx.doi.org/10.1073/pnas.0507681102
13. Murphy S V and Atala A, 2014, 3D bioprinting of tissues and organs. *Nature Biotechnology*, vol.32: 773–785. http://dx.doi.org/10.1038/nbt.2958
14. Klebe R J, 1988, Cytoscribing: A method for micropositioning cells and the construction of two- and three-dimensional synthetic tissues. *Experimental Cell Research*, vol.179(2): 362–373. http://dx.doi.org/10.1016/0014-4827(88)90275-3
15. Singh M, Haverinen H M, Dhagat P, *et al.*, 2010, Inkjet printing — process and its applications. *Advanced Materials*, vol.22(6): 673–685. http://dx.doi.org/10.1002/adma.200901141
16. Cui X, Dean D, Ruggeri Z M, *et al.*, 2010, Cell damage evaluation of thermal inkjet printed Chinese hamster ovary cells. *Biotechnology and Bioengineering*, vol.106(6): 963–969. http://dx.doi.org/10.1002/bit.22762
17. Tasoglu S and Demirci U, 2013, Bioprinting for stem cell research. *Trends in Biotechnology*, vol.31(1): 10–19. http://dx.doi.org/10.1016/j.tibtech.2012.10.005
18. Xu C, Zhang M, Huang Y, *et al.*, 2014, Study of droplet formation process during drop-on-demand inkjetting of living cell-laden bioink. *Langmuir*, vol.30(30): 9130–9138. http://dx.doi.org/10.1021/la501430x
19. Demirci U and Montesano G, 2007, Single cell epitaxy by acoustic picolitre droplets. *Lab on a Chip*, vol.7(9): 1139–1145. http://dx.doi.org/10.1039/B704965J
20. Derby B, 2012, Printing and prototyping of tissues and scaffolds. *Science*, vol.338(6109): 921–926. http://dx.doi.org/10.1126/science.1226340
21. Skardal A, Mack D, Kapetanovic E, *et al.*, 2012, Bioprinted amniotic fluid-derived stem cells accelerate healing of large skin wounds. *Stem Cells Translational Medicine*, vol.1(11): 792–802. http://dx.doi.org/10.5966/sctm.2012-0088
22. Cui X, Breitenkamp K, Finn MG, *et al.*, 2012, Direct human cartilage repair using three-dimensional bioprinting technology. *Tissue Engineering: Part A*, vol.18(11–12): 1304–1312. http://dx.doi.org/10.1089/ten.TEA.2011.0543
23. Duocastella M, Colina M, Fernández-Pradas J M, *et al.*, 2007, Study of the laser-induced forward transfer of liquids for laser bioprinting. *Applied Surface Science*, vol.253(19): 7855–7859. http://dx.doi.org/10.1016/j.apsusc.2007.02.097
24. Mézel C, Souquet A, Hallo L, *et al.*, 2010, Bioprinting by laser-induced forward transfer for tissue engineering applications: Jet formation modeling. *Biofabrication*, vol.2(1): 014103. http://dx.doi.org/10.1088/1758-5082/2/1/014103
25. Ali M, Pages E, Ducom A, *et al.*, 2014, Controlling laser-induced jet formation for bioprinting mesenchymal stem cells with high viability and high resolution. *Biofabrication*, vol.6(4): 045001. http://dx.doi.org/10.1088/1758-5082/6/4/045001
26. Hopp B, Smausz T, Krez N, *et al.*, 2005, Survival and proliferative ability of various living cell types after laser-induced forward transfer. *Tissue Engineering*, vol.11(11–12): 1817–1823. http://dx.doi.org/10.1089/ten.2005.11.1817
27. Guillotin B, Souquet A, Catros S, *et al*., 2010, Laser assisted bioprinting of engineered tissue with high cell density and microscale organization. *Biomaterials*, vol.31(28): 7250–7256. http://dx.doi.org/10.1016/j.biomaterials.2010.05.055
28. Zopf D A, Hollister S J and Nelson M E, 2013, Bioresorbable airway splint created with a three-dimensional printer. *The New England Journal of Medicine*, vol.368: 2043–2045. http://dx.doi.org/10.1056/NEJMc1206319
29. Michael S, Sorg H, Peck C-T, *et al.*, 2013, Tissue engineered skin substitutes created by laser-assisted bioprinting form skin-like structures in the dorsal skin fold chamber in mice. *PLoS ONE*, vol.8(3): e57741. http://dx.doi.org/10.1371/journal.pone.0057741
30. Keriquel V, Guillemot F, Arnault I, *et al*., 2010, *In vivo* bioprinting for computer- and robotic-assisted medical intervention: Preliminary study in mice. *Biofabrication*, vol.2(1): 014101. http://dx.doi.org/10.1088/1758-5082/2/1/014101
31. Ragaert K, Cardon L, Dekeyser A, *et al.*, 2010, Machine design and processing considerations for the 3D plotting of thermoplastic scaffolds. *Biofabrication*, vol.2(1): 014107. http://dx.doi.org/10.1088/1758-5082/2/1/014107
32. Zhang X and Zhang Y, 2015, Tissue engineering applications of three-dimensional bioprinting. *Cell Biochemistry and Biophysics*, vol.72(3): 777–782. http://dx.doi.org/10.1007/s12013-015-0531-x
33. Malda J, Visser J, Melchels F P, *et al.*, 2013, 25th anniversary article: Engineering hydrogels for biofabrication.

Advanced Materials, vol.25(36): 5011–5028.
http://dx.doi.org/10.1002/adma.201302042

34. Tirella A, Vozzi F, Vozzi G, *et al*., 2011, PAM2 (Piston Assisted Microsyringe): A new rapid prototyping technique for biofabrication of cell incorporated scaffolds. *Tissue Engineering: Part C*, vol. 17(2): 229–237.
http://dx.doi.org/10.1089/ten.tec.2010.0195
35. DeSimone E, Schacht K, Jungst T, *et al*., 2015, Biofabrication of 3D constructs: Fabrication technologies and spider silk proteins as bioinks. *Pure and Applied Chemistry*, vol.87(8): 737–749.
http://dx.doi.org/10.1515/pac-2015-0106
36. Chang R, Nam J and Sun W, 2008, Effects of dispensing pressure and nozzle diameter on cell survival from solid freeform fabrication–based direct cell writing. *Tissue Engineering: Part A*, vol.14(1): 41–48.
http://dx.doi.org/10.1089/ten.a.2007.0004
37. Khalil S, Nam J and Sun W, 2005, Multi-nozzle deposition for construction of 3D biopolymer tissue scaffolds. *Rapid Prototyping Journal*, vol.11(1): 9–17.
http://dx.doi.org/10.1108/13552540510573347
38. Jakab K, Norotte C, Marga F, *et al*., 2010, Tissue engineering by self-assembly and bio-printing of living cells. *Biofabrication*, vol.2(2): 022001.
http://dx.doi.org/10.1088/1758-5082/2/2/022001
39. Duan B, Hockaday L A, Kang K H, *et al*., 2013, 3D bioprinting of heterogeneous aortic valve conduits with alginate/gelatin hydrogels. *Journal of Biomedical Materials Research A*, vol.101A(5): 1255–1264.
http://dx.doi.org/10.1002/jbm.a.34420
40. Chang R, Nam J and Sun W, 2008, Direct cell writing of 3D microorgan for *in vitro* pharmacokinetic model. *Tissue Engineering Part C: Methods*, vol.14(2): 157–166.
http://dx.doi.org/10.1089/ten.tec.2007.0392
41. Xu F, Celli J, Rizvi I, *et al*., 2011, A three-dimensional in vitro ovarian cancer coculture model using a high-throughput cell patterning platform. *Biotechnology Journal*, vol.6(2): 204–212.
http://dx.doi.org/10.1002/biot.201000340
42. Melchels F P W, Feijen J and Grijpma D W, 2010, A review on stereolithography and its applications in biomedical engineering. *Biomaterials*, vol.31(24): 6121–6130.
http://dx.doi.org/10.1016/j.biomaterials.2010.04.050
43. Castro N J, O'Brien J and Zhang LG, 2015, Integrating biologically inspired nanomaterials and table-top stereolithography for 3D printed biomimetic osteochondral scaffolds. *Nanoscale*, vol.7(33): 14010.
http://dx.doi.org/10.1039/c5nr03425f
44. Grogan S P, Chung P H, Soman P, *et al*., 2013, Digital micromirror device projection printing system for meniscus tissue engineering. *Acta Biomaterialia*, vol.9(7): 7218–7226.
http://dx.doi.org/10.1016/j.actbio.2013.03.020
45. Guo M, Qu X, Zhu W, *et al*., 2014, Bio-inspired detoxification using 3D-printed hydrogel nanocomposites. *Nature Communications*, vol.5: 3774.
http://dx.doi.org/10.1038/ncomms4774
46. Dhariwala B, Hunt E and Boland T, 2014, Rapid prototyping of tissue-engineering constructs, using photopolymerisable hydrogels and stereolithography. *Tissue Engineering*, vol.10(9–10): 1316–1322.
http://dx.doi.org/10.1089/ten.2004.10.1316
47. Lee K Y and Mooney D J, 2001, Hydrogels for tissue engineering. *Chemical Reviews*, vol.101(7): 1869–1879.
http://dx.doi.org/10.1021/cr000108x
48. Hutmacher D W, Goh J C and Teoh S H, 2001, An introduction to biodegradable materials for tissue engineering applications. *Annals of the Academy of Medicine, Singapore*, vol.30: 183–191.
49. Drury J L, Mooney D J and 2003, Hydrogels for tissue engineering: Scaffold design variables and applications. *Biomaterials*, vol.24(24): 4337–4351.
http://dx.doi.org/10.1016/S0142-9612(03)00340-5
50. O'Brien F J, 2011, Biomaterials & scaffolds for tissue engineering. *Materials Today*, vol.14(3): 88–95.
http://dx.doi.org/10.1016/S1369-7021(11)70058-X
51. Iwasaki N, Yamane S T, Majima T, *et al*., 2004, Feasibility of polysaccharide hybrid materials for scaffolds in cartilage tissue engineering: evaluation of chondrocyte adhesion to polyion complex fibers prepared from alginate and chitosan. *Biomacromolecules*, vol.5(3): 828–833.
http://dx.doi.org/10.1021/bm0400067
52. Costa V C, Costa H S, Vasconcelos W L, *et al*., 2007, Preparation of hybrid biomaterials for bone tissue engineering. *Materials Research*, vol.10(1): 21–26.
http://dx.doi.org/10.1590/S1516-14392007000100006
53. Shah A A, Hasan F, Hameed A, *et al*., 2008, Biological degradation of plastics: A comprehensive review. *Biotechnology Advances*, vol.26(3): 246–265.
http://dx.doi.org/10.1016/j.biotechadv.2007.12.005
54. Göpferich A, 1996, Mechanisms of polymer degradation and erosion. *Biomaterials*, vol.17(2): 103–114.
http://dx.doi.org/10.1016/0142-9612(96)85755-3
55. Salacinski H J, Tai N R, Carson R J, *et al*., 2002, *In vitro* stability of a novel compliant poly(carbonate-urea) urethane to oxidative and hydrolytic stress. *Journal of Biomedical Materials Research*, vol.59(2): 207–218.
http://dx.doi.org/10.1002/jbm.1234
56. Steven M M and George G H, 2005, Exploring and engineering the cell surface interface. *Science*, vol.310(5751): 1135–1138.
http://dx.doi.org/10.1126/science.1106587
57. Seidlits S K, Khaing Z Z, Petersen R R, *et al*., 2010, The effects of hyaluronic acid hydrogels with tunable mechanical properties on neural progenitor cell differentiation. *Biomaterials*, vol.31(14): 3930–3940.
http://dx.doi.org/10.1016/j.biomaterials.2010.01.125

58. Murphy C M, Matsiko A, Haugh M G, *et al.*, 2012, Mesenchymal stem cell fate is regulated by the composition and mechanical properties of collagen-glycosaminoglycan scaffolds. *Journal of the Mechanical Behaviour of Biomedical Materials*, vol.11: 53–62. http://dx.doi.org/10.1016/j.jmbbm.2011.11.009
59. Shim J H, Kim J Y, Park M, *et al.*, 2011, Development of a hybrid scaffold with synthetic biomaterials and hydrogel using solid freeform fabrication technology. *Biofabrication*, vol.3(3): 034102. http://dx.doi.org/10.1088/1758-5082/3/3/034102
60. Ahn S H, Kim Y B, Lee H J, *et al.*, 2012, A new hybrid scaffold constructed of solid freeform-fabricated PCL struts and collagen struts for bone tissue regeneration: fabrication, mechanical properties, and cellular activity. *Journal of Materials Chemistry*, vol.22(31): 15901–15909. http://dx.doi.org/10.1039/C2JM33310D
61. Tan H and Marra K G, 2010, Injectable, biodegradable hydrogels for tissue engineering applications. *Materials*, vol.3(3): 1746–1767. http://dx.doi.org/10.3390/ma3031746
62. Zhu J and Marchant R E, 2011, Design properties of hydrogel tissue-engineering scaffolds. *Expert Review of Medical Devices*, vol.8(5): 607–626. http://dx.doi.org/10.1586/erd.11.27
63. Hunt JA, Chen R, van Veen T, *et al.*, 2014, Hydrogels for tissue engineering and regenerative medicine. *Journal of Materials Chemistry B*, vol.2(33): 5319–5338. http://dx.doi.org/10.1039/C4TB00775A
64. Ahmed E M, 2015, Hydrogel: Preparation, characterization, and applications: A review. *Journal of Advanced Research*, vol.6(2): 105–121. http://dx.doi.org/10.1016/j.jare.2013.07.006
65. Skardal A and Atal A 2015, Biomaterials for integration with 3-D bioprinting. *Annals of Biomedical Engineering*, vol.43(3): 730–746. http://dx.doi.org/10.1007/s10439-014-1207-1
66. Vu LT, Jain G, Veres B D, *et al.*, 2015, Cell migration on planar and three-dimensional matrices: A hydrogel-based perspective. *Tissue Engineering Part B: Reviews*, vol.21(1): 67–74. http://dx.doi.org/10.1089/ten.TEB.2013.0782
67. Amsden B, 1998, Solute diffusion within hydrogels. Mechanisms and models. *Macromolecules*, vol.31(23): 8382–8395. http://dx.doi.org/10.1021/ma980765f
68. Tan H, Li H, Rubin J P, *et al.*, 2011, Controlled gelation and degradation rates of injectable hyaluronic acid-based hydrogels through a double crosslinking strategy. *Journal of Tissue Engineering and Regenerative Medicine*, vol.5(10): 790–797. http://dx.doi.org/10.1002/term.378
69. Müller M, Becher J, Schnabelrauch M, *et al.*, 2015, Nanostructured Pluronic hydrogels as bioinks for 3D bioprinting. *Biofabrication*, vol.7(3): 035006. http://dx.doi.org/10.1088/1758-5090/7/3/035006
70. Barry RA, Shepherd R F, Hanson J N, *et al.*, 2009, Direct-write assembly of 3D hydrogel scaffolds for guided cell growth. *Advanced Materials*, vol.21(23): 2407–2410. http://dx.doi.org/10.1002/adma.200803702
71. Cha C, Soman P, Zhu W, *et al.*, 2014, Structural reinforcement of cell-laden hydrogels with microfabricated three dimensional scaffolds. *Biomaterials Science*, vol.2(5): 703–709. http://dx.doi.org/10.1039/C3BM60210A
72. Geckil H, Xu F, Zhang X, *et al.*, 2010, Engineering hydrogels as extracellular matrix mimics. *Nanomedicine (London)*, vol.5(3): 469–484. http://dx.doi.org/10.2217/nnm.10.12
73. Frantz C, Stewart K M and Weaver V M, 2010, The extracellular matrix at a glance. *Journal of Cell Science*, vol.123: 4195–4200. http://dx.doi.org/10.1242/jcs.023820
74. Taubenberger A V, Woodruff M A, Bai H, *et al.*, 2010, The effect of unlocking RGD-motifs in collagen I on pre-osteoblast adhesion and differentiation. *Biomaterials*, vol.31(10): 2827–2835. http://dx.doi.org/10.1016/j.biomaterials.2009.12.051
75. Galus R, Antiszko A and Wlodarski P, 2006, Clinical applications of hyaluronic acid. *Polski Merkuriusz Lekarski*, vol.20(119): 606–608.
76. Skardal A, Zhang J, McCoard L, *et al.*, 2010, Photocrosslinkable hyaluronan-gelatin hydrogels for two-step bioprinting. *Tissue Engineering: Part A*, vol.16(8): 2675–2685. http://dx.doi.org/10.1089/ten.TEA.2009.0798
77. Skardal A, Zhang J, McCoard L, *et al.*, 2010, Dynamically crosslinked gold nanoparticle-hyaluronan hydrogels. *Advanced Materials*, vol.22(42): 4736–4740. http://dx.doi.org/10.1002/adma.201001436
78. Jackson M R, 2001, Fibrin sealants in surgical practice: An overview. *The American Journal of Surgery*, vol.182(2): S1–S7. http://dx.doi.org/10.1016/S0002-9610(01)00770-X
79. Traver M A and Assimos D G, 2006, New generation tissue sealants and hemostatic agents: Innovative urologic applications. *Reviews in Urology*, vol.8(3): 104–111.
80. Ahmed T A, Dare EV and Hincke M, 2008, Fibrin: a versatile scaffold for tissue engineering applications. *Tissue Engineering Part B: Reviews*, vol.14(2): 199–215. http://dx.doi.org/10.1089/ten.teb.2007.0435
81. Masutani E M, Kinoshita C K, Tanaka T T, *et al.*, 2014, Increasing thermal stability of gelatin by UV-induced cross-linking with glucose. *International Journal of Biomaterials*, vol.2014: Article ID 979636. http://dx.doi.org/10.1155/2014/979636
82. Sun J and Tan H, 2013, Alginate-based biomaterials for

regenerative medicine applications. *Materials*, vol.6(4): 1285–1309.
http://dx.doi.org/10.3390/ma6041285

83. Duan B, Kapetanovic E, Hockaday L A, *et al.*, 2014, Three-dimensional printed trileaflet valve conduits using biological hydrogels and human valve interstitial cells. *Acta Biomaterialia*, vol.10(5): 1836–1846.
http://dx.doi.org/10.1016/j.actbio.2013.12.005
84. Kundu J, Shim J-H, Jang J, *et al.*, 2013, An Additive manufacturing-based PCL-alginate-chondrocyte bioprinted scaffold for cartilage tissue engineering. *Journal of Tissue Engineering and Regenerative Medicine*, vol.9(11): 1286–1297.
http://dx.doi.org/10.1002/term.1682
85. Rutz A L, Hyland K E, Jakus A E, *et al.*, 2015, A multimaterial bioink method for 3D printing tunable, cell-compatible hydrogels. *Advanced Materials*, vol.27(9): 1607–1614.
http://dx.doi.org/10.1002/adma.201405076
86. Ozbolat I T, Chen H and Yu Y, 2014, Development of 'multi-arm bioprinter' for hybrid biofabrication of tissue engineered constructs. *Robotics and Computer-Integrated Manufacturing*, vol.30(3): 295–304.
http://dx.doi.org/10.1016/j.rcim.2013.10.005
87. Khalil S and Sun W, 2009, Bioprinting endothelial cells with alginate for 3D tissue constructs. *Journal of Biomedical Engineering*, vol.131(11): 111002.
http://dx.doi.org/10.1115/1.3128729
88. Nakamura M, Iwanaga S, Henmi C, *et al.*, 2010, Biomatrices and biomaterials for future developments of bioprinting and biofabrication. *Biofabrication*, vol.2(1): 014110.
http://dx.doi.org/10.1088/1758-5082/2/1/014110
89. Pati F, Jang J, Ha D-H, *et al.*, 2013, Printing three-dimensional tissue analogues with decellularized extracellular matrix bioink. *Nature Communications*, vol.5: Article number 3935.
http://dx.doi.org/10.1038/ncomms4935
90. Xu T, Jin J, Gregory C, *et al.*, 2005, Inkjet printing of viable mammalian cells. *Biomaterials*, vol.26(1): 93–99.
http://dx.doi.org/10.1016/j.biomaterials.2004.04.011
91. Kolesky D B, Truby R L, Gladman A S, *et al.*, 2014, 3D bioprinting of vascularized, heterogenous cell-laden tissue constructs. *Advanced Materials*, vol.26(19): 3124–3130.
http://dx.doi.org/10.1002/adma.201305506
92. Williams C G, Malik A N, Kim T K, *et al.*, 2005, Variable cytocompatibility of six cell lines with photoinitiators used for polymerizing hydrogels and cell encapsulation. *Biomaterials*, vol. 26(11): 1211–1218.
http://dx.doi.org/10.1016/j.biomaterials.2004.04.024
93. Bianco P and Robey P G, 2001, Stem cells in tissue engineering. *Nature*, vol.414: 118–121.
http://dx.doi.org/10.1038/35102181
94. Gimble J M and Guilak F, 2003, Adipose-derived adult stem cells: Isolation, characterization, and differentiation potential. *Cytotherapy*, vol.5(5): 362–369.
http://dx.doi.org/10.1080/14653240310003026
95. Winter A, Breit S, Parsch D, *et al.*, 2003, Cartilage-like gene expression in differentiated human stem cell spheroids: A comparison of bone marrow–derived and adipose tissue–derived stromal cells. *Arthritis and Rheumatology*, vol.48(2): 418–429.
http://dx.doi.org/10.1002/art.10767
96. Barry F P and Murphy J M, 2004, Mesenchymal stem cells: Clinical applications and biological characterization. *The International Journal of Biochemistry and Cell Biology*, vol.36(4): 568–584.
http://dx.doi.org/10.1016/j.biocel.2003.11.001
97. Dalby M J, Riehle M O, Johnstone H, *et al.*, 2002, *In vitro* reaction of endothelial cells to polymer demixed nanotopography. *Biomaterials*, vol.23(14): 2945–2954.
http://dx.doi.org/10.1016/S0142-9612(01)00424-0
98. Knoepfler P S, 2009, Deconstructing stem cell tumorigenicity: A roadmap to safe regenerative medicine. *Stem cells*, vol.27(5): 1050–1056.
http://dx.doi.org/10.1002/stem.37
99. Vats A, Tolley N S, Bishop A E, *et al.*, 2005, Embryonic stem cells and tissue engineering: delivering stem cells to the clinic. *Journal of the Royal Society of Medicine*, vol.98(8): 346–350.
http://dx.doi.org/10.1258/jrsm.98.8.346
100. Tsai C C, Su P F, Huang Y F, *et al.*, 2012, Oct4 and Nanog directly regulate Dnmt1 to maintain self-renewal and undifferentiated state in mesenchymal stem cells. *Molecular Cell*, vol.47(2): 169–182.
http://dx.doi.org/10.1016/j.molcel.2012.06.020
101. Körbling M, Estrov Z and Champlin R, 2003, Adult stem cells and tissue repair. *Bone Marrow Transplantation*, vol.32: S23–S24.
http://dx.doi.org/10.1038/sj.bmt.1703939
102. Pittenger M F, Mackay A M, Beck S C, *et al.*, 1999, Multilineage potential of adult human mesenchymal stem cells. *Science*, vol.284: 143–147.
http://dx.doi.org/10.1126/science.284.5411.143
103. Sterodimas A, de Faria J Nicaretta B, *et al.*, 2010, Tissue engineering with adipose-derived stem cells (ADSCs): Current and future applications. *Journal of Plastic, Reconstructive & Aesthetic Surgery*, vol.63(11): 1886–1892.
http://dx.doi.org/10.1016/j.bjps.2009.10.028
104. Zuk P 2013, Adipose-derived stem cells in tissue regeneration: A review. *International Scholarly Research Notices*, vol.2013: Article ID 713959.
http://dx.doi.org/10.1155/2013/713959
105. Takahashi K and Yamanaka S, 2006, Induction of pluripotent stem cells from mouse embryonic and adult fibroblast cultures by defined factors. *Cell*, vol.126(4): 663–676.

http://dx.doi.org/10.1016/j.cell.2006.07.024

106. Wang A, Tang Z, Park I-H, *et al.*, 2011, Induced pluripotent stem cells for neural tissue engineering. *Biomaterials*, vol.32(22): 5023–502. http://dx.doi.org/10.1016/j.biomaterials.2011.03.070
107. Diekman B O, Christoforou N, Willard V P, *et al.*, 2012, Cartilage tissue engineering using differentiated and purified induced pluripotent stem cells. *Proceedings of the National Academy of Sciences of the United States of America*, vol.109: 19172–19177. http://dx.doi.org/10.1073/pnas.1210422109
108. De Peppo G M, Marcos-Campos I, Kahler D J, *et al.*, Engineering bone tissue substitutes from human induced pluripotent stem cells. *Proceedings of the National Academy of Sciences of the United States of America*, vol.110: 8680–8685. http://dx.doi.org/10.1073/pnas.1301190110
109. Cho H-J, Lee C-S, Kwon Y-W, *et al.*, 2010, Induction of pluripotent stem cells from adult somatic cells by protein-based reprogramming without genetic manipulation. *Blood*, vol.116(3): 386–395. http://dx.doi.org/10.1182/blood-2010-02-269589
110. Peerani R, Rao B M, Bauwens C, *et al.*, 2007, Niche-mediated control of human embryonic stem cell self-renewal and differentiation. *The EMBO Journal*, vol.26: 4744–4755. http://dx.doi.org/10.1038/sj.emboj.7601896
111. Park J, Cho C H, Parashurama N, *et al.*, 2007, Microfabrication-based modulation of embryonic stem cell differentiation. *Lab on a Chip*, vol.7(8):1018–1028. http://dx.doi.org/10.1039/B704739H
112. Raof NA, Schiele N R, Xie Y, *et al.*, 2011, The maintenance of pluripotency following laser direct-write of mouse embryonic stem cells. *Biomaterials*, vol.32(7): 1802–1808. http://dx.doi.org/10.1016/j.biomaterials.2010.11.015
113. Gruene M, Deiwick A, Koch L, *et al.*, 2011, Laser printing of stem cells for biofabrication of scaffold-free autologous grafts. *Tissue Engineering Part C: Methods*, vol.17(1): 79–87. http://dx.doi.org/10.1089/ten.tec.2010.0359
114. Le Visage C, Dunham B, Flint P, *et al.*, 2004, Coculture of mesenchymal stem cells and respiratory epithelial cells to engineer a human composite respiratory mucosa. *Tissue Engineering*, vol.10(9–10): 1426–1435. http://dx.doi.org/10.1089/ten.2004.10.1426
115. Gaebel R, Ma N, Liu J, *et al.*, 2011, Patterning human stem cells and endothelial cells with laser printing for cardiac regeneration. *Biomaterials*, vol.32(35): 9218–9230. http://dx.doi.org/10.1016/j.biomaterials.2011.08.071
116. Teoh G Z, Crowley C, Birchall M A, *et al.*, 2015, Development of resorbable nanocomposite tracheal and bronchial scaffolds for paediatric applications. *British Journal of Surgery*, vol.102(2): e140–e150. http://dx.doi.org/10.1002/bjs.9700
117. Wang S, Lee J M, and Yeong W Y, 2015, Smart hydrogels for 3D bioprinting. *International Journal of Bioprinting*, vol.1: 3–14. http://dx.doi.org/10.18063/IJB.2015.01.005
118. Seras-Franzoso J, Tsimbouri P M, Burgess K V, *et al.*, 2014, Topographically targeted osteogenesis of mesenchymal stem cells stimulated by inclusion bodies attached to polycaprolactone surfaces. *Nanomedicine*, vol.9(2): 207–220. http://dx.doi.org/10.2217/nnm.13.43
119. Gruene M, Pflaum M, Deiwick A, *et al.*, 2011 Adipogenic differentiation of laser-printed 3D tissue grafts consisting of human adipose-derived stem cells. *Biofabrication*, vol.3(1): 015005. http://dx.doi.org/10.1088/1758-5082/3/1/015005
120. Gao G, Yonezawa T, Hubbell K, *et al.*, 2015, Inkjet-bioprinted acrylated peptides and PEG hydrogel with human mesenchymal stem cells promote robust bone and cartilage formation with minimal printhead clogging. *Biotechnology Journal*, vol.10(10): 1568–1577. http://dx.doi.org/10.1002/biot.201400635
121. Holmes B and Zhang L G, 2013, Enhanced human bone marrow mesenchymal stem cell functions in 3D bioprinted biologically inspired osteochondral construct. *The American Society of Chemical Engineers Proceedings*, vol.3A: V03AT03A002. http://dx.doi.org/10.1115/IMECE2013-66118
122. Lee V, Singh G, Tarasatti J P, *et al.*, 2014, Design and fabrication of human skin by three-dimensional bioprinting. *Tissue Engineering Part C: Methods*, vol.20(6): 473–484. http://dx.doi.org/10.1089/ten.TEC.2013.0335
123. Censi R, Schuurman W, Malda J, *et al.*, 2011, A printable photopolymerizable thermosensitive p(HPMAm-lactate)-PEG hydrogel for tissue engineering. *Advanced Functional Materials*, vol.21(10): 1833–1842. http://dx.doi.org/10.1002/adfm.201002428
124. Jackson N and Stam F, 2015, Optimization of electrical stimulation parameters for electro-responsive hydrogels for biomedical applications. *Journal of Applied Polymer Science*, vol.132(12): 41687(1–8). http://dx.doi.org/10.1002/app.41687
125. Giani G, Fedi S and Barbucci R, 2012, Hybrid magnetic hydrogel: A potential system for controlled drug delivery by means of alternating magnetic fields. *Polymers*, vol.4(2): 1157–1169. http://dx.doi.org/10.3390/polym4021157
126. Pati F, Jang J, Ha D-H, *et al.*, 2014, Printing three-dimensional tissue analogues with decellularized extracellular matrix bioink. *Nature Communications*, vol.5: Article Number 3935. http://dx.doi.org/10.1038/ncomms4935

REVIEW ARTICLE

Preventing bacterial adhesion on scaffolds for bone tissue engineering

Sandra Sánchez-Salcedo[1,2], Montserrat Colilla[1,2], Isabel Izquierdo-Barba[1,2] and María Vallet-Regí[1,2*]

[1] Department of Inorganic and Bioinorganic Chemistry, Faculty of Pharmacy, Complutense University of Madrid, Sanitary Research Institute "Hospital 12 de Octubre i+12". Plaza Ramón y Cajal S/N, E-28040 Madrid, Spain

[2] Center on Bioengineering, Biomaterials and Nanomedicine (CIBER-BBN), Spain

Abstract: Bone implant infection constitutes a major sanitary concern which is associated to high morbidity and health costs. This manuscript focused on overviewing the main research efforts committed up to date to develop innovative alternatives to conventional treatments, such as those with antibiotics. These strategies mainly rely on chemical modifications of the surface of biomaterials, such as providing it of zwitterionic nature, and tailoring the nanostructure surface of metal implants. These surface modifications have successfully allowed inhibition of bacterial adhesion, which is the first step to implant infection, and preventing long-term biofilm formation compared to pristine materials. These strategies could be easily applied to provide three-dimensional (3D) scaffolds based on bioceramics and metals, of which its manufacture using rapid prototyping techniques was reviewed. This opens the gates for the design and development of advanced 3D scaffolds for bone tissue engineering to prevent bone implant infections.

Keywords: Antibacterial adhesion, biofilm formation, zwitterionic surfaces, nanostructured surfaces, rapid prototyping 3D scaffolds, bone tissue engineering.

*Correspondence to: María Vallet-Regí, Department of Inorganic and Bioinorganic Chemistry, Faculty of Pharmacy, Complutense University of Madrid, Institute of Investigation Sanitaria Hospital 12 de Octubre i+12. Ramón and Cajal Plaza s/n, E-28040 Madrid, Spain; Email: vallet@ucm.es

Received: October 27, 2015; **Accepted:** December 8, 2015; **Published Online:** December 28, 2015

Citation: Sánchez-Salcedo S, Colilla M, Izquierdo-Barba I, *et al*., 2016, Preventing bacterial adhesion on scaffolds for bone tissue engineering. *International Journal of Bioprinting*, vol.2(1): 20–34. http://dx.doi.org/10.18063/IJB.2016.01.008.

1. Introduction

The infection risk of bone implants is a major clinical concern that could lead to implant failure and subsequent serious postoperative complications of surgical procedures with high morbidity and costs to the national healthcare systems. Bone implant infections are usually caused by bacterial attachment and colonization on the implant surface[1]. Bacterial adhesion and subsequent growth usually results in slime enclosed biofilm formation on the implant surface[2,3]. In fact, it has been estimated that 65–80% of bacterial infections treated by clinicians in the developed world are caused by organisms growing on biofilms[4]. A biofilm is a microbial-derived sessile community consisting of prokaryotic cells permanently attached to a substratum one to each other, embedded in a matrix of extracellular polymeric substances that it had produced[2]. Bacteria forming biofilms are resistant to host defenses and conventional antibacterial therapies such as vaccines and antibiotics that are effective to eliminate infections caused by planktonic bacteria[5]. Therefore, the initial bacterial adhesion to the biomaterial surface becomes critical in infection pathogenesis.

Of late, new approaches have been proposed to

control and prevent bacterial contamination of implants. One strategy consisted of tailoring the antibacterial properties of the implant surface. Thus, different surface modifications and coating techniques have been proposed, such as direct impregnation with antibiotics, immobilization of bactericidal agents or coating with antimicrobial active metals such as copper and silver, nitric oxide-releasing materials, and TiO_2 films[6]. Nonetheless, whatever antimicrobial strategies used, implants must fulfill the non-fouling requirements or biomacromolecules and dead microorganisms would easily accumulate on the implant surface and hinder the antimicrobial activity of its functional groups[7]. For this reason, great research efforts have been devoted to develop new strategies to modify the surface of biomaterials to provide antibacterial adhesion capability. With the aim of hampering the attachment of microorganism onto surfaces, a widely investigated method consisted of grafting surfaces with hydrophilic polymers, and highlighting polyethylene glycol (PEG) derivatives. Steric repulsion caused by a water hydration layer formed via hydrogen bonding has often been proposed to explain the resistance of hydrophilic surfaces to protein and bacterial adhesion[8,9]. A major concern that limits biological applications of PEG is that this polyether autoxidizes relatively quickly[10], which made PEG coatings having restricted attainment in preventing long-term biofilm formation.

Recently, zwitterionization of biomaterials has emerged as a groundbreaking strategy to confer surfaces of high resistance to nonspecific protein adsorption, bacterial adhesion and/or biofilm formation[9]. Zwitterions are characterized by owning an equal number of both positively and negatively charged groups within a molecule hence maintaining overall electrical neutrality. The non-fouling ability of zwitterionic materials, as in the case of hydrophilic materials, is correlated with a hydration layer on the surface, since a closely bound water layer forms a physical and energetic barrier to avoid bacterial adhesion. Since zwitterionic materials contain both positive and negative charged units, it can bind water molecules even more strongly than hydrophilic materials via electrostatically induced hydration, becoming an important part in affording interfacial bioadhesion resistance[9,11].

On the other hand, it has been demonstrated that surface nanotopography and architecture plays an essential role in bacterial attachment and biofilm formation[12–15]. In fact, Campoccia *et al.*[16] indicated that the use of nanostructured surfaces with inhibited bacterial adhesion could represent a challenging alternative to antibiotics[17–19]. Varied surface modification techniques have been widely used in the fabrication of artificial antibacterial surfaces[20–22]. These surfaces comprised a range of nanotubes and nanoparticle-based surfaces, and nanostructured coatings produced by glancing angle deposition technique by magnetron sputtering (MS-GLAD)[23,24].

The potential of these antibacterial strategies into the bone tissue engineering (BTE) landscape would be essential in manufacturing advanced three-dimensional (3D) scaffolds. The different techniques used in the manufacturing of scaffolds must permit an accurate control of different length scales from nano, micro to macro[25], attending to clinical needs. 3D scaffolds for BTE must fulfill the following requirements[26]: (i) highly interconnected pore networks to allow cell growth, nutrients supply and metabolic waste; (ii) both biocompatible and bioresorbable behavior with tunable degradation and resorption rates to ensure tissue replacement; (iii) appropriate surface chemistry for selective cell attachment, proliferation, and differentiation; and (iv) mechanical properties similar to those of the tissues at the implantation site[26,27].

This review begins with a description of the different recent surface modification strategies aimed at inhibiting bacterial adhesion. Among the diverse approaches, we centered on the chemical modification of biomaterials via zwitterionization, and the modification of metal implants by tailoring its surface nanotopography. In addition, this review focused on the potential application of these antibacterial strategies in BTE. To this aim, the more sophisticated techniques for the fabrication of 3D scaffolds are overviewed.

2. Bone Implant Infections

In this section we overviewed the recent advances developed to date concerning the design and development of zwitterionic surfaces and nanostructured coatings to inhibit bacterial adhesion and biofilm formation onto implantable biomaterials.

2.1 Zwitterionization of Biomaterials

Zwitterionic materials are very promising next-generation biomaterials with a wide variety of potential biomedical applications. Herein, we summarized the methods reported to date to provide metal substrates and bioceramics of zwitterionic nature aimed at designing bacterial anti-adhesive biomaterials.

(1) *Zwitterionization of metal substrates*

Zwiterionic polymers such poly(sulfobetaine methacrylate) (pSBMA) and poly(carboxybetaine methacrylate) (pCBMA), possessing mixed positively and negatively charged functional groups within the same polymer chain and total neutral charge, exhibit ultra-low fouling capabilities, able to inhibit nonspecific protein adsorption, bacterial adhesion and biofilm formation[28–32]. The most widely used method to graft zwitterionic polymers to surfaces is the surface-initiated atom transfer radical polymerization (SI-ATRP)[33]. Among zwitterionic polymers, pSBMA has been grafted to different substrates such as gold[33], glass[34] and poly(tetrafluoroethylene) membranes[35] to attain unfouling surfaces.

Recently, an improved strategy for surface zwitterionization of metallic surfaces, such as commercial pure titanium (pTi)[36] and biomedical grade 316L type stainless steel (SUS 316L)[37], by SI-ATRP of pSBMA has been reported (Figure 1A). Zwitterionization can

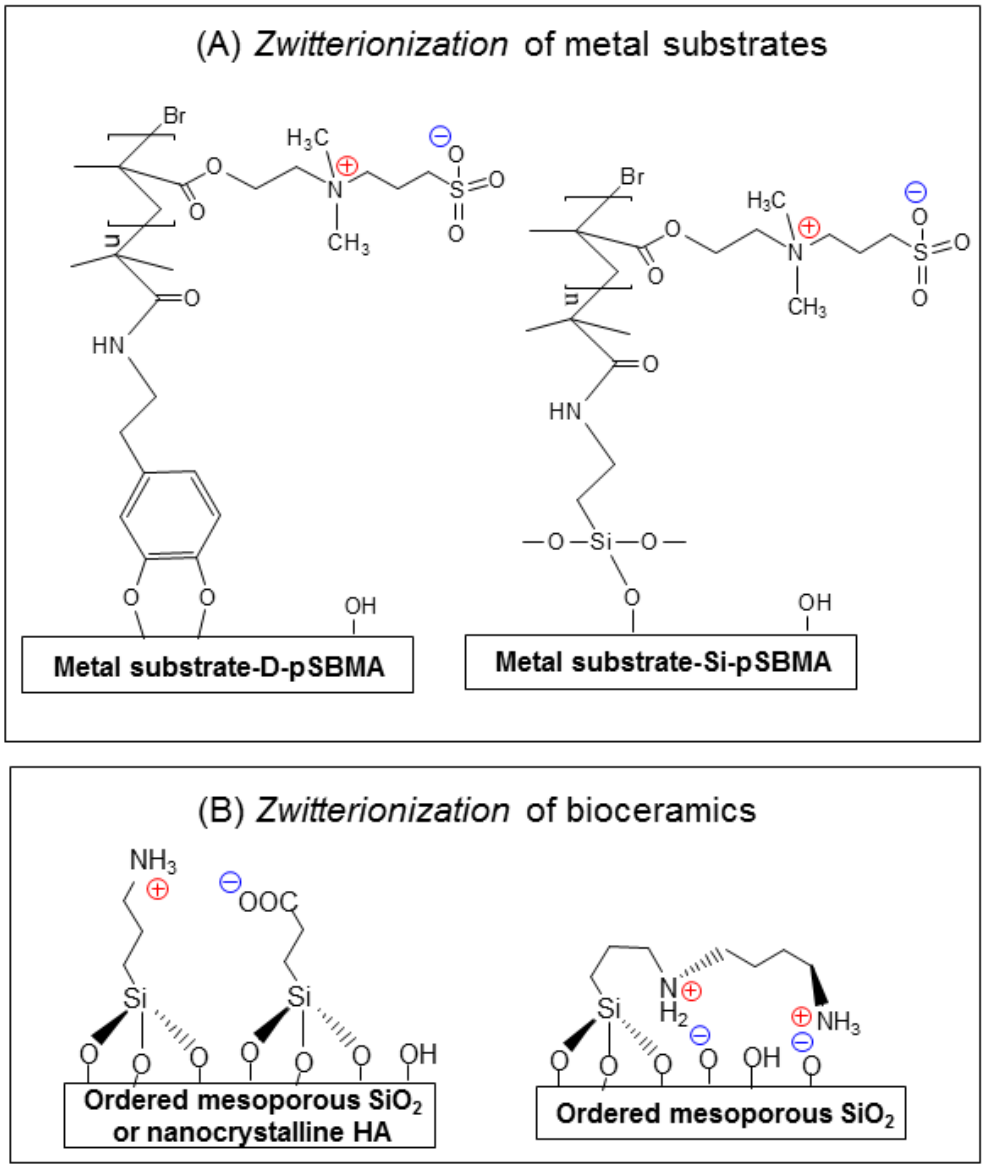

Figure 1. Schematic depiction of the developed strategies to functionalize biomaterials. **(A)** Zwitterionization of metal substrates with poly(carboxybetaine methacrylate) (pCBMA) by covalently bonding dopamine (D) (left) or an organosilane (Si) (right), grafting of an initiator and polymerization of SBMA monomers via surface-initiated atom transfer radical polymerization (SI-ATRP) **(B)** Zwitterionization of bioceramics (ordered mesoporous silica or nanocrystalline hydroxyapatite, HA) by using 3-aminopropyltrimethoxysilane (APTES) and carboxyethylsilanetriol sodium salt (CES) (left) or (N-(2-aminoethyl)-3-aminopropyl-trimethoxysilane) (DAMO) (right).

be divided into four stages[8,9]: (i) treating of the bare metal with ultraviolet (UV) light; (ii) immobilization of either dopamine (D) or an organosilane (Si); (iii) grafting of the initiator, 2-bromoisobutyl bromide (BiBB); and (iv) polymerization of SBMA monomers from the BiBB-tethered surface via ATRP. *In vitro* bacterial adhesion assays were tested using two of the most commonly seen clinical bacteria, *E. coli* and *S. epidermidis*. Bacterial adhesion tests on pTi surfaces indicated that bare metal surface was fully covered by *E. coli* and *S. epidermidis* after 24 hours of assay[36]. However, very few bacteria were attached to SI-ATRP-treated surfaces, reduced to *ca.* 95% relative to uncoated pTi surfaces. This opened up promising expectations in the field of metallic implants.

(2) *Zwitterionization of bioceramics*

Bioceramics are excellent candidates to manufacture bone-like scaffolds[38,39]. It can be designed to release biologically active molecules to repair, maintain, restore or improve bone functions. Different strategies have been developed to provide bioceramics of zwitterionic nature aimed at inhibiting bacterial adhesion and preventing bone implant infections. In this case, inhibition of bacterial colonization must be compatible with adhesion of bone-forming cells to allow osseointegration, which is an essential requisite to warrant a successful implant performance.

Among bioceramics, silica-based ordered mesoporous materials have been broadly proposed for bone tissue regeneration[39–42]. These materials display high surface areas and pore volumes, tailored and narrow pore size distributions, and functionalizable surfaces. These characteristics allow these materials to act as host matrices for a wide range of therapeutic molecules, such as drugs, peptides and small proteins, to be subsequently released in a sustained fashion at the implantation site[43]. Providing the surface of mesoporous matrices of zwitterionic nature to inhibit bacterial adhesion would constitute and add value for the biomedical application of these materials. Thus, the synthesis of zwitterionic SBA-15 type mesoporous material bearing $–NH_3^{\oplus}/–COO^{\ominus}$ groups has been reported (Figure 1B)[44]. This material was synthesized by the co-condensation method using 3-aminopropyltriethoxysilane (APTES) and carboxyethyl silanetriol sodium salt (CES) silanes as $–NH_3^{\oplus}$ and $–COO^{\ominus}$ sources respectively, during the synthesis of SBA-15. The zwitterionic nature of this material in aqueous medium was conserved at pH values around 5.5, as confirmed by determining its isoelectric point by ζ potential measurements. The capability of these materials to inhibit bacterial adhesion was *in vitro* evaluated by simulating severe inflammation/infection conditions, which are usually associated to a decrease in normal pH values[45]. *In vitro* bacterial adhesion assays using *E. coli* indicated that bacterial adhesion in zwitterionic SBA-15 was reduced to *ca.* 93% relative to that for pure silica SBA-15. Moreover, *in vitro* tests with cultured human Saos-2 osteoblasts were performed to investigate the biocompatibility of zwitterionic materials at 7.4, i.e., once normal physiological pH conditions have recovered. The results demonstrated that zwitterionic SBA-15 exhibited good biocompatibility with Saos-2 osteoblasts adhering, proliferating and maintaining its morphological and functional characteristics[45].

Recently, the design and synthesis of a new zwitterionic SBA-15 type bioceramic with dual antibacterial ability has been reported[46]. Its non-fouling capability was derived from the inherent zwitterionic nature of the surface, while the bactericidal capability resulted from its capability to host antibiotics into the mesopores. In this case, zwitterionic SBA-15 mesoporous material was synthetized by using an alkoxysilane bearing primary and secondary amine groups (N-(2-aminoethyl)-3-aminopropyl-trimethoxysilane) (DAMO) based on the co-condensation route. The zwitterionic nature of SBA-15 comes from the $–NH_3^{\oplus}/–SiO^{\ominus}$ and $<NH_2^{\oplus}/–SiO^{\ominus}$ zwitterionic pairs present on the material surface (Figure 1B). *In vitro* adhesion test with *S. aureus* revealed that this zwitterionic bioceramic was capable of decreasing relative bacterial adhesion from 100% (corresponding to pure silica SBA-15) to values lower than 0.1%. This was the first time that such a huge bacterial inhibition capability was found for a mesoporous bioceramic at a physiological pH of 7.4. Moreover, *in vitro* loading and release assays using cephalexin as a model antibiotic demonstrated that zwitterionic SBA-15 can host drugs into its mesopores, releasing it in more than 15 days. This finding unlocks outstanding insights into the design of new bone implants able to play a dual role to treat infections. The zwitterionic nature allowed inhibiting bacterial adhesion, i.e., the first stage of implant infection, whereas release of antibiotics would help eliminate planktonic bacteria in the implant surroundings.

The above-mentioned results opened up promising expectations in the management and prevention of bone implant infections. However, the great scientific challenge is providing bioceramics currently in clini-

cal use with anti-bacterial adhesion properties while preserving its biocompatibility. Nanocrystalline hydroxyapatite (HA) is a calcium phosphate-based bioceramic widely used in dental and orthopedic reconstructive medicine owing to its biocompatibility, bioactivity and osteoconductivity[47]. Although the inherent brittleness of HA limits its use in the restoration of large bone defects, its applications include dental implants, periodontal treatment, alveolar ridge reconstruction and augmentation, orthopedics, maxillofacial surgery, and otolaryngology[47,48]. Thus, HA is commercially available in several physical forms, including powders, particles, granules, dense blocks, self-setting cements, porous 3D scaffolds, implant coatings and composite components. The possibility to provide HA of anti-bacterial adhesion capability would be an added value. The research group of Prof. Vallet-Regí reported the preparation of stoichiometric HA, $Ca_{10}(PO_4)_6(OH)_2$, exhibiting zwitterionic surface capable of inhibiting bacterial adhesion while allowing osteoblast colonization[49]. APTES and CES organosilanes were used to functionalize the surface of HA with $–NH_3^{\oplus}$ and $–COO^{\ominus}$ groups, respectively (Figure 1B). In a first approach, the functionalization process was optimized in HA powders prepared using the controlled crystallization method. Then, the validity of this functionalization method for application in HA substrates shaped in several forms was assessed. For this purpose, HA 3D scaffolds were fabricated by RP technique (see Section 3.1 for further description of this technique) and the resulting 3D-HA scaffolds were functionalized using APTES and CES. *In vitro* bacterial adhesion using *E. coli* under physiological conditions proved that bacterial adhesion in zwitterionic powder HA and 3D-HA decreased 92% and 99% respectively with respect to unmodified HA materials (Figure 2A). The presence of $–NH_3^{\oplus}/–COO^{\ominus}$ zwitterionic pairs onto HA surface accounts for its bacterial anti-adhesive properties. To evaluate the biocompatibility of these HA surfaces, *in vitro* assays were performed using HOS cell cultures. Thus, zwitterionic and pristine HA samples, both as powder and 3D scaffolds were used to carry out the *in vitro* tests. Osteoblastic like-cell spreading was observed in all samples. High magnification scanning electron microscopy (SEM) micrographs showed viable and well-spread cells, which preserved the typical osteoblast morphology (Figure 2B). Regarding cell morphology, there were no differences between zwitterionic and bare HA samples. Moreover, HA-3D scaffolds exhibited different scales of porosity, i.e., channels of *ca.* 800 μm and macropores at 0.01–600 μm range, allowing good cellular internalization with adequate cell anchorage and cell colonization over the entire surface of the scaffolds.

2.2 Development of Nanostructured Surfaces

Albeit a well-established application of nanotechnology in electronic and optical engineering, the use of nanostructured materials in medicine and biology is still at its infancy. In this sense, it had demonstrated the major role of surface nanotopography in bacterial adhesion and biofilm formation[15-17,50]. Different studies using modeled nanostructured surfaces have demonstrated the influence of the nanostructure in the inhibition of bacterial adhesion[18,51,52].

Nature constitutes an unexhausted font of inspiration for scientists and engineers, particularly in biomimetics[13]. Several natural surfaces are able to maintain a contaminant-free status despite the innate abundance of contaminants in the surroundings[53–57]. Most of these surfaces owe its non-fouling characteristics to its superhydrophobic properties, which in turn are largely due to its nanotopography. Many animals (e.g., the wing of cicadae[13], mosquitos[58], etc.) and plants (e.g., lotus (*Nelumbo nucifera*[59])) possess a hierarchical surface with nanotopologic characteristics that significantly increase its hydrophobicity, often to the point of becoming superhydrophobic[60], and repellent to microorganism adhesion. Its antibacterial effects are exclusively due to surface nanostructure and not to surface chemical effect. Several surface modification techniques have been widely used in the construction of artificial antibacterial surfaces based in nanostructured surfaces[22]. These surfaces comprised a range of polymers, nanotubes and nanoparticle-based surfaces in nanoscale, exhibiting bactericidal or anti-biofouling effect.

It should be highlighted that the development of surfaces with simultaneous opposite responses toward osteoblasts and bacterial proliferation would represent a significant achievement in orthopedic implantology[50]. However, there have been very few studies analyzing surfaces that fulfill both conditions[61,62]. The idea of tailoring surfaces with customized and selective responses toward specific cell types (eukaryotic and prokaryotic cells) should be mandatory in the design of biomaterials for TE purposes[63]. In this sense, the key role of surface nanotopography in the stimulation of osteoblast-like cells while reducing bacterial

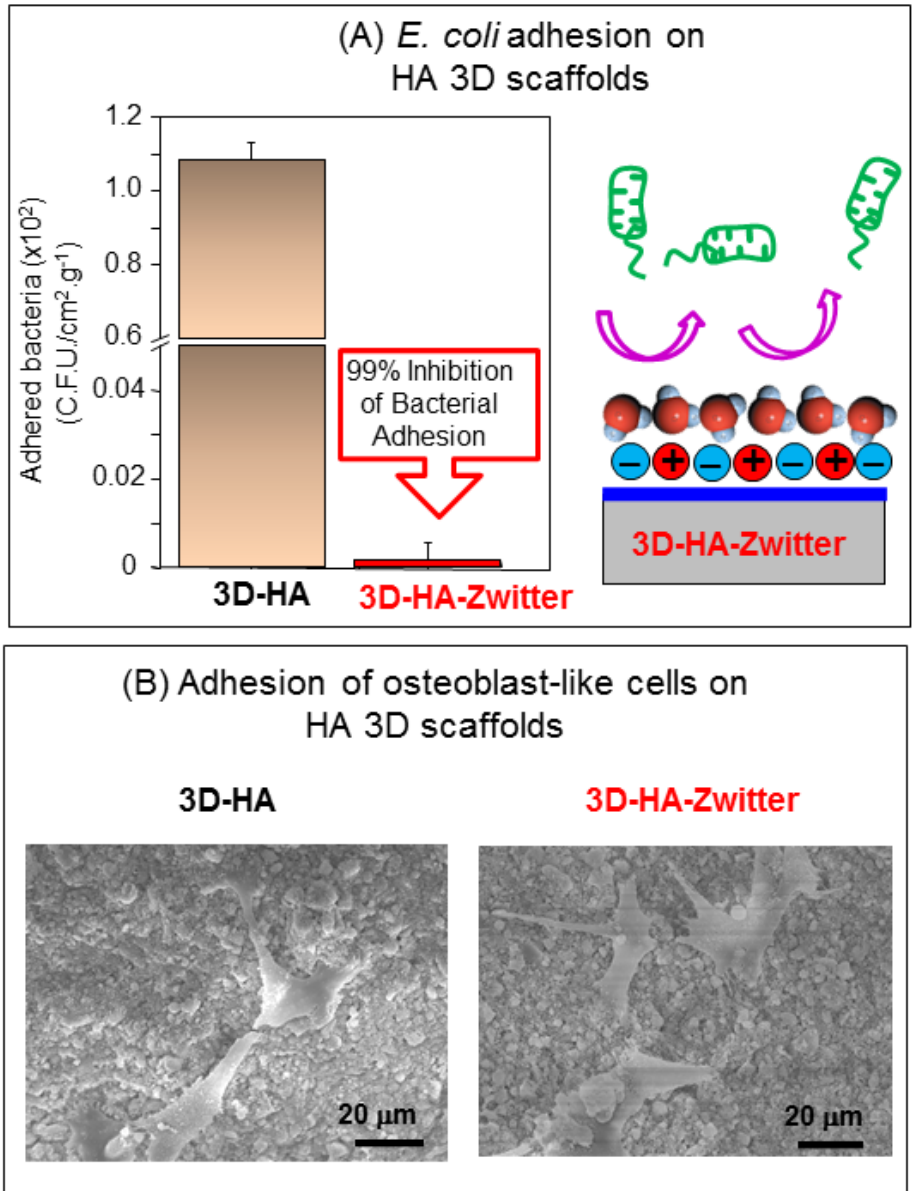

Figure 2. (A) *E. coli* adhesion onto 3D HA scaffolds (3D-HA) before and after being submitted to the zwitterionization process with 3-aminopropyltrimethoxysilane (APTES) and carboxyethyl silanetriol sodium salt (CES) (3D-HA-Zwitter). Schematic representation of the performance of 3D-HA-Zwitter surface during the bacterial adhesion assay was also included. **(B)** SEM micrographs at 1000x magnification of the surface of 3D-HA and 3D-HA-Zwitter scaffolds after 24 hours of cell spreading assay with the HOS osteoblast culture.

adhesion and proliferation can be explained by a mathematical model[63]. Recently, MS-GLAD has been used to produce nanostructured coatings in pure titanium and Ti6Al4V alloy implants[24]. MSGLAD is a powerful technique for producing nanostructured coatings in large areas and with a great variety of morphologies[64]. It is based on exploiting atomic shadowing effects during physical vapor deposition under high vacuum conditions. In this sense, the main processes responsible for the formation of the nanostructures are the atomic self-shadowing mechanism at the surface and the collisional processes of the sputtered atoms in the plasma phase, mediated by the tilt angle of the substrate and the value of the argon background pressure[65].

Figure 3A indicated SEM micrographs corresponding to Ti6Al4V substrates before and after (Nano-Ti6Al4V) MSGLAD processing, displaying different topological surface features. Nano-Ti6Al4V substrate appeared fully coated, with patterns at the

nanoscale consisting of almost vertically aligned nanocolumns with lengths between 250 and 350 nm with a diameter between 40 and 60 nm, separated (from center to center) by 100–200 nm. This nanostructure is very similar to the nanostructure of cicada wings as previously reported[13]. Moreover, this kind of dense, highly packed nanotopography, together with the separation between nanofeatures can lead to a significant

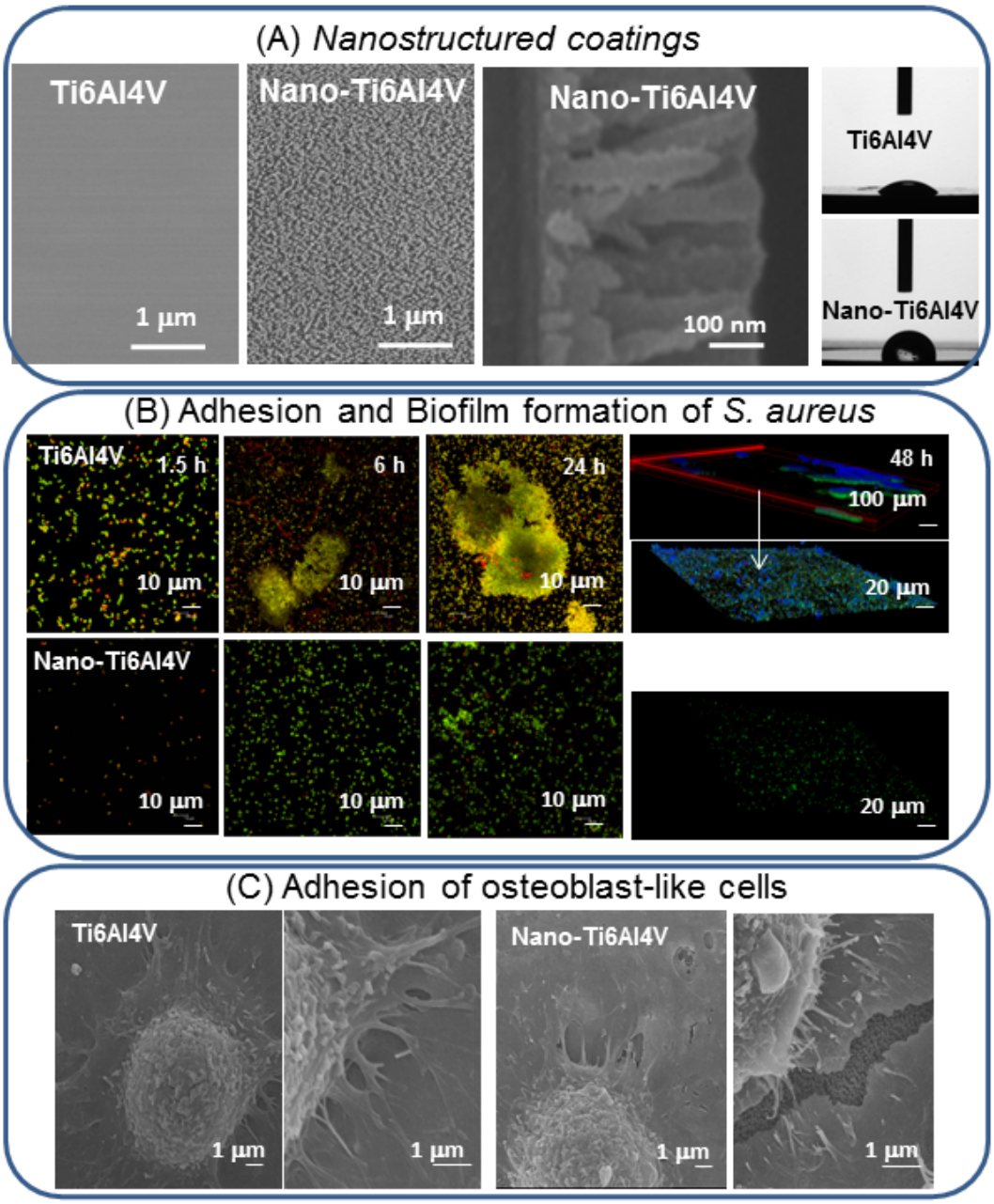

Figure 3. (A) Characterization of nanostructured coating by SEM. Micrographs of Ti6Al4V substrate (smooth surfaces) and Nano-Ti6Al4V surfaces (nanostructured pattering formed by nanocolumns). Evaluation of surface wettability showing the increase of hydrophobicity after coated with nanostructures pattering. **(B)** Images collected by confocal fluorescence microscopy after 1.5, 6 and 24 hours of culture with *S. aureus* on Ti6Al4V and Nano-Ti6Al4V surfaces. Ti6Al4V showed initial bacterial adherence and the subsequent development of a biofilm (6 and 24 hours, arrows). No biofilms were observed in the modified material Nano-Ti6Al4V, and only cells and small conglomerates can be seen. Confocal 3D reconstruction of the Ti6Al4V surface after 48 hours. Extracellular matrix (blue stain) was only observed in Ti6Al4V substrate, on the contrary only live individual bacterial cells was detected on Nano-Ti6Al4V surfaces, with no biofilm formation. **(C)** Osteoblast adhesion after 24 hours on a Ti6Al4V substrate and a Nano-Ti6Al4V sample showing similar behavior.

decrease in wettability due to a ''lotus leaf effect'' on the material surface[56]. To estimate the wettability of the different surface samples, contact angles measurements were measured. The contact angle for the initial Ti6Al4V substrate was 56º whilst that of the Nano-Ti6Al4V was 102º showing a drastic increase in the hydrophobicity for the nanostructured surfaces. The antibacterial effect of the Nano-Ti6Al4V surfaces was evaluated by means of bacterial adhesion experiments and compared with those on medical grade Ti6Al4V substrates. Different *S. aureus* strains from a collection strain and six clinical strains isolated from different patients were used. Results showed that Nano-Ti6Al4V exhibited a notable decrease in *S. aureus* adhesion for both the collection and clinical strains (around 70%) with respect to the untreated Ti6Al4V surfaces.

Concerning biofilm formation, confocal microscopy was used to characterize sequential biofilm formation after different periods (Figure 3B). The presence of a few scattered bacteria on the Nano-Ti6Al4V surface was noted, as well as the absence of biofilm after 24 hours of incubation. Additional confocal microscopy experiments were performed using calcofluor fluorescent stains to stain the extracellular matrix of biofilms after 48 hours (Figure 3B). The confocal 3D images corresponding to biofilm formation demonstrated that non-coated Ti6Al4V substrates clearly show biofilm formation from the blue staining of typical extracellular matrix covering the bacterial colonies. In contrast, blue staining was absent in Nano-Ti6Al4V.

In vitro biocompatibility was assessed by culturing the HOS cell line on the Nano-Ti6Al4V. Results have indicated similar behavior regarding the initial osteoblast adhesion and mitochondrial activity between both surfaces, indicating a good biocompatibility. SEM micrographs after 1 day of culture confirmed that Nano-Ti6Al4V behaved as well as pristine Ti6Al4V with respect to human osteoblasts (Figure 3C). The surfaces in both cases appeared fully covered by cells, exhibiting good adhesion, proliferation and degree of extension. Higher magnification images showed the anchoring elements spread by the cells.

3. Scaffolds for Bone Tissue Engineering

The application of the above-mentioned antibacterial strategies to implants manufactured as 3D scaffolds would represent a step forward in bone tissue engineering (BTE).

Since the emergence of TE in the mid-1980s, a wide variety of shaping methodologies for manufacturing 3D porous scaffolds have been developed. There are many manufacturing methods ranging from the more conventional ones, which lead to randomly interconnected porous scaffolds and that which are principally based on the incorporation of porogen particles[66], use of foam replica technique[67], gel-casting of foams[68], cold isostatic pressing[69], deproteinization of bovine bone[70], particulate leaching[71], freeze-drying[72], gas foaming[73], and a combination of the methods[74]; to more sophisticated technologies based on solid free form (SFF) fabrication such as rapid prototyping (RP). RP techniques allowed accurate control in the macro-microporosity scales and fabricating custom-made implants, which allowed the fabrication of scaffolds both of bioceramic and metallic nature[75]. These techniques constituted a general strategy in which 3D parts are printed layer-by-layer based on a computer-aided-design (CAD) to fabricate 3D interconnected porous scaffolds at a large scale[76,77]. Thus, the scaffold architecture can be adjusted and optimized to attain the adequate mechanical response, accelerate bone regeneration process, and guide bone formation with the anatomic cortical-trabecular structure[78]. Several RP techniques have been used for scaffolds preparation, such as robocasting (RC), selective laser sintering (SLS), selective laser melting (SLM), stereolithography (SLA)[79–82], 3D printing (3DP)[83–85] and fused deposition modeling (FDM)[86,87]. Herein we reviewed the two main RP techniques, namely robocasting (RC) and selective laser based techniques as SLS and SLM, used for the manufacture of bioceramic and metallic scaffolds by itself or in combination with polymers.

3.1 Robocasting (RC)

RC technology also known as direct-printing assembly, is distinctive among these processes because it allowed the building of ceramic scaffolds using water-based inks with minimal organic content (<1wt.%)[88]. Slurries developed from RC must fulfill two important criteria[89]. Firstly, its viscoelastic properties must allow it to flow through a deposition nozzle and then "set" instantaneously so that its shape is preserved as additional layers are deposited or when it span gaps in the underlying structure. Secondly, the suspension must have a high solid volume concentration to reduce shrinkage[90]. The stability of these slurries demands high dispersive forces between particles, where the role of the dispersant is critical[90,91]. The resulting

scaffolds display a high percent of porosity and interconnectivity, easily controllable with enhanced mechanical properties in comparison to conventional scaffold processing (Figure 4A)[92]. Thus, 3D scaffolds based on composites (ceramic-polymer) such as silicon doped hydroxyapatite (SiHA), and mesoporous bioactive glass such as ceramic and polycaprolactone (PCL) and gelatin as polymers have been carried out[93–97]. One of the advantages of RC is the possibility to integrate nanostructural features into micro-macrostructure matrices to fine-tune cellular responses. Thus, the use of sol-gel process combined with RC technique, where the sol can be directly printed before gelation in a one-pot procedure, permits the design of hierarchical 3D meso-macroporous[98]. Hence, the versatility of RC allowed the addition of biodegradable polymers into the slurries avoiding high temperature processing and improving its mechanical properties.

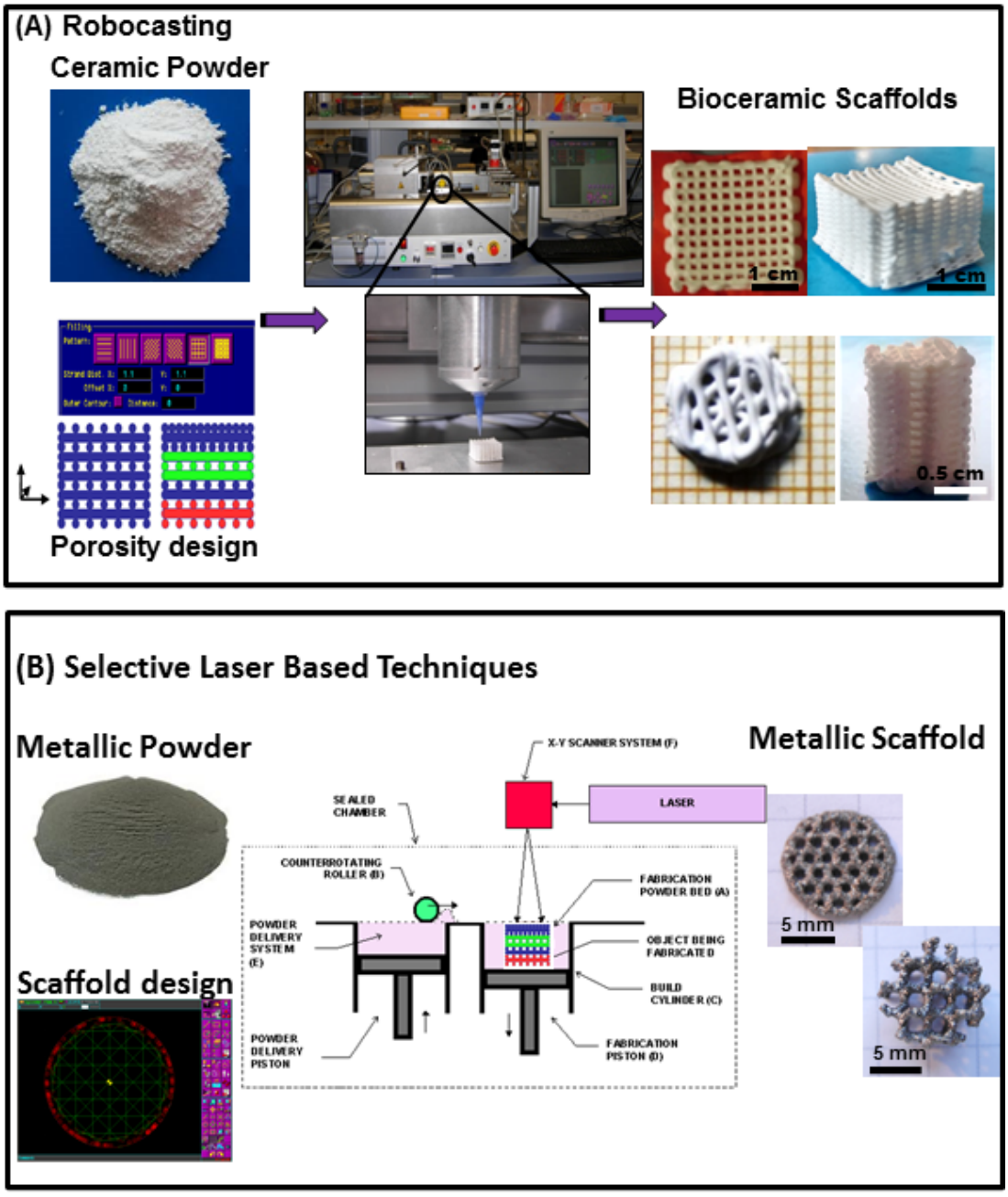

Figure 4. Schematics of two rapid prototyping (RP) methods for the manufacture of 3D scaffolds based in bioceramics and metals via **(A)** robocasting (RC) and **(B)** selective laser based techniques.

This feature permits incorporating biologically active molecules, such as therapeutic drugs and osteoinductive agents, during the manufacture of the scaffold. Thus, 3D scaffolds based in demineralized bone matrix (DBM) containing nanocrystalline silicon doped hydroxyapatite (HA) and PCL have been fabricated[99].

3.2 Selective Laser Based Techniques

Among the most used laser-assisted additive manufacturing are the SLS and SLM techniques[100]. These techniques involved selective use of a laser to build up a model layer by layer from a fine powder bed (Figure 4B). The fine powder particles adhere and sinter when illuminated by a laser beam. Each layer is scanned according to its corresponding cross-section as calculated from the CAD model. The immediate advantage offered by these techniques is that there is no requirement of support structures, since the un-sintered powder provides support during the build and leads to the possibility of obtaining polymeric, ceramic and metallic based-scaffolds[101–102]. Usually, ceramic and polymeric 3D scaffolds are manufactured by the SLS technique, which permits fabricating complex geometries with controllable internal architecture such as those required for BTE applications[47,85,103,104]. *In vivo* evaluations revealed that the 3D ceramic scaffolds were biocompatible and that the macropores were filled by mineralization. For instance, porous calcium phosphate ceramic scaffolds have been fabricated using different weight ratios of tricalcium phosphate (TCP)/HA via SLS. Rapid heating and cooling of SLS were used, which reduced the decomposition of HA due to shorter exposure at high temperature[105].

SLM, which emerged to alleviate some of the issues associated to SLS technique, uses a high-energy laser beam to directly fuse the high-temperature metallic powder layers consecutively deposited as ultra-thin 2D cross-sections. In this sense, SLM has been proven to be beneficial for the manufacture of bone tissue engineering metallic scaffolds and implants by producing very fine and porous structures with mechanical properties similar to those of bulk materials[100,106].

4. Conclusion

Recent scientific advances have permitted the development of novel alternatives to antibiotics treatment for the management and prevention of bone implant infections. The fine tuning of chemical and nano-structural properties of biomaterial surfaces permits providing bioceramic and metallic substrates antibacterial properties by notably reducing bacterial adhesion and biofilm formation compared to bare substrates. The application of these approaches to 3D scaffolds augur promising opportunities in the field of bone tissue engineering.

Conflict of Interest and Funding

The authors declare no conflict of interest. The authors would like to acknowledge the Ministry of Economy and Competitiveness (MINECO), Spain, for funding through projects MAT2012-35556 and CSO2010-11384-E (Agening Network of Excellence).

References

1. Nablo B J, Rothrock A R and Schoenfisch M H, 2005, Nitric oxide-releasing sol-gels as antibacterial coatings for orthopedic implants. *Biomaterials*, vol.26(8): 917–924. http://dx.doi.org/10.1016/j.biomaterials.2004.03.031
2. Costerton J W, Montanaro L and Arciola C R, 2005, Biofilm in implant infections: its production and regulation. *International Journal of Artificial Organs*, vol.28(11): 1062–1068.
3. Bjarnsholt T, 2013, The role of bacterial biofilms in chronic infections. *Acta Pathologica, Microbiologica et Immunologica Scandinavica*, vol.121(136): 1–51. http://dx.doi.org/10.1111/apm.12099
4. Lebeaux D, Chauhan A, Rendueles O, *et al.*, 2013, From in vitro to *in vivo* models of bacterial biofilm-related infections. *Pathogens*, vol.2(2): 288–356. http://dx.doi.org/10.3390/pathogens2020288
5. Davies D, 2003, Understanding biofilm resistance to antibacterial agents. *Nature Reviews Drug Discovery*, vol.2(2): 114–122. http://dx.doi.org/10.1038/nrd1008
6. Simchi A, Tamji E, Pishbin F, *et al.*, 2011, Recent progress in inorganic and composite coatings with bactericidal capability for orthopaedic applications. *Nanomedicine: Nanotechnology, Biology and Medicine*, vol.7(1): 22–39. http://dx.doi.org/10.1016/j.nano.2010.10.005
7. Klibanov A M, 2007, Permanently microbicidal materials coatings. *Journal of Materials Chemistry*, vol.17(24): 2479–2482. http://dx.doi.org/10.1039/B702079A
8. Zheng J, Li L, Tsao H K, *et al.*, 2005, Strong repulsive forces between protein and oligo(ethylene glycol) self-assembled monolayers: a molecular simulation study. *Biophysical Journal*, vol.89(1): 158–166.

http://dx.doi.org/10.1529/biophysj.105.059428

9. Chen S, Li L, Zhao, *et al.*, 2010, Surface hydration: Principles and applications toward low-fouling/non-fouling biomaterials. *Polymer*, vol.51(23): 5283–5293. http://dx.doi.org/10.1016/j.polymer.2010.08.022
10. Ostuni E, Chapman R G, Holmlin R E, *et al.*, 2001, A survey of structure-property relationships of surfaces that resist the adsorption of protein. *Langmuir*, vol.17(18): 5605–5020. http://dx.doi.org/10.1021/la010384m
11. Tanaka M, Sato K, Kitakami E, *et al.*, 2015, Design of biocompatible and biodegradable polymers based on intermediate water concept. *Polymer Journal*, vol.47: 114–121. http://dx.doi.org/10.1038/pj.2014.129
12. Chung K K, Schumacher J F, Sampson E M, *et al.*, 2007, Impact of engineered surface microtopography on biofilm formation of *Staphylococcus aureus*. *Biointerphases*, vol.2(2): 89–94. http://dx.doi.org/10.1116/1.2751405
13. Ivanova E P, Hasan J, Webb H K, *et al.*, 2012, Natural bactericidal surfaces: Mechanical rupture of *Pseudomonas aeruginosa* by cicada wings. *Small*, vol.8(16): 2489–2494. http://dx.doi.org/10.1002/smll.201200528
14. Bazaka, K, Crawford R J and Ivanova E P, 2011, Do bacteria differentiate between degrees of nanoscale surface roughness? *Biotechnology Journal*, vol.6(9): 1103–1114. http://dx.doi.org/10.1002/biot.201100027
15. Truonga V K, Lapovok R, Estrin Y S, *et al.*, 2010, The influence of nano-scale surface roughness on bacterial adhesion to ultrafine-grained titanium. *Biomaterials*, vol.31(13): 3674–3683. http://dx.doi.org/10.1016/j.biomaterials.2010.01.071
16. Campoccia D, Montanaro L and Arciola C R, 2013, A review of the biomaterials technologies for infection-resistant surfaces. *Biomaterials*, vol.34(34): 8533–5854. http://dx.doi.org/10.1016/j.biomaterials.2013.07.089
17. Puckett S D, Taylor E, Raimondo T, *et al.*, 2010, The relationship between the nanostructure of titanium surfaces and bacterial attachment. *Biomaterials*, vol.31(4): 706–713. http://dx.doi.org/10.1016/j.biomaterials.2009.09.081
18. Díaz C, Schilardi P L, Salvarezza R C, *et al.*, 2007, Nano/microscale order affects the early stages of biofilm formation on metal surface. *Langmuir*, vol.23(22): 11206–11210. http://dx.doi.org/10.1021/la700650q
19. Jahed Z, Lin P, Seo B B, *et al.*, 2014, Responses of *Staphylococcus aureus* bacterial cells to nanocrystalline nickel nanostructures. *Biomaterials*, vol.35(14): 4249–4254. http://dx.doi.org/10.1016/j.biomaterials.2014.01.080
20. Tiraferri A, Vecitis C D and Elimelech M, 2011, Covalent binding of single-walled carbon nanotubes to polyamide membranes for antimicrobial surface properties. *ACS Applied Materials and Interfaces*, vol.3(8): 2869–2877. http://dx.doi.org/10.1021/am200536p
21. Knetsch M L W and Koole L H, 2011, New strategies in the development of antimicrobial coatings: The example of increasing usage of silver and silver nanoparticles. *Polymers*, vol.3(1): 340–366. http://dx.doi.org/10.3390/polym3010340
22. Kelly P J, Lia H, Whitehead K A, *et al*., 2009, A study of the antimicrobial and tribological properties of TiN/Ag nanocomposite coatings. *Surface and Coatings Technology*, vol.204(6–7): 1137–1140. http://dx.doi.org/10.1016/j.surfcoat.2009.05.012
23. Sengstock C, Lopian M, Motemani Y, *et al.*, 2014, Structure-related antibacterial activity of a titanium nanostructured surface fabricated by glancing angle sputter deposition. *Nanotechnology*, vol.25(19): 195101–195702. http://dx.doi.org/10.1088/0957-4484/25/19/195101
24. Izquierdo-Barba I, García-Martín J M, Álvarez R, *et al.*, 2015, Nanocolumnar coatings with selective behavior towards osteoblast and *Staphylococcus aureus* proliferation. *Acta Biomaterialia*, vol.15: 20–28. http://dx.doi.org/10.1016/j.actbio.2014.12.023
25. Anselme K, 2000, Osteoblast adhesion on biomaterials. *Biomaterials*, vol.21(7): 667–681. http://dx.doi.org/10.1016/S0142-9612(99)00242-2
26. Hutmacher D W, 2000, Scaffolds in tissue engineering bone and cartilage. *Biomaterials*, vol.21(24): 2529–2543. http://dx.doi.org/10.1016/S0142-9612(00)00121-6
27. Hollister S J, 2009, Scaffold design and manufacturing: from concept to clinic. *Advanced Materials*, vol. 21(32–33), 3330–3342. http://dx.doi.org/10.1002/adma.200802977
28. Cheng G, Zhang Z, Chen S, *et al.*, 2007, Inhibition of bacterial adhesion and biofilm formation on zwitterionic surfaces. *Biomaterials*, vol.28(29): 4192–4199. http://dx.doi.org/10.1016/j.biomaterials.2007.05.041
29. Cheng G, Xue H, Zhang Z, *et al.*, 2008, A switchable biocompatible polymer surface with self-sterilizing and nonfouling capabilities. *Angewandte Chemie International Edition*, vol.120(46): 8963–8966. http://dx.doi.org/10.1002/ange.200803570
30. Cheng G, Li G, Xue H, *et al.*, 2009, Zwitterionic carboxybetaine polymer surfaces and their resistance to long-term biofilm formation. *Biomaterials*, vol.30(28): 5234–5240. http://dx.doi.org/10.1016/j.biomaterials.2009.05.058
31. Jiang S and Cao Z, 2010, Ultralow-fouling, functiona-

lizable, and hydrolyzable zwitterionic materials and their derivatives for biological applications. *Advanced Materials*, vol.22(9): 920–932. http://dx.doi.org/10.1002/adma.200901407

32. Lalani R and Liu L, 2012, Electrospun zwitterionic poly(sulfobetaine methacrylate) for nonadherent, superabsorbent, and antimicrobial wound dressing applications. *Biomacromolecules*, vol.13(6): 1853–1863. http://dx.doi.org/10.1021/bm300345e
33. Zhang Z, Chen S, Chang Y, *et al*., 2006, Surface grafted sulfobetaine polymers via atom transfer radical polymerization as superlow fouling coatings. *Journal of Physical Chemistry B*, vol.110(22): 10799–10804. http://dx.doi.org/10.1021/jp057266i
34. Zhang Z, Chao T, Chen S, *et al.*, 2006, Superlow fouling sulfobetaine and carboxybetaine polymers on glass slides. *Langmuir*, vol.22(24): 10072–10077. http://dx.doi.org/10.1021/la062175d
35. Liu Y L, Han C C, Wei T-C, *et al*., 2010, Surface-initiated atom transfer radical polymerization from porous poly(tetrafluoroethylene) membranes using the C-F groups as initiators. *Journal of Polymer Science: Part A: Polymer Chemistry*, vol.48(10): 2076–2083. http://dx.doi.org/10.1002/pola.23975
36. Yu B Y, Zheng J, Chang Y, *et al.*, 2014, Surface zwitterionization of titanium for a general bio-inert control of plasma proteins, blood cells, tissue cells, and bacteria. L*angmuir*, vol.30(25): 7502–7512. http://dx.doi.org/10.1021/la500917s
37. Sin M C, Sun Y M and Chang Y, 2014, Zwitterionic-based stainless steel with well-defined polysulfobetaine brushes for general bioadhesive control. *ACS Applied Materials and Interfaces*, vol.6(2): 861–873. http://dx.doi.org/10.1021/am4041256
38. Vallet-Regí M and Ruiz-Hernández E, 2011, Bioceramics: from bone regeneration to cancer nanomedicine. *Advanced Materials*, vol.23(44): 5177–5218. http://dx.doi.org/10.1002/adma.201101586
39. Vallet-Regí M, 2014, *Bio-ceramics with clinical applications*, John Wiley & Sons Ltd, Chichester, United Kingdom. http://dx.doi.org/10.1002/9781118406748
40. Vallet-Regí M, 2006, Ordered mesoporous materials in the context of drug delivery systems and bone tissue engineering. *Chemistry–A European Journal*, vol.12(23): 5934–5943. http://dx.doi.org/10.1002/chem.200600226
41. Vallet-Regí M, Colilla M and González B, 2011, Medical applications of organic-inorganic hybrid materials within the field of silica-based bioceramics. *Chemical Society Reviews*, vol.40(2): 596–607. http://dx.doi.org/10.1039/C0CS00025F
42. Vallet-Regí M, Izquierdo-Barba I and Colilla M, 2012, Structure and functionalization of mesoporous bioceramics for bone tissue regeneration and local drug delivery. *Philosophical Transactions of the Royal Society of Chemistry A*, vol.370(1963): 1400–1421. http://dx.doi.org/10.1098/rsta.2011.0258
43. Vallet-Regí M, Balas F and Arcos D, 2007, Mesoporous materials for drug delivery. *Angewandte Chemie International Edition*, vol.46(40): 7548–7558. http://dx.doi.org/10.1002/anie.200604488
44. Colilla M, Izquierdo-Barba I, Sánchez-Salcedo S, *et al.*, 2010, Synthesis and characterization of zwitterionic SBA-15 nanostructured materials. *Chemistry of Materials*, vol.22(23): 6459–6466. http://dx.doi.org/10.1021/cm102827y
45. Izquierdo-Barba I, Sánchez-Salcedo S, Colilla M, *et al.*, 2011, Inhibition of bacterial adhesion on biocompatible zwitterionic SBA-15 mesoporous materials. *Acta Biomaterialia*, vol.7(7): 2977–2985. http://dx.doi.org/10.1016/j.actbio.2011.03.005
46. Colilla M, Martínez-Carmona M, Sanchez-Salcedo S, *et al.*, 2014, A novel zwitterionic bioceramic with dual antibacterial capability. *Journal of Materials Chemistry B*, vol.2(34): 5639–5651. http://dx.doi.org/10.1039/C4TB00690A
47. Vallet-Regí M and Navarrete D A, 2015, *Nanoceramics in clinical use: From materials to applications*. 2nd ed., Royal Society of Chemistry, Cambridge, United Kingdom. http://dx.doi.org/10.1039/9781782622550
48. Dorozhkin S V, 2010, Bioceramics of calcium orthophosphates. *Biomaterials*, vol.31(7): 1465–1485. http://dx.doi.org/10.1016/j.biomaterials.2009.11.050
49. Sánchez-Salcedo S, Colilla M, Izquierdo-Barba I, *et al.*, 2013, Design and preparation of biocompatible zwitterionic hydroxyapatite. *Journal of Materials Chemistry B*, vol.1(11): 1595–1606. http://dx.doi.org/10.1039/C3TB00122A
50. Anselme, K, Davidson P, Popa A M, *et al.*, 2010, The interaction of cells and bacteria with surfaces structured at the nanometre scale. *Acta Biomaterialia*, vol.6(10): 3824–3846. http://dx.doi.org/10.1016/j.actbio.2010.04.001
51. Whitehead K A, Colligon J and Verran J, 2005, Retention of microbial cells in substratum surface features of micrometer and sub-micrometer dimensions. *Colloids Surfaces B: Biointerfaces*, vol.41(2–3): 129–138. http://dx.doi.org/10.1016/j.colsurfb.2004.11.010
52. Campoccia D, Montanaro L, Agheli H, *et al.*, 2006, Study of *Staphylococcus aureus* adhesion on a novel nanostructured surface by chemiluminometry. *International Journal of Artificial Organs*, vol.29(6): 622–629.
53. Marmur A, 2004, The Lotus effect: Superhydrophobici-

ty and metastability. *Langmuir*, vol.20(9): 3517–3519. http://dx.doi.org/10.1021/la036369u

54. Su Y, B Ji and Hwang K C, 2010, Nature's design of hierarchical superhydrophobic surfaces of a water strider for low adhesion and low-energy dissipation. *Langmuir*, vol.26(24): 18926–18937. http://dx.doi.org/10.1021/la103442b
55. Bhushan B and Jung Y C, 2011, Natural and biomimetic artificial surfaces for superhydrophobicity, self-cleaning, low adhesion, and drag reduction. *Progress in Materials Science*, vol.56(1): 1–108. http://dx.doi.org/10.1016/j.pmatsci.2010.04.003
56. Guo Z, Liu W and Su B L, 2011, Superhydrophobic surfaces: From natural to biomimetic to functional. *Journal of Colloid and Interface Science*, vol.353(2): 335–355. http://dx.doi.org/10.1016/j.jcis.2010.08.047
57. Webb H K, Hasan J, Truong V K, *et al*., 2011, Nature inspired structured surfaces for biomedical applications. *Current Medicinal Chemistry*, vol.18(22): 3367–3375. http://dx.doi.org/10.2174/092986711796504673
58. Gao X, Yan X, Yao X, *et al*., 2007, The dry-style antifogging properties of mosquito compound eyes and artificial analogues prepared by soft lithography. *Advanced Materials*, vol.19(17): 2213–2217. http://dx.doi.org/10.1002/adma.200601946
59. Bhushan B, Jung Y C, Niemitz A, *et al*., 2009, Lotus-like biomimetic hierarchical structures developed by the self-assembly of tubular plant waxes. *Langmuir*, vol.25(3): 1659–1666. http://dx.doi.org/10.1021/la802491k
60. Koch K, Bhushan B, Yong C J, *et al*., 2009, Fabrication of artificial lotus leaves and significance of hierarchical structure for superhydrophobicity and low adhesion. *Soft Matter*, vol.5(7): 1386–1393. http://dx.doi.org/10.1039/B818940D
61. Ploux L, Anselme K, Dirani A, *et al*., 2009, Opposite responses of cells and bacteria to micro/nanopatterned surfaces prepared by pulsed plasma polymerization and UV-irradiation. *Langmuir*, vol.25(14): 8161–8169. http://dx.doi.org/10.1021/la900457f
62. Mei S, Wang H, Wang W, *et al*., 2014, Antibacterial effects and biocompatibility of titanium surfaces with graded silver incorporation in titania nanotubes. *Biomaterials*, vol.35(14): 4255–4265. http://dx.doi.org/10.1016/j.biomaterials.2014.02.005
63. Decuzzi P and Ferrari M, 2010, Modulating cellular adhesion through nanotopography. *Biomaterials*, vol.31(1): 173–179. http://dx.doi.org/10.1016/j.biomaterials.2009.09.018
64. Alvarez R, García-Martín J M, Macías-Montero M, *et al*., 2013, Growth regimes of porous gold thin films deposited by magnetron sputtering at oblique incidence: From compact to columnar microstructures. *Nanotechnology*, vol.24(4): 045604. http://dx.doi.org/10.1088/0957-4484/24/4/045604
65. García-Martín J M, Álvarez R, Romero-Gómez P, *et al*., 2010, Tilt angle control of nanocolumns grown by glancing angle sputtering at variable argon pressures. *Applied Physics Letters*, vol.97(17): 173103. http://dx.doi.org/10.1063/1.3506502
66. Liu D M, 1996, Fabrication and characterization of porous hydroxyapatite granules. *Biomaterials*, vol.17(20): 1955–1957. http://dx.doi.org/10.1016/0142-9612(95)00301-0
67. Padilla S, Román J and Vallet-Regí M, 2002, Synthesis of porous hydroxyapatite by combination of gelcasting and foams burn out methods. *Journal Materials Science: Materials in Medicine*. vol.13(12): 1193–1197. http://dx.doi.org/10.1023/A:1021162626006
68. Padilla S, Sánchez-Salcedo S and Vallet-Regí M, 2007, Bioactive glass as precursor of designed-architecture scaffolds for tissue engineering. *Journal Biomedical Materials Research*, vol.81(1): 224–232. http://dx.doi.org/10.1002/jbm.a.30934
69. Slosarczyk A J, 1999, Porous hydroxyapatite ceramics. *Journal Materials Science: Materials in Medicine*, vol.18(14): 1163–1165. http://dx.doi.org/10.1023/A:1006677806537
70. Al Ruhaimi K A, 2001, Bone graft substitutes: Acomparative qualitative histologic review of current osteoconductive grafting materials. *International Journal of Oral & Maxillofacial Implants*, vol.16(1): 105–114.
71. Sánchez-Salcedo S, Balas F, Izquierdo-Barba I, *et al*., 2009, *In vitro* structural changes in porous HA/beta-TCP scaffolds under simulated body fluid. *Acta Biomaterialia*, vol.5(7): 2738–2751. http://dx.doi.org/10.1016/j.actbio.2009.03.025
72. Deville S, Saiz E, Nalla R K, *et al*., 2006, Freezing as a path to build complex composites, *Science*, vol.311(5760): 515–518. http://dx.doi.org/10.1126/science.1120937
73. Locs J, Zalite V, Berzina-Cimdina L, *et al*., 2013, Ammonium hydrogen carbonate provided viscous slurry foaming — a novel technology for the preparation of porous ceramics. *Journal of the European Ceramic Society*, vol.33(15–16): 3437–3443. http://dx.doi.org/10.1016/j.jeurceramsoc.2013.06.010
74. Sánchez-Salcedo S, Werner J and Vallet-Regí M, 2008, Hierarchical pore structure of calcium phosphate scaffolds by combination of the gel casting and multiple tape casting methods. *Acta Biomaterialia*, vol.4: 913–922. http://dx.doi.org/10.1016/j.actbio.2008.02.005
75. Hutmacher D W, Sittinger M and Risbud M V, 2004,

Scaffold-based tissue engineering: Rationale for computer-aided design and solid free-form fabrication systems. *Trends in Biology*, vol.22(7): 354–362. http://dx.doi.org/10.1016/j.tibtech.2004.05.005

76. Hutmacher D W, 2001, Scaffold design and fabrication technologies for engineering tissues — state of the art and future perspectives. *Journal Biomaterials Science Polymer Edition*, vol.12(1): 107–124. http://dx.doi.org/10.1163/156856201744489
77. Leong K F, Cheah C M and Chua C K, 2003, Solid freeform fabrication of three-dimensional scaffolds for engineering replacement tissues and organs. *Biomaterials*, vol.24(13): 2363–2378. http://dx.doi.org/10.1016/S0142-9612(03)00030-9
78. Fu Q, Saiz E, Rahaman M N, *et al.*, 2011, Bioactive glass scaffolds for bone tissue engineering: State of the art and future perspectives. *Materials Science and Engineering C*, vol.31(7): 1245–1256. http://dx.doi.org/10.1016/j.msec.2011.04.022
79. Coward T J, Watson R M and Wilkinson I C, 1999, Fabrication of a wax ear by rapid-process modeling using stereolithography. *International Journal of Prosthodontics*, vol.12(1): 20–27.
80. Sánchez-Salcedo S, Nieto A and Vallet-Regí M, 2008, Hydroxyapatite/β-tricalciumphosphate/agarose macroporous scaffolds for bone tissue engineering. *Chemical Engineering Journal*, vol.137(1): 62–71. http://dx.doi.org/10.1016/j.cej.2007.09.011
81. Padilla P, Sánchez-Salcedo S and Vallet-Regí M, 2007, Bioactive glass as precursor of designed-architecture scaffolds for tissue engineering. *Journal of Biomedical Materials Research*, vol.81A(1): 224–232. http://dx.doi.org/10.1002/jbm.a.30934
82. Ryan G E, Pandit A S and Apatsidis D P, 2008, Porous titanium scaffolds fabricated using a rapid prototyping and powder metallurgy technique. *Biomaterials*, vol.29(27): 3625–3635. http://dx.doi.org/10.1016/j.biomaterials.2008.05.032
83. Giordano R A, Wu B M, Borland S W, *et al.*, 1996, Mechanical properties of dense polylactic acid structures fabricated by three dimensional printing. *Journal of Biomaterials Science, Polymer Edition*, vol.8(1): 63–75. http://dx.doi.org/10.1163/156856297X00588
84. Lopez-Heredia M A, Sohier J, Gaillard C, *et al.*, 2008, Rapid prototyped porous titanium coated with calcium phosphate as a scaffold for bone tissue engineering. *Biomaterials*, vol. 29(17): 2608–2615. http://dx.doi.org/10.1016/j.biomaterials.2008.02.021
85. Wiria F E, Shyan J Y M, Lim P N, *et al*., 2010, Printing of titanium implant prototype. *Materials and Design*, vol.31(1): S101–S105. http://dx.doi.org/10.1016/j.matdes.2009.12.050
86. Zein I, Hutmacher D W, Tan K C, *et al.*, 2002, Fused deposition modeling of novel scaffold architectures for tissue engineering applications. *Biomaterials*, vol.23(4): 1169–1185. http://dx.doi.org/10.1016/S0142-9612(01)00232-0
87. Hutmacher D W, Schantz T, Zein I, *et al*., Mechanical properties and cell cultural response of polycaprolactone scaffolds designed and fabricated via fused deposition modelling. *Journal of Biomedical Materials Research*, vol.55(2): 203–216. http://dx.doi.org/10.1002/1097-4636%28200105%2955%3A2%3C203%3A%3AAID-JBM1007%3E3.0.CO%3B2-7
88. Cesarano J, Segalman R and Calvert P, 1998, Robocasting provides mold less fabrication from slurry deposition. *Ceramic Industry*, vol.148: 94–102.
89. Smay J E, Cesarano J and Lewis J A, 2002, Colloidal inks for directed assembly of 3-D periodic structures. *Langmuir*, vol.18(14): 5429–5437. http://dx.doi.org/10.1021/la0257135
90. Michna S, Wu W and Lewis J A, 2005, Concentrated hydroxyapatite inks for direct-write assembly of 3-D periodic scaffolds. *Biomaterials*, vol.26(28): 5632–5639. http://dx.doi.org/10.1016/j.biomaterials.2005.02.040
91. Barnes C P, Sell S A, Boland E D, *et al.*, 2007, Nanofiber technology: Designing the next generation of tissue engineering scaffolds. *Advanced in Drug Delivery Reviews*, vol.59(14): 1413–1433. http://dx.doi.org/10.1016/j.addr.2007.04.022
92. Perera F H, Martínez-Vázquez F J, Miranda P, *et al.*, 2010, Clarifying the effect of sintering conditions on the microstructure and mechanical properties of beta-tricalcium phosphate. *Ceramics International*, vol.36(6): 1929–1935. http://dx.doi.org/10.1016/j.ceramint.2010.03.015
93. Yun H S, Kim S E and Hyeon Y T, 2007, Design and preparation of bioactive glasses with hierarchical pore networks. *Chemical Communications*, vol.21(21): 2139–2141. http://dx.doi.org/10.1039/B702103H
94. García, A, Izquierdo-Barba I, Colilla M, *et al.*, 2011, Preparation of 3-D scaffolds in the SiO_2–$P2O_5$ system with tailored hierarchical meso-macroporosity. *Acta Biomaterialia*, vol.7(3): 1265–1273. http://dx.doi.org/10.1016/j.actbio.2010.10.006
95. Sánchez-Salcedo S, Shruti S, Salinas A J, *et al*., 2014, *In vitro* antibacterial capacity and cytocompatibility of SiO_2–CaO–P_2O_5 meso-macroporous glass scaffolds enriched with ZnO. *Journal Materials Chemistry B*, vol.2(30): 4836–4847. http://dx.doi.org/10.1039/C4TB00403E
96. Martínez-Vázquez F J, Cabañas M V, Paris J L, *et al.*, 2015, Fabrication of novel Si-doped hydroxyapatite/

gelatine scaffolds by rapid prototyping for drug delivery and bone regeneration. *Acta Biomaterialia*, vol.15: 200–209.
http://dx.doi.org/0.1016/j.actbio.2014.12.021

97. Shruti S, Salinas A J, Lusvardi G, *et al*., 2013, Mesoporous bioactive scaffolds prepared with cerium-, gallium- and zinc-containing glasses. *Acta Biomaterialia*, vol.9(1): 4836–4844.
http://dx.doi.org/10.1016/j.actbio.2012.09.024
98. Cicuéndez M, Malmsten M, Doadrio J C, *et al.*, 2014, Tailoring hierarchical meso–macroporous 3D scaffolds: From nano to macro. *Journal of Materials Chemistry B*, vol.2(1): 49–58.
http://dx.doi.org/10.1039/C3TB21307B
99. Meseguer-Olmo, L, Vicente-Ortega V, Alcaraz-Baños M, *et al*., 2013, *In-vivo* behavior of Si-Hydroxyapatite/polycaprolactone/DMB scaffolds fabricated by 3D printing. *Journal of Biomedical Materials Research A*, vol.101A(7): 2038–2048.
http://dx.doi.org/10.1002/jbm.a.34511
100. Riza S H, Masood S H and Wen C, 2014, Laser-assisted additive manufacturing for metallic biomedical scaffolds, *Comprehensive Materials Processing*, vol.10: 285–301.
http://doi.org/10.1016/B978-0-08-096532-1.01017-7
101. Berry E, Brown J M, Connell M, *et al*., 1997, Preliminary experience with medical applications of rapid prototyping by selective laser sintering. *Medical Engineering & Physics*, vol.19(1): 90–96.
http://dx.doi.org/10.1016/S1350-4533(96)00039-2
102. Kruth J-P, Mercelis P, Vaerenbergh J V, *et al*., 2005, Binding mechanisms in selective laser sintering and selective laser melting. *Rapid Prototyping Journal*, vol.11(1): 26–36.
http://dx.doi.org/10.1108/13552540510573365
103. Wiria F E, Leong K F, Chua C K, *et al.*, 2007, Poly-Ɛ-caprolactone/hydroxyapatite for tissue engineering scaffold fabrication via selective laser sintering. *Acta Biomaterialia*, vol.3(1): 1–12.
http://dx.doi.org/10.1016/j.actbio.2006.07.008
104. Tan K H, Chua C K, Leong K F, *et al*., 2005, Selective laser sintering of biocompatible polymers for applications in tissue engineering. *Biomedical Materials Engineering*, vol.15(1–2): 113−124.
105. Shuai C, Li P, Liu J, *et al.*, 2013, Optimization of TCP/HAP ratio for better properties of calcium phosphate scaffold via selective laser sintering. *Materials Characterization*, vol.77: 23–31.
http://dx.doi.org/10.1016/j.matchar.2012.12.009
106. Lin C Y, Wirtz T, LaMarca F, *et al.*, 2007, Structural and mechanical evaluation of a topology optimized titanium interbody fusion cage fabricated by selective laser melting process. *Journal of Biomedical Material Research*, vol.83A(2): 272–279.
http://dx.doi.org/10.1002/jbm.a.31231

RESEARCH ARTICLE

Utilising inkjet printed paraffin wax for cell patterning applications

Christopher Chi Wai Tse[1*], Shea Shin Ng[1], Jonathan Stringer[3], Sheila MacNeil[4], John W. Haycock[5] and Patrick J. Smith[2]

[1] Additive Manufacturing Centre, University of Sheffield, Western Bank, Sheffield, South Yorkshire S10 2TN, UK
[2] Department of Mechanical Engineering, University of Sheffield, Western Bank, Sheffield, South Yorkshire S10 2TN, UK
[3] Composite Systems Innovation Centre, PDRA (Inkjet Printing), University of Sheffield, Western Bank, Sheffield, South Yorkshire S10 2TN, UK
[4] Faculty of Engineering, University of Sheffield, Western Bank, Sheffield, South Yorkshire S10 2TN, UK
[5] Centre for Biomaterials and Tissue Engineering, University of Sheffield, Western Bank, Sheffield, South Yorkshire S10 2TN, UK

Abstract: We describe a method to prepare patterned environments for eukaryotic cells by inkjet printing paraffin wax onto a substrate. This technique bypasses the requirement to create a master mould, typically required with the use of polydimethylsiloxane techniques and the printed structure could be immediately used to guide cell proliferation. In a space of 2–3 hours, the desired pattern could be created with computer assisted design, printed and have cells seeded onto the scaffold, which could reduce the cycle time of prototyping micropattern designs. Human dermal fibroblasts and RN22 Schwann cells were seen to proliferate within the fabricated patterns and survive for more than 7 days. Additionally, the wax constructs could be readily removed from the substrate at any stage after cell seeding with the cells continuing to proliferate. Thus, we report on a simple but novel approach for the controlled physical positioning of live cells by wax inkjet printing.

Keywords: cell patterning, bioprinting, paraffin wax

*Correspondence to: Christopher Chi Wai Tse, Additive Manufacturing Centre, University of Sheffield, Western Bank, Sheffield, South Yorkshire S10 2TN, UK; Email: mtp11cct@sheffield.ac.uk

Received: August 18, 2015; **Accepted:** October 14, 2015; **Published Online:** October 30, 2015

Citation: Tse C W C, Ng S S, Stringer J, *et al*. 2016, Utilising inkjet printed paraffin wax for cell patterning applications. *International Journal of Bioprinting*, vol.2(1): 35–44. http://dx.doi.org/10.18063/IJB.2016.01.001.

1. Introduction

Research into cell patterning and spatial coordination are growing fields, as new technologies enable researchers to accurately position populations of cells and promote the design of better biological systems[1,2]. Geometry and topology are important factors that affect anchorage-dependent cells[3–5], as living cells actively investigate their surroundings, which can influence function and morphology[6]. Cell behaviour can be better elucidated if there was a technique that allowed the rapid creation of appropriate environments to better understand the dynamic mechanism that affects cell architecture, polarity, morphology, survival and division within their surrounding environments[3,7,8]. With much interdisciplinary use of mechanical techniques being applied in the further study of tissue engineering, much has been learnt recently about cell behaviour in a microenvironment and the creation of microstructures,

that are essential in the understanding of fabricating microdevices to control cell-substrate interactions[9–12]. The importance of such research was highlighted in a special themed issue of *Soft Matter* in 2014 on cells in patterned environments[13]. Being able to control the deposition and location of cells onto a surface allows the creation of scaffolds suitable for tissue engineering, biosensors, the formation of neuronal networks, cell-based assays and for the study of cell-cell interactions.

The current "gold standard" for preparing patterned environments for cells uses PDMS (polydimethylsiloxane) during the construction of lab-on-a-chip devices and micropatterning[14]. With the ability to modify mechanical, optical and chemical properties, patterning on glass[15] or silicon[16], PDMS is a versatile material. An essential requirement when using PDMS is the creation of a master mould, into which PDMS can be poured, cured and removed to create the desired construct. There has been research in reducing and making the process easier, as the pattern design can be created on the master mould through soft-lithography, or through etching into silicon. The photomask can be created using high resolution printers[15] or photo-plotters[17], but a clean room environment is required for fabrication. Solid object printers have been used to create the initial patterns for the master mould[18], with resolutions of >250 µm. Other techniques have also been investigated by researchers, which deposit a cell attractive or repelling agent onto a substrate, with cells thereafter physically restrained to grow within the confines[19,20]. Such approaches, however, do not allow the user to remove such a physical confine at a later time.

The use of PDMS is advantageous if several copies of the master pattern are required. However, when the user requires a large range of variances in their design during prototyping, a typical need exists to create tens, or even hundreds of master moulds. In contrast, the direct patterning of a design using wax printed on a substrate bypasses the conventional process of using PDMS. Potential applications of our proposed method are found in the field of simulation studies and optimising microdevice prototypes[6,21].

Using inkjet printing to produce patterned environments offers fewer limitations compared to previously mentioned techniques that use UV exposure, photomasks and organic and toxic solvents, and require long processing times, complicated machinery, etching and multiple steps. Avoiding these drawbacks would aid in the fabrication of microfluidic devices in research and industry settings, as the turnaround times inherent in these techniques can be reduced, from around 24 hours (with the majority of this time being used for mould preparation), to hours.

With respect to inkjet printing for cell guidance, this typically involves depositing a biologically active molecule such as fibronectin, collagen and/or polymers, to selectively adhere cells at specific places on a substrate[21,22]. The use of wax for the creation of microfluidic devices has been used to create paper and glass-based devices as a simple and inexpensive method using commercially available materials[23–25]. This ability to create biosensors has been investigated to an extent with inkjet printing technology[26–29].

In this paper we have described for first time inkjet printing paraffin wax on tissue culture plastic and on a plain glass substrate and these formed structures were then used to guide cell attachment, spreading and proliferation, without further processing steps. Previous research using paraffin wax for the creation of microfluidic devices described wax deposition integrated with paper, film or combined with PDMS stamping[30–33]. The current approach for cell patterning involves creating the desired pattern by CAD software (Figure 1A), bypassing the need to create a master mould or use of PDMS, and thereafter the immediate seeding of cells after fabrication (Figure 1B). The inkjet printing system was able to move through three

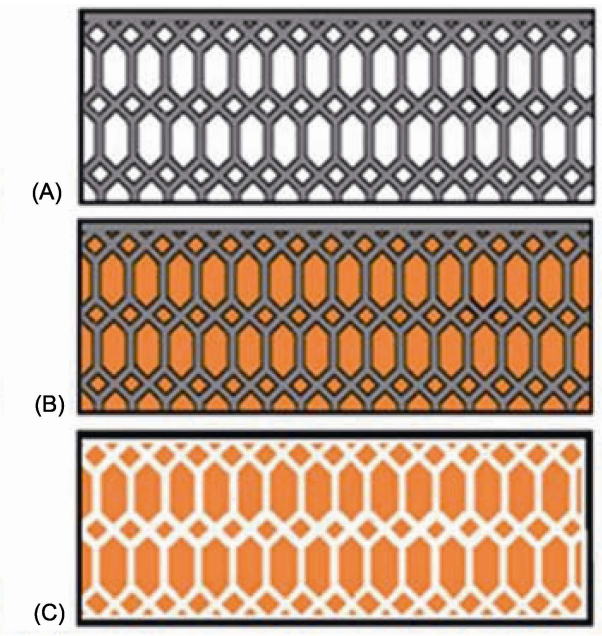

Figure 1. (A) Wax was printed in the desired micrometre scale shape on a substrate; **(B)** cells were seeded onto the substrate and left to attach, spread and proliferate; **(C)** when required, the wax could be physically removed, to leave the cells *in situ*.

axes (*x*,*y*,*z*) and was therefore not limited to 2D design structures. 3D and topologically irregular surfaces could be printed. At any point during the experiment, the wax could be removed to allow cells to freely migrate on the substrate, permitting the further study of cell behaviour (Figure 1C).

2. Materials and Methods

2.1 Inkjet Printing System

A single nozzle piezoelectric inkjet device (MicroFab, Texas, USA) was used to print paraffin wax. Specifically, a Jetlab4 xl-A table top printing platform with position accuracy and repeatability of 25 µm and 5 µm respectively, with a 50 µm orifice diameter (PH-04a Polymer Jet™) high-temperature, drop-on-demand printhead, was used. This was a drop-on-demand printhead that was connected together to the cartridge reservoir through an integrated filter. It allows print-on-the-fly and point-to-point printing, through vector and raster printing modes.

Such a system had a 30 mL stainless steel reservoir and the system could heat up to 240°C. A CT-PT4 four-channel pressure controller was used, made by Microfab to maintain a slight negative pressure within the system to control the creation of the correct nozzle meniscus level for optimal jetting. The print head was made of a glass capillary tapered to the stated orifice size and encased in a metal body surrounded by a piezoelectric actuator. JetDrive III software was used to drive the electronics to control the generation of a waveform to provide complex drive waveforms to tailor the jetting parameters of the print heads. Prior to jetting, all the tubings, reservoirs and the print head were flushed with 1% Micro-90 cleaning solution and distilled de-ionised water.

2.2 RN22 Schwann Cells and Dermal Fibroblasts

Rat RN22 Schwann cells were purchased from the European Collection of Cell Cultures (ECACC) (Public Health England, Porton Down, Salisbury, UK). Human dermal fibroblasts were obtained from abdominoplasty or breast reduction operations according to local ethically approved guidelines (under an HTA Research Tissue Bank license number 12179). All cell types were cultured independently and grown in Dulbecco's Modified Eagle Medium (DMEM) containing 10% (v/v) fetal calf serum (FCS), 1% (v/v) glutamine, 1% (v/v) penicillin/streptomycin, and 0.5% amphotericin B (under serum-free conditions) in a humidified atmosphere with 5% CO_2 at 37°C. Prior to seeding, cells were grown to near confluence, and detached with 0.05% trypsin/EDTA (GIBCO, Invitrogen, Karlsruhe, Germany). A Neubauer chamber was used to count the cells. Passages 20 to 22 were used for RN22 Schwann cells and dermal fibroblasts respectively.

2.3 Paraffin Wax

Paraffin wax was placed inside the cartridge reservoir and the printing system was heated up to 75°C for printing, while the printing platform was heated to 30°C to improve the topography of the printed structures. Wax viscosity was measured with a rheometer (AR 2000, TA Instruments) at different temperatures (Figure 2). When the temperature reached above 60°C, the viscosity was less than 10 mPa·s (10 centipoise). Specification guidelines from Microfab stated that inks should have a viscosity below 20 mPa·s (20 centipoise) for successful droplet formation during inkjet printing. At the temperature of printing (75°C) the viscosity was 6.02 mPa·s (6 centipoise), which was within optimal printing limits.

2.4 Wax Patterning

Using a combination of Microsoft Paint and MS Windows-based computer aided design software environment (Jetlab4, Microfab), varying shapes and designs of wax structures were created with varying channel widths and complexity onto tissue culture plastic and glass substrates. Inkjet printing parameters were optimised to create a single wax droplet per ejection, with droplet spacing of 40 µm between each droplet to create an impermeable scaffold block of wax. The volume of wax that was ejected from the piezoelectric print head could be manipulated through the fine tuning of its printing parameters, such as the

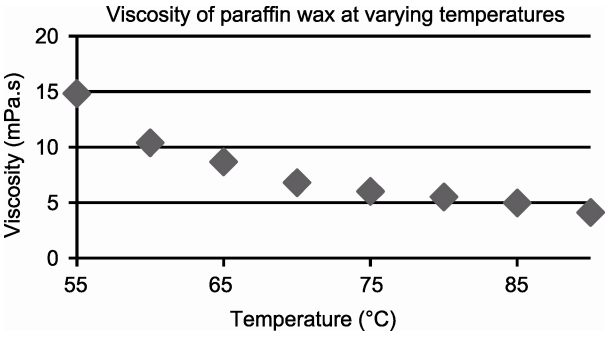

Figure 2. Viscosity values of paraffin wax over a range of temperatures, which was Newtonian when molten. Printing parameters below 20 mPa·s are optimal for printing.

voltage, rise and echo time, which alters the size and velocity of the wax droplet to create optimum conditions to print on varying surfaces and resolutions. When required during the study, the wax was removed by physical lifting with a scalpel.

2.5 Cell Seeding

After the wax template had been printed onto the substrate (tissue culture plastic or glass substrates), the sample was placed in a petri dish and cells were seeded at 2×10^4 cells per sample in 1 mL, and left in the incubator for 60 minutes. After this time, the sample was supplemented with 10 mL cell medium to cover the entire substrate, and left to proliferate for up to 7 days and wax removal when necessary, during which images were captured to record cell growth along the substrate with and without the patterned wax.

2.6 Analysis of Samples

Images were obtained using an inverted Olympus CK40 phase contrast microscope. Images were captured of samples prior to cell seeding, after cell seeding and after wax removal through physical lift off with a sharp scalpel.

2.7 Image Processing

All image processing was performed with ImageJ (U.S. National Institutes of Health). The orientation field was obtained using the ImageJ plugin, OrientationJ. The colour survey was set with the following settings — Hue: Orientation, Saturation: Coherency, Brightness: Original-Image. With this, it was possible to better visualise the orientation of cells along the patterned substrate, with and without the wax template over time.

2.8 Confocal Fluorescence Microscopy

For confocal fluorescence imaging, RN22 Schwann cells and dermal fibroblasts were seeded on the scaffolds at 2×10^4 cells per sample, stained with phalloidin-fluorescein isothiocyanate (FITC) for F-actin filaments and 4',6-diamidino-2-phenylindole dihydrochloride (DAPI) for nuclear staining.

Samples were fixed with 3.7% formaldehyde in PBS for 30 minutes at room temperature and permeabilised with 0.1% (v/v) Triton X-100 in PBS for 30 minutes. Phalloidin:FITC was added at 1:1000 in PBS in combination with DAPI at 1:1000 (300 nM) for 30 minutes, washed and stored in PBS at 4°C until imaging. Cells were washed with PBS (×3) for 5 minutes between each step.

A confocal scanning microscope (Carl Zeiss LSM-510-META, Germany) with magnification ×10 and ×40 long-range water-dipping lenses were used. FITC channel (λ_{ex} = 485 nm; λ_{em} = 520 nm). DAPI (λ_{ex} 400 nm; λ_{em} = 460 nm). Image acquisition and analysis were carried out with Carl Zeiss Laser Scanning Systems LSM 510 software.

3. Results and Discussion

3.1 Inkjet Printing of Wax Guides

A variety of designs were created that were suitable for isolating and connecting islands of cells on substrates (Figure 3A–C). Under high magnification, as exemplified in Figure 3A single wax rows of droplets appeared to have a slightly uneven topography due to scalloping behaviour. The final shape and surface texture of the resultant printed structure was dependent on conditions that include the wettability of the substrate and its temperature, print head temperature, gap distance from the print head to the substrate and droplet material[34–36]. The scalloping behaviour was due to the droplets being cooled quicker than optimal during jetted flight, after landing on the substrate, merging with the previous deposited droplet and partially retained their individual rounded contact lines[37]. Printing wax allowed the creation of a range of different complexities and channel widths that allowed the creation of thick impermeable blocks, to channels as small as 30 µm. The smallest dimensions that can be created with the wax struts is a single line of inkjet printed paraffin wax. Using a 50 µm diameter printhead nozzle, wax lines with a minimum width of 50 µm could be created to act as a barrier between each compartment.

3.2 Cell Seeding

Human dermal fibroblasts and RN22 rat Schwann cells were seeded and imaged to show cell compartmentalisation and connection within the wax structures. Figure 4A and B show images taken after 24 hours of cell culture with fibroblasts and Schwann cells on a glass substrate, respectively. Figure 4C and D show cells that have proliferated after 5 days, where the cells were able to grow in a wax-containing environment on tissue culture plastic. No cells were observed growing across and over the wax structures, showing how this technique was effective at impeding the cell interactions between individual compartments and creating separate environments for collections of

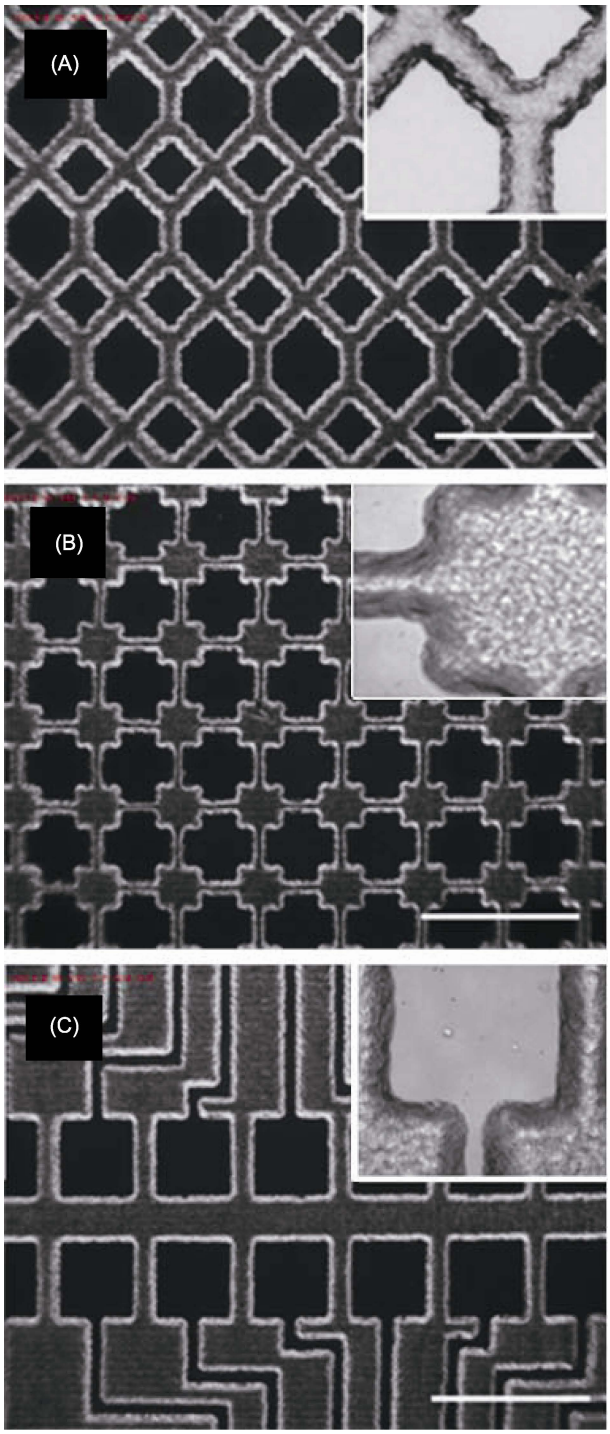

Figure 3. Micrographs of printed wax on glass. **(A–C)** show different patterns that were produced. Magnified light microscopy images are shown in the small frame. Bar = 200 µm.

cells to grow.

With isolated arrays, cells proliferated in random shapes with no obvious direction (Figure 4A and B), but when a linear patterned structure was created, cells aligned in the direction of the structure (Figure 4C and D). Figure 5 show cells aligning to the same orientation as the channel, and through the use of ImageJ software, the orientation of cells could be clearly observed following the direction of the channel. Cell alignment could be investigated with this methodology as in the research reported by Duclos *et al.*[8], who described how NIH-3T3 mouse embryo fibroblasts aligned on confined strips from 30 µm to 1.5 mm.

After fibroblasts or Schwann cells were seeded, they adhered, had spread and thereafter proliferated into the desired positions and orientation. The wax structures were easily removed from the samples with a sharp scalpel, which was used to physically peel the wax off, to leave the cells to grow without any space limitations. Figure 6 shows images of the fabricated wax structures, patterned cells before and after wax removal. Cells maintained their position and orientation for at least 7 days after seeding as shown.

3.3 Cell Proliferation After Removal of Wax

A wax scaffold with channel widths of 40 µm and 30 µm connected together at one end were created and fibroblasts were seeded into the structure and cultured. After 2 days of culture and prior to wax removal, fibroblasts had aligned within the shape of the open channels (Figure 7A). Upon wax removal, cells were not limited to the channel space (Figure 7B) and had spread to cover the substrate, which was observed 24 to 48 hours after wax removal (Figure 7C and D). The wax printing technique could therefore be used initially to deposit cells in the desired areas spatially. The ability of the wax to be removed from the substrate, without the addition of new substances into the environment, allowed for a new method to analyse cell migration and proliferation on open substrates to be studied over time. We observed a high level of alignment to the direction of channels with diameters of less than 160 µm, and consequently the authors of this paper suggest that this work would have immediate applications in cell migration and "scratch assay" type studies, commonly used in wound healing and cancer cell migration research.

Cells were able to remain attached onto the substrate even after wax removal. An exception to this occurred when cell concentration exceeded confluence. From this study, when cell density began to reach confluency (typically more than 300 cells/mm^2) an increased proportion of cells detached. All cells within the scaffold were removed when cell density reached above 700 cells/mm^2. It was postulated that this was

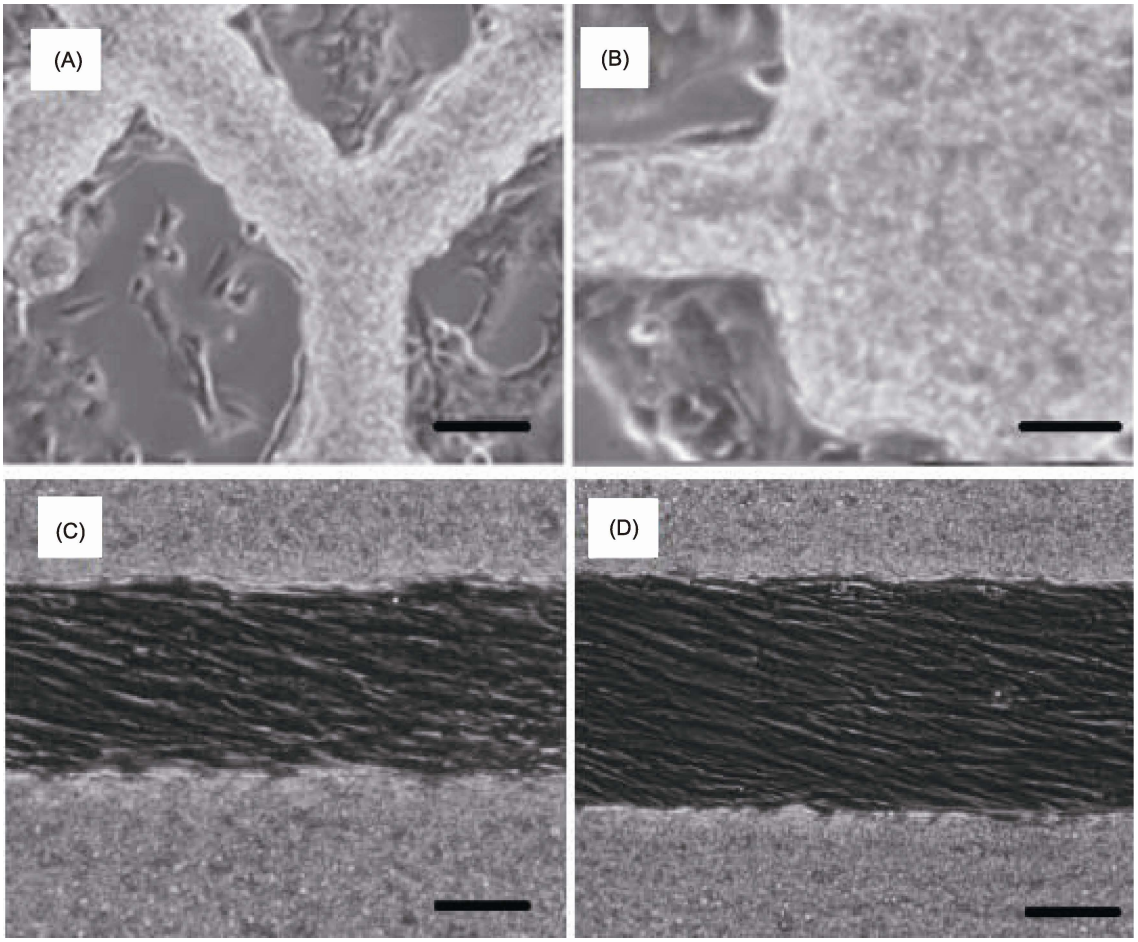

Figure 4. Micrographs of **(A)** fibroblasts after 24 hours on glass substrate, **(B)** RN22 Schwann cells after 24 hours on glass, **(C)** fibroblasts after 5 days cultured on tissue culture plastic, **(D)** RN22 Schwann cells after 5 days cultured on tissue culture plastic, with inkjet printed wax scaffolds. Bars = 50 μm, 40 μm, 100 μm and 100 μm respectively.

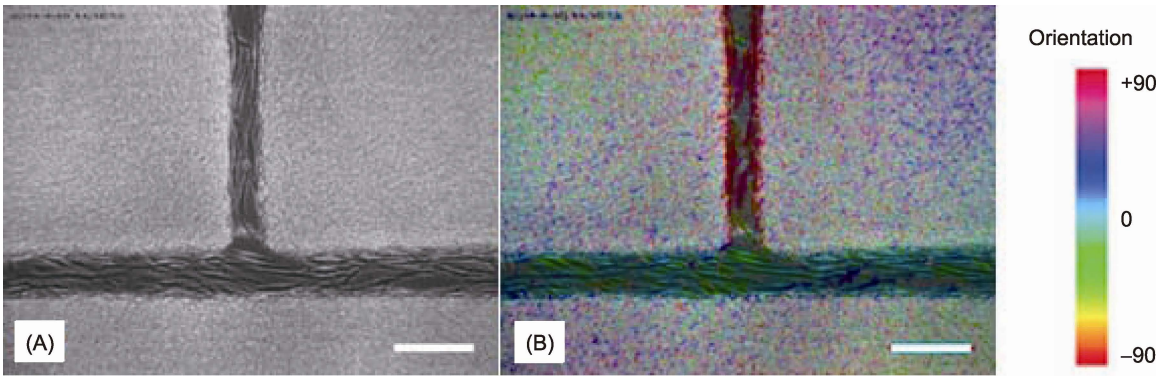

Figure 5. Micrographs showing **(A)** a wax pattern on glass where fibroblasts are proliferating and orientating along the channel after 2 days in culture and **(B)** the same picture after processing with OrientationJ to highlight the alignment of cells within the channel. Channel widths are 40 μm and 60 μm and bar = 100 μm.

caused by adhered cells depositing a proportionate amount of extracellular matrix along their local environment, which had spread over time and was able to bind onto the substrate, wax and cells. When there was a high concentration of cells, the volume of extracellular matrix that was produced was enough to create a sheet on which the cells grew on, and allowed the cells to be peeled off along with the wax when the

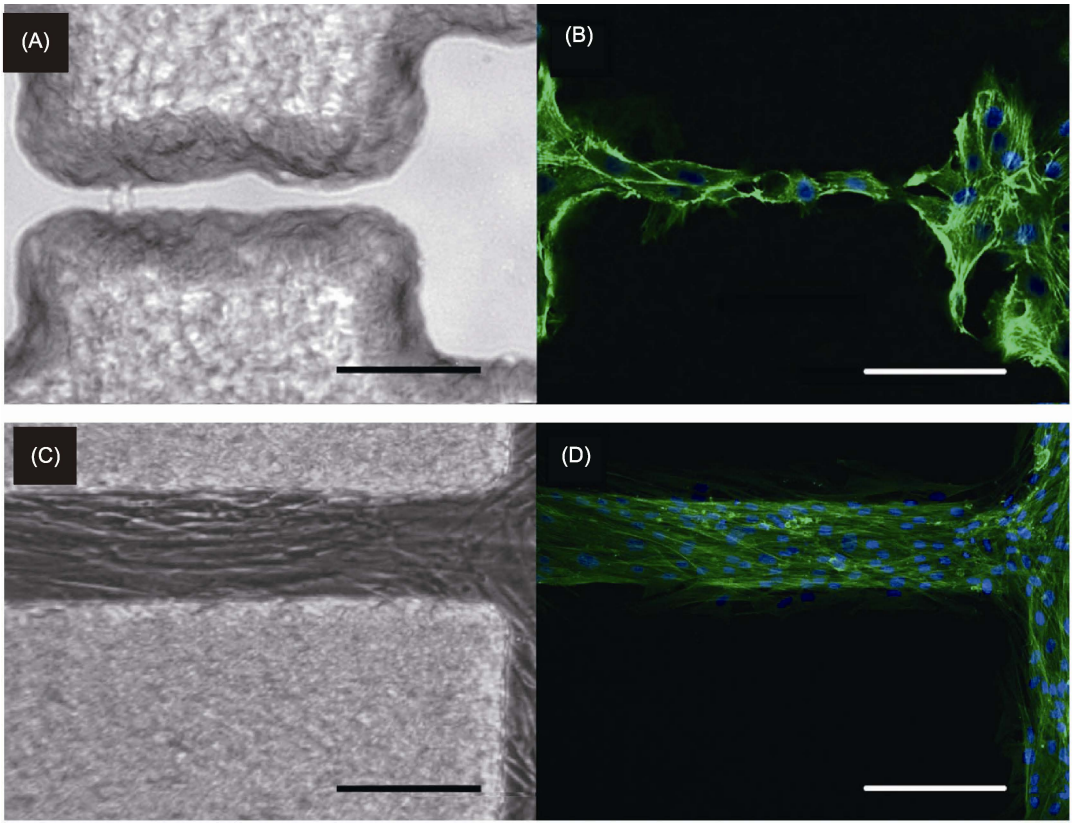

Figure 6. Light microscopy and confocal micrograph images that showed Schwann cells proliferated and aligned between two compartments through an open channel; **(A)** printed paraffin wax on glass; **(B)** confocal image immediately after wax removal, after 2 days of Schwann cells cultured on wax structures, stained for actin (green; phalloidin-FITC) and nuclei (blue; DAPI); **(C)** Schwann cells proliferated and remained within the confines of the wax structures, with the channel width that spanned several cell widths; **(D)** confocal image of Schwann cells immediately after wax removal, after 7 days of culture, cells were seen firmly adhered and aligned with the orientation of the channel stained for actin (green; phalloidin-FITC) and nuclei (blue; DAPI). Channel widths averaged 30 µm (i.e.， the confines of the wax). Bars = 100 µm, 100 µm, 200 µm, 200 µm respectively.

wax was lifted off. This could be considered a limitation of this study; as the extracellular matrix deposited caused the cells to adhere on the wax.

4. Conclusion

A new method of creating cell guided structures through the use of paraffin wax deposited by inkjet printing has been presented. Channel widths of 30 µm and wax widths of 50 µm could be produced. RN22 Schwann and dermal fibroblast cells were seen to proliferate for over 7 days as exemplars, with and without wax present, on tissue culture plastic and glass substrates. The design of the wax pattern could be easily changed and directly patterned onto a substrate through CAD, without multiple processes or use of lithography techniques to create a master mould, which is advantageous when experimental procedures require slight variances in each microdevice design to be fabricated. Such examples include optimising the channel width, length, height and complexity of a prototype lab-on-a-chip for cell study. Compared to other cell guidance techniques, this technique does not require the use of harsh chemical treatments, long procedures to create the desired structures, is low cost and easy to fabricate. During cell seeding, the wax scaffold can be removed at any point, so that users can study the behaviour of cells that are allowed to proliferate freely on the substrate. Limitations can arise with this technique when studies involve lifting the wax off when growing cultures to confluence; due to the deposition of extracellular matrix from adhered cells that glue the constituents of the surrounding environment together. More cells are lifted off with increasing cell density and narrower wax channels. A smooth substrate was used in our studies; however the inkjet printing platform was able to move through three axes (*x*, *y*, *z*) and therefore is not limited to 2D design structures. Non-flat surfaces can also be printed on, along with topologically

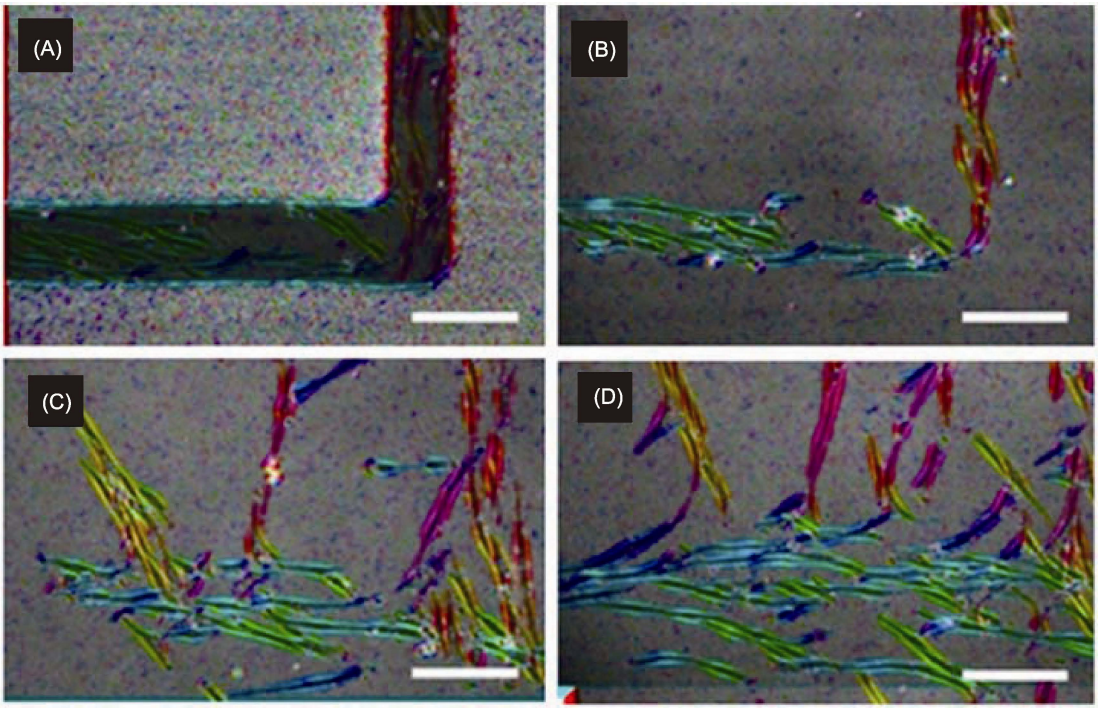

Figure 7. Micrographs showing **(A)** fibroblasts aligning within wax structures on glass, after 2 days of cell culture on wax structures, **(B)** immediately after wax removal, **(C)** 24 hours and **(D)** 48 hours after wax removal taken in the same sample region of interest. Each image was processed with OrientationJ to highlight the alignment of cells within the channel. Bar = 50 µm.

irregular surfaces as a substrate.

Future research will involve the application of patterned environments with co-culture of cells. Organised formations of cell constructs can be created which would be of benefit to fields such as neuronal research. Nerve cells could be patterned onto a sample within an organised wax structure, and once the nerve cells have adhered and the wax has been removed, support cells can be seeded on the sample to create a patterned co-culture environment.

Conflict of Interest and Funding

No conflict of interest was reported by the authors.

References

1. Théry M, 2010, Micropatterning as a tool to decipher cell morphogenesis and functions. *Journal of Cell Science*, vol.123: 4201–4213. http://dx.doi.org/10.1242/jcs.075150
2. Kumar S and LeDuc P R, 2009, Dissecting the molecular basis of the mechanics of living cells. *Experimental Mechanics*, vol.49(1): 11–23. http://dx.doi.org/10.1007/s11340-007-9063-7
3. Chen C S, Mrksich M, Huang S, *et al*., 1997, Geometric control of cell life and death. *Science*, vol.276: 1425–1428. http://dx.doi.org/10.1126/science.276.5317.1425
4. Dike L E, Chen C S, Mrksich M, *et al*., 1999, Geometric control of switching between growth, apoptosis, and differentiation during angiogenesis using micropatterned substrates. *In Vitro Cellular & Developmental Biology-Animal*, vol.35(8): 441–448. http://dx.doi.org/10.1007/s11626-999-0050-4
5. McBeath R, Pirone D M, Nelson C M, *et al*., 2004, Cell shape, cytoskeletal tension, and RhoA regulate stem cell lineage commitment. *Developmental Cell*, vol.6(4): 483–495. http://dx.doi.org/10.1016/S1534-5807(04)00075-9
6. Banerjee S, Sknepnek R and Marchetti M C, 2014, Optimal shapes and stresses of adherent cells on patterned substrates. *Soft Matter*, vol.10(14): 2424–2430. http://dx.doi.org/10.1039/c3sm52647j
7. Geiger B, Spatz J P and Bershadsky A D, 2009, Environmental sensing through focal adhesions. *Nature Reviews Molecular Cell Biology*, vol.10: 21–33. http://dx.doi.org/10.1038/nrm2593
8. Duclos G, Garcia S, Yevick H G, *et al*., 2014, Perfect nematic order in confined monolayers of spindle-shaped cells. *Soft Matter*, vol.10(14): 2346–2353. http://dx.doi.org/10.1039/c3sm52323c
9. Alvarado J, Mulder B M and Koenderink G H, 2014, Alignment of nematic and bundled semiflexible poly-

mers in cell-sized confinement. *Soft Matter*, vol.10(14): 2354–2364.
http://dx.doi.org/10.1039/c3sm52421c

10. Tomba C, Braïni C, Wu B, *et al.*, 2014, Tuning the adhesive geometry of neurons: length and polarity control. *Soft Matter*, vol.10(14): 2381–2387.
http://dx.doi.org/10.1039/c3sm52342j
11. Röttgermann P J F, Alberola A P and Rädler J O, 2014, Cellular self-organization on micro-structured surfaces. *Soft Matter*, vol.10(14): 2397–2404.
http://dx.doi.org/10.1039/c3sm52419a
12. Hampe N, Jonas T, Wolters B, *et al.*, 2014, Defined 2-D microtissues on soft elastomeric silicone rubber using lift-off epoxy-membranes for biomechanical analyses. *Soft Matter*, vol.10(14): 2431–2443.
http://dx.doi.org/10.1039/c3sm53123f
13. Schwarz U S, Nelson C M and Silberzan P, 2014, Proteins, cells, and tissues in patterned environments. *Soft Matter*, vol.10(14): 2337–2340.
http://dx.doi.org/10.1039/c4sm90028f
14. Fujii T, 2002, PDMS-based microfluidic devices for biomedical applications. *Microelectronic Engineering*, vol.61–62: 907–914.
http://dx.doi.org/10.1016/S0167-9317(02)00494-X
15. Duffy D C, McDonald J C, Schueller O J A, *et al.*, 1998, Rapid prototyping of microfluidic systems in poly(dimethylsiloxane). *Analytical Chemistry*, vol.70(23): 4974–4984.
http://dx.doi.org/10.1021/ac980656z
16. Liu J, Enzelberger M and Quake S, 2002, A nanoliter rotary device for polymerase chain reaction. *Electrophoresis*, vol.23: 1531–1536.
http://dx.doi.org/10.1002/1522-2683(200205)23:10<1531::AID-ELPS1531>3.0.CO;2-D
17. Linder V, Wu H, Jiang X, *et al.*, 2003, Rapid prototyping of 2D structures with feature sizes larger than 8 μm. *Analytical Chemistry*, vol.75(10): 2522–2527.
http://dx.doi.org/10.1021/ac026441d
18. McDonald J C, Chabinyc M L, Metallo S J, *et al.*, 2002, Prototyping of microfluidic devices in poly(dimethylsiloxane) using solid-object printing. *Analytical Chemistry*, vol.74(7): 1537–1545.
http://dx.doi.org/10.1021/ac010938q
19. Love J C, Wolfe D B, Jacobs H O, *et al.*, 2001, Microscope projection photolithography for rapid prototyping of masters with micron-scale features for use in soft lithography. *Langmuir*, vol.17(19): 6005–6012.
http://dx.doi.org/10.1021/la010655t
20. Kwon K W, Choi J C, Suh K Y, *et al.*, 2011, Multiscale fabrication of multiple proteins and topographical structures by combining capillary force lithography and microscope projection photolithography. *Langmuir*, vol.27(7): 3238–3243.
http://dx.doi.org/10.1021/la2000156
21. Müller A, Meyer J, Paumer T, *et al.*, 2014, Cytoskeletal transition in patterned cells correlates with interfacial energy model. *Soft Matter*, vol.10(14): 2444–2452.
http://dx.doi.org/10.1039/c3sm52424h
22. Sanjana N E and Fuller S B, 2004, A fast flexible ink-jet printing method for patterning dissociated neurons in culture. *Journal of Neuroscience Methods*, vol.136(2): 151–163.
http://dx.doi.org/10.1016/j.jneumeth.2004.01.011
23. Lu Y, Shi W, Jiang L, *et al.*, 2009, Rapid prototyping of paper-based microfluidics with wax for low-cost, portable bioassay. *Electrophoresis*, vol.30(9): 1497–1500.
http://dx.doi.org/10.1002/elps.200800563
24. Carrilho E, Martinez A W and Whitesides G M, 2009, Understanding wax printing: A simple micropatterning process for paper-based microfluidics. *Analytical Chemistry*, vol.81(16): 7091–7095.
http://dx.doi.org/10.1021/ac901071p
25. Renault C, Koehne J, Ricco A J, *et al.*, 2014, Three-dimensional wax patterning of paper fluidic devices. *Langmuir*, vol.30(23): 7030–7036.
http://dx.doi.org/10.1021/la501212b
26. Yun Y H, Lee B K, Choi J S, *et al.*, 2011, A glucose sensor fabricated by piezoelectric inkjet printing of conducting polymers and bienzymes. *Analytical Science*, vol.27(4): 375-379.
http://dx.doi.org/10.2116/analsci.27.375
27. Setti L, Fraleoni-Morgera A, Ballarin B, *et al.*, 2005, An amperometric glucose biosensor prototype fabricated by thermal inkjet printing. *Biosensors and Bioelectronics*, vol.20(10): 2019–2026.
http://dx.doi.org/10.1016/j.bios.2004.09.022
28. Wang T, Cook C and Derby B, 2009, Fabrication of a glucose biosensor by piezoelectric inkjet printing: *Proceedings of the Third International Conference on Sensor Technologies and Applications, 2009 (SENSORCOMM'09)*, 82–85.
http://dx.doi.org/10.1109/SENSORCOMM.2009.20
29. Bietsch A, Zhang J, Hegner M, *et al.*, 2004, Rapid functionalization of cantilever array sensors by inkjet printing. *Nanotechnology*, vol.15(8): 873–880.
http://dx.doi.org/10.1088/0957-4484/15/8/002
30. Selimović Š, Dokmeci M R and Khademhosseini A, 2013, Research highlights. *Lab on a Chip*, vol.13(3): 325–327.
http://dx.doi.org/10.1039/c2lc90145e
31. Kaigala G V, Ho S, Penterman R, *et al.*, 2007, Rapid prototyping of microfluidic devices with a wax printer. *Lab on a Chip*, vol.7(3): 384–387.
http://dx.doi.org/10.1039/b617764f

32. Li Z, Hou L, Zhang W, *et al*., 2014, Preparation of PDMS microfluidic devices based on drop-on-demand generation of wax molds. *Analytical Methods*, vol.6(13): 4716–4722.
http://dx.doi.org/10.1039/c4ay00798k
33. Simon K A, Park K M, Mosadegh B, *et al*., 2014, Polymer-based mesh as supports for multi-layered 3D cell culture and assays. *Biomaterials*, vol.35: 259–268.
http://dx.doi.org/10.1016/j.biomaterials.2013.09.049
34. De Gans B-J and Schubert U S, 2004, Inkjet printing of well-defined polymer dots and arrays. *Langmuir*, vol.20(18): 7789–7793.
http://dx.doi.org/10.1021/la049469o
35. Li R, Ashgriz N, Chandra S, *et al*., 2008, Shape and surface texture of molten droplets deposited on cold surfaces. *Surface and Coatings Technology*, vol.202(16): 3960–3966.
http://dx.doi.org/10.1016/j.surfcoat.2008.02.009
36. Stringer J and Derby B, 2010, Formation and stability of lines produced by inkjet printing. *Langmuir*, vol.26(12): 10365–10372.
http://dx.doi.org/10.1021/la101296e
37. Schiaffino S and Sonin A, 1997, Molten droplet deposition and solidification at low Weber numbers. *Physics of Fluids*, vol.9(11): 3172–3187.
http://dx.doi.org/10.1063/1.869434

RESEARCH ARTICLE

Patterning of tissue spheroids biofabricated from human fibroblasts on the surface of electrospun polyurethane matrix using 3D bioprinter

Elizabeth V. Koudan[1], Elena A. Bulanova[1], Frederico D A S Pereira[1], Vladislav A. Parfenov[1], Vladimir A. Kasyanov[2], Yousef D. Hesuani[1] and Vladimir A. Mironov[1*]

[1] The Laboratory of Biotechnological Research, 3D Bioprinting Solutions, Kashirskoe Roadway, 68/2, Moscow, Russian Federation

[2] Riga Stradins University and Riga Technical University, Riga, LV-1007, Latvia

Abstract: Organ printing is a computer-aided additive biofabrication of functional three-dimensional human tissue and organ constructs according to digital model using the tissue spheroids as building blocks. The fundamental biological principle of organ printing technology is a phenomenon of tissue fusion. Closely placed tissue spheroids undergo tissue fusion driven by surface tension forces. In order to ensure tissue fusion in the course of post-printing, tissue spheroids must be placed and maintained close to each other. We report here that tissue spheroids biofabricated from primary human fibroblasts could be placed and maintained on the surface of biocompatible electrospun polyurethane matrix using 3D bioprinter according to desirable pattern. The patterned tissue spheroids attach to polyurethane matrix during several hours and became completely spread during several days. Tissue constructions biofabricated by spreading of patterned tissue spheroids on the biocompatible electrospun polyurethane matrix is a novel technological platform for 3D bioprinting of human tissue and organs.

Keywords: tissue spheroids, electrospinning, polyurethane, 3D bioprinting, human fibroblasts, bioprinter, tissue fusion, spreading

*Correspondence to: Vladimir A. Mironov, The Laboratory of Biotechnological Research, 3D Bioprinting Solutions, Kashirskoe Roadway, 68/2, Moscow, Russian Federation; Email: vladimir.mironov54@gmail.com

Received: October 26, 2015; **Accepted:** November 27, 2015; **Published Online:** December 17, 2015

Citation: Koudan E V, Bulanova E A, Pereira F D A S, *et al*., 2016, Patterning of tissue spheroids biofabricated from human fibroblasts on the surface of electrospun polyurethane matrix using 3D bioprinter. *International Journal of Bioprinting*, vol.2(1): 45–52. http://dx.doi.org/10.18063/IJB.2016.01.007.

1. Introduction

3D bioprinting is a rapidly evolving area of biomedical research[1,2] aimed by biofabrication of human tissues and organs to solve one of the most important and urgent medical problems — the shortage of human organs for transplantation. There are different variants of emerging 3D bioprinting technology[3–6]. Organ printing is a variant of 3D bioprinting technology which could be defined as a computer-aided robotic additive biofabrication of functional human tissue and organ constructs according to digital model using tissue spheroids as building blocks[7,8]. Tissue spheroids are closely packed aggregates of living cells. The fundamental biomimetic principle of organ printing technology is a phenomenon of tissue fusion which often occurs during embryonic development[9]. Two closely placed tissue spheroids undergo tissue fusion driven by surface tension forces[10]. Thus, to enable post-printed tissue spheroids fusion it

is necessary to keep them close to each other in three-dimensional space. Several different approaches have been developed to enable controllable tissue spheroids fusion, which include placing tissue sphe-roids inside 3D printed synthetic scaffolds[11–13], using bioprintable hydrogel[14,15] and even metallic rods[16]. The search for the effective methods to keep tissue spheroids close to each other during 3D bioprinting continues and one of the possible perspective approaches is an application of nanotechnology. It have been postulated in recent reviews that application of nanotechnology will enable biofabrication of complex human tissues and even organs[17,18]. Fabrication of nano-/microfibrous synthetic scaffolds by electrospinning is one of popular application of nanotechnology in tissue engineering[19,20]. It has been demonstrated that tissue spheroids can attach, spread and fuse on synthetic electrospun matrices[21,22].

Moreover, recently reported magnetic functionalization of electrospun synthetic matrices with magnetic nanoparticles[23] as well as biofabrication of tissue spheroids from cells labelled with magnetic nanoparticles[24–27] allow the development of magnetic forces-driven biofabrication and even 3D magnetic bioprinting based on principles of magnetic levitation[28–30]. Thus, application of nanotechnology can enable development of novel technology of magnetic 3D bioprinting.

We hypothesize that precise placing of tissue spheroids using 3D bioprinter on biocompatible electrospun polyurethane matrix followed by their attachment and spreading will optimize biofabrication of tissue engineered constructions of desirable pattern and thickness and allow the use of electrospun synthetic matrices as carrier for tissue spheroids. Thus, tissue engineered constructions formed by tissue spheroids patterned, attached and spread on the surface of biocompatible electrospun synthetic matrices could be used as a novel technology platform in organ printing. Reported spreading of patterned tissue spheroids could be also used as an *in vitro* assay for testing biocompatibility of various synthetic electrospun biomaterials.

2. Materials and Methods

2.1 Electrospinning

Polyurethane was kindly provided by Dr Xuejun Wen ((EG-85A, Lubrizol, USA). Electrospinning of micro fibrous polyurethane matrix have been performed using commercial apparatus Professional Electrospinning Lab Device (Yflow, Spain). Electrospinning was performed under voltage 17kV; the distance between needle end and collector was 20 cm; speed of polymer movement was 1.3 mL/h; diameter of needle was 0.84 mm. Polyurethane have been dissolved to concentration 17% in solvents containing 40% N,N-dimethylformamide (DMF) and 60% tetrahydrofuran (THF).

2.2 Biomechanical Testing

Tensile tests were performed for electrospun polyurethane material. Rectangular specimens (n = 5) were cut out using a template (two parallel blades). Dimensions of the trimmed specimens were: width — 5 mm; length — 30 mm. The thickness of samples was measured using a cathetometer KLM-4 (Russia). The precision of measurement was 0.001 mm. For tensile test Zwick-Roell BDO-FB0.5TS Test System (Germany) with load cell 50 N connected to PC was used. Samples were deformed with the speed of 5 mm/min until rupture. Maximal (failure) strain and maximal stress were estimated for each sample using TestExpert software Version 11.02 (Germany). The stiffness of the material was assessed as the slope of the first linear range of the stress-strain curve, and was expressed as a tangential modulus of elasticity.

2.3 Normal Human Dermal Fibroblast Cell Culture

Normal human dermal fibroblasts (NHDF) were obtained from Lonza (cat.# CC-2511). NHDF cells were grown in DMEM (Gibco, cat.# 12491-015) containing 10% FBS (Gibco, cat.# 16000-044) supplemented with antibiotic/antimycotic mix (Gibco, cat.# 15240-062), 1 mM L-glutamine (Paneco, cat.# F032). The cells were cultivated at 37ºC in humidified atmosphere with 5% CO_2 and split at 85–95% confluence.

2.4 Biofabrication of Tissue Spheroids

The tissue spheroids were formed using the 3D petri dishes (Microtissues, cat.# 12-81) according to manufacturing protocol. Briefly, the 3D petri dishes were prepared from 2% agarose in PBS. NHDF monolayer cells reached 95% confluence were rinsed by Versen (Paneco, cat.# R080), harvested from the culture flasks by 0.25% trypsin — 0.53 mM EDTA (Gibco, cat.# 25200-114) and then re-suspended in cell culture medium. The concentrations of the NHDF cells were 6.8×10^6 per milliliter. 190 µL of cell suspension was seeded into the 3D petri dishes. After 40 minutes additional culture medium was added. The 3D petri dishes containing the tissue spheroids were incubated 4 days

at 37ºC in a humidified atmosphere with 5% CO_2.. NHDF spheroids were visualized by inverted light microscopy (Eclipse TS100, Nikon, Japan). Spheroid diameters were measured using ImageJ software. Diameter distribution plots were analyzed using GraphPad Prism software (GraphPad Software, Inc., La Jolla, CA). 4 days tissue spheroids have been used for their robotic placing on electrospun polyurethane matrix.

2.5 Patterning of Tissue Spheroids

The suspension of tissue spheroids have been placed according to digital model (linear and hexagonal order) on the surface of electrospun polyurethane matrix using original 3D bioprinter Fabion with conus-like pipets, allowing precision placing of tissue spheroid one by one.

2.6 Kinetics of Tissue Spheroids Spreading

The kinetics of tissue spheroids spreading on electrospinning polyurethane matrix was evaluated by measuring the spheroid's diameter in the course of attaching and spreading. Several experiments were performed. In each experiment the following time points were evaluated: 4 hours, 24 hours, 48 hours, 4 days and 7 days. 15 to 20 spheroids were measured at each time point.

2.7 Morphometric Analysis of Electrospun Microfibers

Morphometric analysis of diameter of electrospun polyurethane filaments have been performed using scanning electron micrographs under large magnification (n =100).

2.8 Estimation of Viability of Tissue Spheroids

Viability of tissue spheroids from human fibroblasts (NHDF) on electrospun matrix was assessed using the CellTiter-Glo 3D Cell Viability Assay kit (Promega, USA). Briefly, identical samples of electrospun matrix were placed into the wells of 24-well plates. 4-days NHDF spheroids were seeded on electrospun matrix or tissue culture-treated plastic (positive control for determination of 100% viability) at a seeding density 8 spheroids/well. At 24 or 72 hours, the CellTiter-Glo 3D reagent was added to each well. Plates were shaken for 5 minutes, incubated at RT for an additional 25 minutes, then supernatants were transferred to 96-well plates and the luminescence was read using VICTOR X3 Multilabel Plate Reader (Perkin Elmer, USA). Tissue spheroids viability data were analyzed using GraphPad Prism software (GraphPad Software, Inc., La Jolla, CA).

2.9 Scanning Electron Microscopy

Electrospun polyurethane matrix was gold-coated using ion coater (IB-3, EIKO, Japan) and the structure of the microfilaments was characterized by scanning electron microscope (SEM) (JSM-6510LV). Samples were observed at 30 kV accelerating voltage. The samples of tissue spheroids on electrospun polyurethane matrix were fixed with 2.5% glutaraldehyde/0.1Mcacodylate buffer, dehydrated through ethanol series and then were dried in a critical point dryer (*HCP-2*, Hitachi Koki Co. Ltd., *Japan*). The samples are mounted on a stub of metal with adhesive, coated with gold using ion coater (IB-3, EIKO, Japan) and then observed under the microscope JSM -6510 LV (JEOL, Japan).

2.10 Statistical Analysis

The statistical analysis was performed using software GraphPad Prism (USA).

3. Results

The microfibrous synthetic matrix composed of thin filaments was fabricated using electrospinning of polyurethane (Figure 1A). Dense 3D network of thin filaments was formed as a result of fusion of adjacent electrospun filaments at their intersection points (Figure 1B). The average diameter of electrospun polyurethane filaments was 3.24 ± 0.144 μm (n = 100).

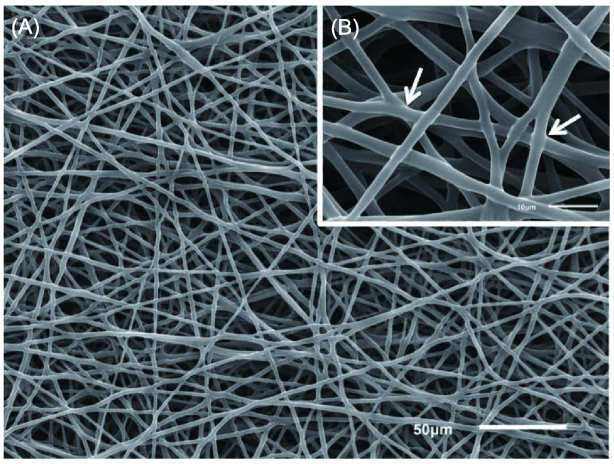

Figure 1. Electrospun polyurethane matrix. **(A)** Dense network of polyurethane matrix formed by electrospun filaments of regular diameter. **(B)** Electrospun polyurethane matrix. Fusion of intersected polyurethane filaments is indicated by arrows. Scanning electron microscopy.

Fusion of filaments with regular diameter leads to the formation of larger diameter filaments. The electrospun polyurethane matrix has typical non-linear stress-strain relationship for synthetic elastic biomaterials (Figure 2). The ultimate stress, ultimate strain and tangential modulus of elasticity were 3.18 ± 0.48 MPa, 200.40 ± 15.74% and 6.66 ± 1.02 MPa, respectively.

Tissue spheroids have been biofabricated using micromolded non-adhesive hydrogel. The suspension of human fibroblasts has been placed into micromolded replica in agarose hydrogel. After overnight incubation, tissue spheroids of standard shape and size have been biofabricated (Figure 3). The redistribution of tissue spheroids diameter is presented at Figure 4. Tissue spheroids have been placed on the electrospun polyurethane matrix using original multifunctional 3D

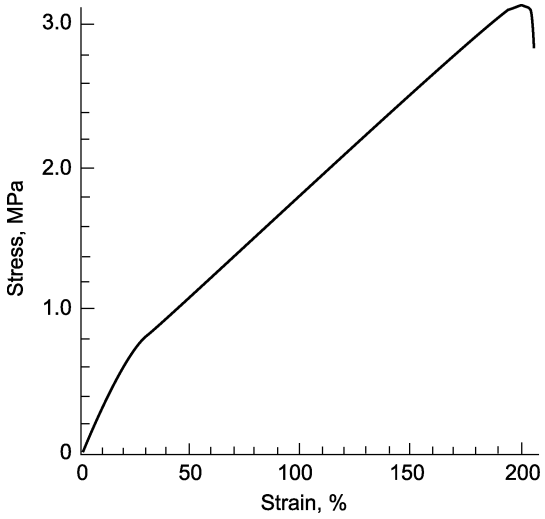

Figure 2. Representative stress-strain curve of the electrospun polyurethane matrix.

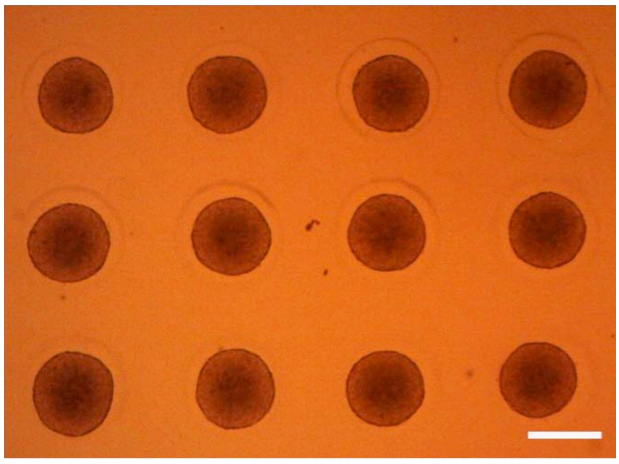

Figure 3. Biofabricated tissue spheroids in micromolded agarose hydrogel. Bar = 200 micrometers.

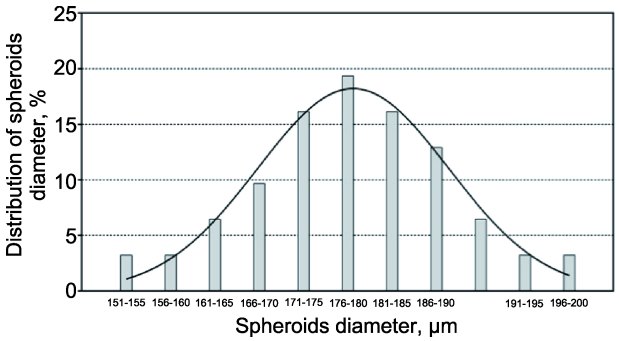

Figure 4. Distribution of diameter of tissue spheroids biofabricated from human fibroblasts using micromolded non-adhesive agarose hydrogel.

bioprinter Fabion (Figure 5). The dispensing of tissue spheroids by conus-like nozzle is documented on Figure 6.

The 3D bioprinter enabled placing and patterning of tissue spheroids in desirable regular patterns according to selected digital model (Figure 7 and 8). The placed tissue spheroids attached to electrospun polyurethane matrix during several hours and became completely spread during several days (Figure 9). The kinetics tissue spheroids spreading was measured and it have been demonstrated that diameter of tissue spheroids increases 8.4-fold during the spreading on electrospun polyurethane matrix (Figure 10). Tissue spheroids demonstrated high viability (95 ± 4.6%).

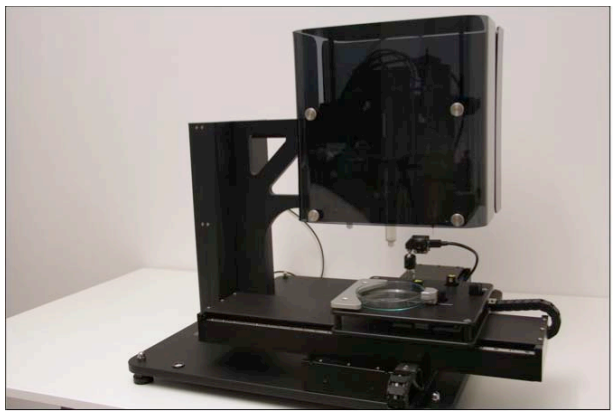

Figure 5. 3D bioprinter Fabion developed by 3D Bioprinting Solutions (Russia) and used for patterning of tissue spheroids on electrospun polyurethane matrix.

4. Discussion

We have demonstrated that tissue spheroids biofabricated from human dermal fibroblasts could be patterned on the surface of electrospun polyurethane using 3D bioprinter. This fact is in good accordance with

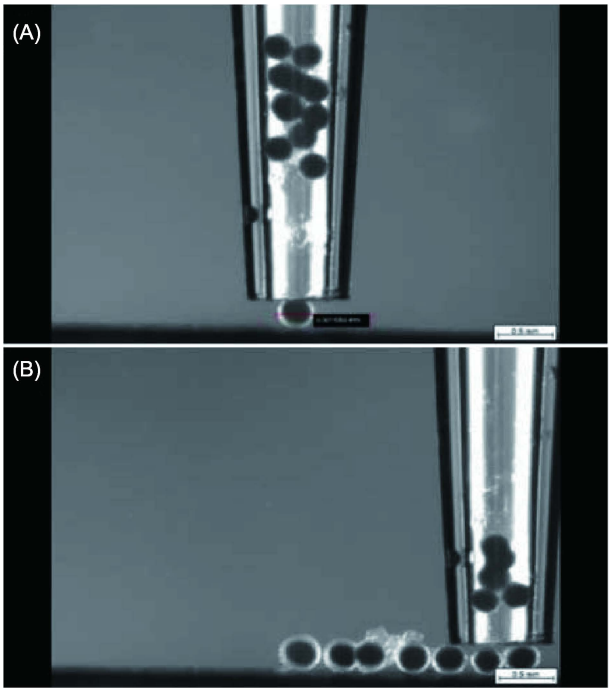

Figure 6. Dispensing of tissue spheroids using 3D bioprinter: **(A)** Beginning of bioprinting, **(B)** Linear pattern of tissue spheroids.

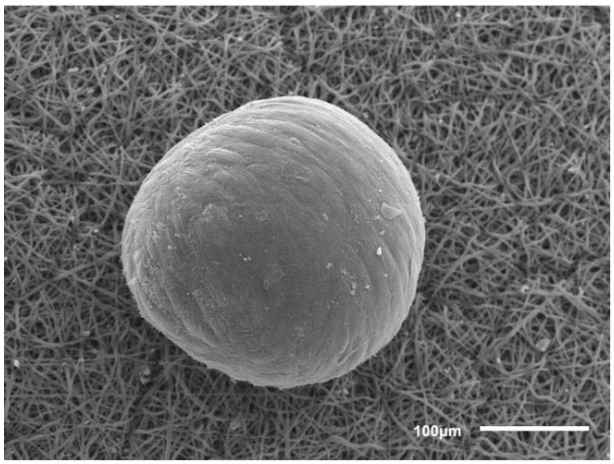

Figure 7. Tissue spheroid on the surface of electrospun polyurethane matrices. Scanning electron microscopy.

previous published reports about attachment, spreading and fusion of tissue spheroids placed manually on electrospun matrices[21,22]. The main advantage in using 3D bioprinter for automated placing of tissue spheroids is a possibility to create regular pattern of their redistribution and, thus, to control the resulted thickness of bioprinted tissue construct. Using this approach the tissue constructs could be rationally designed with desirable thickness (Figure 11). Moreover, in our previous publication we have demonstrated that

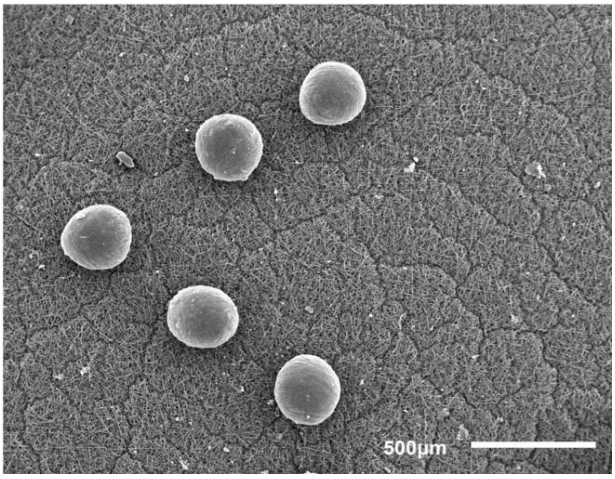

Figure 8. Patterned (regularly placed by 3D bioprinter) tissue spheroids on the surface of electrospun polyurethane matrices. Scanning electron microscopy.

resulted thickness of bioprinted 3D tissue construct including several layers of tissue spheroids could be precisely predicted[31]. The demonstrated rapid attachment and spreading of patterned tissue spheroids on electrospun polyurethane matrix also prove its optimal *in vitro* biocompatibility. In this context quantitative analysis of tissue spheroids attachment and spreading could be used as a novel high throughput *in vitro* assay to test tissue biocompatibility of different electrospun biomaterials. Estimated material properties of electrospun polyurethane could serve as control for future studies of tissue engineered constructs biofabricated on the surface polyurethane matrices. Compared to testing of attachment and spreading of single cells on electrospun matrices, the application of 3D tissue spheroids provides more authentic information about biocompatibility at tissue level because implanted *in vivo* electorspun biomaterials interact with complex 3D connective tissue, not just with single cells. Theoretically, there are three potential outcomes of direct interaction of tissue spheroids with electrospun biomaterials: (i) tissue spheroids can attach and sequentially completely spread as we reported here; (ii) tissue spheroids can only attach but not spread and form so-called tethered spheroids, which already is used in microfluidics toxicity assays[32]; finally, (iii) if electrospun biomaterials are toxic, then spheroids will not attach and will not spread. The cells composing spheroids in case of third theoretical outcome will die as a result of necrosis. Thus, patterned tissue spheroids on novel electrospun biomaterials could be used in toxicology studies. Repeatable patterning of tissue spheroids with 3D bioprinter will enable standardization

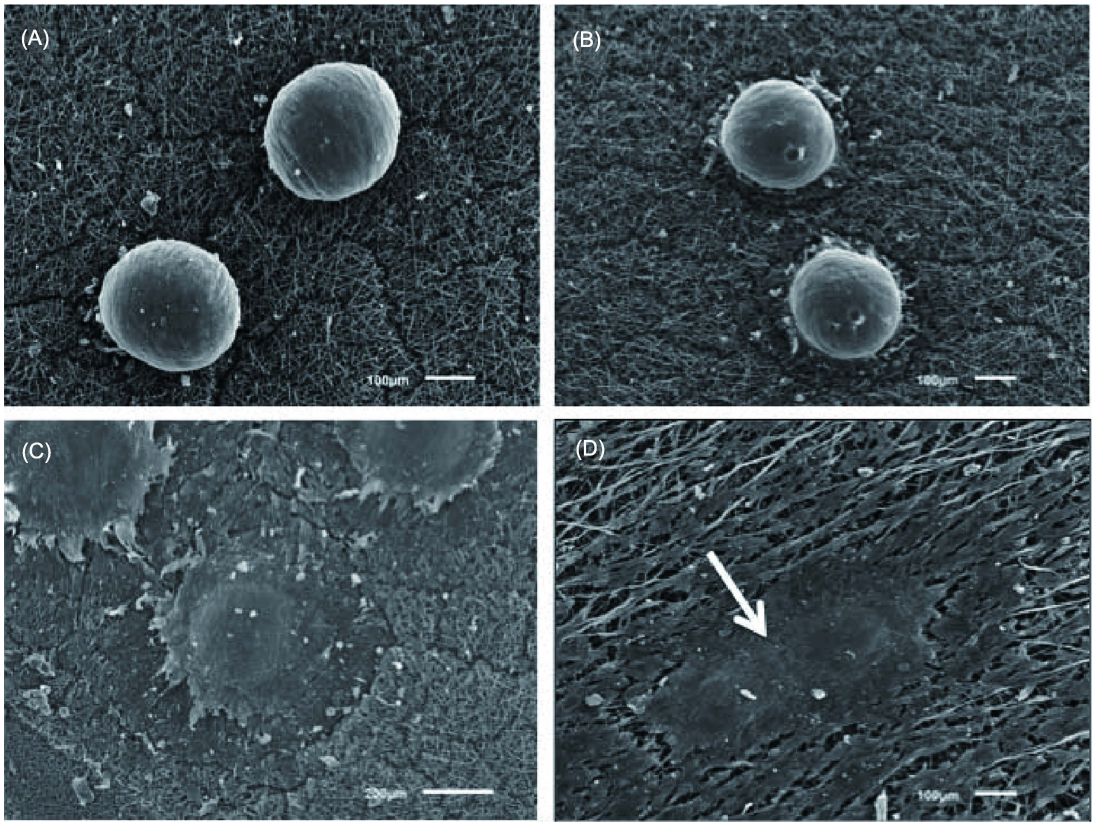

Figure 9. Spreading of tissue spheroids on the surface of electrospun polyurethane matrix: **(A)** 4 hours, scale bar — 100 μm; **(B)** 1 day, scale bar — 100 μm; **(C)** 4 days, scale bar — 200 μm; **(D)** 7 days, white arrow indicates area of tissue fusion of two adjacent spreading tissue spheroids, scale bar — 100 μm. Scanning electron microscopy.

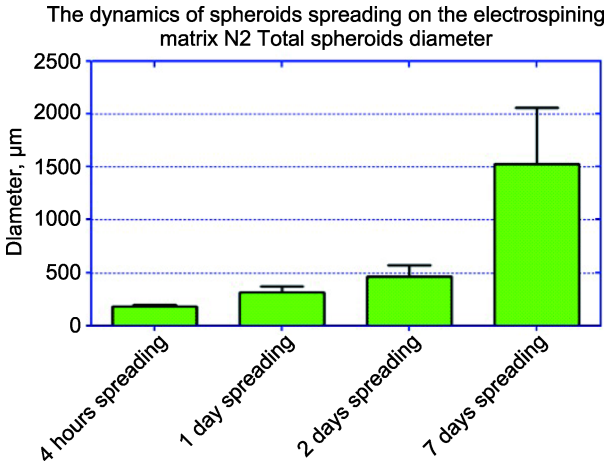

Figure 10. The dynamics of tissue spheroids spreading on the surface of electrospun polyurethane matrix.

of *in vitro* assays.

Another important potential application of patterned tissue spheroids is tissue engineering and biofabrication (Figure 12). Tissue spheroids biofabricated from human fibroblasts spread on electrospun matrices (Figure 12A) could be used for biofabrication of dense connective tissue after decellularization (Figure 12B). Spreading of tissue spheroids from human fibroblast on one side of electrospun polyurethane matrix

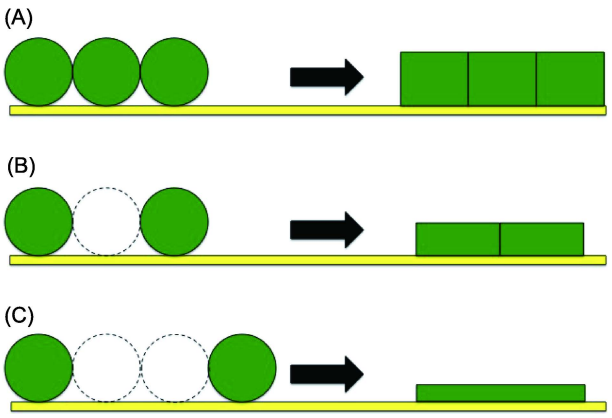

Figure 11. Scheme demonstrating the effect of distance between placed tissue spheroids on thickness of engineered tissue: **(A)** Tissue spheroids are placed in direct contact with each other; **(B)** Tissue spheroids are placed at the distance of one spheroid diameter; **(C)** Tissue spheroids are placed at the distance of two spheroids diameter.

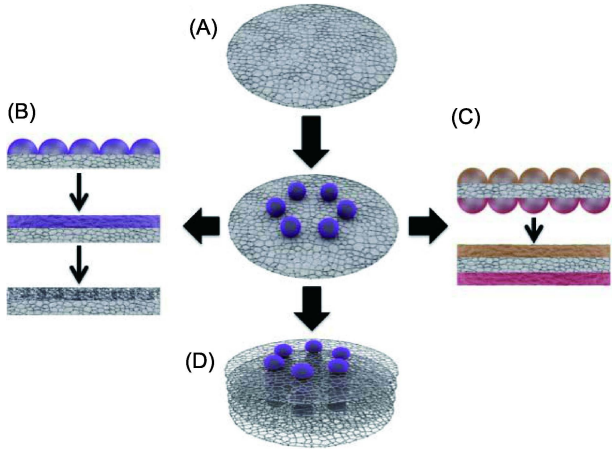

Figure 12. Tissue constructs formed by attachment of patterned tissue spheroids to electrospun polyurethane matrix as a technology platform for 3D bioprinting: **(A)** Patterned tissue spheroids attached to electrospun polyurethane matrix; **(B)** Biofabrication of acellular collagen patches; **(C)** Biofabrication of human skin; **(D)** Biofabrication of cartilage.

and tissue spheroids from keratinocytes on another side of matrix will enable biofabrication of human skin (Figure 12C). Using several layers of chondrospheres attached to electrospun polyurethane matrix will also allow to biofabricate human cartilage (Figure 12D).

Finally, using magnetically functionalized electrospun matrices with magnetic nanoparticles[23] as well as using tissue spheroids biofabricated from cells labelled with magnetic nanoparticles[24–27] will enable the development of novel magnetic 3D bioprinting technology based on principles of magnetic levitation or translocation of tissue constructs using magnetic forces[28–30].

5. Conclusion

Tissue spheroids biofabricated from human fibroblasts have been placed in regular patterns on the surface of electrospun polyurethane matrix using 3D bioprinter. Spreading of patterned tissue spheroids demonstrated an *in vitro* biocompatibiity of electrospun microfibrous polyurethane. The biocompatible electrospun polyurethane matrix could serve as a carrier for tissue spheroids. Thus, tissue spheroids spread on microfibrous electrospun polyurethane matrix is a novel technological platform for advancing biofabrication and 3D bioprinting.

Conflict of Interest and Funding

No conflict of interest was reported by the authors. This research has been supported by grant from Russian Research Fund (project number 15-15-00173).

References

1. Derby B, 2012, Printing and prototyping of tissues and scaffolds. *Science*, vol.338(6109): 921–926. http://dx.doi.org/10.1126/science.1226340
2. Murphy S V and Atala A, 2014, 3D bioprinting of tissues and organs. *Nature Biotechnology*, vol.32(8): 773–785. http://dx.doi.org/10.1038/nbt.2958
3. Atala A and Yoo J J, 2015, *Essentials of 3D Biofabrication and Translation*, Academic Press, United States.
4. Chua C K and Yeong W Y, 2015, *Bioprinting: Principles and Applications*, World Scientific Publishing Company, Singapore.
5. Gao G and Cui X, 2015, Three-dimensional bioprinting in tissue engineering and regenerative medicine. *Biotechnology Letters*, vol.37(12): 1–9. http://dx.doi.org/10.1007/s10529-015-1975-1
6. Ozbolat IT, 2015, Bioprinting scale-up tissue and organ constructs for transplantation. *Trends in Biotechnology*, vol.33(7): 395–400. http://dx.doi.org/10.1016/j.tibtech.2015.04.005
7. Mironov V, Kasyanov V, Drake C, *et al.*, 2008, Organ printing: Promises and challenges. *Regenerative Medicine*, vol.3(1): 93–103. http://dx.doi.org/10.2217/17460751.3.1.93
8. Mironov V, Visconti R P, Kasyanov V, *et al.*, 2009, Organ printing: Tissue spheroids as building blocks. *Biomaterials*, vol.30(12): 2164–2174. http://dx.doi.org/10.1016/j.biomaterials.2008.12.084
9. Perez-Pomares J M and Foty R A, 2006, Tissue fusion and cell sorting in embryonic development and disease: Biomedical implications. *BioEssays*, vol.28(8): 809–821. http://dx.doi.org/10.1002/bies.20442
10. Hajdu Z, Mironov V, Mehesz A N, *et al.*, 2010, Tissue spheroid fusion-based *in vitro* screening assays for analysis of tissue maturation. *Journal of Tissue Engineering and Regenerative Medicine*, vol.4(8): 659–664. http://dx.doi.org/10.1002/term.291
11. Huang G S, Tseng C S, Linju Yen B, *et al.*, 2013, Solid freeform-fabricated scaffolds designed to carry multicellular mesenchymal stem cell spheroids for cartilage regeneration. *European Cells and Materials*, vol.26: 179–194; discussion 194.
12. Ozbolat IT and Yu Y, 2013, Bioprinting toward organ fabrication: Challenges and future trends. *IEEE Transactions on Biomedical Engineering*, vol.60(3): 691–699. http://dx.doi.org/10.1109/TBME.2013.2243912
13. Schon B S, Schrobback K, van der Ven M, *et al.*, 2012, Validation of a high-throughput microtissue fabrication process for 3D assembly of tissue engineered cartilage constructs. *Cell and Tissue Research*, vol.347(3): 629–642.

http://dx.doi.org/10.1007/s00441-011-1311-6

14. Jakab K, Neagu A, Mironov V, *et al.*, 2004, Engineering biological structures of prescribed shape using self-assembling multicellular systems. *Proceeding of the National Academy of Science of the United States of America*, vol.101(9): 2864–2869. http://dx.doi.org/10.1073/pnas.0400164101
15. Skardal A and Atala A, 2015, Biomaterials for integration with 3-D bioprinting. *Annals of Biomedical Engineering*, vol.43(3): 730–746. http://dx.doi.org/10.1007/s10439-014-1207-1
16. Itoh M, Nakayama K, Noguchi R, *et al.*, 2015, Scaffold-free tubular tissues created by a bio-3D printer undergo remodeling and endothelialization when implanted in rat aortae. *PLOS ONE*, vol.10(9): e0136681. http://dx.doi.org/10.1371/journal.pone.0136681
17. Dvir T, Timko B P, Kohane D S, *et al.*, 2011, Nanotechnological strategies for engineering complex tissues. *Nature Nanotechnology*, vol.6(1): 13–22. http://dx.doi.org/10.1038/nnano.2010.246
18. Rezende R A, Azevedo F S, Pereira F D A S, *et al.*, 2012, Nanotechnological strategies for biofabrication of human organs. *Journal of Nanotechnology*, vol.2012: 1–10. http://dx.doi.org/10.1155/2012/149264
19. Mironov V, Kasyanov V and Markwald R R, 2008, Nanotechnology in vascular tissue engineering: From nanoscaffolding towards rapid vessel biofabrication. *Trends in Biotechnology*, vol.26(6): 338–344. http://dx.doi.org/10.1016/j.tibtech.2008.03.001
20. Pham Q P, Sharma U and Mikos A G, 2006, Electrospinning of polymeric nanofibers for tissue engineering applications: A review. *Tissue Engineering*, vol.12(5): 1197–1211. http://dx.doi.org/10.1089/ten.2006.12.1197
21. Beachley V, Kasyanov V, Nagy-Mehesz A, *et al.*, 2014, The fusion of tissue spheroids attached to pre-stretched electrospun polyurethane scaffolds. *Journal of Tissue Engineering*, vol.5: 1–11. http://dx.doi.org/10.1177/2041731414556561
22. Chua K N, Lim W S, Zhang P, *et al.*, 2005, Stable immobilization of rat hepatocyte spheroids on galactosylated nanofiber scaffold. *Biomaterials*, vol.26(15): 2537–2547. http://dx.doi.org/10.1016/j.biomaterials.2004.07.040
23. Lee H J, Lee S J, Uthaman S, *et al.*, 2015, Biomedical applications of magnetically functionalized organic/inorganic hybrid nanofibers. *International Journal of Molecular Sciences*, vol.16(6): 13661–13677. http://dx.doi.org/10.3390/ijms160613661
24. Ho V H, Muller K H, Barcza A, *et al.*, 2010, Generation and manipulation of magnetic multicellular spheroids. *Biomaterials*, vol.31(11): 3095–3102. http://dx.doi.org/10.1016/j.biomaterials.2009.12.047
25. Lin R Z, Chu W C, Chiang C C, *et al.*, 2008, Magnetic reconstruction of three-dimensional tissues from multicellular spheroid. *Tissue Engineering Part C: Methods*, vol.14(3): 197–205. http://dx.doi.org/10.1089/ten.tec.2008.0061
26. Mattix B, Olsen T R, Gu Y, *et al.*, 2014, Biological magnetic cellular spheroids as building blocks for tissue engineering. *Acta Biomaterialia*, vol.10(2): 623–629. http://dx.doi.org/10.1016/j.actbio.2013.10.021
27. Whatley B R, Li X, Zhang N, *et al.*, 2014, Magnetic-directed patterning of cell spheroids. *Journal of Biomedical Materials Research A*, vol.102(5): 1537–1547. http://dx.doi.org/10.1002/jbm.a.34797
28. Durmus N G, Tekin H C, Guven S, *et al.*, 2015, Magnetic levitation of single cells. *Proceedings of the National Academy of Science of the United States of America*, vol.112(28): E3661–3668. http://dx.doi.org/10.1073/pnas.1509250112
29. Mirica K A, Ilievski F, Ellerbee A K, *et al.*, 2011, Using magnetic levitation for three dimensional self-assembly. *Advanced Materials*, vol.23(36): 4134–4140. http://dx.doi.org/10.1002/adma.201101917
30. Tasoglu S, Yu C H, Liaudanskaya V, *et al.*, 2015, Magnetic levitational assembly for living material fabrication. *Advanced Healthcare Materials*, vol.4(10): 1469–1476, 1422. http://dx.doi.org/10.1002/adhm.201500092
31. Kasyanov V, Brakke K, Vilbrandt T, *et al.*, 2011, Toward organ printing: Design characteristics, virtual modelling and physical prototyping vascular segments of kidney arterial tree. *Virtual and Physical Prototyping*, vol.6(4): 197–213. http://dx.doi.org/10.1080/17452759.2011.631738
32. Xia L, Sakban R B, Qu Y, *et al.*, 2012, Tethered spheroids as an *in vitro* hepatocyte model for drug safety screening. *Biomaterials*, vol.33(7): 2165–2176. http://dx.doi.org/10.1016/j.biomaterials.2011.12.006

RESEARCH ARTICLE

Polyelectrolyte gelatin-chitosan hydrogel optimized for 3D bioprinting in skin tissue engineering

Wei Long Ng[1,2], Wai Yee Yeong[1*] and May Win Naing[2]

[1] Singapore Centre for 3D Printing (SC3DP), School of Mechanical and Aerospace Engineering, Nanyang Technological University (NTU), 50 Nanyang Avenue, Singapore 639798, Singapore

[2] Singapore Institute of Manufacturing Technology (SIMTech), Agency for Science, Technology and Research, 71 Nanyang Drive, Singapore 638075, Singapore

Abstract: Bioprinting is a promising automated platform that enables the simultaneous deposition of multiple types of cells and biomaterials to fabricate complex three-dimensional (3D) tissue constructs. Collagen-based biomaterial used in most of the previous works on skin bioprinting has poor printability and long crosslinking time. This posed an immense challenge to create 3D constructs with pre-determined shape and configuration at high throughput. Recently, the use of chitosan for wound healing applications has attracted huge attention due to its attractive traits such as its antimicrobial properties and ability to trigger hemostasis. In this paper, we optimized polyelectrolyte gelatin-chitosan hydrogel for 3D bioprinting. Modification to the chitosan was carried out via the oppositely charged functional groups from chitosan and gelatin at a specific pH of ~pH 6.5 to form polyelectrolyte complexes. The polyelectrolyte hydrogels were evaluated in terms of physical interactions within polymer blend, rheological properties (viscosities, storage and loss modulus), printing resolution at varying pressures and feed rates and biocompatibility. The polyelectrolyte gelatin-chitosan hydrogels formulated in this work was optimized for 3D bioprinting at room temperature to achieve high shape fidelity of the printed 3D constructs and good biocompatibility with fibroblast skin cells.

Keywords: 3D printing, bioprinting, rapid prototyping, additive manufacturing, skin tissue engineering

*Correspondence to: Wai Yee Yeong, Singapore Centre for 3D Printing (SC3DP), School of Mechanical and Aerospace Engineering, Nanyang Technological University (NTU), 50 Nanyang Avenue, Singapore 639798, Singapore; Email: wyyeong@ntu.edu.sg

Received: October 22, 2015; **Accepted:** December 17, 2015; **Published Online:** December 29, 2015

Citation: Ng W L, Yeong W Y and Naing M W, 2016, Polyelectrolyte gelatin-chitosan hydrogel optimized for 3D bioprinting in skin tissue engineering. *International Journal of Bioprinting*, vol.2(1): 53–62. http://dx.doi.org/10.18063/IJB.2016.01.009

1. Introduction

Tissue engineering has emerged as a multi-disciplinary field that involves clinicians, scientists and engineers to create anatomically relevant tissue constructs that alleviate the shortage of donor tissues/organs[1]. Despite major advancements in the field of tissue engineering, simple cell seeding over pre-formed polymeric scaffolds is not sufficient to fully replicate the sophisticated cell-matrix interactions within the native tissues[2]. The heterogeneity in extracellular matrix (ECM) composition within both epidermal and dermal regions of the skin plays numerous roles ranging from regulation of cellular proliferation to manipulation of stem cell fate. Bioprinting, which is an emerging technology, can be defined as "the use of 3D printing technology that incorporates viable living cells with biomaterials to fabricate sophisticated tissues/organs"[3]. The bioprinting technology not only enables the simultaneous deposition of different biomaterials and multiple cell types, but also provides flexibility in the design and fabrication of customizable patient-specific tissue-engineered constructs[4], demonstrating great potential for fabrica-

tion of complex 3D multicellular tissue constructs.

Despite being in its stage of infancy, bioprinting has already demonstrated great potential for fabrication of multi-layered skin[5–7], cartilage[8,9] and liver constructs[10]. It was highly anticipated that production of less-sophisticated human tissues/organs such as skin would be a reality in the near future[3]. Some current works on bioprinting of skin constructs include fabrication of hydrogel constructs consisting of different skin cells (keratinocytes and fibroblasts)[5,6] and *in-situ* printing of skin cells and biomaterials directly over the wound site[11]. Contrary to the common misconception that skin is a relatively simple 2D tissue, the thin layer of human skin has a unique pattern created by the natural compartmentalization of different types of skin cells that are positioned relative to each other at high degree of specificity[12]. This specific arrangement of skin cells is essential for cell-cell interactions that initiate autocrine and paracrine signaling within the native human skin[13].

As skin cells (fibroblasts) are capable of producing their own ECM proteins, the bio-inks serve as temporary 3D templates to guide the tissue morphogenesis. Collagen type I, the most abundant ECM protein in human skin, is widely used for bioprinting of skin constructs. Most of the biomaterials used in those studies[5,6,14–16] were mainly collagen-based, which has relatively poor printability. Lee *et al.* printed layers of collagen to create a 3D bioprinted collagen construct with stacking height of 1.2 mm[5]. Another work demonstrated printing of multi-layered cell-laden collagen constructs on non-planar surface using nebulized crosslinking reagent[15]. Only planar sandwich constructs were fabricated using the valve-based technique due to the slow pH-dependent crosslinking of collagen prior to printing of subsequent layers. Koch *et al.* printed layers of encapsulated keratinocytes and fibroblasts onto a decellularized dermal matrix sheet via laser-based method[6]. The printed construct comprised high number of keratinocytes and fibroblasts (different from representative cellular density within native human skin) and there is no variation in the extracellular matrix density across the depth of printed structure[17].

Progress in bioprinting of skin is severely hindered due to limited choices of printable biomaterials. Over the recent years, the attractive traits of chitosan polymer have gained huge attention for wound healing applications[18–20]. Chitosan is a linear polysaccharide of D-glucosamine and *N*-acetyl-D-glucosamine, which can be prepared by the *N*-deacetylation of insoluble chitin in the presence of alkaline solution[21]. In the presence of lysozymes, chitosan undergoes *in vivo* degradation via enzymatic hydrolysis to form by-product, glucosamine, which does not pose any toxicity[22]. Furthermore, chitosan triggers hemostasis and accelerates tissue regeneration due to the migration of inflammatory cells and activation of fibroblasts that produce multiple cytokines[23]. Notably, chitosan-based biomaterials have antimicrobial properties which can help to reduce the incidence of sepsis[24]. Chitosan powders are generally soluble at acidic pH and the amine groups in chitosan are protonated at pH lower than 6 to confer the poly-cationic behavior to chitosan. With increasing pH, the amine groups become deprotonated to form insoluble chitosan polymer. This soluble-insoluble transition occurs at its pK_a value around pH 6–6.5, which is dependent on degree of *N*-deacetylation and molecular weight[25]. Despite its attractive properties, chitosan alone has poor printability[26,27] and further modifications are required to increase the printability of chitosan-based hydrogels.

Gelatin, which is commonly used for biomedical applications, exhibits negative charges when the pH of medium is above its isoelectric point (pH_{iso} = 4.7)[28]. As such, interactions between the positively charged ammonium ions from chitosan react with carboxylate groups from the ampholytic gelatin result in the formation of a polyelectrolyte complex. Prior works on polyelectrolyte gelatin-chitosan scaffolds/films[29–32] have demonstrated great potential for skin tissue engineering applications. The polyelectrolyte gelatin-chitosan hydrogel did not experience significant contraction in the *in-vitro* cell culture test over 4 weeks[32] and also demonstrated potential antimicrobial activity[33]. An *in-vivo* study over a period of 16 weeks revealed that the chitosan/gelatin hydrogel was efficient in inducing fibrin formation and vascularization at the implant-host interface[34]. The polyelectrolyte gelatin-chitosan scaffolds are commonly prepared via freeze-drying[29,31,32] or solvent-casting approaches[29,30].

In this paper, gelatin was modified with chitosan to form polyelectrolyte gelatin-chitosan (PGC) hydrogels to demonstrate its potential for bioprinting applications. The interactions between the chitosan and gelatin within the polyelectrolyte complex were evaluated, followed by rheological characterization of the PGC hydrogels at varying shear rates and temperatures. Next, different combinations of printing pressures and feed rates were utilized for different PGC hydrogels to

determine the highest possible printing resolution and printing accuracy at room temperature. Lastly, biocompatibility tests were conducted to evaluate the potential use of PGC hydrogels for bioprinting of skin constructs. These outcomes will provide valuable insights into development of printable hydrogels for bioprinting of 3D tissue constructs.

2. Materials and Methods

2.1 Materials and Cells

Chitosan (low molecular weight, 75–85% deacetylation) and gelatin (porcine skin, Type A) powders were obtained from (Sigma Aldrich, Singapore). Other reagents like acetic acid, sodium hydroxide (NaOH) and phosphate buffered saline (PBS) solution (pH 7.4 at 0.01 M) were sterile-filtered before use. Neonatal human foreskin fibroblasts (HFF-1 from ATCC® SCRC-1041™) were used in this study. The cell line was cultured in a HERAcell 150i cell incubator (Thermo Scientific) at 37°C in 5% CO_2 using ATCC-formulated Dulbecco's Modified Eagle's Medium (DMEM) supplemented with 15% fetal bovine serum (HyClone™ from GE Healthcare). Culture media was changed every 3 days and the cells were routinely passaged in tissue culture flasks (cells were not used after Passage 6). The adherent HFF-1 cells were harvested using 0.25% trypsin/ethylenediaminetetraacetic acid (EDTA) (Invitrogen) at 90% confluency.

2.2 Synthesis of Polyelectrolyte Gelatin-chitosan Hydrogels

Modification of chitosan was carried out via the addition of gelatin to create a polyelectrolyte gelatin-chitosan hydrogel[30]. 2.5% w/v chitosan was dissolved in acetic acid and mechanically agitated for three hours to obtain a homogeneous gel. Varying concentration of gelatin solutions (2.5%, 5% and 7.5% w/v) were dissolved in sterile PBS solution and stirred at 40°C for complete dissolution of gelatin powder. The gelatin solution of varying concentration was then added separately to the chitosan gel at a pH greater than 4.7 to initiate the formation of polyelectrolyte complex between the positively-charged chitosan and negatively charged gelatin and they were designated hereafter as 2.5%, 5% and 7.5% PGC respectively. Equal volume of gelatin solution was added to the chitosan gel in a drop-wise manner under constant mechanical agitation, followed by subsequent addition of NaOH solution to the gelatin-chitosan polymer blend in a drop-wise manner till the pH of the mixture reaches ~ 6.5 to initiate the pH-dependent crosslinking using a pH meter (HM Digital. Inc.).

2.3 FTIR Characterization

The interactions between chitosan and gelatin within the polymer blend were investigated with dried gelatin-chitosan hydrogels using a Fourier Transform Infrared (FTIR) Spectrometer (Bruker Vertex 80v, Germany). Each dried gelatin-chitosan hydrogel was placed within the enclosed vacuum chamber one at a time and FTIR spectra were collected within the range of 800–2000 cm^{-1} via attenuated total reflectance (ATR) technique. The measurements were conducted in triplicate and presented in the transmittance mode.

2.4 Rheological Characterization

The rheological properties of PGC hydrogels were evaluated using the Discovery hybrid rheometer (TA instruments, USA). The values of the strain amplitude were first verified to ensure that all measurements were performed within the linear viscoelastic region. Next, the viscosities of PGC hydrogels were evaluated for shear rates ranging from 0.1 to 100 s^{-1} at a constant temperature of 27°C (room temperature). To evaluate the sol-gel transition state of the hydrogels, (i) storage modulus (G') and (ii) loss modulus (G") of the 2.5%, 5% and 7.5% PGC were then measured at varying temperatures from 20 to 40°C at a fixed shear strain of 2%. The sol-gel transition state can be determined by the G'/G" ratio, whereby G'/G" = 1 is the gelling point. All measurements were conducted in triplicate.

2.5 Bioprinting of Biomaterials

A 3-D bioprinter, Biofactory® (regenHU Ltd., Switzerland), was used for printing of PGC hydrogels. The PGC bio-ink was loaded into a sterile printing cartridge and the printing process was conducted using an extrusion-based print-head. The hydrogel was deposited via extrusion-based printing approach and the material flow for each print-head was controlled by individual pressure regulators. Pre-defined structures were input into BioCAD (regenHU Ltd., Switzerland).

The printability of different PGC hydrogels was evaluated using a combination of different printing pressures (1–3.5 bars) and feed rates (600–1000 mm/min) using a constant nozzle diameter of 210 µm. Adjacent filaments of 2 cm length at inter-spacing of 1 mm (n = 6) were printed and measured in terms of filament

widths at varying printing pressures and feed rates using ImageJ processing software. To demonstrate its ability to fabricate a multi-layered hydrogel construct, a 3-layered hydrogel construct with grid-like patterns was fabricated by printing each layer of grid-like patterns directly over the previous layer using an optimal combination of feed rates and printing pressures.

2.6 Biocompatibility of PGC Hydrogels

To assess the biocompatibility of PGC hydrogels, PGC hydrogels were manually casted followed by seeding 150,000 HFF-1 cells on surface of PGC hydrogels in each of the 6-well plates (n = 5) and 2 mL of complete growth medium was added into each well plate. A control setup with 2.5% chitosan was used in this study. The cells were incubated for 4 days prior to performing cell viability assay on Day 4 using Molecular Probes® Live/Dead staining kits (Life-Technologies) according to the manufacturer's manual. The calcein AM will stain the viable cells green, while the ethidium homodimer-1 will stain the dead cells red. The samples were washed twice with PBS and 1 mL of staining solution was added to each of the 6-well plates containing the PGC hydrogels and incubated for an hour before observation under Carl Zeiss Axio Vert. A1 Inverted Microscopy.

3. Results and Discussion

An ideal printable material should provide good shape fidelity and high printing resolution. An important characteristic of printable biomaterials is to have consistent flow that facilitates deposition at high repeatability. Notably, the hydrogel-based bio-inks with natural porosity offer good permeability to oxygen and nutrients[35].

3.1 FTIR Characterization

To evaluate the interactions between the chitosan and gelatin within the polymer blend, FTIR analysis was conducted. The IR spectra of the gelatin-chitosan polymer blend and their respective polymers were shown in Figure 1. The IR spectrum of chitosan polymer displayed saccharide peaks at approximately 896 and 1152 cm^{-1}, an amino characteristic peak at 1550 cm^{-1} and an amide I peak of the acetyl group at 1643 cm^{-1}. Gelatin polymer was characterized by its amino peak at 1539 cm^{-1} and carbonyl peak at 1628 cm^{-1}. The gelatin-chitosan polymer blend led to slight adjustment in the spectrum, i.e., shifting of both carbonyl

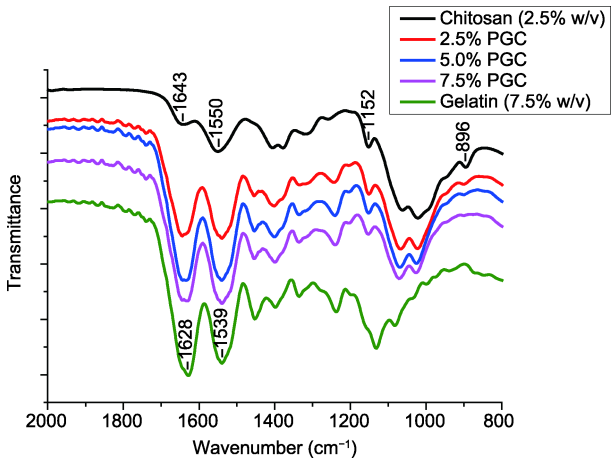

Figure 1. IR spectra of gelatin-chitosan polymer blend along with their individual polymers. The shifting of both carbonyl and amino bands indicate the formation of hydrogen bonds between chitosan and gelatin molecules in the polyelectrolyte complex.

(from 1643 to 1628 cm^{-1}) and amino bands (from 1550 to 1539 cm^{-1}). This illustrated that hydrogen bonding are formed between chitosan and gelatin molecules in the polyelectrolyte complex, which is supported by other reported results[36]. The shifting of the peaks implied that hydrogen bonding occurs between the chitosan and gelatin polymers to form polyelectrolyte hydrogels, which is consistent with previous reported results[30,36,37].

3.2 Rheological Characterization

The rheological properties of different PGC hydrogels were investigated at 27°C to analyze how varying shear rates affect viscosity of the hydrogels during printing process at room temperature. A force is required to overcome yield stress of the hydrogel before it undergoes a shear-thinning process with increasing shear rates. It was reported that a suitable range of printing viscosity is ~ 4 to 30 Pa·s for extrusion-based printing[38]. The generated shear rate in our printing process was estimated in the range of 20–60 s^{-1}. As shown in Figure 2, PGC hydrogels with higher gelatin concentrations exhibited higher yield stress and viscosity. The increased gelatin concentration resulted in more interactions between the positively-charged ammonium ions from chitosan and negatively-charged carboxylate groups from the ampholytic gelatin, resulting in higher viscosity. It was observed that as the shear rate increases, viscosity of 2.5% PGC hydrogels falls out of the ideal printing viscosity. The resultant low viscosity would result in poor printing accuracy

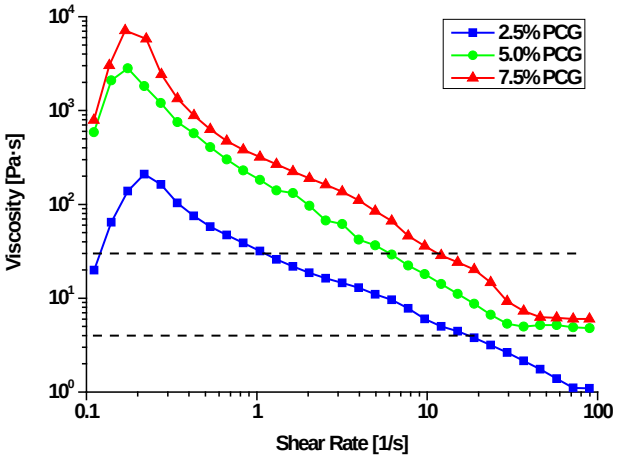

Figure 2. Rheological behavior of PGC hydrogels at varying shear rates (0.1–100 s^{-1}) at 27°C (room temperature). All 3 different PGC hydrogels fall within the suitable range of printing viscosity (~ 4 to 30 Pa·s) at varying shear rates.

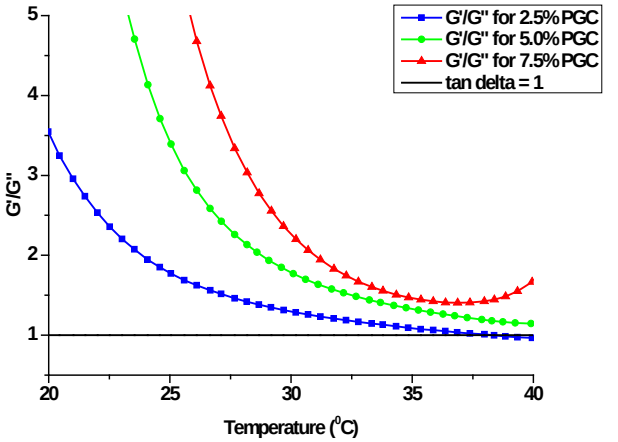

Figure 3. G'/G" ratio of different PGC hydrogels at varying temperatures at fixed shear strain of 2%. A high G'/G" ratio (>1) would offer good shape fidelity of the printed structures.

but both 5% and 7.5% PGC hydrogels have relatively more suitable printing viscosities.

As gelatin is a thermo-sensitive polymer, it is important to evaluate the rheological behaviour of PGC hydrogels at varying temperatures. The storage and loss modulus of PGC hydrogels were evaluated over a temperature range of 20–40°C. Prior to the addition of NaOH, all the PGC hydrogels were in sol state with low viscosity at temperatures above 25°C, as such it is difficult to achieve good shape fidelity above printing temperatures of 25°C. To analyze sol-gel transition state of the PGC hydrogels, the storage (G') and loss modulus (G") of the PGC hydrogels were measured. The ratio of G'/G" (tan α) determines the sol-gel state of the hydrogel. When tan α is greater than 1, it indicates that the material is in a gel state, while a tan α lower than 1 indicates that the material is in a sol state. As shown in Figure 3; only 5% and 7.5% PGC hydrogels exhibit gel-like behaviour within the temperature range of 20–40°C. The tan α of 2.5% PGC hydrogel approaches 1 near 37°C and its tanα value decreases below 1 at temperatures above 37°C. As such, 2.5% PGC hydrogel will not be used in the bioprinting process as loss of shape fidelity might occur during the incubation of the printed construct at higher temperature. Conversely, both 5% and 7.5% PGC hydrogels exhibit significantly high G'/G" ratio, which would offer good shape fidelity of the printed structures.

3.3 Bioprinting of Biomaterials

There are currently two different modes of printing; one is the deposition of cell-laden hydrogel and the other approach is to print the hydrogel and cells separately. The latter approach offers better control over the cellular density and distribution across each printed layer. As such in our printing process, we focus on the printing of acellular biomaterials using the extrusion-based printing technique.

As shown in Figure 4, the suitable range of printing pressures for each PGC hydrogel is different. Generally, higher pressures are required to extrude the more viscous hydrogels[39]. It was observed that the filament widths of 2.5% PGC hydrogels increase exponentially with increasing printing pressures. This is probably due to the intrinsic low viscosity of 2.5% PGC hydrogel which causes higher extent of filament spreading when a larger printing pressure was used. A similar trend was also observed in 5% PGC hydrogel; the filament widths increase in a linear manner from printing pressures of 2–2.8 bars and subsequently increase in an exponential manner when the printing pressures are above 2.8 bars. In contrast, the most viscous 7.5% PGC hydrogels demonstrated a linear relationship between printing pressures and filament widths throughout 2.6 bars to 3.4 bars. It is likely that the high viscosity of 7.5% PGC hydrogel reduces the extent of filament spreading at higher printing pressures (above 3 bars). It was also observed that standard deviation of printed filament widths decreases with PGC hydrogels of higher viscosity. Hence, a more viscous hydrogel offers higher printing consistency and better control over the printed filament widths at increasing printing pressure.

Generally, a higher feed rate would result in a thinner

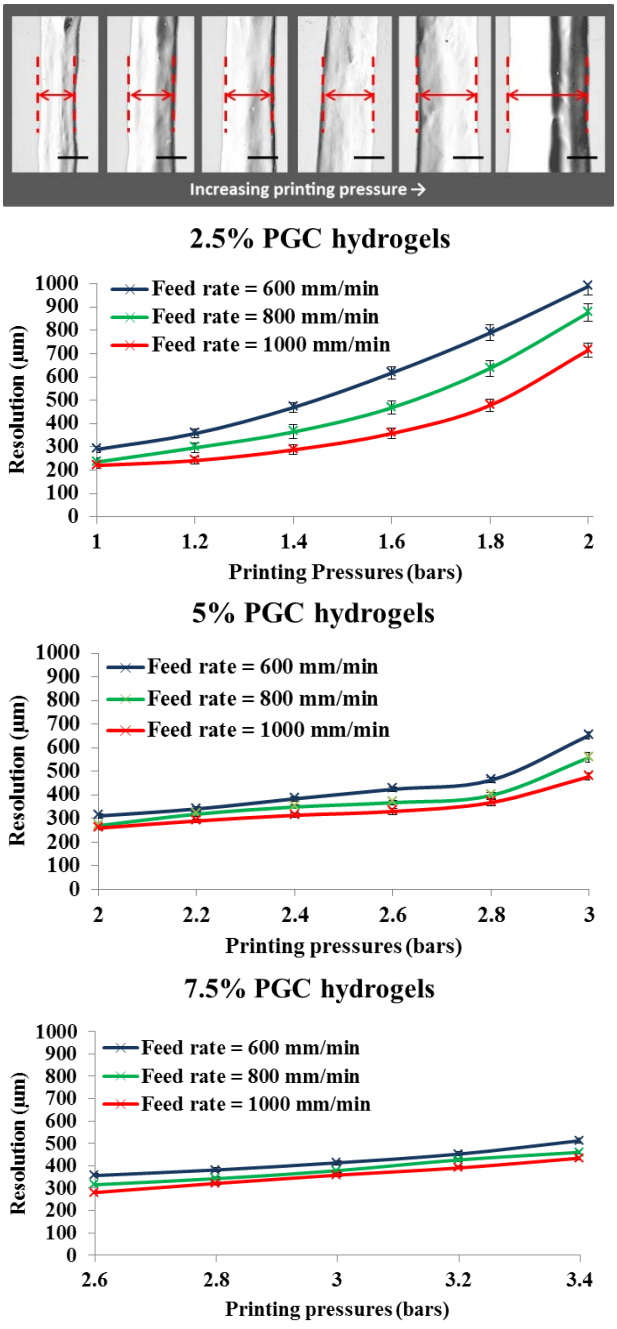

Figure 4. Effect of printing pressures on printed filament widths.

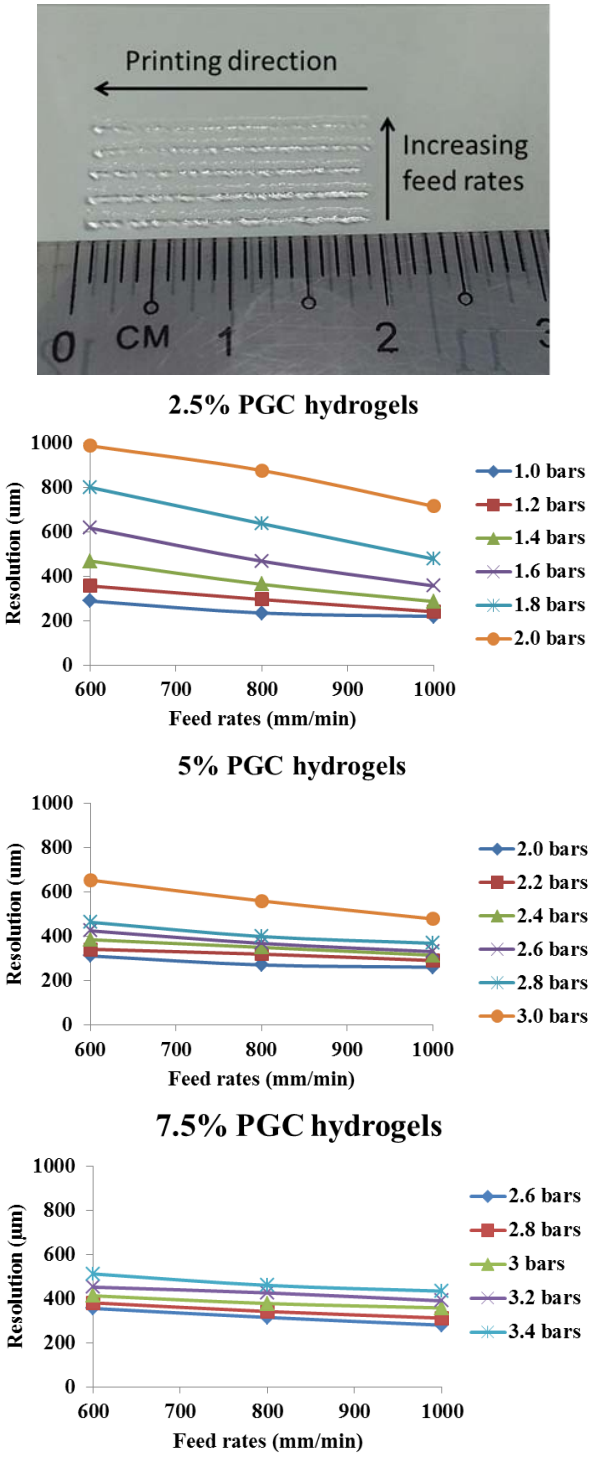

Figure 5. Effect of feed rates on printed filament widths.

filament width (Figure 5). It was observed in 2.5% PGC hydrogels that the printed filament widths increase to a larger extent with decreasing feed rates when higher printing pressures were used (indicated by the gradient of the plotted lines). Conversely, the most viscous 7.5% PGC hydrogels exhibited a linear relationship between the feed rates and printed filament widths within its suitable range of printing pressures. Hence, varying feed rates has significant effect on the less viscous hydrogels such as 2.5% PGC hydrogels with increasing printing pressures.

As shown in Figure 6, an optimal combination of both printing pressures and feed rates is required to obtain a complete grid-like pattern. A high printing pressure would result in excessive material deposition,

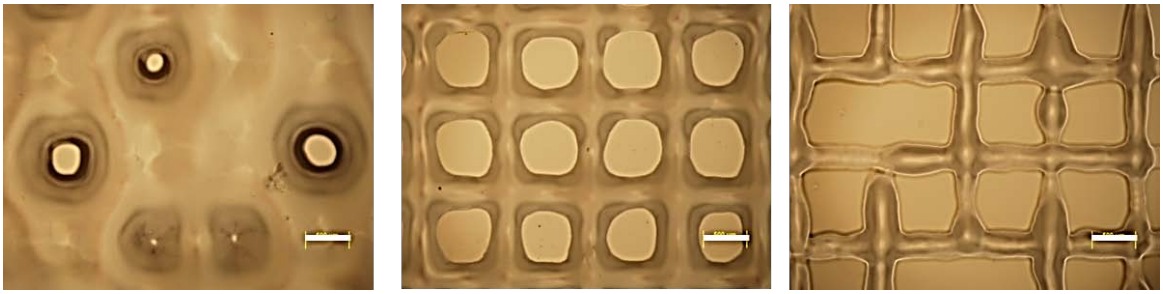

Figure. 6. (Left) Excessive material deposition, (Middle) optimal printing parameters, (Right) incomplete printing (scale bar: 500 µm).

while a low printing pressure would result in incomplete patterning. Among all the PGC hydrogels and different combinations of printing pressures and feed rates, the 5% PGC hydrogels at printing conditions of 2.4 bars and 1000 mm/min feed rate enables the fabrication of complete grid-like patterns at highest printing resolution. Using the optimal combination of printing pressures and feed rates and a pre-defined layer thickness of 160 µm, a 3-layered PGC hydrogel construct with grid-like structures was printed and shown in Figure 7. It was observed that the estimated height of the printed construct (~400 µm) was lower than the pre-defined height of 480 µm and the filament widths increased from ~314 µm (1-layer) to ~ 450 µm (3-layers). It is likely that the nozzle tip transversed within the layer and induced compression of each printed layer (lower height and higher filament widths). Further optimization to the layer thickness is required to improve the accuracy of printed 3D constructs.

3.4 Biocompatibility of PGC Hydrogels

To evaluate the biocompatibility of the PGC hydrogel, 5% PGC hydrogel was manually casted onto 6 well plates followed by seeding of HFF-1 cells onto the surface and a control set-up with 2.5% chitosan was used in this study. The seeded HFF-1 cells were generally round in shape and evenly distributed over the surface of PGC hydrogels. Live-dead staining was conducted to visually inspect the cell viability and morphology after 4 days. As shown in Figure 8, the green viable fibroblast cells exhibited the spindle-like morphology indicating that they were able to attach and proliferate. It was noted that a small number of dead HFF-1 cells, as represented by red colour, was also present in the 3D construct. A greater number of viable HFF-1 cells were observed on 5% PGC hydrogel as compared to the 2.5% chitosan hydrogel. The incorporation of gelatin within the polymer blend improved the biocompatibility by shielding the excessive positive charges on chitosan polymer to a suitable charge density[30]. This enables the cells to attach and proliferate better as compared to the pure chitosan biomaterial[40].

4. Conclusion

We envision that the bioprinting of both biomaterials and cells with pre-defined structures will eventually

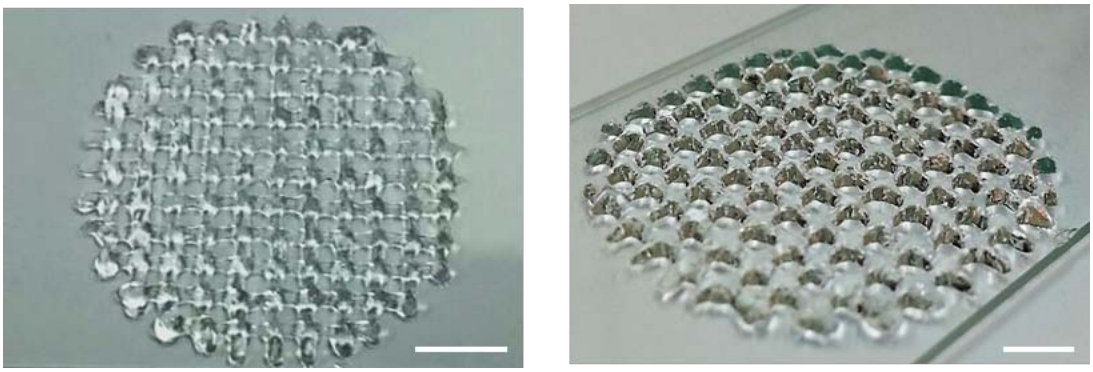

Figure 7. 3D printed multi-layered PGC hydrogel structure view at various persepectives. The resultant 3D construct has a lower height than the pre-defined value and the filament widths increased with increasing layers. 5% PGC hydrogel was tested for the fabrication of 3D hydrogel construct, number of layers 3, scale bar = 5 mm

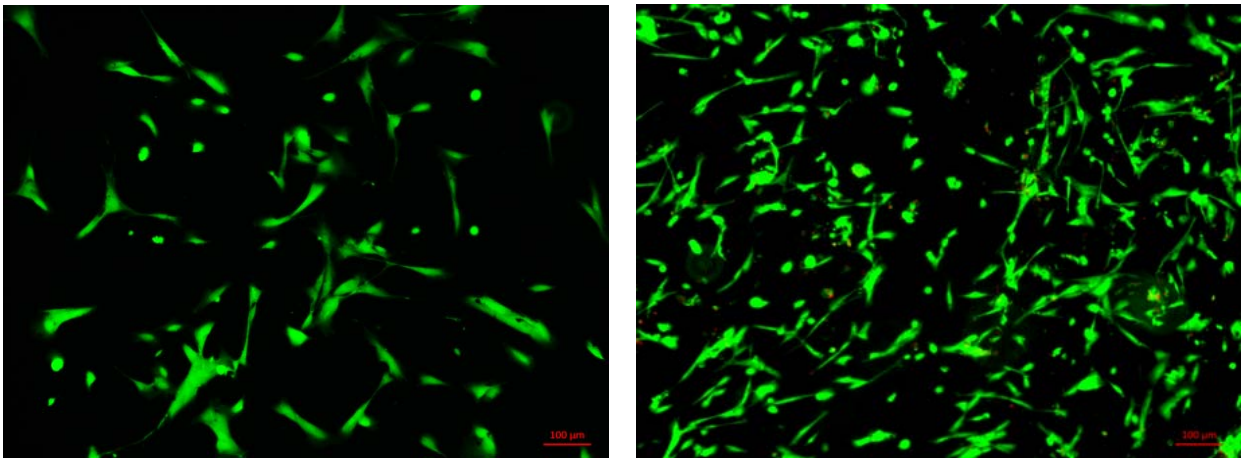

Figure 8. Live-dead staining on Day 4. (Left) chitosan hydrogel, (Right) 5% PGC hydrogel (scale bar: 100 μm).

mature to form a functional tissue. As such, 3D bioprinting serves as an attractive platform to facilitate cellular and matrix deposition in a spatially-controlled 3D matrix. Chitosan is a promising polymer used in wound healing applications due to its antimicrobial and hemostasis properties. In this work, modification to the chitosan was carried out via the addition of gelatin to form printable polyelectrolyte gelatin-chitosan (PGC) hydrogels. We have optimized PGC hydrogels for bioprinting of skin constructs. The PGC hydrogels exhibited a sufficiently high viscosity that is suitable for our printing chamber which has a temperature of 27°C and its high G'/G" ratio resulted in good shape fidelity of the printed constructs. The highest resolution for the grid-like pattern using the 210 μm nozzle tip was 314 μm at an optimal combination of 2.4 bars and 1000 mm/min feed rate. The important functions of bioengineered skin are to provide barrier function and a temporary scaffold to guide tissue morphogenesis[41]. The use of bioprinting offers good spatial control over deposition of selected biomaterials at specific regions to fabricate customizable tissue-engineered constructs correlating to wound area and depth. Full-thickness human skin ranges between 1.5–2.5 mm in thickness. The epidermal region is approximately 75 to 150 μm in thickness and the dermal region is usually less than 2 mm. The printed constructs (~400 μm for 3 layers) are representative of the outer epidermal layer and part of the dermal region. These results suggest the potential use of PGC hydrogels for bioprinting applications. More work needs to be conducted on thixotropy and swelling behavior of the PCG hydrogels to further optimize the printing process.

Conflict of Interest and Funding

No conflict of interest was reported by the authors.

Acknowledgments

The first author would like to thank the scholarship sponsorship by A*STAR Graduate Academy.

References

1. Lanza R, Langer R and Vacanti J P, 2011, *Principles of Tissue Engineering*, 4th edn, Academic Press, San Diego.
2. Watt F M and Fujiwara H, 2011, Cell-extracellular matrix interactions in normal and diseased skin. *Cold Spring Harbor Perspectives in Biology*, vol.3(4): a005124. http://dx.doi.org/10.1101/cshperspect.a005124
3. Murphy S V and Atala A, 2014, 3D bioprinting of tissues and organs, *Nature biotechnology*, vol.32: 773–785. http://dx.doi.org/10.1038/nbt.2958
4. Ozbolat I T and Yu Y, 2013, Bioprinting towards organ fabrication: Challenges and future trends. *IEEE Transactions on Bio-Medical Engineering*, vol.60(3): 691–693. http://dx.doi.org/10.1109/TBME.2013.2243912
5. Lee V, Singh G, Trasatti C, *et al.*, 2013, Design and fabrication of human skin by three-dimensional bioprinting. *Tissue Engineering Part C: Methods*, vol.20(6): 473–484. http://dx.doi.org/10.1089/ten.TEC.2013.0335
6. Koch L, Deiwick A, Schlie S, *et al*., 2012, Skin tissue generation by laser cell printing. *Biotechnology and Bioengineering*, vol.109(7): 1855–1863. http://dx.doi.org/10.1002/bit.24455
7. Pereira R F, Barrias C C, Granja P L, *et al.*, 2013, Advanced biofabrication strategies for skin regeneration and repair. *Nanomedicine*, vol.8(4): 603–621.

http://dx.doi.org/10.2217/nnm.13.50

8. Cui X, Breitenkamp K, Finn M, *et al*., 2012, Direct human cartilage repair using three-dimensional bioprinting technology. *Tissue Engineering Part A*, vol.18(11-12): 1304–1312. http://dx.doi.org/10.1089/ten.tea.2011.0543
9. Kundu J, Shim J H, Jang J, *et al.*, 2013, An additive manufacturing-based PCL alginate-chondrocyte bioprinted scaffold for cartilage tissue engineering. *Journal of Tissue Engineering and Regenerative Medicine*, vol.9(11): 1286–1297. http://dx.doi.org/10.1002/term.1682
10. Chang R, Emami K, Wu H, *et al*., 2010, Biofabrication of a three-dimensional liver micro-organ as an *in vitro* drug metabolism model. *Biofabrication*, vol.2(4): 045004. http://dx.doi.org/10.1088/1758-5082/2/4/045004
11. Binder K W, Zhao W X, Aboushwareb T, *et al*., 2010, *In situ* bioprinting of the skin for burns. *Journal of the American College of Surgeons*, vol.211(3): S76. http://dx.doi.org/10.1016/j.jamcollsurg.2010.06.198
12. Tobin D J, 2006, Biochemistry of human skin—our brain on the outside. *Chemical Society Reviews*, vol.35(1): 52–67. http://dx.doi.org/10.1039/B505793K
13. Ng W L, Yeong W Y and Naing M W, 2015, Cellular approaches to tissue-engineering of skin: A review. *Journal of Tissue Science & Engineering*, vol.6: 150. http://dx.doi.org/10.4172/2157-7552.1000150
14. Michael S, Sorg H, Peck C-T, *et al.*, 2013, Tissue engineered skin substitutes created by laser-assisted bioprinting form skin-like structures in the dorsal skin fold chamber in mice. *Plos One*, vol.8: e57741. http://dx.doi.org/10.1371/journal.pone.0057741
15. Lee W, Debasitis J C, Lee V K, *et al.*, 2009, Multi-layered culture of human skin fibroblasts and keratinocytes through three-dimensional freeform fabrication. *Biomaterials*, vol.30(8): 1587–1595. http://dx.doi.org/10.1016/j.biomaterials.2008.12.009
16. Lee W, Lee V, Polio S, *et al.*, 2010, On-demand three-dimensional freeform fabrication of multi-layered hydrogel scaffold with fluidic channels. *Biotechnology and Bioengineering*, vol.105(6): 1178–1186. http://dx.doi.org/10.1002/bit.22613
17. Weber L, Kirsch E, Müller P, *et al.*, 1984, Collagen type distribution and macromolecular organization of connective tissue in different layers of human skin. *Journal of Investigative Dermatology*, vol.82(2): 156–160. http://dx.doi.org/10.1111/1523-1747.ep12259720
18. Muzzarelli R A, 2009, Chitins and chitosans for the repair of wounded skin, nerve, cartilage and bone. *Carbohydrate Polymers*, vol.76(2): 167–182. http://dx.doi.org/10.1016/j.carbpol.2008.11.002
19. Dash M, Chiellini F, Ottenbrite R M, *et al*., 2011, Chitosan—A versatile semi-synthetic polymer in biomedical applications. *Progress in Polymer Science*, vol.36(8): 981–1014. http://dx.doi.org/10.1016/j.progpolymsci.2011.02.001
20. Jayakumar R, Prabaharan M, Kumar P S, *et al.* 2011, Biomaterials based on chitin and chitosan in wound dressing applications. *Biotechnology Advances*, vol.29(3): 322–337. http://dx.doi.org/10.1016/j.biotechadv.2011.01.005
21. Rinaudo M, 2006, Chitin and chitosan: Properties and applications. *Progress in Polymer Science*, vol.31(7): 603–632. http://dx.doi.org/10.1016/j.progpolymsci.2006.06.001
22. Kim I Y, Seo S J, Moon H S, *et al.*, 2008, Chitosan and its derivatives for tissue engineering applications. *Biotechnology Advances*, vol.26(1): 1–21. http://dx.doi.org/10.1016/j.biotechadv.2007.07.009
23. Ueno H, Nakamura F, Murakami M, *et al.*, 2001, Evaluation effects of chitosan for the extracellular matrix production by fibroblasts and the growth factors production by macrophages. *Biomaterial*s, vol.22(15): 2125–2130. http://dx.doi.org/10.1016/S0142-9612(00)00401-4
24. Kong M, Chen X G, Xing K, *et al.*, 2010, Antimicrobial properties of chitosan and mode of action: A state of the art review. *International Journal of Food Microbiology*, vol.144(1): 51–63. http://dx.doi.org/10.1016/j.ijfoodmicro.2010.09.012
25. Cho Y-W, Jang J, Park C R, *et al.*, 2000, Preparation and solubility in acid and water of partially deacetylated chitins. *Biomacromolecules*, vol.1(4): 609–614. http://dx.doi.org/10.1021/bm000036j
26. Geng L, Feng W, Hutmacher D W, *et al*., 2005, Direct writing of chitosan scaffolds using a robotic system. *Rapid Prototyping Journal*, vol.11(2): 90–97. http://dx.doi.org/10.1108/13552540510589458
27. Ng W L, Yeong W Y and Naing M W, 2014, Potential of bioprinted films for skin tissue engineering, in *Proceedings of the 1st International Conference on Progress in Additive Manufacturing* (eds C K Chua, W Y Yeong, M J Tan and E Liu).
28. Malafaya P B, Silva G A and Reis R L, 2007, Natural–origin polymers as carriers and scaffolds for biomolecules and cell delivery in tissue engineering applications. *Advanced Drug Delivery Reviews*, vol.59(4–5): 207–233. http://dx.doi.org/10.1016/j.addr.2007.03.012
29. Huang Y, Onyeri S, Siewe M, *et al.*, 2005, *In vitro* characterization of chitosan–gelatin scaffolds for tissue engineering. *Biomaterials*, vol.26(36): 7616–7627. http://dx.doi.org/10.1016/j.biomaterials.2005.05.036

30. Yin Y, Li Z, Sun Y, *et al*., 2005, A preliminary study on chitosan/gelatin polyelectrolyte complex formation. *Journal of Materials Science*, vol.40(17): 4649–4652. http://dx.doi.org/10.1007/s10853-005-3929-9
31. Mao J, Zhao L G, Yin Y J, *et al*., 2003, Structure and properties of bilayer chitosan–gelatin scaffolds. *Biomaterials*, vol.24(6): 1067–1074. http://dx.doi.org/10.1016/S0142-9612(02)00442-8
32. Mao J , Zhao L, de Yao K, *et al*., 2003, Study of novel chitosan-gelatin artificial skin *in vitro*. *Journal of Biomedical Materials Research Part A*, vol.64A(2): 301–308. http://dx.doi.org/10.1002/jbm.a.10223
33. Pereda M, Ponce A, Marcovich N, *et al.*, 2011, Chitosan-gelatin composites and bi-layer films with potential antimicrobial activity. *Food Hydrocolloids*, vol.25(5): 1372–1381. http://dx.doi.org/10.1016/j.foodhyd.2011.01.001
34. Wang X, Yu X, Yan Y, *et al.*, 2008, Liver tissue responses to gelatin and gelatin/chitosan gels. *Journal of Biomedical Materials Research Part A*, vol.87(1): 62–68. http://dx.doi.org/10.1002/jbm.a.31712
35. Nguyen K T and West J L, 2002, Photopolymerizable hydrogels for tissue engineering applications. *Biomaterials*, vol.23(22): 4307–4314. http://dx.doi.org/10.1016/S0142-9612(02)00175-8
36. Cheng M, Deng J, Yang F, *et al.*, 2003, Study on physical properties and nerve cell affinity of composite films from chitosan and gelatin solutions. *Biomaterials*, vol.24(17): 2871–2880. http://dx.doi.org/10.1016/S0142-9612(03)00117-0
37. Yin Y J, Yao K D, Cheng G X, *et al*., 1999, Properties of polyelectrolyte complex films of chitosan and gelatin. *Polymer International*, vol.48(6): 429–432. http://dx.doi.org/10.1002/(SICI)1097-0126(199906)48:6<429::AID-PI160>3.0.CO;2-1
38. Das S, Pati F, Choi Y J, *et al*., 2015, Bioprintable, cell-laden silk fibroin–gelatin hydrogel supporting multilineage differentiation of stem cells for fabrication of three-dimensional tissue constructs. *Acta Biomaterialia*, vol.11: 233–246. http://dx.doi.org/10.1016/j.actbio.2014.09.023
39. Swope V B, Supp A P and Boyce S T, 2002, Regulation of cutaneous pigmentation by titration of human melanocytes in cultured skin substitutes grafted to athymic mice. *Wound Repair and Regeneration*, vol.10(6): 378–386. http://dx.doi.org/10.1046/j.1524-475X.2002.10607.x
40. Mao J S, Cui Y L, Wang X H, *et al.* 2004, A preliminary study on chitosan and gelatin polyelectrolyte complex cytocompatibility by cell cycle and apoptosis analysis. *Biomaterials*, vol.25(18): 3973–3981. http://dx.doi.org/10.1016/j.biomaterials.2003.10.080
41. MacNeil S, 2007, Progress and opportunities for tissue-engineered skin. *Nature*, vol.445: 874–880. http://dx.doi.org/10.1038/nature05664

RESEARCH ARTICLE

Investigation of process parameters of electrohydrodynamic jetting for 3D printed PCL fibrous scaffolds with complex geometries

Hui Wang[1], Sanjairaj Vijayavenkataraman[2], Yang Wu[2], Zhen Shu[1], Jie Sun[1] and Jerry Fuh Ying Hsi[1,2*]

[1] NUS Suzhou Research Institute (NUSRI), No. 377 Linquan Street, Dushu Lake Science and Education Innovation District, Suzhou Industrial Park, Suzhou, Jiangsu, China 215123

[2] Department of Mechanical Engineering, National University of Singapore, 9 Engineering Drive 1, Singapore 117575

Abstract: Tissue engineering is a promising technology in the field of regenerative medicine with its potential to create tissues *de novo*. Though there has been a good progress in this field so far, there still exists the challenge of providing a 3D micro-architecture to the artificial tissue construct, to mimic the native cell or tissue environment. Both 3D printing and 3D bioprinting are looked upon as an excellent solution due to their capabilities of mimicking the native tissue architecture layer-by-layer with high precision and appreciable resolution. Electrohydrodynamic jetting (E-jetting) is one type of 3D printing, in which, a high electric voltage is applied between the extruding nozzle and the substrate in order to print highly controlled fibres. In this study, an E-jetting system was developed in-house for the purpose of 3D printing of fibrous scaffolds. The effect of various E-jetting parameters, namely the supply voltage, solution concentration, nozzle-to-substrate distance, stage (printing) speed and solution dispensing feed rate on the diameter of printed fibres were studied at the first stage. Optimized parameters were then used to print Polycaprolactone (PCL) scaffolds of highly complex geometries, i.e., semi-lunar and spiral geometries, with the aim of demonstrating the flexibility and capability of the system to fabricate complex geometry scaffolds and biomimic the complex 3D micro-architecture of native tissue environment. The spiral geometry is expected to result in better cell migration during cell culture and tissue maturation.

Keywords: 3D printing, PCL scaffolds, E-jet printing

*Correspondence to: Jerry Fuh Ying Hsi, Department of Mechanical Engineering, National University of Singapore, 9 Engineering Drive 1, Singapore 117575; Email: jerry.fuh@nus.edu.sg

Received: October 26, 2015; **Accepted:** November 24, 2015; **Published Online:** January 5, 2016

Citation: Wang H, Vijayavenkataraman S, Wu Y, *et al*., 2016, Investigation of process parameters of electrohydrodynamic jetting for 3D printed PCL fibrous scaffolds with complex geometries. *International Journal of Bioprinting*, vol.2(1): 63–71. http://dx.doi.org/10.18063/IJB.2016.01.005.

1. Introduction

Scaffolds have a significant role in tissue engineering. In brief, cells are cultured *in vitro* on a scaffold and allowed to migrate, proliferate and differentiate, which eventually attached to the scaffold and developed into a tissue. Most of the times, the engineered tissue is incubated in a bioreactor to facilitate maturation. The structure and properties of the final engineered tissue predominantly depends on the material, structure and properties of the scaffold. Many requirements are expected in order for scaffolds

to be successful in engineering a tissue[1–2], namely (i) scaffold should biomimic the native tissue environment as close as possible, (ii) material selection, should be biocompatible and biodegradable, (iii) appropriate surface chemistry to promote cell attachment, proliferation and differentiation, (iv) adequate mechanical properties, and (v) fabrication flexibility to have a variety of shapes and sizes. The utmost challenge with the current tissue engineering techniques is imitation of the native tissue environment. Traditional tissue engineering methods use 2D materials or scaffolds for cell culture and tissue construction. The main drawback of 2D substrate is that it fails to provide the cell with its native architecture. Most importantly, native tissue micro-architecture is highly complex and highly oriented due to its 3D environment. Obviously, when a 3D environment is provided rather than 2D or 2.5D, the cells grow, proliferate and differentiate closer to the native tissue[3–5]. There are several techniques to create a3D environment, such as solvent-casting particulate-leeching, gas foaming, phase separation, melt moulding, solution casting, freeze drying and emulsion freeze drying, however, they suffer from the drawback of producing only a foam structure, and not a highly controlled porous 3D micro-architecture, which leads to several other problems[6]. Though microscale fabrication technologies like soft lithography were able to create a microscale resolution scaffold[7–8], they also suffer from several limitations associated with inflexibility in fabricating complex geometries and the optimization of scaffold architecture[9]. Electrospinning is looked at as an alternate technology to fabricate nanofibrous scaffolds for tissue engineering applications[10–14] and shows a considerable progress with several reports portraying its successfulness. Nonetheless, electrospinning technology suffers from the limitation of randomly oriented fibres and inability to fabricate a controlled uniformly porous scaffolds. 3D printing is currently seen as the potential solution to fabricate layer by layer, controlled 3D porous scaffolds[6,15–19]. A new term known as 3D bioprinting has emerged recently and researchers are working towards the realization of printing functional human organs with this novel technology. An *et al*.[20] reviewed vastly on various state-of-the-art 3D printing technologies for tissue engineering applications, limitations of the current technologies and the possible future improvements. Electrohydrodynamic Jetting, which is also known as EHD-Jetting or E-jetting is one type of bioprinting technology. E-jetting has the same working principle as Electrospinning technique which is widely used to fabricate controlled porous scaffolds for tissue engineering applications[21–26]. Various studies were made on the effect of Electrospinning parameters on the electrospun fibres[27–28]. Subsequently, the most important parameters that have been identified were namely, the volumetric charge density, distance from nozzle to collector, initial jet/orifice radius, relaxation time, and viscosity[29]. Numerous novel and hybrid techniques of Electrospinning were developed in order to overcome the limitation of non-orientated random fibres from the Electrospinning process. Bu *et al*.[30] developed a mechano-electrospinning technique for fabricating oriented nanofibres and the controlled parameter was the moving speed of the substrate. Chanthakulchan *et al*.[31] developed an Electrospinning-based rapid prototyping method for fabrication of patterned scaffolds but only achieved a certain level, due to the challenges of controlling the vibration. Auyson *et al*.[32] studied the effect of various parameters of the hybrid Electrospinning / Fused Depositio Modelling (FDM) on the fabricated scaffold and concluded that two most important parameters to get a continuous jet are the voltage applied and the standoff distance between the nozzle and the substrate. On the other hand, a low voltage near-field Electrospinning method reported by Bisht *et al*.[33] was able to pattern nanofibres continuously on both 2D and 3D substrates, respectively. Besides that, other vital parameters were namely, the viscosity and elasticity of the polymer ink[34].

In this study, an E-jetting setup was built in-house in order to fabricate 3D scaffolds out of PCL material. PCL material is widely used as a biomaterial for scaffolds which possess extremely good mechanical properties. The structure of the printed scaffold depends on two important elements namely, the fibre diameter and the pore size. The parameters of the E-jetting system, i.e. the supply voltage, solution concentration, nozzle-to-substrate distance, stage (printing) speed and solution dispensing feed rate greatly influences the fibre diameter of the printed structure. Briefly, the relation between these parameters and the fibre diameter were discussed in this work. Parameters were optimized and scaffolds of complex geometries i.e. semi-lunar and spiral shapes have been successfully printed.

2. Experimental Section

2.1 Materials

Acetate (Aladdin A116171, electronic grade, >99.7%)

which is commonly referred to acetic acid was used as the solvent. Polycaprolactone (PCL) pellets with an average molecular weight of 80 kDa (Polycaprolactone, Scientific Polymer Products Inc, Ontario, NY) was used as the solute biomaterial. PCL pellets were put in the acetic acid solution (50%, 60%, 70%, 80% and 90%) (w/v) and sonicated by using an ultrasonic sonicator at 30°C and 40 kHz for 3 hours. Then, the mixture was stirred well and re-sonicated for another 1.5 hours in order to obtain a homogeneous solution. The solution was left at room temperature for a while before unloaded it into the syringe for E-jetting purpose. Polished silicon wafers with the diameter of 100 mm were used as substrates.

2.2 Experimental Setup

An E-jetting system was built in-house for the purpose of fabrication of scaffolds. The schematic diagram of the experimental setup and the actual system are shown in Figure 1 and Figure 2, respectively. The main components of the system are namely, the high voltage power source, a high precision XYZT stage along with the controller, a syringe pump and a computer. The software for stage control, connecting tubes, syringes and needles are other components. A 13 mm internal diameter syringe and 0.5 mm internal diameter needle were used in all the experimental trials. The high precision stage, purchased from Aerotech Company (Pittsburgh, PA, USA) was driven by linear motors. The X and Y axis has the travel distance of up to 150 mm and can be precisely controlled up to 3 μm, while the Z axis has the travel distance of 50 mm and can be precisely controlled up to 5 μm. Ensemble

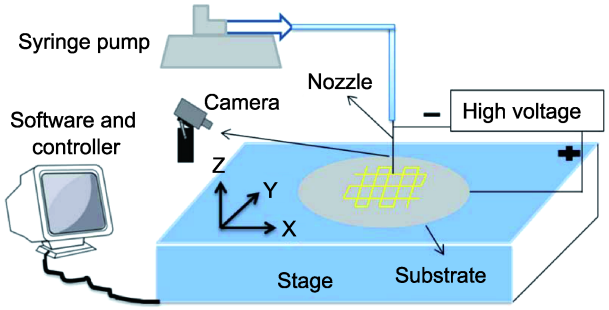

Figure 1. Conceptual diagram of E-jetting system.

IDE is the software that controls the movement of the XYZT stage through a communication interface, which also gives the real-time position and velocity information for effective monitoring and control.

The working principle is based on the balance between the electrostatic force and the combined surface tension and viscoelastic force of the liquid. A high voltage (DC) is applied between the nozzle and the substrate, typically in the order of 2–3 kV. The surface tension force of the liquid at the nozzle tip was overcome by the electrostatic force between the nozzle and substrate, hence forcing the solution to come out of the nozzle and printed onto the substrate. The whole process happens in two stages. The first stage was the formation of the Taylor cone at the apex of the conical meniscus, due to which the electric field stretches the liquid. Then it progresses to the second stage of Rayleigh-Plateau instability. As the electric field force increases, Rayleigh-Plateau instability becomes larger than the combined surface tension and viscoelastic force, while a jet of liquid is formed and ejected continuously onto the substrate. The substrate

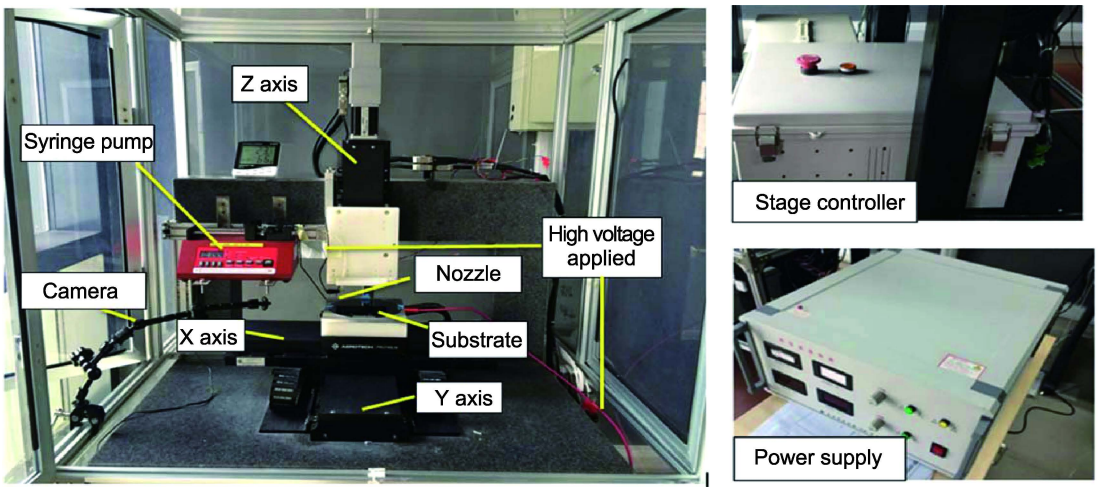

Figure 2. In-house E-jetting system.

was placed on the XYZT stage and moved in accordance to the computer program pertaining to the desired geometry, pore size and number of layers. A square-mesh pattern is used for the optimization studies of various parameters and its effects on the fibre diameter. The traverse path of square-mesh scaffolds is shown in Figure 3.

2.3 Characterization of Fibrous Scaffolds

The morphology of fibre was analysed under an Optical Microscope (OLYMPUS, BX51M) and FESEM (FEI Quanta 250 FEG, FEI Inc, OR, USA) at an accelerating voltage of 15 kV. Acceleration voltage is the voltage in which the electrons are accelerated down the SEM column. In other words, it is the highest voltage applied to the filament. The higher the accelerating voltage, the faster the electrons travel down the column and the more penetrating power they have, reducing spherical abberation of the system and thereby increasing the resolution. The diameter of the fibre was measured both using the optimal microscope images (MShot Digital Imaging System software) and FESEM. Six measurements were made and the average value was calculated. The images from optical microscope and SEM are shown in Figure 4. The sample size for each data point for all the experiments was three whereas the standard deviation (SD) was less than 20 μm. In fact, most of the data points had a SD of 2–5 μm.

3. Results and Discussion

3.1 Effect of Stage Speed on Fibre Diameter

The effect of varying stage speed on fibre diameter is shown in Figure 5. Stage speed is varied from 10 mm/s to 140 mm/s, while all other parameters are kept constant (Fd = 6 μL/min, D = 3 mm, V = 3 kV), at two different solution concentrations (C) viz. 50% and 70% w/v. As expected, the size of the fibre diameter decreased with the increment of stage speed. This is due to the fact that at higher speed, the duration of e-jetting at a particular point of substrate have lessened and the fibre's diameter was also reduced naturally. However, at very high speeds, discontinuous fibres resulted. This might be because of the fact that the frictional force between the jetted fibre and the substrate increases greatly at very high speeds, which at a certain critical value exceeds the viscoelastic force and hence results in discontinuous fibres. In other words, when the stage speed was increased to more than 160 mm/s, the traction force caused by the adhesion in-between the nozzle and substrate could exceed the viscoelastic force of the PCL fibre, thus resulting in the formation of discontinuous fibres

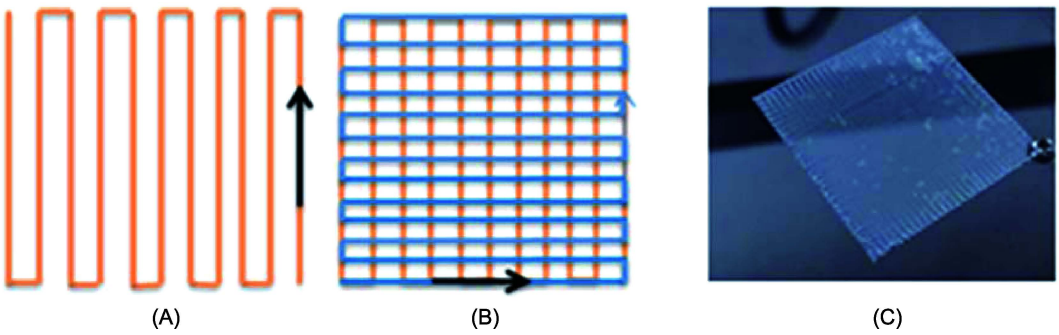

Figure 3. Traverse path of the square-mesh scaffold, **(A)** first layer **(B)** second layer **(C)** E-jetted square- mesh PCL scaffold, 40 x 40 mm, pore size of 0.5 x 0.5 mm and fibre diameter of 100 μm.

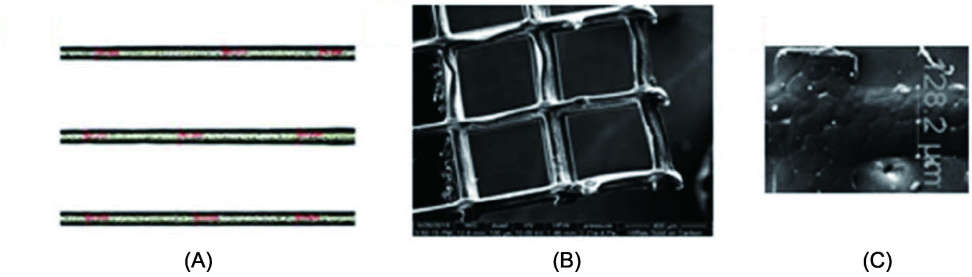

Figure 4. Characterization of fibre through **(A)** Optical Microscope and **(B)** SEM. **(C)** A closer view of the SEM measurement.

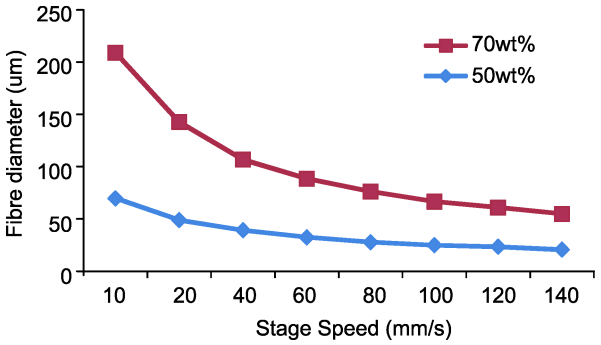

Figure 5. Effect of stage speed on fibre diameter.

or no fibre being attached onto the substrate. On top of that, the effect of stage speed on fibre diameter was found to be different at various solution concentrations. With increase in concentration the fibre diameter is larger, at the same stage speed . As seen from Figure 5, at a particular stage speed, the fibre diameter of 70% w/v solution is much higher than that of 50% w/v solution. On an average, the difference is more than 40%, which is predominantly due to the increase in the viscoelastic force, with increase in the concentration. The effect was more pronounced at lower speeds and the differences were narrowed down slowly as the stage speed increases, which apparently prove the same fact.

3.2 Effect of Solution Feed Rate on Fibre Diameter

The feed rate at which the solution was delivered by the syringe pump to the nozzle and onto the substrate plays a significant role in determining the final fibre diameter. Figure 6 shows the relationship between the solution feed rate and fibre diameter. The solution feed rate was varied from 4 to 20 µL/min, while the other parameters were kept constant (D = 2.5 mm, V = 3 kV and S = 150 mm/s). The study was conducted in three different solution concentrations (60%, 70% and 90%) (w/v). The fibre diameter increased with increase in solution feed rate, as expected. At the same stage speed and voltage, when the feed rate is increased, the amount of solution that is e-jetted out of the nozzle per unit of time will also increase, thereby resulting in deposition of an increased volume of solution on the substrate and hence, the fibre diameter also increases. Also, at the same feed rate, solutions with higher concentration resulted in greater fibre diameter than the solution with lower concentration, which is due to the dominant viscoelastic force as discussed in the previous section. One important observation to make is that at very high concentration (90% w/v), the effect of solution feed rate is much less pronounced compared to the low concentration solutions. To put it in other words, for the same range of feed rate variation (4–20 µL/min), the variation range of fibre diameter is larger in low concentration solutions (50 µm to as large as 200 µm), whereas the fibre diameter range is considerably lesser in high concentration solution (100 µm to 140 µm only). This is attributed to the reason that the viscoelastic force due to the higher solution concentration is so dominant that the effect of increased feed rate becomes very less.

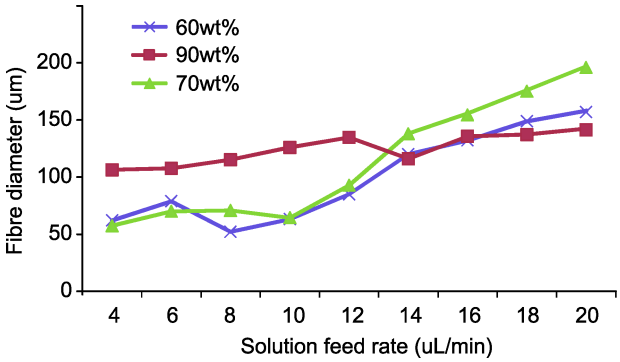

Figure 6. Effect of solution feed rate on fibre diameter.

3.3 Effect of Supply Voltage on Fibre Diameter

Supply voltage is a very important parameter in the E-jetting process, not only for the integrity of the fibre structure but also a safety concern. Too high values may result in sparking, eventually leading to greater safety risks. It is important to know the effect of supply voltage on fibre diameter so as to not exceed a certain value for safety reasons. The relationship between the supply voltage and the fibre diameter is shown in Figure 7. Voltage is varied from 2 kV to 3.5 kV, in small steps, with all other parameters constant (D = 2.5 mm, Fd = 10µL/min, S = 150 mm/s) and at three different solution concentrations (60% w/v, 70% w/v and 80% w/v). Voltage values below 2 kV resulted in discontinuous jet formations because of the inability of the electric field force to overcome the surface tension and viscoelastic force of the solution. The relationship is not well established and the trend is not regular. However, two regions could be identified. In the first region, at lower voltages, a small change in voltage resulted in a major change in the fibre diameter, For instance, at a solution concentration of 60% w/v, when the voltage is increased from 2 to 2.4 kV, the diameter increased from 20 to 100 µm and at solution concentration of 70%

w/v, when the voltage is increased from 2 to 2.4 kV, the diameter increased from 55 to 95 µm. This is followed by the second region, where the effect of increased voltage has less pronounced effect on the fibre diameter. This may be due to the reason that in region one, there lies the transition point at which the electric field force reaches a critical value and when it exceeds the combined effect of surface tension and viscoelastic forces. However, at a higher solution concentration, the trend looks murky and no stable pattern and the effect is also less pronounced, due to the dominant viscoelastic force. This may also be attributed to the complex interaction between the supply voltage and nozzle-to-substrate distance, which goes hand in hand.

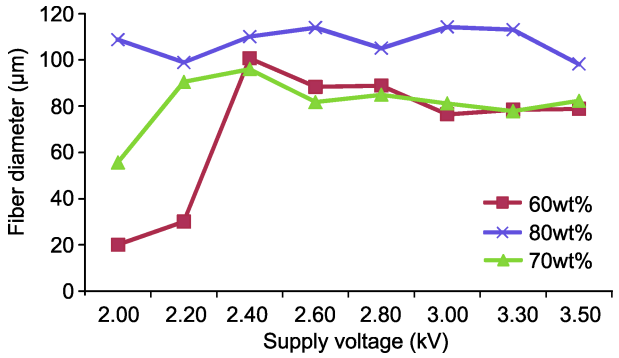

Figure 7. Effect of supply voltage on fibre diameter.

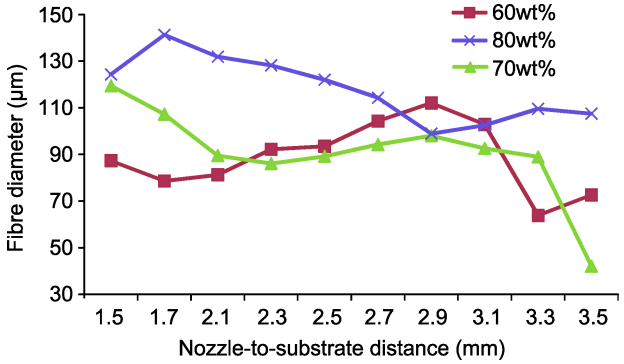

Figure 8. Effect of nozzle-to-substrate distance on fibre diameter.

3.4 Effect of Nozzle-to-substrate Distance on Fibre Diameter

Another important parameter which plays a significant role in the E-jetting process is the gap between the nozzle and the substrate. This parameter works relative to the supply voltage, i.e., if the gap is very small, applying a higher voltage will result in sparking and if the gap is very large, a very high voltage is required to overcome the surface tension and viscoelastic forces of the solution. The relationship between the nozzle-to-substrate distance and the fibre diameter is shown in Figure 8. Nozzle-to-substrate distance is varied from 1.5 to 3.5 mm, in small steps, with all other parameters constant (V = 2.5 kV, Fd = 10µL/min, S = 150 mm/s) and at three different solution concentrations (60% w/v, 70% w/v and 80% w/v). Values below 1.5 mm resulted in sparking. The observed relationship has no regular trend. But certain important observations can be made. While at lower values of gap, the fibre diameter increases at some concentrations and decreases at some other concentrations when the gap is increased, eventually there is a plateau region, where the fibre diameter doesn't vary much and is stable. After a certain higher value of nozzle-to-substrate distance, the fibre diameter tends to decrease drastically. This is due to the reason that when the gap is larger, at the same supply voltage, the electric field force at the nozzle tip reduces greatly and hence unable to overcome the surface tension and viscoelastic forces and also the fibres were not very stable and discontinuous. The trend is a bit different at very high solution concentration; in the plateau (middle) region where for other lower concentrations (60% w/v, 70% w/v) the fibre diameter does not vary much, it decreases in the higher concentration solution (80% w/v), again due to the dominant viscoelastic force.

3.5 3D Printing of PCL Scaffolds with Complex Geometries

From the parametric study, the E-jetting process was optimized and range for each parameter is obtained so as to get stable, continuous E-jetting fibres. The concentration of the PCL solution was fixed at 70% w/v, stage speed at 150 mm/s, supply voltage 2.5 to 3 kV, solution feed rate 4-10µL/min and nozzle -to-substrate distance 2.5 or 3 mm for all the subsequent experimental trials. Scaffolds of different geometries, with complex architecture were printed. Semi-lunar or curved scaffolds are printed as shown in Figure 9. This geometry is necessary for reconstruction of soft tissues especially the knee meniscus[35]. The E-jetting parameters were C = 70%, Fd = 8uL/min, V = 3 kV, S = 150 mm/s and D = 2.5 mm. Several trials were made and the fibre diameter measured was 90 ± 5 µm. A novel spiral scaffold was also printed as shown in Figure 10 for the first time. The E-jetting parameters were, for Figure 10C, C = 70%, Fd = 6 uL/min, V = 2.5 kV, S = 100 mm/s and D = 3 mm, and for Figure 10D, C = 70%, Fd = 0.4 uL/min, V = 2.55 kV, S = 100 mm/s and

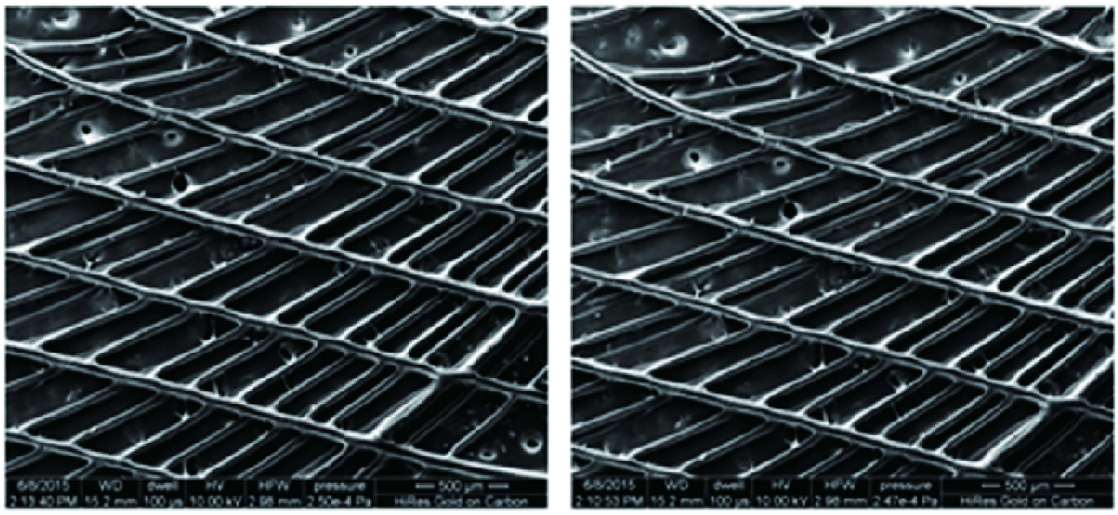

Figure 9. SEM Images of semi-lunar PCL scaffolds.

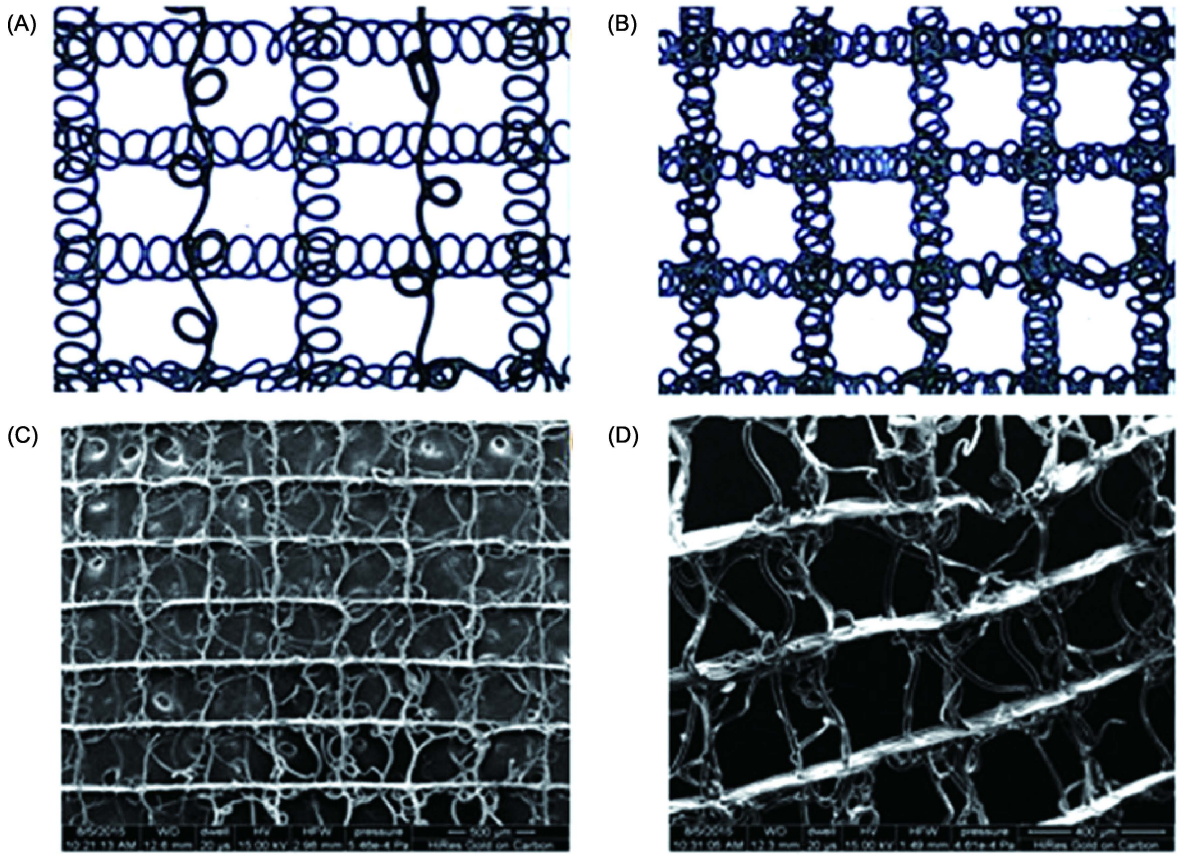

Figure 10. (A) & **(B)** Conceptual images of spiral scaffold. **(C)** & **(D)** SEM Images of spiral PCL scaffolds.

D = 3 mm. Different types of cells show different proliferation responses to the environment. Spiral scaffolds may be suitable for tissue engineering of soft tissues, with the spiral design improving the cell migration and formation of cell-cell junctions.

4. Conclusion

Development of the field of tissue engineering and successful clinical translation of this technology depends on how closely the engineered tissue biomimic

the native tissue architecture. 3D printing of scaffolds for tissue engineering and 3D Bioprinting are relatively new technologies which have the potential to meet this requirement. In this study, E-jetting process is studied in detail and the effect of various parameters on the printed fibre diameter analysed, pertaining to PCL biomaterial. The relationship between these parameters, in combination, is complex. Hence, a detailed parametric study has to be performed for finding the optimum parameters of E-jetting to print stable, regular, continuous fibres and hence scaffolds with good structural and spatial properties. In fact, the greatest advantage of this technology is the patterning and orientation of fibres in a controlled manner in desired architecture. The complex geometries like semi-lunar and spiral shaped scaffolds are printed using this technique, which will be very useful for certain complex soft tissues in body like the knee meniscus or tendon. These different complex shapes are also expected to influence the cell proliferation positively, in terms of better cell migration within the scaffold and formation of cell-cell junctions, which has to be validated by future in vitro studies. Development of the field of tissue engineering and successful clinical translation of this technology depends on how closely the engineered tissue biomimic the native tissue architecture. Both 3D printing of scaffolds for tissue engineering and 3D bioprinting are relatively new technologies which have the potential to meet this requirement. In this study, E-jetting process is studied in detail and the effect of various parameters on the printed fibre diameter analyzed, pertaining to PCL biomaterial. The relationship between these parameters, in combination, is complex. Hence, a detailed parametric study has to be performed for finding the optimum parameters of E-jetting process to print stable, regular, continuous fibres and hence scaffolds with good structural and spatial properties. In fact, the greatest advantage of this technology is the patterning and orientation of fibres in a controlled manner in desired architecture. The complex geometries like semi-lunar and spiral shaped scaffolds are printed using this technique, which will be very useful for certain complex soft tissues in body like the knee meniscus or tendon. These different complex shapes are also expected to influence the cell proliferation positively, in terms of better cell migration within the scaffold and formation of cell-cell junctions, which has to be validated by future *in vitro* studies.

Conflict of Interest and Funding

No conflict of interest was reported by the authors.

References

1. Hutmacher D W, 2001, Scaffold design and fabrication technologies for engineering tissues — state of the art and future perspectives. *Journal of Biomaterials Science, Polymer Edition*, vol.12(1): 107–124. http://dx.doi.org/10.1163/156856201744489
2. Hutmacher D W, Schantz T, Zein I, *et al*., 2001, Mechanical properties and cell cultural response of polycaprolactone scaffolds designed and fabricated via fused deposition modelling. *Journal of Biomedical Materials Research*, vol.55(2): 203–216. http://dx.doi.org/10.1002/1097-4636(200105)55:23.0.CO;2-7
3. Cukierman E, Pankov R, Stevens D R, *et al*., 2001, Taking cell-matrix adhesions to the third dimension. *Science*, vol.294(5547): 1708–1712. http://dx.doi.org/10.1126/science.1064829
4. Cukierman E, Pankov R and Yamada K M, 2002, Cell interactions with three-dimensional matrices. *Current Opinion in Cell Biology*, vol.14(5): 633–640. http://dx.doi.org/10.1016/S0955-0674(02)00364-2
5. Edelman D B and Keefer E W, 2005, A cultural renaissance: *In vitro* cell biology embraces three-dimensional context. *Experimental Neurology*, vol.192(1): 1–6. http://dx.doi.org/10.1016/j.expneurol.2004.10.005
6. Sachlos E and Czernuszka J T, 2003, Making tissue engineering scaffold work: Review on the application of SFF technology to the production of tissue engineering scaffolds. *European Cells and Materials*, vol.5(1): 29–40.
7. Whitesides G M, Ostuni E, Takayama S, *et al*., 2001, Soft lithography in biology and biochemistry. *Annual Review of Biomedical Engineering*, vol.3(1): 335–373. http://dx.doi.org/10.1146/annurev.bioeng.3.1.335
8. Walker G M, Zeringue H C and Beebe D J, 2004, Microenvironment design considerations for cellular scale studies. *Lab on a Chip*, vol.4(2): 91–97. http://dx.doi.org/10.1039/b311214d
9. Khademhosseini A, Langer R, Borenstein J, *et al*., 2006, Microscale technologies for tissue engineering and biology. *Proceedings of the National Academy of Sciences of the United States of America*, vol.103(8): 2480–2487. http://dx.doi.org/10.1073/pnas.0507681102
10. Lannutti J, Reneker D, Ma T, *et al*., 2007, Electrospinning for tissue engineering scaffolds. *Materials Science and Engineering: C*, vol.27(3): 504–509. http://dx.doi.org/10.1016/j.msec.2006.05.019
11. Agarwal S, Wendorff J H and Greiner A, 2009, Progress in the field of electrospinning for tissue engineering applications. *Advanced Materials*, vol.21(32–33): 3343–3351. http://dx.doi.org/10.1002/adma.200803092

12. Li W J, Laurencin C T, Caterson E J, *et al*., 2002, Electrospun nanofibrous structure: A novel scaffold for tissue engineering. *Journal of Biomedical Materials Research*, vol.60(4): 613–621. http://dx.doi.org/10.1002/jbm.10167
13. Sill T J and von Recum H A, 2008, Electrospinning: Applications in drug delivery and tissue engineering. *Biomaterials*, vol.29(13): 1989–2006. http://dx.doi.org/10.1016/j.biomaterials.2008.01.011
14. Yang F, Murugan R, Wang S, *et al*., 2005, Electrospinning of nano/micro scale poly (L-lactic acid) aligned fibers and their potential in neural tissue engineering. *Biomaterials*, vol.26(15): 2603–2610. http://dx.doi.org/10.1016/j.biomaterials.2004.06.051
15. Richards D J, Tan Y, Jia J, *et al*., 2013, 3D printing for tissue engineering. *Israel Journal of Chemistry*, vol.53(9–10): 805–814. http://dx.doi.org/10.1002/ijch.201300086
16. Mironov V, Boland T, Trusk T, *et al*., 2003, Organ printing: Computer-aided jet-based 3D tissue engineering. *Trends in Biotechnology*, vol.21(4): 157–161. http://dx.doi.org/0.1016/S0167-7799(03)00033-7
17. Hollister S J, 2005, Porous scaffold design for tissue engineering. *Nature Materials*, vol.4(7): 518–524. http://dx.doi.org/10.1038/nmat1421
18. Boland T, Xu T, Damon B, *et al*., 2006, Application of inkjet printing to tissue engineering. *Biotechnology Journal*, vol.1(9): 910–917. http://dx.doi.org/10.1002/biot.200600081
19. Yeong W Y, Chua C K, Leong K F, *et al*., 2004, Rapid prototyping in tissue engineering: Challenges and potential. *Trends in Biotechnology*, vol.22(12): 643–652. http://dx.doi.org/10.1016/j.tibtech.2004.10.004
20. An J, Teoh J E M, Suntornnond R, *et al*., 2015, Design and 3D printing of scaffolds and tissues. *Engineering*, vol.1(2), 261–268. http://dx.doi.org/10.15302/J-ENG-2015061
21. Gupta A, Seifalian A M, Ahmad Z, *et al*., 2007, Novel electrohydrodynamic printing of nanocomposite biopolymer scaffolds. *Journal of Bioactive and Compatible Polymers*, vol.22(3), 265–280. http://dx.doi.org/10.1177/0883911507078268
22. Wei C and Dong J, 2013, Direct fabrication of high-resolution three-dimensional polymeric scaffolds using electrohydrodynamic hot jet plotting. *Journal of Micromechanics and Microengineering*, vol.23(2): 025017. http://dx.doi.org/10.1088/0960-1317/23/2/025017
23. Ahmad Z, Rasekh M and Edirisinghe M, 2010, Electrohydrodynamic direct writing of biomedical polymers and composites. *Macromolecular Materials and Engineering*, vol.295(4): 315–319. http://dx.doi.org/10.1002/mame.200900396
24. Li J L, Cai Y L, Guo Y L, *et al*., 2014, Fabrication of three-dimensional porous scaffolds with controlled filament orientation and large pore size via an improved E-jetting technique. *Journal of Biomedical Materials Research Part B: Applied Biomaterials*, vol.102(4): 651–658. http://dx.doi.org/10.1002/jbm.b.33043
25. Gasperini L, Maniglio D, Motta A, *et al*., 2014, An electrohydrodynamic bioprinter for alginate hydrogels containing living cells. *Tissue Engineering Part C: Methods*, vol.21(2): 123–132. http://dx.doi.org/10.1089/ten.TEC.2014.0149
26. Cai Y, Li J L, Poh C K, *et al*., 2013, Collagen grafted 3D polycaprolactone scaffolds for enhanced cartilage regeneration. *Journal of Materials Chemistry B*, vol.1(43): 5971–5976. http://dx.doi.org/0.1039/C3TB20680G
27. Doshi J and Reneker D H, 1993, Electrospinning process and applications of electrospun fibers, In *Industry Applications Society Annual Meeting, Conference Record of the 1993 IEEE*: 1698–1703.
28. Mitchell G R, Ahn K H and Davis F J, 2011, The potential of electrospinning in rapid manufacturing processes. *Virtual and Physical Prototyping*, vol.6(2): 63–77. http://dx.doi.org/10.1080/17452759.2011.590387
29. Thompson C J, Chase G G, Yarin A L, *et al*., 2007, Effects of parameters on nanofiber diameter determined from electrospinning model. *Polymer*, vol.48(23): 6913–6922. http://dx.doi.org/10.1016/j.polymer.2007.09.017
30. Bu N, Huang Y, Wang X, *et al*., 2012, Continuously tunable and oriented nanofiber direct-written by mechano-electrospinning. *Materials and Manufacturing Processes*, vol.27(12): 1318–1323. http://dx.doi.org/10.1080/10426914.2012.700145
31. Chanthakulchan A, Koomsap P, Auyson K, *et al*., 2015, Development of an electrospinning-based rapid prototyping for scaffold fabrication. *Rapid Prototyping Journal*, vol.21(3): 329–339. http://dx.doi.org/10.1108/RPJ-11-2013-0119
32. Auyson K, Koomsap P, Chanthakulchan A, *et al*., 2013, Investigation of applying electrospinning in fused deposition modeling for scaffold fabrication. In High Value Manufacturing: Advanced Research in Virtual and Rapid Prototyping, *Proceedings of the 6th International Conference on Advanced Research in Virtual and Rapid Prototyping*, CRC Press: 149.
33. Bisht G S, Canton G, Mirsepassi A, *et al*., 2011, Controlled continuous patterning of polymeric nanofibers on three-dimensional substrates using low-voltage near-field Electrospinning. *Nano Letters*, vol.11(4): 1831–1837. http://dx.doi.org/10.1021/nl2006164
34. Chang C, Limkrailassiri K and Lin L, 2008, Continuous near-field electrospinning for large area deposition of orderly nanofiber patterns. *Applied Physics Letters*, vol.93(12): 123111. http://dx.doi.org/10.1063/1.2975834
35. Li J L, Guo Y L, Thian E S, *et al*., 2013, 3-Dimensional meniscal fibrillar scaffolds, apparatus and process for the fabrication thereof, UK Patent filing, 2013. Application No. 1315074.3.

RESEARCH ARTICLE

Microstereolithography-fabricated microneedles for fluid sampling of histamine-contaminated tuna

Ryan D. Boehm[1], Panupong Jaipan[2], Kai-Hung Yang[2], Thomas N. Stewart[3] and Roger J. Narayan[1,2*]

[1] Joint Department of Biomedical Engineering, University of North Carolina and North Carolina State University, Box 7115, Raleigh NC 27695, USA

[2] Department of Material Science Engineering, North Carolina State University, Box 7907, Raleigh, NC 27695, USA

[3] Mercury Science Inc., Raleigh, NC 27607, USA

Abstract: A custom-designed microneedle sampling system was prepared using dynamic mask microstereolithography; this sampling system was used for determination of histamine content in fresh, histamine-spiked, and spoiled tuna flesh. Lateral flow (test strip) assays were successfully utilized in the microneedle sampling system to assess histamine content. Good agreement was noted between data obtained from the microneedle sampling system and a commercially available histamine detection kit. A discrepancy was noted in the results from the microneedle sampling system and the commercially available histamine detection kit at low (negative) levels of histamine. There was an improvement in the agreement between the microneedle sampling system and the commercially available histamine detection kit at higher histamine levels. The results, which showed an improvement in the test duration and the amount of reagent needed for histamine detection, indicate the promise of printed microneedle sampling systems for histamine detection in seafood samples and other types of food testing.

Keywords: microneedles, dynamic mask microstereolithography, histamine, lateral flow, tuna

*Correspondence to: Roger J. Narayan, Joint Department of Biomedical Engineering, University of North Carolina and North Carolina State University, Box 7115, Raleigh NC 27695, USA; Email: roger_narayan@msn.com

Received: November 18, 2015; **Accepted:** December 22, 2015; **Published Online:** December 30, 2015

Citation: Boehm R D, Jaipan P, Yang K-H, *et al*., 2016, Microstereolithography-fabricated microneedles for fluid sampling of histamine-contaminated tuna. *International Journal of Bioprinting*, vol.2(1): 72–80. http://dx.doi.org/10.18063/IJB.2016.01.010

1. Introduction

Food poisoning is a concern when consuming fish that has been exposed to elevated temperatures for extended periods of time. Histamine fish poisoning is one of the most common types of seafood consumption-related illnesses in the United States[1]. Histamine fish poisoning (HFP), which is sometimes referred to as scrombroid fish poisoning, is associated with mishandling of the *Scrombridae* family of fish (e.g., tuna and mahi-mahi), which have high levels of histidine in their muscles[2]. A biogenic amine known as histamine is formed during bacterial decarboxylation of histidine in the raw fish[3–5]. Although histamine is naturally present in humans and humans possess a protective mechanism in the digestive tract to handle small amounts of consumed histamine, ingestion of tainted fish with high levels of histamine may overwhelm the protective mechanism and result in histamine intoxication, which resembles an allergic reaction[6,7]. Histamine levels that are greater than or equal to 500 mg/kg of fish tissue are noted to be toxic when ingested[8]; the United States Food & Drug Administration has set the acceptability limit at 50 mg/kg[9]. It is concerning to note that fish with unacceptable levels of histamine may not exhibit a different appearance or emit a different odor than fish that has not been compromised[8,10]. Furthermore, heating fish to

normal cooking temperatures does not necessarily alter the histamine levels within the fish[1].

Due to concerns associated with histamine contamination of fish, a number of methods have been developed to screen fish flesh and ensure that it does not contain dangerous levels of histamine. Screening of histamine levels in fish may be conducted using a variety of methods, including high purity liquid chromatography (HPLC)[11], enzymatic test kits, enzyme-linked immunosorbent assays (ELISA), and lateral flow immunochromatographic test strips[12]. The lateral flow test strips are particularly useful for fieldwork since they do not require complex equipment for analysis. Lateral flow tests, sometimes referred to as dipsticks, are used in many environmental and healthcare applications (e.g., colorimetric pregnancy tests)[13]. For example, lateral flow tests have been used for botulinum neurotoxin, aflatoxin B1, and virus detection[14–17]. One such lateral flow test is the Reveal® for Histamine test kit (Neogen® Corporation, Lansing, MI, USA), which can screen for histamine in tuna and mahi-mahi; the Reveal® for Histamine test kit was used as the histamine detection mechanism in this study.

One procedure that is described in many histamine detection methods is homogenization of fish flesh; most assays are performed on fluid extracts from the homogenized fish flesh. In this study, we investigated use of a microstereolithography-prepared microneedle sampling system for detecting histamine in fish flesh. Systems containing microneedle arrays have previously been developed for sampling of analytes in transdermal blood and/or interstitial fluid[18–20]. For instance, systems containing microneedles arrays have been developed for detection of glutamate[21], glucose[22,23], and potassium ions[24]. In this study, microneedle arrays were used as a sampling mechanism for detection of histamine in fish flesh. Visible light dynamic mask microstereolithography was used to prepare customized microneedle arrays; this approach has been previously used to create microneedle arrays for drug delivery[25–28] and biosensing applications[21,29]. Reveal® for Histamine lateral flow test strips were integrated with the microneedle sampling system. Flesh from fresh, histamine-spiked, and spoiled tuna was examined with the microneedle sampling system; the results from the microneedle sampling system were compared to results from the manufacturer's protocol that involved homogenization of tuna flesh.

2. Materials and Methods

2.1 Microneedle and Lateral Flow Test Holder

To sample the tuna flesh for histamine, arrays of microneedles were used to capture fluid from the tuna samples. A custom lateral flow test strip holder was designed to stabilize a microneedle array, allowing the sampled fluid to be washed off of the microneedle array and into a reservoir for wetting of a lateral flow test (Figure 1). Both of these components were custom designed using computer-aided design software (SolidWorks Education Edition 2014–2015, Dassault Systémes SolidWorks Corporation, Concord, NH, USA). The microneedle arrays were composed of nine offset microneedles, which exhibited a thin pyramidal shape and a trapezoidal eyelet design to capture fluid (Figure 1A). The test strip and microneedle holder (Figure 1C) was designed with three chambers: (i) a washed sample reservoir for placement of the lateral flow test, (ii) the microneedle holder/wash chamber, and (iii) an

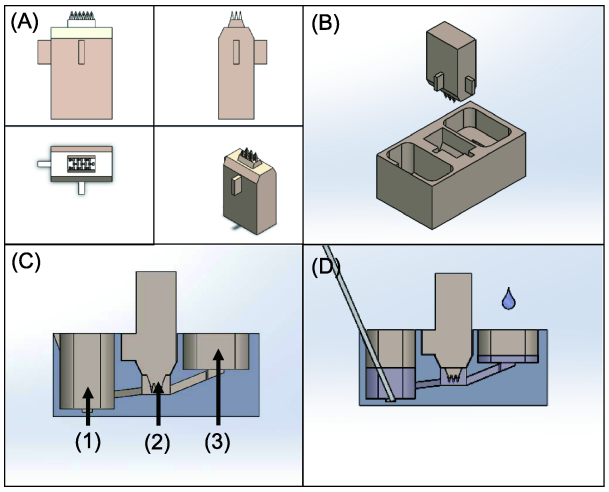

Figure 1. Computer aided design schematic of the microneedle array and the custom lateral flow test holder. **(A)** Front, left, top, and isometric views of the microneedle design are shown clockwise from upper left position. **(B)** Insertion of the microneedle into the central chamber of the test strip holder following application of the microneedle array to the tuna sample. **(C)** Section view of the custom test strip holder showing: (1) the washed sample reservoir for the test strip, (2) the central chamber holding the microneedle array in place, and (3) the inlet port for the sample diluent. **(D)** The sample diluent is added to the port at site (3), where it runs through the channel to (2) the central chamber, washing the acquired sample from the microneedle array into the reservoir at site (1). The lateral flow test strip is placed into the groove at site (1) and is wetted by the microneedle array wash/diluent at the beginning of the screening test.

inlet port for the sample diluent.

The devices were fabricated using a photosensitive acrylate-based, class-IIa biocompatible polymer known by the tradename eShell 200 (Envisiontec, Ferndale, USA)[30]. This material was polymerized into the desired component geometries based on STL files, which were created using computer aided design software. A Perfactory III SXGA+ visible light dynamic mask microstereolithography system with an Enhanced Resolution Module (EnvisionTEC GmbH, Gladbeck, Germany) was utilized to fabricate the devices in an additive layer-by-layer manner. A z-direction step size of 50 µm was used to build the devices; the dynamic mask was illuminated with visible light at a lamp power of 550 mW.

Following the microstereolithography step, the devices were rinsed with isoproponal 2–3 times and dried with compressed air. The test strip holders were immersed in isopropanol for 15 minutes and sonicated in an ultrasonic bath. The parts were then removed, dried with compressed air, and hand-rinsed with isopropanol as needed to remove unpolymerized resin. Both types of devices were dried in a heated chamber at 30°C for at least 30 minutes before undergoing a post curing procedure. For post curing, the parts were loaded into an Otoflash Post Curing Light Pulsing Unit (EnvisionTEC GmbH, Gladbeck, Germany) and exposed to two sets of 2000 light pulses. This units utilizes light pulses in the 300–700 nm spectral range at 10 Hz to polymerize residual unpolymerized material within the devices[31]. The devices were imaged with a VHX-5000 optical microscope (Keyence, Itaska, IL, USA).

2.2 Fish Preparation

Tuna steaks that were cut to a 1-inch thickness were used to perform histamine testing. The tuna samples were acquired from a local fresh fish market. To calibrate the microneedle testing procedure, tuna pieces were incubated overnight in histamine solutions within vacuum seal bags in a refrigerator. Pieces of tuna were trimmed to ~100 g pieces and loaded into individual vacuum seal bags. Histamine (Sigma-Aldrich Co. LLC, St. Louis, MO, USA) solutions were prepared in 1 × phosphate buffered saline (PBS) to 0.5 mg/mL and 1.0 mg/mL concentrations; 1 × PBS alone was used as a negative control. A volume of 5 mL of each of these solutions was added to individual vacuum bags containing the tuna and zip-sealed; most of the air in the bags was then removed. The tuna samples were incubated overnight with the histamine solutions in a 4°C refrigerator.

In addition, tuna samples were prepared for a time course examination, which involved placing samples in the refrigerator for up to seven days. Tuna steaks again were cut into approximately 100 g individual pieces, placed into vacuum bags, and zip sealed; in this study, the bags were not vacuumed to remove air. Five time points were used to measure the fish spoilage over the course of the seven day period. For the "Day 0" time point, a piece of tuna flesh was immediately frozen. Tuna flesh from days 1, 3, 5, and 7 were also removed from incubation in the refrigerator and frozen for histamine testing at a later time.

Lastly, a piece of spoiled tuna was examined with the microneedle sampling system procedure and the manufacturer-described procedure to obtain a comparison between the two procedures. The tuna flesh for this study was stored in a vacuum sealed bag containing 1 × PBS with the air removed by vacuum; the sample was then placed in a refrigerator overnight. The tuna flesh was originally designated as a negative control during the calibration steps described above; however, it was determined that the tuna flesh was spoiled upon acquisition from the source. This occurrence provided an opportunity to study a tuna flesh sample acquired from a commercial source in an authentic spoilage scenario.

2.3 Histamine Testing Procedure

To conduct the histamine screening, colorimetric lateral flow tests were acquired as components of Reveal® for Histamine screening test kits (Neogen® Corporation, Lansing, MI, USA), which provide a detection threshold of 50 ppm. For the microneedle sampling system procedure, the microneedle array was pressed into the tuna sample for 5 seconds to acquire a fluid sample. The microneedle array was then placed into the test strip holder as seen in Figure 1. With the microneedle array in place, 1000 µL of the sample diluent provided in the test kit was added to the input port of the test strip holder. This fluid flowed over the microneedle array, washing the test fluid sample into the reservoir, where one of the Reveal® test strips was placed to begin the screening. The test strip was allowed to incubate in the sample fluid for 10 minutes or less before the result was determined.

To more objectively compare positive test results and negative test results, an Accuscan® Gold (Neogen® Corporation, Lansing, MI, USA) test strip reader

was used to optically measure the intensities of the colored test and control lines in the lateral flow strip. Each test strip has colored control and test lines that appear upon introduction of a fluid sample. The ratio of the color intensities of these lines was used to assess if a sample was positive or negative for histamine at the 50 ppm level. The Accuscan® reader provided a ratiometric readout of the lines, which was used to differentiate between a positive result and a negative result. If the ratio of the test:control lines was greater than or equal to one, the test was read as negative for histamine. If the ratio of the test:control lines was less than one, the test was read as positive for histamine. For each test lateral flow strip, three measurements were taken in short succession with the reader; the average ratio was used to determine positive versus negative for the individual strip. For the calibration studies with the 1 × PBS, 0.5 mg/mL histamine, and 1.0 mg/mL histamine solutions, nine test strips were used for each type of tuna sample. Five test strips were used for the time course study. Four test strips for each method were used in the time course study.

For the calibration studies and the spoiled fish study, the protocol[32] described by the Reveal® for histamine test kits was used to validate the findings of the microneedle sampling system procedure. Briefly, the procedure involved acquiring a 10 g piece of tuna flesh, blending the tuna flesh in a food prep blender until it was homogenized, and adding 190 mL of deionized water to the blended sample. The sample was then hand-shaken for 20 seconds and allowed to rest for 5 minutes; the shaking and resting sequence was then repeated. Immediately prior to sampling the blended fluid, the container was shaken; the tuna sample was allowed to settle in the suspension and 100 µL of fluid was removed. This 100 µL sample was added to a bottle containing sample diluent and then mixed. 200 µL of fluid was removed from the sample diluent bottle provided in the test kit; this fluid was added to a small sample cup, which contained a lateral flow test strip. The lateral flow test strip was allowed to develop in the solution for at least 5 minutes and then evaluated with the Accuscan® reader. A positive result from the Accuscan® reader indicated that the sample contained greater than 50 ppm of histamine.

3. Results and Discussion

3.1 Microneedle and Test Holder Fabrication

The microstereolithography process was successful in creating (a) the microneedle arrays for sample acquisition from the tuna samples, (b) the microneedle holder, and (c) the lateral flow test holder. As seen in Figure 2A–C, the microneedles were arranged in staggered 3 × 3 rows in each microneedle sampling system. The trapezoidal eyelet extending from the microneedle base toward the microneedle tip served as a capture point for fluid from the tuna sample. The microneedles had heights of 1150 µm and base widths of 950 µm. Figure 2B–C show the insertion of the microneedle array into a piece of tuna and the indention left in the tuna sample upon removal of the microneedle array.

As illustrated in Figure 1B–D, following insertion of the microneedle array into the tuna sample, the microneedle array was inserted into the central chamber of the test strip and microneedle array holder. Once in place, a lateral flow test strip was placed in the washed sample reservoir and 1000 µL of sample diluent from the Reveal® kit was added to the inlet port chamber of the device. The diluent traveled through the inlet channel, washed over the microneedles that were used to sample the tuna flesh, and entered the chamber holding the lateral flow test strip. Figure 2F shows an example of a completed test that followed this procedure. The lateral flow strip is shown to extend vertically out from the reservoir chamber, having been exposed to the diluent that flowed over the microneedles located in the central chamber. The lateral flow test strip in Figure 2F shows a positive histamine reading; a pink control band is observed in the upper portion and a more faintly pink test band is observed in the central portion. A ratio of the test: control line color intensity below 1 is indicative of a positive reading.

3.2 Comparison of Testing Methods with Histamine-Spiked Tuna Samples

For calibration of the microneedle sampling system procedure with the tuna flesh, pieces of tuna were incubated overnight in solutions of 1 × PBS (negative control), 0.5 mg/mL histamine, and 1.0 mg/mL histamine. The microneedle sampling system procedure was used to obtain fluid from the tuna sample. The same tuna sample was then evaluated using the manufacturer-described procedure (i.e., the procedure described in the Reveal® for Histamine kit). Comparisons between the data acquired from both testing methods for each solution type were made using a difference of the means with a 95% confidence interval.

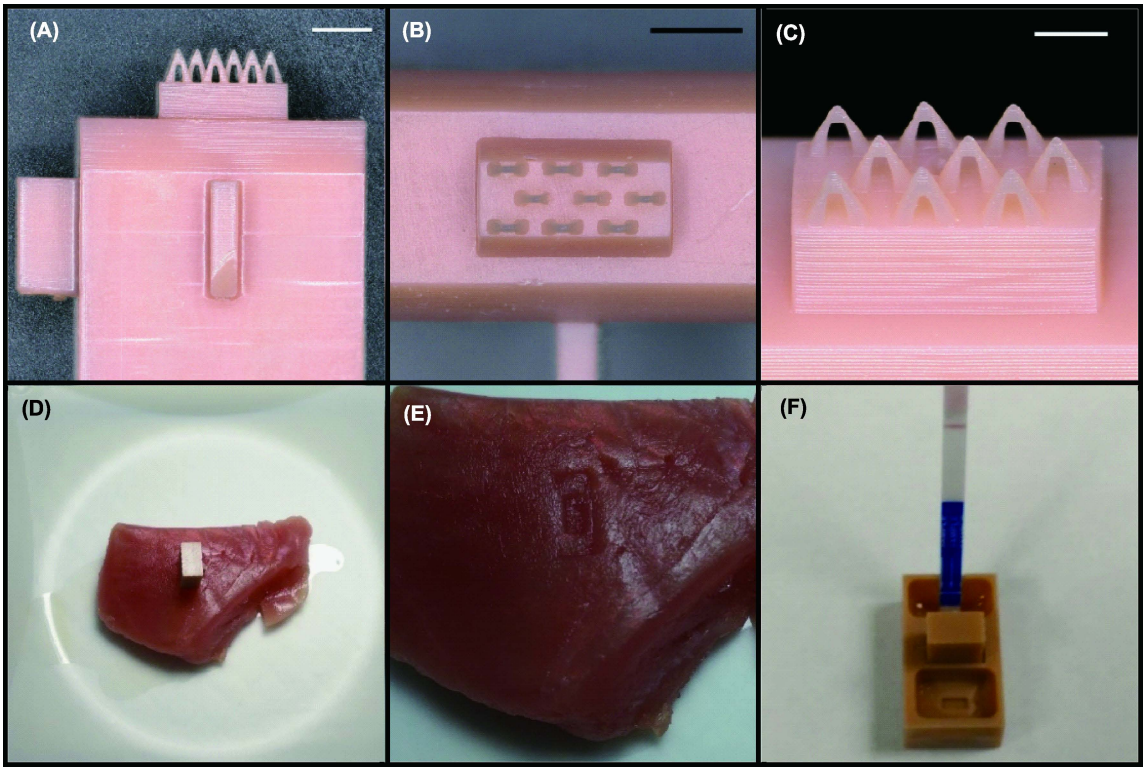

Figure 2. Optical micrographs of the microstereolithography-fabricated microneedles **(A–C)**, including **(A)** a front view of the microneedles showing the trapezoidal cutouts, **(B)** a top view of the microneedles showing the thin pyramidal geometries and the staggered orientation, **(C)** an angled view of the microneedle array; the scale bars in these images are 2 mm. In **(D)** a microneedle is inserted into a fresh piece of tuna. After removal in **(E)**, indentations of the hand-applied microneedle array are noted in the tuna sample. An example of a positive test is shown in **(F)**; in this figure, a lateral flow test strip was placed in the sample chamber and was allowed to develop after incubating in diluent. The diluent washed over a microneedle array that had sampled a piece of histamine-spiked tuna.

The following formulas were used to compare results from the tuna samples and establish the difference of means confidence interval:

$$C.I.Upper = (M_1 - M_2) + (t_{0.95})(S_{M_1-M_2}) \quad (3.1)$$

$$C.I.Lower = (M_1 - M_2) - (t_{0.95})(S_{M_1-M_2}) \quad (3.2)$$

$$S_{M_1-M_2} = \sqrt{\left(\frac{S_1^2}{n_1}\right) + \left(\frac{S_2^2}{n_2}\right)} \quad (3.3)$$

The upper and lower limits of the confidence interval were calculated using Equations 3.1 and 3.2, with M_1 and M_2 representing the means of the microneedle sampling system procedure and manufacturer-described procedure Accuscan® reading ratios, respectively. The $t_{0.95}$ value is the *t*-table value at 95% confidence level. The $S_{M_1-M_2}$ represents the standard deviation for the difference of means; it was calculated by use of Equation 3.3. In this equation, S_1^2 and S_2^2 are the variance and n_1 and n_2 as the number of samples for the microneedle sampling system procedure and the manufacturer-described procedure measurements, respectively. Upon calculating the confidence intervals, if the range of the interval spans both positive and negative values, no statistical difference exists between the two means within the indicated level of confidence.

Using this method, the confidence intervals comparing the difference of means for the microneedle sampling system procedure and the manufacturer-described procedure were compared. For the negative control with PBS, the 95% C.I. range was calculated to be $-0.14 \geq S_{M_1-M_2} \geq -10.76$, with a difference of means of -5.45. Based on this calculation, a slight statistical difference was noted between the test methods for PBS. When examining the 0.5 mg/mL test comparison, the 95% C.I. range was $-3.96 \geq S_{M_1-M_2} \geq -4.21$, with a difference of means of -0.13. Looking at the 1.0 mg/mL values, the 95% C.I. spanned

$0.52 \geq S_{M_1-M_2} \geq -0.01$, with a difference of means of 0.25. For the nine samples tested using each method in this comparison, no statistical difference was observed at a 95% confidence level between the microneedle sampling system procedure results and the manufacturer- described procedure results. Although a difference between the microneedle sampling system procedure results and the manufacturer-described procedure results was noted for the PBS-incubated samples, the histamine-spiked samples showed comparable results for the microneedle sampling system procedure and the manufacturer-described procedure. Figure 3 shows the mean values of Accuscan® ratio readings for each type of sample. A decrease in the relative differences between the ratios of the microneedle sampling system procedure results and the manufacturer-described procedure results was noted as the sample type changed from PBS-spiked to histamine-spiked.

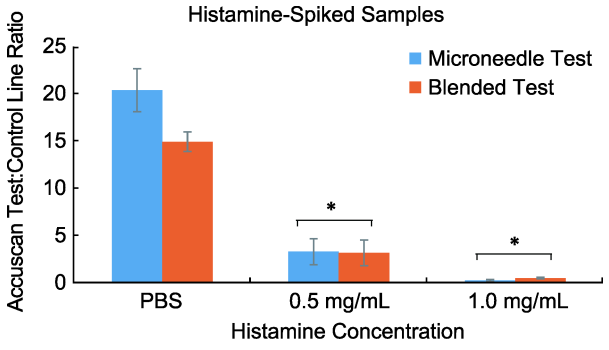

Figure 3. Graph of the mean (± S.E.M.) of the Accuscan® reader test:control ratio data for histamine-spiked tuna samples acquired through the microneedle sampling system procedure and the manufacturer-described procedure. For comparisons marked with "*", no statistical difference was noted between the results from the microneedle sampling system procedure and the manufacturer-described procedure when looking at the difference of means 95% confidence intervals for $n = 9$ of each test type.

3.3 Testing of Tuna from Time Course and Spoiled Samples

In addition to the histamine-spiked tuna samples that were used to compare the microneedle sampling system procedure and the manufacturer-described procedure, tuna samples that were left in a refrigerator for seven days were tested using both procedures. Figure 4 shows the test:control ratio values and standard error of the mean values for each set of measurements at Day 0 – Day 7 time points. Large differences were noted between results from the microneedle sampling system procedure and results from the manufacturer-described procedure for Day 0 – Day 3. These results from both procedures were well into the negative ratio values; although a large discrepancy in the results from the two procedures was noted, both procedures showed that the samples were negative for histamine at the 50 ppm threshold. The Day 5 results showed a dip in the ratio readings. Both procedures detected increasing levels of histamine; however, both procedures showed that the samples were negative for histamine at the 50 ppm threshold. A substantial dip in the microneedle sampling system procedure results was noted at Day 5. At the Day 7 time point, the decrease in readings for both test procedures continued. Using the confidence interval comparison method described previously, no difference between the results from the two test methods was noted at Day 7. The results remained negative at the 50 ppm histamine detection level at all time points over the 7-day time course.

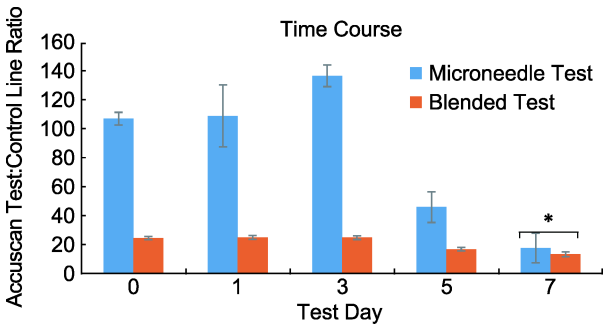

Figure 4. Graph of the mean (± S.E.M.) of the Accuscan® reader test:control ratio data for tuna samples over the refrigerated 7-day time course. Color intensity ratios acquired through the microneedle sampling system procedure and the manufacturer-described procedure were compared. For comparison marked with "*", no statistical difference was noted between the microneedle sampling system procedure and the manufacturer-described procedure when looking at the difference of means 95% confidence intervals for $n = 5$ of each test type.

While the testing of time course samples remained negative, a spoiled piece of tuna was identified during the study. As described earlier, pieces of tuna that were incubated in PBS overnight under refrigerated conditions were meant to serve as negative controls during the histamine-spiking tests. However, one of the pieces of tuna that was tested in this manner returned a positive result for histamine. It was determined that the tuna sample was spoiled upon acquisition from the local fresh market. This spoiled tuna sample provided an opportunity to compare the mi-

croneedle sampling system procedure and the manufacturer-described procedure. The positive results were initially detected using the microneedle procedure; four independent test strips were used to assess that particular piece of tuna. Upon obtaining these unexpected positive results, the histamine detection procedure outlined by the commercial Reveal® test kits was used to assess whether or not the tuna contained histamine. Four independent test strips were conducted on the tuna sample, which indicated that the tuna sample was spoiled and contained levels of histamine above the 50 ppm threshold. Figure 5 shows the mean color intensity ratios of the two test methods acquired from the Accuscan® reader. Using the difference of means calculation with a 95% C.I., no statistical difference was observed between the two test methods. The 95% C.I. for the difference of means for these samples was $-0.008 \leq S_{M_1-M_2} \leq 0.028$. It is interesting to note that the microneedle sampling system procedure was successfully able to detect histamine contamination in a tuna sample that had unexpectedly spoiled.

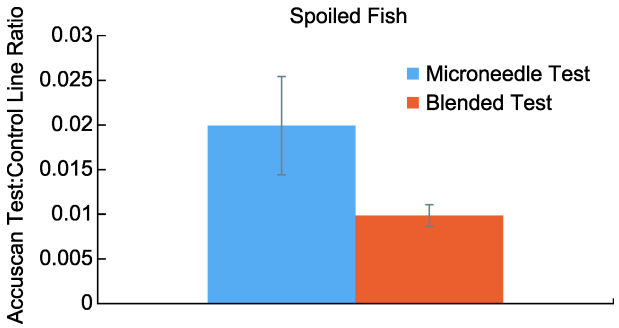

Figure 5. Graph of the mean (± S.E.M.) of the Accuscan® reader test:control ratio data for the spoiled tuna sample. Color intensity ratios acquired through the microneedle sampling system procedure and the manufacturer-described procedure were compared. In a comparison of the difference of means 95% confidence intervals for $n = 4$ of each test type, no statistical difference was noted between the microneedle sampling system procedure and the manufacturer-described procedure.

Other benefits of the microneedle sampling system procedure were noted throughout the course of the study. The amount of sample diluent used to process a sample was lower for the microneedle sampling system procedure than for the commercially available histamine detection kit procedure. The commercially available histamine detection kit provides sample diluent bottles containing 7 mL of solution to be used with each test strip. On the other hand, the microneedle sampling system utilizes only 1 mL of solution. In addition, the amount of time required to perform the microneedle sampling system procedure was much lower than the time required to perform the commercially available histamine detection kit procedure. The commercially available histamine detection kit procedure involves weighing 10 g of the sample, homogenization of the sample, addition of water, mixing, dilution, and use of the lateral flow test strip assay. On the other hand, the microneedle sampling system procedure involved application of the microneedle array to the sample for a few seconds, placement of the microneedle array into the sample holder, pipetting 1 mL of diluent into the holder, and use of the lateral flow test strip assay. The homogenization step associated with the commercially available histamine detection kit procedure added ten or more minutes of preparation time per sample. The microneedle sampling system procedure does not involve homogenization of the sample or cleaning of the homogenizer/blender between samples. The microneedle sampling system can be implemented as a single-use disposable unit, which minimizes the time needed for histamine detection.

4. Conclusion

A custom-designed microneedle sampling system was designed and used for determination of histamine content in fresh, histamine-spiked, and spoiled tuna samples. Lateral flow test strip assays were successfully integrated with the microneedle sampling system for determining histamine levels in tuna samples. Good agreement was noted between the microneedle sampling system procedure and the procedure outlined in a commercially available histamine detection kit. A discrepancy between the results from the microneedle sampling system procedure and the commercial procedure was noted at low (negative) levels of histamine; at higher histamine levels, an improvement in the statistical agreement between the procedures was noted. The microneedle sampling system procedure showed an improvement in the amount of time needed and the amount of reagent needed to screen for histamine in tuna samples. As such, the microneedle sampling system shows promise for future food testing studies.

References

1. Arvanitoyannis I S, Kotsanopoulos K V and Papadopoulou A, 2014, Rapid detection of chemical hazards

(toxins, dioxins, and PCBs) in seafood. *Critical Reviews in Food Science and Nutrition*, vol.54(11): 1473–1528. http://dx.doi.org/10.1080/10408398.2011.641132

2. Hungerford J M, 2010, Scrombroid poisoning: A review. *Toxicon*, vol.56(2): 231–243. http://dx.doi.org/10.1016/j.toxicon.2010.02.006
3. Rawles D D, Flick G J and Martin R E, 1996, Biogenic amines in fish and shellfish. *Advances in Food Nutrition Research*, vol.39: 329–364. http://dx.doi.org/10.1016/S1043-4526(08)60076-5
4. Santos M H S, 1996, Biogenic amines: Their importance in foods. *International Journal of Food Microbiology*, vol.29(2–3): 213–231. http://dx.doi.org/10.1016/0168-1605(95)00032-1
5. Dadáková E, Křížek M and Pelikánová T, 2009, Determination of biogenic amines in foods using ultra-performance liquid chromatography (UPLC). *Food Chemistry*, vol.116(1): 365–370. http://dx.doi.org/10.1016/j.foodchem.2009.02.018
6. Shalaby A R, 1996, Significance of biogenic amines to food safety and human health. *Food Research International*, vol.29(7): 675–690. http://dx.doi.org/10.1016/S0963-9969(96)00066-X
7. Önal A, 2007, A review: Current analytical methods for the determination of biogenic amines in foods. *Food Chemistry*, vol.103(4): 1475–1486. http://dx.doi.org/10.1016/j.foodchem.2006.08.028
8. Lehane L and Olley J, 2000, Histamine fish poisoning revisited. *International Journal of Food Microbiology*, vol.58(1–2): 1–37. http://dx.doi.org/10.1016/S0168-1605(00)00296-8
9. Prester L, 2011, Biogenic amines in fish, fish products and shellfish: A review. *Food Additives and Contaminants: Part A*, vol.28(11): 1547–1560. http://dx.doi.org/10.1080/19440049.2011.600728
10. Sapin-Jaloustre H and Sapin-Jaloustre, J, 1957, [A little-known food poisoning: Histamine poisoning from tuna]. *Concours Médical*, vol.79(22): 2705–2708, In French, English abstract.
11. Evangelista W P, Tette P A S and Gloria M B A, 2013, Quality control of the analysis of histamine in fish by proficiency test. *Journal of Physics: Conference Series*, vol.575: 012035. http://dx.doi.org/10.1088/1742-6596/575/1/012035
12. Hungerford J and Wu W-H, 2012, Comparison study of three rapid test kits for histamine in fish: BiooScientific MaxSignal enzymatic assay, Neogen Veratox ELISA, and the Neogen Reveal Histamine Screening test. *Food Control*, vol.25(2): 448–457. http://dx.doi.org/10.1016/j.foodcont.2011.11.007
13. Posthuma-Trumpie G A, Korf J and van Amerongen A, 2009, Lateral flow (immuno)assay: Its strengths, weaknesses, opportunities and threats. A literature survey. *Analytical and Bioanalytical Chemistry*, vol.393(2): 569–582. http://dx.doi.org/10.1007/s00216-008-2287-2
14. Čapek P and Dickerson T J, 2010, Sensing the deadliest toxin: Technologies for botulinum neurotoxin detection. *Toxins*, vol.2(1): 24–53. http://dx.doi.org/10.3390/toxins2010024
15. Liao J-Y and Li H, 2010, Lateral flow immunodipstick for visual detection of aflatoxin B_1 in food using immune-nanoparticles composed of a silver core and a gold shell. *Microchimica Acta*, vol.171(3–4): 289–295. http://dx.doi.org/10.1007/s00604-010-0431-0
16. Nimitphak T, Meemetta W, Arunrut N, *et al*., 2010, Rapid and sensitive detection of *Penaeus monodon* nucleopolyhedrovirus (PemoNPV) by loop-mediated isothermal amplification combined with a lateral-flow dipstick. *Molecular and cellular probes*, vol.24(1): 1–5. http://dx.doi.org/10.1016/j.mcp.2009.09.004
17. Moon J, Kim, G and Lee S, 2012, A gold nanoparticle and aflatoxin B1-BSA conjugates based lateral flow assay method for the analysis of aflatoxin B1. *Materials*. vol.5(4): 634–643. http://dx.doi.org/10.3390/ma5040634
18. Li C G, Lee C Y, Lee K, *et al*., 2013, An optimized hollow microneedle for minimally invasive blood extraction. *Biomedical Microdevices*, vol.15(1): 17–25. http://dx.doi.org/10.1007/s10544-012-9683-2
19. Donnelly R F, Mooney K, Caffarel-Salvador E, *et al*., 2014, Microneedle-mediated minimally invasive patient monitoring. *Therapeutic Drug Monitoring*, vol.36(1): 10–17. http://dx.doi.org/10.1097/FTD.0000000000000022
20. Romanyuk A V, Zvezdin V N, Samant P, *et al*., 2014, Collection of analytes from microneedle patches. *Analytical Chemistry*, vol.86(21): 10520–10523. http://dx.doi.org/10.1021/ac503823p
21. Windmiller J R, Valdés-Ramirez G Zhou N, *et al*., 2011, Bicomponent microneedle array biosensor for minimally-invasive glutamate monitoring. *Electroanalysis*, vol.23(10): 2302–2309. http://dx.doi.org/10.1002/elan.201100361
22. Sakaguchi K, Hirota Y, Hashimoto N, *et al*., 2012, A minimally invasive system for glucose area under the curve measurement using interstitial fluid extraction technology: evaluation of the accuracy and usefulness with oral glucose tolerance tests in subjects with and without diabetes. *Diabetes Technology & Therapeutics*, vol.14(6): 485–491. http://dx.doi.org/10.1089/dia.2011.0255
23. Jina A, Tierney M J, Tamada J A, *et al*., 2014, Design, development, and evaluation of a novel microneedle ar-

ray-based continuous glucose monitor. *Journal of Diabetes Science and Technology*, vol.8(3): 483–487. http://dx.doi.org/10.1177/1932296814526191

24. Miller P R, Xiao X, Brener I, *et al.*, 2014, Microneedle-based transdermal sensor for on-chip potentiometric determination of K(+). *Advanced Healthcare Materials*, vol.3(6): 876–881. http://dx.doi.org/10.1002/adhm.201300541
25. Boehm R D, Miller P R, Hayes S L, *et al.*, 2011, Modification of microneedles using inkjet printing. *AIP Advances*, vol.1(2): 022139. http://dx.doi.org/10.1063/1.3602461
26. Boehm R D, Miller P R, Singh R, *et al.*, 2012, Indirect rapid prototyping of antibacterial acid anhydride copolymer microneedles. *Biofabrication*, vol.4(1): 011002. http://dx.doi.org/10.1088/1758-5082/4/1/011002
27. Boehm R D, Miller P R, Schell W A, *et al.*, 2013, Inkjet printing of amphotericin B onto biodegradable microneedles using piezoelectric inkjet printing. *JOM*, vol.65(4): 525–533. http://dx.doi.org/10.1007/s11837-013-0574-7
28. Boehm R D, Miller P R, Daniels J. *et al.*, 2014, Inkjet printing for pharmaceutical applications. *Materials Today*, vol.17(5): 247–252. http://dx.doi.org/10.1016/j.mattod.2014.04.027
29. Miller P R, Gittard S D, Edwards T L. *et al.*, 2011, Integrated carbon fiber electrodes within hollow polymer microneedles for transdermal electrochemical sensing. *Biomicrofluidics*, vol.5(1): 013415. http://dx.doi.org/10.1063/1.3569945
30. Technical data 1: EnvisionTEC E-shell® 200 series, viewed October 28, 2015, <http://envisiontec.com/envisiontec/wp-content/uploads/MK-MTS-EShell200Series-V01-FN-EN.pdf>
31. Technical data 2: EnvisionTEC Otoflash post curing light flashing unit, viewed October 28, 2015, <http://media.envisiontec.com/envisiontec/wp-content/uploads/MK-MCS-Otoflash-V01-FN-EN.pdf>
32. Reveal product information: Reveal® histamine screening test, viewed November 1, 2015, <http://www.neogen.com/FoodSafety/pdf/ProdInfo/R-Hist.pdf>

RESEARCH ARTICLE

Electrospun 3D multi-scale fibrous scaffold for enhanced human dermal fibroblasts infiltration

Wen Shing Leong[1], Shu Cheng Wu[1,2], Kee Woei Ng[1] and Lay Poh Tan[1*]

[1] School of Materials Science and Engineering, Nanyang Technological University, 50 Nanyang Avenue, Singapore 639798, Singapore

[2] School of Engineering, Ngee Ann Polytechnic, Singapore 599489, Singapore

Abstract: Electrospun polymeric nanofibrous scaffold possesses significant potential in the field of tissue engineering due to its extracellular matrix mimicking topographical features that modulate a variety of key cellular activities. However, traditional two-dimensional (2D) electrospun scaffolds are generally close-packed fiber mats which prohibit cell infiltration and proliferation. Consequently, the applications of electrospun scaffolds in regenerative medicine are limited. In this study, we detail the use of a needle collector to fabricate three-dimensional (3D) electrospun poly-ε-caprolactone (PCL) scaffolds with multi-scale fiber dimensions. The resultant pore size is 4 times larger than conventional 2D electrospun scaffolds with interweaving micro (3.3 ± 0.6 μm) and nano (240 ± 50 nm) fibers. The scaffold was surface modified by grafting with gelatin molecules. It was found that surface modification significantly improved human dermal fibroblasts (HDFs) cell infiltration throughout the 3D multi-scale scaffold. Even after an extended culture period of up to 28 days, cell proliferation was well supported in the surface-modified 3D multi-scale scaffold as confirmed by Ki67 staining. Extracellular matrix proteins secreted by the HDFs was evident on the 3D multi-scale PCL scaffold showing promising potential to facilitate tissue regeneration, in particular dermal tissue engineering.

Keywords: tissue engineering, 3D electrospinning scaffold, human dermal fibroblasts, three-dimensional scaffold, cell infiltration

*Correspondence to: Lay Poh Tan, School of Materials Science and Engineering, Nanyang Technological University, 50 Nanyang Avenue, Singapore 639798, Singapore; Email: lptan@ntu.edu.sg

Received: September 4, 2015; **Accepted:** October 14, 2015; **Published Online:** November 18, 2015

Citation: Leong W S, Wu S C, Ng K W, *et al*., 2016, Electrospun 3D multi-scale fibrous scaffold for enhanced human dermal fibroblasts infiltration. *International Journal of Bioprinting*, vol.2(1): 81–92. http://dx.doi.org/10.18063/IJB.2016.01.002.

1. Introduction

Tissue engineering aims to improve the health and quality of human lives by restoring, maintaining, or enhancing the function of tissue and organ[1]. Among all, skin tissue engineering is one of the most developed areas where engineered skin substitutes are commercially available (e.g., Integra™, Dermagraft™, Apligraf™). However, they do not fully recreate the function and aesthetics of the skin. As a result, it leads to unsatisfactory treatment, especially for full thickness[2] and chronic non-healing wound[3].

Continuous effort is focused on developing biomimicry scaffolds to trigger cell response and function as those tissues of which they aim to restore. One of the approaches is to replicate extracellular matrix (ECM) environment using nanofibrous scaffold. Nanofibers have been demonstrated to promote vascularization[4] and mimic the native ECM[5,6] to potentially develop functional tissue. Recently, nanofibers which are known to have great influence over cellular behavior have been incorporated as promising scaffold feature

for skin tissue regeneration and wound healing[7]. Scaffold fabrication techniques, e.g., electrospinning, self-assembling peptides and phase separation, have been outlined as the three promising methods to create scaffold of fiber sizes close to the ECM fibrils in nanoscale[8]. Among them, electrospinning offers superior versatility capable of fabricating nanofibrous scaffold of high porosity at controllable structure, low cost, and high repeatability from a wide range of polymers. Furthermore, the use of electrospinning allows tailoring of scaffold's properties according to targeted tissue. The large surface to volume ratio of the nanofiber scaffold also promotes cell adhesion and cell migration.

Conventional electrospinning collects nanofibers on a plate collector where nanofibers are formed and collected as a 2D mat. This results in densely packed nanofibers with reduced pore size and porosity and it is challenging to build a scaffold with thickness beyond 100 μm using this conventional method[9]. The limited cell infiltration due to the densely packed structure and small pore size has restricted the application of electrospun scaffold[10]. Numerous approaches have been reported to increase the pore size of the traditional electrospun scaffold[11,12], including mechanical expansion[13], inclusion of porogen[14], increment of the fiber diameter[15], incorporation of sacrificial fibers[16,17], cryogenic electropinning[18], and addition of microscale (3~10 μm)[19,20] or macroscale (~300 μm)[21,22] fibers into the nanoscale fiber (~600 nm) scaffold. However, the fabricated scaffold's thickness is still limited and cellular infiltration was either not studied or limited to the surface of the scaffold.

A thicker scaffold, with versatility to be optimized to the dimension of wound size, may be helpful for treatment of deep skin injury where greater structural support is required to enhance wound healing. To overcome this inherent limitation associated with traditional electrospinning technique, several variants of electrospinning have been devised[23,24]. In recent studies, collector design has been changed from traditional flat surface to protruded shape to increase pore size in electrospun scaffold[23,25]. For example, fabrication of cotton ball-like 3D scaffold called FLUF (Focused, Low density, and Uncompressed nanoFibrous) mesh used an array of point collectors embedded in a spherical dish[23]. The pore size of the FLUF mesh was increased from typical <1 μm to between 2 μm to 5 μm as viewed under scanning electron microscopy (SEM). The cell infiltration was demonstrated at ~300 μm below scaffold surface using rat insulinoma cell line INS-1. This research demonstrated the feasibility to produce porous nanofibrous 3D scaffold using electrospinning with customized collector. Even though the response of human cells was not investigated in the FLUF mesh, this study has proven the concept of changing collection method in a way of changing the electrical field to collect electrospinning fibers in 3D. However, such a collector must be tailor-made to individual electrospinning setup due to the difference in the dimension and environment which may interfere with the electrical field. Practically this system is difficult to be implemented to different kinds of conventional setup as there are too many parameters which may affect the fiber formation. These parameters include the diameter, thickness and material of the spherical dish, position, number, length and diameter of the needles.

In this work, we aim to fabricate 3D poly-ε-caprolactone (PCL) scaffold with multi-scale fibers via an improved electrospinning process based on the conventional setup. The method is easy to set up and can be adapted by any conventional electrospinning setup. The scaffold fabricated was then surface modified to improve the hyrophilicity of the PCL material for better cell adhesion and penetration. Human dermal fibroblasts (HDFs) were used to check the effectiveness of the 3D multi-scale scaffold for cell infiltration and ECM protein deposition. This strategy provides a cost-effective and feasible solution for overcoming the current challenges based on conventional electrospinning to produce 3D instead of 2D scaffold and has great potential across a wide range of tissue engineering applications[26].

2. Materials and Methods

2.1 Materials

Poly (ε-caprolactone) (PCL) (Mn 80,000) granules, Type A gelatin derived from porcine skin, 25% glutaraldehyde, and ethylenediamine (Fluka) were purchased from Sigma Aldrich. Organic solvent dichloromethane (DCM) was purchased from TEDIA, USA. N,N-Dimethylformamide (DMF) was purchased from Merck, USA. HDFs were purchased from Life Technologies, USA. Phosphate buffer saline (PBS), low glucose Dulbecco's Modified Eagle Medium (DMEM), high glucose DMEM, gold fetal bovine serum (FBS), L-glutamine and 1% penicillin-streptomycin were purchased from PAA Laboratories, Pasching, Austria.

Minisart High Flow 0.2 µm syringe filter unit was purchased from Sartorius Stedim Biotech S.A., Aubagne, France. *Jung tissue* freezing medium was purchased from Leica Instruments, Germany.

2.2 Fabrication of Electrospun Scaffold

Electrospun scaffolds were fabricated using electrospinning chamber, Nanon-01A (Mecc Co. Ltd, Japan). Briefly, PCL was dissolved in DCM and DMF at 3.5:6.5 (v/v) ratio to obtain 13% (w/v) solution. The polymer solution was spun through 21G metal nozzle at accelerating voltage 18kV and flow rate 0.5 mL/h. Working distance was set at 15 cm for 2D scaffold collected on collector plate, and 7.5 cm for 3D scaffold collected on a 7.5 cm stainless steel medical hypodermic 18G needle insulated from ground. Electrospinning was carried out for 4 hours for collection of 2D scaffold and 30 minutes for collection of 3D scaffold. Collected electrospun scaffolds were dried in vacuum oven at 37°C for 1 week to remove any residual solvent.

2.3 Surface Modification

Gelatin was grafted onto the electrospun fiber surface through aminolysis[27]. Briefly, scaffolds were washed in 70% ethanol and deionized (DI) water, followed by immersion in 40%(v/v) ethylenediamine at room temperature for 14 hours. Scaffolds were then rinsed 3 times with DI water for 10 minutes to remove free ethylenediamine. After that, scaffolds were immersed in 2.5% (by weight) glutaraldehyde (GA) for 4 hours at room temperature, followed by washing 3 times with DI water for 10 minutes. GA grafted scaffolds were then incubated in 3 mg/mL filtered gelatin at 37°C for 24 hours. Gelatin immobilized scaffolds were then rinsed 3 times with DI water for 10 minutes to remove free gelatin. Lastly, prior to cell culture, scaffolds were sterilized under ultraviolet light for 10 minutes.

All chemical treatment and washing processes involving the use of solution were carried out within vacuum chamber to ensure complete perfusion of the solution. Prior to subsequent characterization, all scaffolds were freeze-dried to ensure the volume and shape of the scaffolds remained intact, and no moisture was trapped within the scaffolds.

2.4 Contact Angle Measurement

Static water contact angle measurements on 2D electrospun scaffold membranes were carried out using FTA 200 (First Ten Angstroms, USA) via the sessile drop method with 0.5 µL of DI dispensed from the syringe of the system.

2.5 Mechanical Testing

The mechanical properties of 2D electrospun scaffolds were investigated using Instron microtester 5848. The samples were die cut into dumbbell shapes according to ASTM D638. The sample was tested under a crosshead speed of 10 mm/min at room temperature. 5 surface modified scaffolds and 5 surface non-modified scaffolds were tested to investigate the effect of surface modification on the mechanical properties of the scaffolds.

2.6 SEM Characterization and Fiber Diameter Measurements

The electrospun PCL scaffolds were sputter coated with gold for 30 seconds at 18mA. The size and morphology of scaffolds were observed using SEM (JEOL JSM-5310). Fiber diameters were measured using ImageJ[28] from triplicates. At least 50 measurements were taken at random locations in SEM micrograph.

2.7 Porosity and Pore Size Measurements

Micrometritics Autopore IV 9500 Mercury Porosimeter was used to investigate pore size and porosimetry of non-modified 3D and 2D electrospun scaffold. The range of pore diameters, d_p, could be calculated using the Washburn equation (Equation (1)).

$$d_p = \frac{-4\gamma \cos\theta}{P} \quad (1)$$

where γ is the surface tension of mercury, θ is the contact angle between the mercury and the scaffold and P is the pressure. As reported in literature[29], a contact angle of 140° between PCL and mercury in air was used. Four replicates were measured for each scaffold type.

2.8 Cell Seeding

HDFs were cultured in fibroblasts cell basal medium (high glucose DMEM supplemented with 10% Gold FBS, 1% penicillin streptomycin, 1% Amphotericin B). To prepare scaffolds for cell culture, 3D scaffolds were cut into 0.6×0.6×0.6 cm^3 cube while 2D scaffolds were cut into 1.6×1.7×0.08 cm^3 sheet. The cells were seeded at same density (500 cells/mm^3) on 2D and 3D scaffolds. Cell culture media were changed every two days.

2.9 Cell Infiltration Characterization

Cryosectioning technique was employed to obtain the information of cell infiltration. HDFs were cultured on electrospun scaffold for 24 hours. After that, the cells were washed with phosphate buffer saline, and then fixed with 4% paraformaldehyde for 20 minutes, followed by 3 times rinsing in PBS for 10 minutes. The fixed samples were embedded in tissue embedding medium (*Jung tissue* freezing medium), leaving in a fridge overnight at 4°C to allow full penetration. The samples were then frozen in liquid nitrogen and cut into 5 µm thick sections in the center part via a cryostat (CM3050S, Leica Microsystems, Bannockburn, IL). All the samples were placed onto glass slides coated with 1% gelatin. The nucleus of cells were stained with 4',6-diamidino-2-phenylindole (DAPI) that emitted blue fluorescence when viewed under a fluorescent microscope (Eclipse 80*i* microscope, Nikon). Triplicates were viewed and captured for each scaffold type.

2.10 Detection of ECM Proteins Deposited by HDFs

Surface modified 3D multi-scale scaffold were seeded with HDFs for 21 and 28 days. The scaffolds were then immersed in *Jung tissue* freezing medium and frozen in liquid nitrogen before kept in a –80°C freezer. Staining of proliferation marker, Ki67 and ECM proteins, including Collagen I, Collagen III, Fibronectin and Elastin, were carried out according to standard protocols. Positive control (mouse multi-tissue) and negative control (samples stained in the absence of primary antibody) were stained for comparison during immunohistochemistry study.

2.11 Statistical Analysis

Experimental data were expressed as means ± standard deviation (SD). Student's *t*-test assuming unequal variance was used to calculate *p*-values, where $p<0.05$ were considered significant.

3. Results and Discussion

3.1 Surface Modification of 2D Electrospun PCL Scaffold

When hydrophobic PCL was electrospun into a 2D fiber mat with high surface roughness and pores, the wettability was significantly decreased further. The contact angle of this 2D electrospun PCL fiber mat measured with sessile drops method was 116°, showing the high hydrophobicity of the surface. The superhydrophobic nature of 2D electrospun PCL fiber mat limits diffusion of polar fluid such as cell culture medium and cell containing solution into electrospun PCL fiber mat, thereby limiting the functions of a scaffold in promoting cellular infiltration and mass transfer. In order to address this concern, surface modification was carried out in this study. Here, polar amino group was introduced onto the fiber surface by aminolysis. Subsequently, glutaraldehyde was introduced as bifunctional linker to link proteins to fiber surface. Therefore, this allows the modified PCL nanofiber to couple with various hydrophilic biomolecules (e.g., collagen, gelatin, peptides) that would be recognized by cell receptor. Among all, gelatin is chosen in this study because it is recognized as one of the most cost-effective peptides with great potential to promote epithelization and granulation tissue formation during wound healing[30]. After grafting with gelatin molecules, the contact angle measured on 2D electrospun PCL fiber mat was significantly reduced from 116° to 46°, showing enhanced surface wettability. This enhanced surface wettability and bioactivity provided by the gelatin molecules would be essential to promote cell infiltration and proliferation, as well as nutrient exchange within the scaffold.

3.2 Morphology and Mechanical Properties of Surface Modified 2D Electrospun PCL Scaffold

The effect of surface modification on the electrospun fibrous scaffold physical properties was examined with SEM and tensile testing. As shown in Figure 1, SEM micrographs revealed that surface modification process did not alter the electrospun fiber network structure. Gelatin grafted electrospun fibers remained intact with fiber diameter and arrangement similar to pristine electrospun PCL scaffold. Tensile test also demonstrated similar Young's modulus, yield stress, ultimate tensile stress, yield strain and elongation at break for both 2D electrospun PCL scaffold with and without surface modification, as summarized in Table 1. It can be concluded that surface modification process neither disrupted the fiber morphology nor altered the mechanical properties of electrospun PCL, despite the concern of strong basicity of diamine on the bulk mechanical property of electrospun PCL[27]. Even though 2D instead of 3D scaffold was used to demonstrate the effect of surface modifcation on the scaffold property, it is expected that 3D scaffold would not behave differently because the response would be an inherent property of the material.

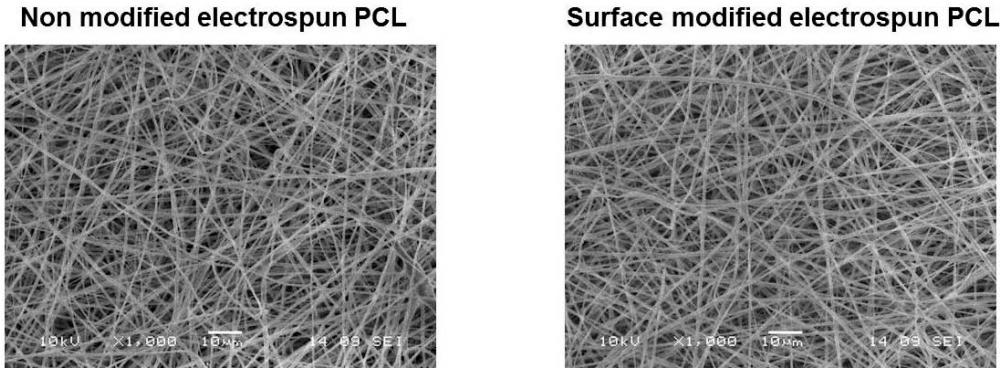

Figure 1. SEM micrographs of electrospun PCL without and with surface modification reveal no physical deterioration despite the chemical treatment.

Table 1. Table showing similar mechanical properties observed between 2D electrospun PCL scaffold with or without surface modification

	Young's modulus, E [Mpa]	Yield stress, σ_y [Mpa]	Ultimate tensile stress, σ_{UTS} [Mpa]	Yield strain [%]	Elongation at break, ε_f [%]
Surface modified	15.86±4.00	3.14±0.48	5.91±0.17	20.34±2.98	321.13±118.25
Non modified	13.96±5.35	2.48±0.28	6.28±1.47	19.14±5.06	260.79±58.65

3.3 Fabrication of 3D Multi-scale Scaffold Using Hypodermic Needle Collector

Replacing the plate collector with a hypodermic needle collector completely transforms the physical structure of fibrous scaffold. Instead of a dense 2D mat as shown, the structure collected using the needle collector was a fluffy ball of loosely interwoven fibers as shown in Figure 2A. The fiber diameter of such 3D scaffold was measured to be a mixture of micro- (3.3 ± 0.6 μm) and nano- (240 ± 50 nm) fibers. The collected scaffold also replicates the inherent micro-nanoscale features in ECM that is essential in triggering series of cell activities[31–36]. The scaffold is therefore termed 3D multi-scale scaffold herein. In comparison, the 2D electrospun PCL collected on traditional plate collector has a relatively uniform fiber diameter with a value of 0.7 ± 0.3 μm (Figure 2C). Mercury porosimetry measurements provided insights into the pore structure of the scaffold collected on the two different scaffolds (Figure 3). Remarkably, the use of a needle collector resulted in an approximately four-fold increment in scaffold pore size (~42 μm) while maintaining the high porosity of about 92%.

The function of the hypodermic needle is to disrupt the closely packed fiber deposition pattern collected using a conventional electrospinning setup (Figure 4A). Hypodermic needle collector has a much smaller collector area compared to plate collector. It confines the electric field from spreading but form into spindle shape[37]. The fibers are therefore randomly deposited around the needle tip which has the highest electric field. When the positively charged polymer solution is deposited onto the needle collector, these positive charges are not discharged rapidly enough due to insulation from grounded conductor plate, and inherent poor conductivity of polymer fibers. As a result, the deposited fibers have residue positive charges. Therefore, repulsive static force exists between the deposited polymer fiber and the subsequent depositing polymer solution jet. This results in the formation of loosely packed electrospun fibers. Over time, the loose structure increased in volume on the needle collector. At the same time, during the collection of fiber on the needle collector, the non-conducted positive charges on needle tip, as well as the movement of spinneret, created a dynamic electrical field that drives the polymer solution to spin into fibers of different diameters.

Unlike the design of tip collector with protruded metal struts[37] or point collector with sharp tip[38] reported earlier, hypodermic needle used in this study is a hollow tube with slanted cylindrical opening (Figure 4B). The slanted area of needle opening offered alternate landing surface for fiber deposition when the sharpest tip was occupied and reduced in electrical conductivity. Therefore, deposited fibers would fold on the needle collector when subsequent fibers landed on the

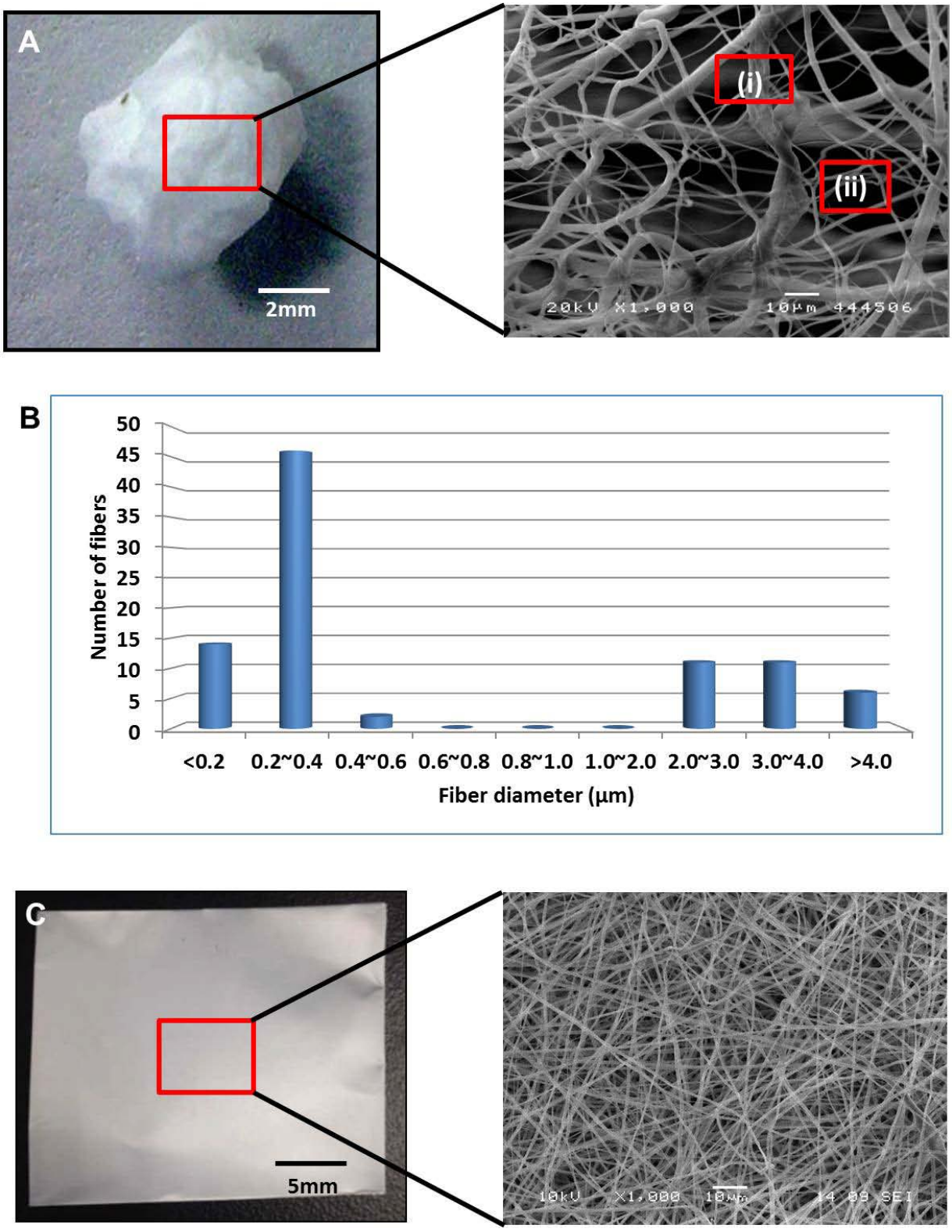

Figure 2. Comparison between 3D multi-scale scaffold and 2D electrospun scaffold. **(A)** 3D multi-scale scaffold has folded into cotton ball like shape. Scanning electron image on the right shows a mixture of (i) micro-fibers of 3.3 µm diameter and (ii) nano-fibers of 0.2 µm diameter. **(B)** Diameters of fibers in 3D multi-scale scaffold are mostly in the range of 0.2~0.4 µm, or 2~4 µm. **(C)** 2D scaffold electrospun scaffold collected on aluminium foil wrapped on plate collector. Micro-fibers of 0.7 µm are densely packed in traditional 2D scaffold.

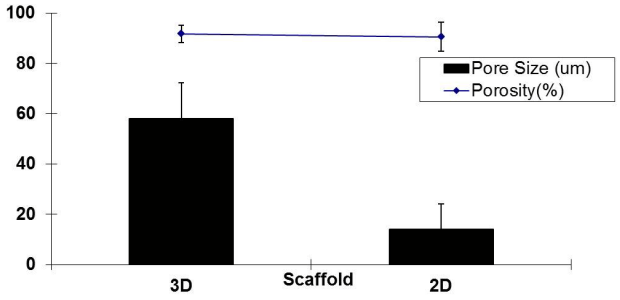

Figure 3. Mercury porosimeter revealed a four-fold increment in pore size in 3D scaffold in comparison with 2D scaffold, with little change in porosity.

slanted needle opening instead of the needle tip. Eventually, newly spun fibers would wrap around the needle tip and develop into a cotton-like scaffold. The scaffold thickness collected within 30 minutes was more than 6 mm and this is about 75 times more than that in 2D electrospun PCL scaffold. On the other hand, existence of a mixture of micro- and nano- fiber could play a part in disrupting fibers packing, resulting in an increase of the pore size of the scaffold[19–22]. Larger pore size offers higher opportunities for cell infiltration and mass transfer without sacrificing the ECM mimicry nanofeatures.

3.4 Comparison of HDFs Distribution Between 2D Electrospun and 3D Multi-scale Scaffold

Both 2D electrospun and 3D multi-scale scaffold were examined to study the effect of pore size of electrospun scaffold on cellular distribution in scaffold after cell seeding. Both types of scaffolds were surface modified with the chosen surface modification method demonstrated in Section 3.1, and compared to that without surface modification. As discussed earlier, surface modification significantly enhanced hydrophilicity of the PCL scaffold without deteriorating the architectural properties. As shown in Figure 5, 3D multi-scale electrospun PCL improved in water absorption and expanded in phosphate buffer solution only after effective surface modification.

Cell culture results as shown in Figure 6 revealed the difficulty for HDFs to be seeded into traditional 2D electrospun scaffold. Traditional 2D PCL electrospun scaffold had desired porosity for tissue engineering but the dense fiber packing resulted in small pore size which restricted cell to be seeded throughout the whole scaffold (Figure 6A). Even with the aid of gelatin grafting to improve wettability and cell-scaffold interaction, no significant improvement in cellular distribution was observed. HDFs seeded on gelatin grafted 2D electrospun scaffold were found to adhere on the top surface only, despite the enhanced wettability (Figure 6B). This is a common issue that has restricted the application of electrospun scaffold[9,10]. By increasing the pore size of the scaffold using needle

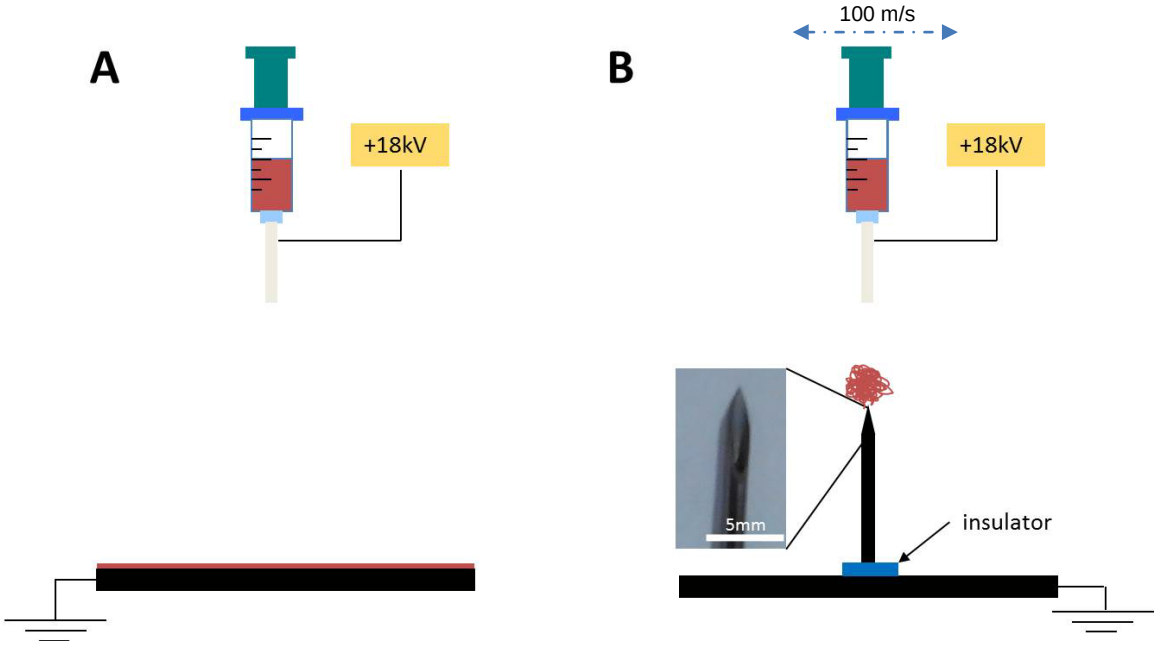

Figure 4. Electrospinning setup. **(A)** Collection of 2D electrospun scaffold on plate collector; **(B)** Collection of 3D electrospun scaffold on needle collector.

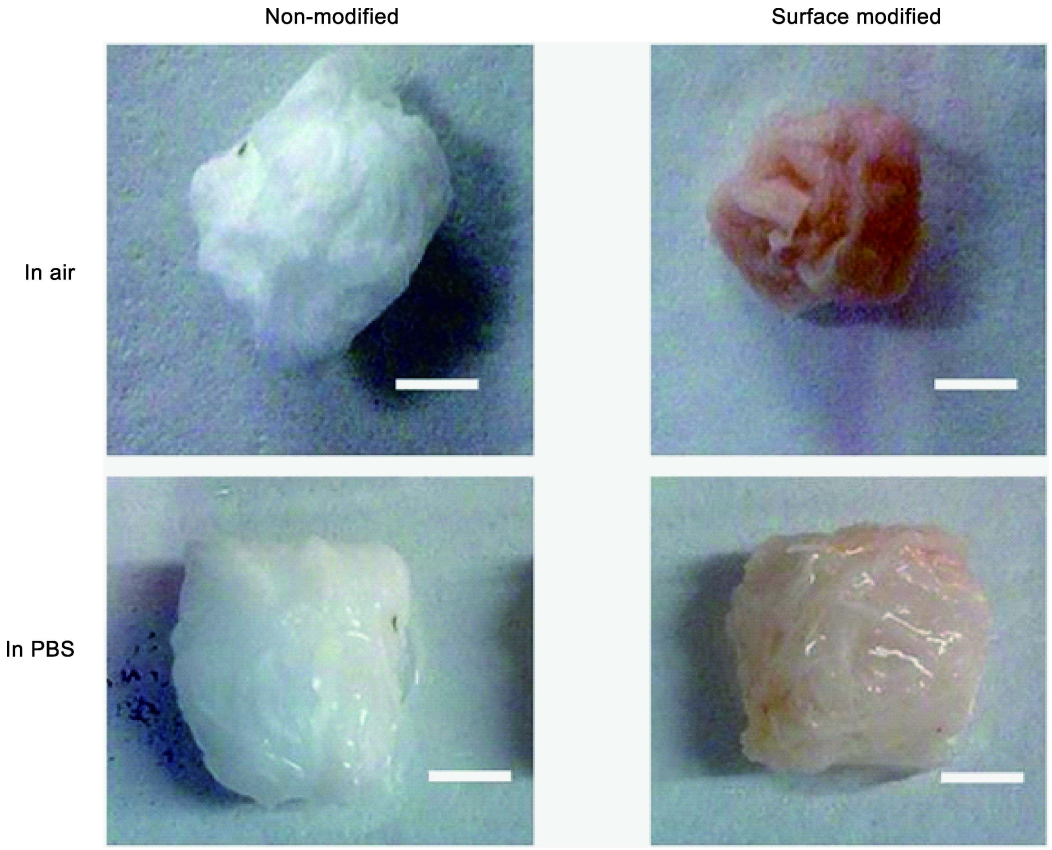

Figure 5. Surface modification on 3D multi-scale scaffold. PBS can penetrate into modified but not non modified 3D multi-scale scaffold easily. Therefore, surface modified 3D multi-scale scaffold absorbs PBS and expand in size when immersed in PBS. Scale bar = 2 mm.

collector, better cellular distribution at seeding was observed even for the unmodified 3D multi-scale scaffold. The images of the cryo-sectioned scaffold demonstrated HDFs infiltration after 24 hours of cell seeding but was limited to 21% (1.2 mm) of the total depth (6 mm), presumably due to the hydrophobic surface which retarded further infiltration of medium and cells (Figure 6C). Whereas in the gelatin modified 3D multi-scale scaffold, cells were distributed through the whole thickness of the scaffold (Figure 6D). The low cell number observed here is due to the low initial seeding density which was deliberate in order to have a more definite observation of the effect of cell distribution. It is evident from this study that improvement in 3D scaffold architecture with larger pores, wettability and bioactivity enhance uniform cellular distribution throughout the thickness of the scaffold. Although some studies have reported electrospun scaffold fabricated with enlarged pore size, few have demonstrated the complete cellular distribution throughout the scaffold. Our study has highlighted that in addition to having large enough pore size, it is also important to have hydrophilic and conducive surface properties to promote cell infiltration and migration. This has bridged the electrospinning technology with its potential application by showing thorough cellular distribution and active proliferation into electrospun scaffold with a thickness of a few millimeters.

3.5 Gelatin Grafted 3D Multi-scale Scaffold for Dermal Tissue Engineering

HDFs were seeded in gelatin grafted 3D multi-scale scaffold for 21 and 28 days prior to characterization for its proliferation marker and ECM deposition respectively. As shown in Figure 7, HDFs were proliferating throughout 28 days of culturing as indicated by positive staining of cellular marker for proliferation, Ki67, in cell nuclei. Despite the large scaffold size and high cell density anchor on scaffold‘s surface, HDFs has successfully penetrated into the scaffold and remained viable with the proliferative protein expressed. This has indicated efficient nutrient and mass transfer in and out of the millimeter-thick multi-scale scaffold. However, the cell number was observed to be on the

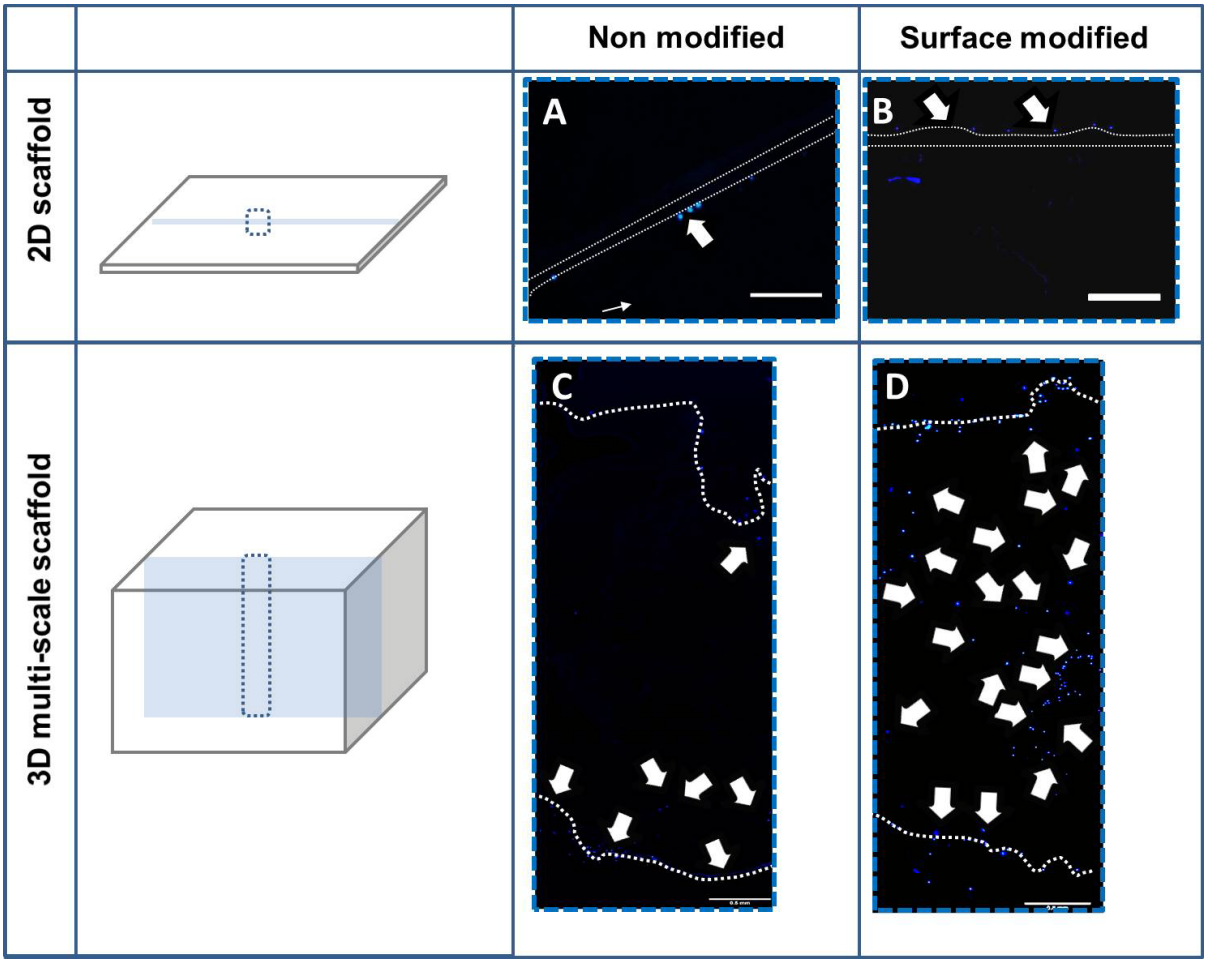

Figure 6. Cross-section images of scaffold comparing cell distribution on 2D **(A,B)** versus 3D multi-scale scaffold **(C,D)** after 24 hours of culturing. White dotted line indicates the boundary of scaffold. **(A,B)** HDFs were seen only at the external surface of scaffold for both non-modified and surface modified 2D electrospun scaffold. **(C)** Cross-section of 3D multi-scale scaffold shows cells attached to only the sub-surface region of the scaffold without surface modification. **(D)** After surface modification, HDFs were seen to have penetrated throughout the 3D multi-scale scaffold. Solid white arrows show cells. **(A,B)** Scale bar = 100 μm and **(C,D)** Scale bar = 0.5 mm.

low side due to the low initial seeding density and therefore perhaps a longer culture time or higher seeding density would be required to resolve this issue.

ECM deposition by cells is an essential process for remodelling and repair of skin defects[39] and therefore it is important to characterize this cellular behavior on the scaffold. Deposition of the two fibroblastic origin extracellular matrix proteins, Collagen I and Collagen III, was observed after both 21 and 28 days of culturing in gelatin grafted 3D multi-scale scaffold (Figure 7B and Figure 7C). Elastin, which determines the elasticity of the skin tissue, was also observed to increase in amount over time (Figure 7D). Fibronectin, which is involved in cell adhesion, growth, migration and differentiation, was found to increasingly deposit in bundle format within the scaffold over time, as an evidence of cell-extracellular matrix adhesion (Figure 7E). These encouraging positive stainings of ECM proteins indicated favorable interaction between 3D scaffold and HDFs, which is essential for the eventual application in tissue engineering.

Taken together, the presence of large, interconnectted pores in gelatin grafted 3D electrospun scaffold promoted infiltration of HDFs throughout the millimeter-thick scaffold, and also encouraged nutrients and mass exchange which are all crucial requirements of tissue engineering scaffolds. This study has successfully demonstrated a user-friendly and cost-effective needle collector technique to produce 3D electrospining scaffold with enlarged pores. Coupled with simple surface modification, the scaffold showed promising cellular interaction and support.

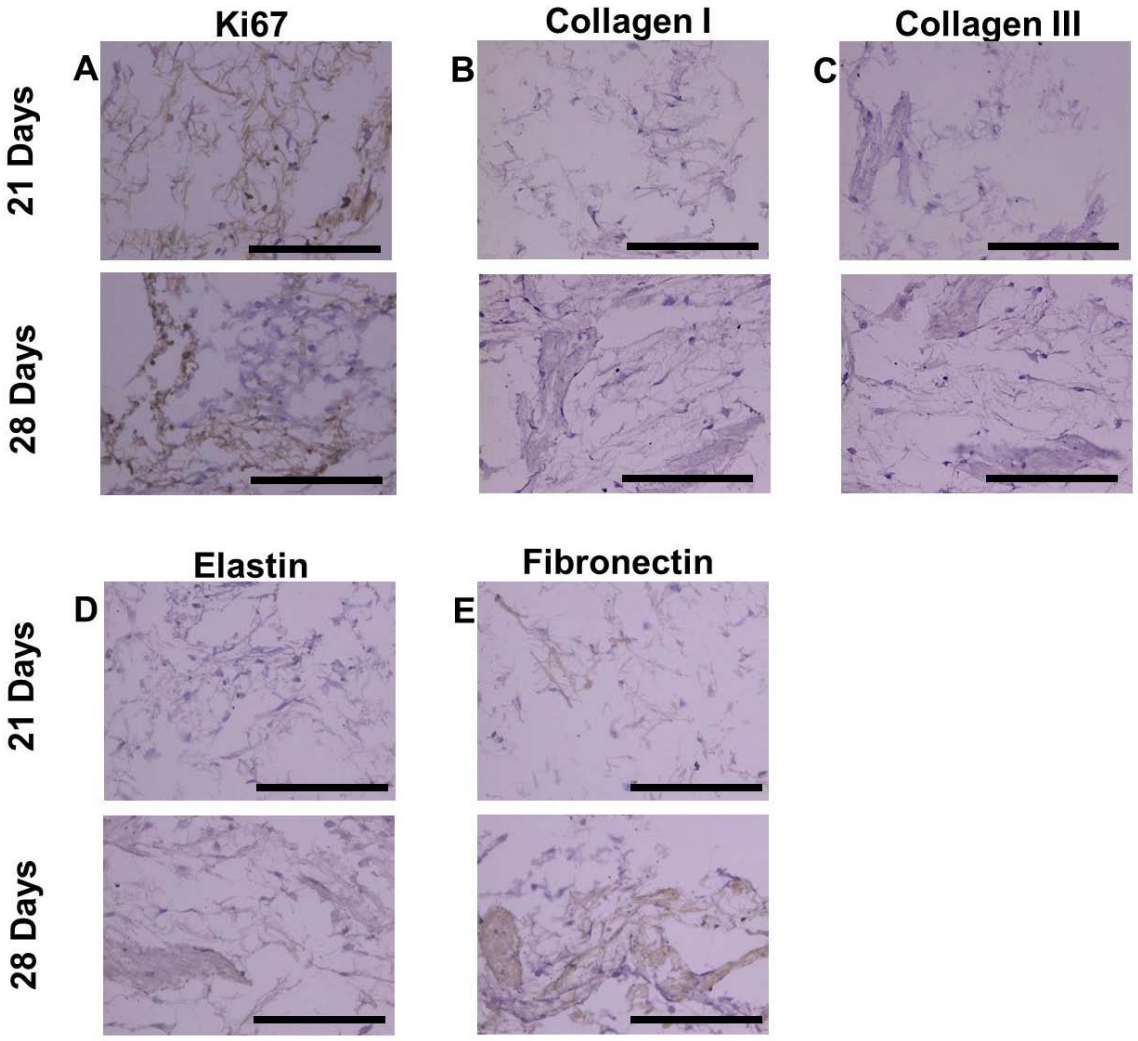

Figure 7. Histology staining of 3D multi-scale scaffold seeded with HDFs for 21 days and 28 days. Ki67 was positively stained throughout the culturing period, which suggests that cells are proliferative. Furthermore, increased deposition of various ECM proteins (Collagen I, Collagen III, Elastin, and Fibronectin) was observed from 21 days to 28 days. Scale bar = 200 μm.

4. Conclusion

Application of electrospun scaffold in tissue engineering has been hindered by limited cell infiltration into the scaffold due to its dense 2D structure. This study has successfully resolved this issue via two approaches. Firstly, we improvised the collector such that the resultant scaffold would be deposited into a 3D structure with sufficiently large pores for cell infiltration. Besides enlarged pore sizes, the fibers forming 3D scaffold mimicked closely the ECM architecture with multi-scale diameters (from ~200 nm to 3 μm). Secondly, we improved the surface wettability and bioactivity of electrospun scaffold through surface modification. As a result, cell infiltration throughout the entirety of the 6 mm fibrous scaffold was observed after 24 hours of cell seeding. Proliferation and ECM deposition of HDFs in the gelatin grafted 3D scaffold were observed up to 28 days of cell culture. The conducive environment of gelatin grafted 3D multi-scale scaffold for attachment, infiltration and ECM deposition of HDFs may find wide applications in the biomedical field particularly in tissue engineering or as fillers.

Conflict of Interest and Funding

No conflict of interest has been reported by the authors.

Acknowledgements

The authors would like to acknowledge the support by Nanyang Technological University.

References

1. Atala A, Thomson J A and Nerem R M, 2011, *Principles of Regenerative Medicine*, 2nd edn, Elsevier Inc.
2. Jayarama R V, Radhakrishnan S, Ravichandran R, *et al*., 2013, Nanofibrous structured biomimetic strategies for skin tissue regeneration. *Wound Repair and Regeneration*, vol.21(1): 1–16. http://dx.doi.org/10.1111/j.1524-475X.2012.00861.x
3. Metcalfe A D and Ferguson M W J, 2007, Tissue engineering of replacement skin: The crossroads of biomaterials, wound healing, embryonic development, stem cells and regeneration. *Journal of The Royal Society Interface*, vol.4(14): 413–417. http://dx.doi.org/10.1098/rsif.2006.0179
4. Xu C Y, Inai R, Kotaki M, *et al*., 2004, Aligned biodegradable nanofibrous structure: A potential scaffold for blood vessel engineering. *Biomaterials*, vol.25(5): 877–886. http://dx.doi.org/10.1016/S0142-9612(03)00593-3
5. Barnes C P, Sell S A, Boland E D, *et al*., 2007, Nanofiber technology: Designing the next generation of tissue engineering scaffolds. *Advanced Drug Delivery Reviews*, vol.59(14): 1413–1433. http://dx.doi.org/10.1016/j.addr.2007.04.022
6. Smith L A and Ma P X, 2004, Nano-fibrous scaffolds for tissue engineering. *Colloids and Surfaces B: Biointerfaces*, vol.39(3): 125–131. http://dx.doi.org/10.1016/j.colsurfb.2003.12.004
7. Powell H M, Supp D M and Boyce S T, 2008, Influence of electrospun collagen on wound contraction of engineered skin substitutes. *Biomaterials*, vol.29(7): 834–843. http://dx.doi.org/10.1016/j.biomaterials.2007.10.036
8. Ayres C E, Jha B S, Sell S A, *et al*., 2010, Nanotechnology in the design of soft tissue scaffolds: Innovations in structure and function. *Wiley Interdisciplinary Reviews: Nanomedicine and Nanobiotechnology*, vol.2(1): 20–34. http://dx.doi.org/10.1002/wnan.55
9. Lowery J L, Datta N and Rutledge G C, 2010, Effect of fiber diameter, pore size and seeding method on growth of human dermal fibroblasts in electrospun poly(ε-caprolactone) fibrous mats. *Biomaterials*, vol.31(3): 491–504. http://dx.doi.org/10.1016/j.biomaterials.2009.09.072
10. Gelain F, 2008, Novel opportunities and challenges offered by nanobiomaterials in tissue engineering. *International Journal of Nanomedicine*, vol.3(4): 415–424. http://dx.doi.org/10.2147/IJN.S3795
11. Zhong S P, Zhang Y Z and Lim C T, 2012, Fabrication of large pores in electrospun nanofibrous scaffolds for cellular infiltration: A review. *Tissue Engineering Part B: Reviews*, vol.18(2): 77–87. http://dx.doi.org/10.1089/ten.TEB.2011.0390
12. Rnjak-Kovacina J and Weiss A S, 2011, Increasing the pore size of electrospun scaffolds. *Tissue Engineering Part B: Reviews*, vol.17(5): 365–372. http://dx.doi.org/10.1089/ten.teb.2011.0235
13. Shim I K, Jung M R, Kim K H, *et al*., 2010, Novel three-dimensional scaffolds of poly(L-lactic acid) microfibers using electrospinning and mechanical expansion: Fabrication and bone regeneration. *Journal of Biomedical Materials Research Part B: Applied Biomaterials*, vol.95(1): 150–160. http://dx.doi.org/10.1002/jbm.b.31695
14. Nam J, Huang Y, Agarwal S, *et al*., 2007, Improved cellular infiltration in electrospun fiber via engineered porosity. *Tissue Engineering*, vol.13(9): 2249–2257. http://dx.doi.org/10.1089/ten.2006.0306
15. Balguid A, Mol A, van Marion M H, *et al*., 2009, Tailoring fiber diameter in electrospun poly(ε-caprolactone) scaffolds for optimal cellular infiltration in cardiovascular tissue engineering. *Tissue Engineering Part A*, vol.15(2): 437–444. http://dx.doi.org/10.1089/ten.tea.2007.0294
16. Baker B M, Gee A O, Metter R B, *et al*., 2008, The potential to improve cell infiltration in composite fiber-aligned electrospun scaffolds by the selective removal of sacrificial fibers. *Biomaterials*, vol.29(15): 2348–2358. http://dx.doi.org/10.1016/j.biomaterials.2008.01.032
17. Guimaraes A, Martins A, Pinho E D, *et al*., 2010, Solving cell infiltration limitations of electrospun nanofiber meshes for tissue engineering applications. *Nanomedicine (London)*, vol.5(4): 539–554. http://dx.doi.org/10.2217/nnm.10.31
18. Simonet M, Schneider O D, Neuenschwander P, *et al*., 2007, Ultraporous 3D polymer meshes by low-temperature electrospinning: Use of ice crystals as a removable void template. *Polymer Engineering and Science*, vol.47(12): 2020–2026. http://dx.doi.org/10.1002/pen.20914
19. Pham Q P, Sharma U and Mikos A G, 2006, Electrospun poly(ε-caprolactone) microfiber and multilayer nanofiber/microfiber scaffolds: Characterization of scaffolds and measurement of cellular infiltration. *Biomacromolecules*, vol.7(10): 2796–2805. http://dx.doi.org/10.1021/bm060680j
20. Soliman S, Pagliari S, Rinaldi A, *et al*., 2010, Multiscale three-dimensional scaffolds for soft tissue engineering via multimodal electrospinning. *Acta Biomaterialia*, vol.6(4): 1227–1237. http://dx.doi.org/10.1016/j.actbio.2009.10.051
21. Moroni L, Hamann D, Schotel R, *et al*., 2008, 3D fiber-deposited electrospun intergrated scaffolds enhance cartilage tissue formation. *Advanced Functional Materials*, vol.18(1): 53–60.

http://dx.doi.org/10.1002/adfm.200601158

22. Kim G, Son J, Park S, *et al*., 2008, Hybrid process for fabricating 3D hierarchical scaffolds combining rapid prototyping and electrospinning. *Macromolecular Rapid Communications*, vol.29(19): 1577–1581. http://dx.doi.org/10.1002/marc.200800277
23. Blakeney B A, Tambralli A, Anderson J M, *et al*., 2011, Cell infiltration and growth in a low density, uncompressed three-dimensional electrospun nanofibrous scaffold. *Biomaterials*, vol.32(6): 1583–1590. http://dx.doi.org/10.1016/j.biomaterials.2010.10.056
24. Tzezana R, Zussman E, Levenberg S, 2008, A layered ultra-porous scaffold for tissue engineering, created via a hydrospinning method. *Tissue Engineering Part C: Methods*, vol.14(4): 281–288. http://dx.doi.org/10.1089/ten.tec.2008.0201
25. Ahirwal D, Hebraud A, Kadar R, *et al*., 2013, From self-assembly of electrospun nanofibers to 3D cm thick hierarchical foams. *Soft Matter*, vol.9(11): 3164–3172. http://dx.doi.org/10.1039/C2SM27543K
26. Lavery L A, Armstrong D G and Harkless L B, 1996, Classification of diabetic foot wounds. *Journal of Foot and Ankle Surgery*, vol.35(6): 528–531. http://dx.doi.org/10.1016/S1067-2516(96)80125-6
27. Zhu Y, Gao C, Liu X, *et al*., 2002, Surface modification of polycaprolactone membrane via aminolysis and biomacromolecule immobilization for promoting cytocompatibility of human endothelial cells. *Biomacromolecules*, vol.3(6): 1312–1319. http://dx.doi.org/10.1021/bm020074y
28. *ImageJ Download page*, n.d., viewed March 31, 2015, <http://rsb.info.nih.gov/ij/download.html>
29. Grant P V, Tomlins P E, Mikhalovska L, *et al*., 2005, Physical characterization of a polycaprolactone tissue scaffold in *Surface Chemistry in Biomedical and Environmental Science*, Springer, Dordrecht, 215–228.
30. Tanaka A, Nagate T and Matsuda H, 2005, Acceleration of wound healing by gelatin film dressings with epidermal growth factor. *Journal of Veterinary Medical Science*, vol.67(9): 909–913. http://dx.doi.org/10.1292/jvms.67.909
31. Bissell M J, Hall H G and Parry G, 1982, How does the extracellular matrix direct gene expression? *Journal of Theoritical Biology*, vol.99(1): 31–68. http://dx.doi.org/10.1016/0022-5193(82)90388-5
32. Martínez E, Engel E, Planell J A, *et al*., 2009, Effects of artificial micro- and nano-structured surfaces on cell behaviour. *Annals of Anatomy — Anatomischer Anzeiger*, vol.191(1): 126–135. http://dx.doi.org/10.1016/j.aanat.2008.05.006
33. Tay C Y, Irvine S A, Boey F Y C, *et al*., 2011, Micro-/nano-engineered cellular responses for soft tissue engineering and biomedical applications. *Small*, vol.7(10): 1361–1378. http://dx.doi.org/10.1002/smll.201100046
34. Li H, Wong Y S, Wen F, *et al*., 2013, Human mesenchymal stem — cell behaviour on direct laser micropatterned electrospun scaffolds with hierarchical structures. *Macromolecular Bioscience*, vol.13(3): 299–310. http://dx.doi.org/10.1002/mabi.201200318
35. Tay C Y, Koh C G, Tan N S, *et al*., 2013, Mechanoregulation of stem cell fate via micro-/nano-scale manipulation for regenerative medicine. *Nanomedicine*, vol.8(4): 623–638. http://dx.doi.org/10.2217/nnm.13.31
36. Yeong W Y, Yu H, Lim K P, *et al*., 2010, Multiscale topological guidance for cell alignment via direct laser writing on biodegradable polymer. *Tissue Engineering Part C: Methods*, vol.16(5): 1011–1021. http://dx.doi.org/10.1089/ten.TEC.2009.0604
37. Tang C C, Chen J C, Long Y Z, *et al*., 2011, Preparation of curled microfibers by electrospinning with tip collector. *Chinese Physics Letters*, vol.28(5). http://dx.doi.org/10.1088/0256-307X/28/5/056801
38. Kim H Y, Lee M, Park K J, *et al*., 2010, Nanopottery: Coiling of electrospun polymer nanofibers. *Nano Letters*, vol.10(6): 2138–2140. http://dx.doi.org/10.1021/nl100824d
39. Watt F M and Fujiwara H, 2011, Cell-extracellular matrix interactions in normal and diseased skin. *Cold Spring Harbor Perspectives in Biology*, vol.3(4): a005124. http://dx.doi.org/10.1101/cshperspect.a005124

REPORT

Artificial vascularized scaffolds for 3D-tissue regeneration — a report of the ArtiVasc 3D Project

Richard Bibb[1*], Nadine Nottrodt[2] and Arnold Gillner[2]

[1] Design School, Loughborough University, Loughborough, Leicestershire, LE11 3TU, United Kingdom

[2] Biotechnology and Laser Therapy, Fraunhofer Institute for Laser Technology (ILT), Steinbachstrasse 15, 52074 Aachen, Germany

Abstract: The aim of this paper is to raise awareness of the ArtiVasc 3D project and its findings. Vascularization is one of the most important and highly challenging issues in the development of soft tissue. It is necessary to supply cells with nutrition within a multilayer tissue, for example in artificial skin. Research on artificial skin is driven by an increasing demand for two main applications. Firstly, for the field of regenerative medicine, the aim is to provide patients with implants or grafts to replace damaged soft tissue after traumatic injuries or ablation surgery. Secondly, another aim is to substitute expensive and ethically disputed pharmaceutical tests on animals by providing artificial vascularized test beds to simulate the effect of pharmaceuticals into the blood through the skin. This paper provides a perspective on ArtiVasc 3D, a major European Commission funded project that explored the development of a full thickness, vascularized artificial skin. The paper provides an overview of the aims and objectives of the project and describes the work packages and partners involved. The most significant results of the project are summarized and a discussion of the overall success and remaining work is given. We also provide the journal papers resulting from the project.

Keywords: vascular, skin, bioprinting, 3D, additive manufacturing

*Correspondence to: Richard Bibb, Design School, Loughborough University, Loughborough, Leicestershire, LE11 3TU, United Kingdom; Email: r.j.bibb@lboro.ac.uk

Received: October 26, 2015; **Accepted:** November 23, 2015; **Published Online:** December 4, 2015

Citation: Bibb R, Nottrodt N and Gillner A, 2016, Artificial vascularized scaffolds for 3D-tissue regeneration — a report of the ArtiVasc 3D Project. *International Journal of Bioprinting*, vol.2(1): 93–102. http://dx.doi.org/10.18063/IJB.2016.01.004.

1. Background

Vascularization is one of the most important and highly challenging issues in the development of soft tissue. It is necessary to supply cells with nutrition within a multilayer tissue, for example in artificial skin.

Research on artificial skin is driven by an increasing demand for two main applications. Firstly, for the field of regenerative medicine, the aim is to provide patients with implants or grafts to replace damaged soft tissue after traumatic injuries or ablation surgery. Secondly, another aim is to substitute expensive and ethically disputed pharmaceutical tests on animals by providing artificial vascularized test beds to simulate the effect of pharmaceuticals into the blood through the skin.

To date, it has only been possible to cultivate the upper layers of the skin — the epidermis and dermis — with a total thickness of up to 200 micrometers outside the human body. A complete skin system, however, should also include the subcutaneous tissues having an overall thickness of several millimeters. In order to co-cultivate the hypodermis, blood vessels supplying this tissue are imperative. The aim of the ArtiVasc 3D project was to enable significantly more complex tissues to be cultivated *in vitro* by developing artificial blood vessels.

2. Introduction

The aim of this paper is to offer a perspective on this large and ambitious project. It aims to disseminate the main findings and achievements of the ArtiVasc 3D project to the wider international academic and research community. The paper provides an overview of the aims and objectives of the project, summarizes the work conducted and highlights some of the most significant achievements with references to published results where possible. The paper offers a critical review of the project and the relative advantages and disadvantages of the large, multidisciplinary, multi-center approach.

The multidisciplinary ArtiVasc 3D project consisted of a consortium of partners from research and industrial institutions across Europe. The project brought together experts in biomaterials development, cell-matrix interaction, angiogenesis, tissue engineering, simulation, design and additive manufacturing to generate bioartificial vascularized skin in a fully automated and standardized manufacturing approach, rapidly and inexpensively. To achieve these aims, ArtiVasc 3D needed to provide a micro- and nano-scale manufacturing and functionalization technology that would enable the generation of fully vascularized bioartificial tissue capable of the necessary nutrition and metabolism functions (illustrated in Figure 1).

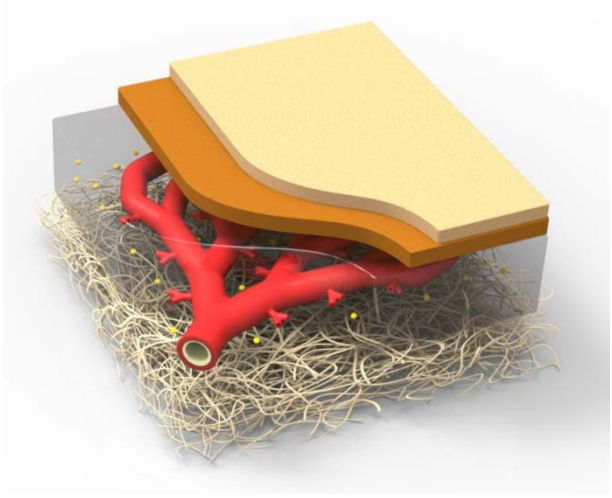

Figure 1. Conceptual illustration of the 3-layer, full thickness, artificial skin construct.

By overcoming these scientific and technical challenges, the project aimed to make a significant contribution to improving and accelerating patient treatment in emergencies and to reducing animal testing to an absolute minimum. The recently completed project was four years in duration starting in November 2011. The project was coordinated by Fraunhofer ILT and involved 20 partners across Europe (see acknowledgments for the full list). The €7.8 million funding was obtained through peer-reviewed open competition from the EU 7th Framework Programme call (FP7-NMP-2010-Large-4, GA no.: 236416). More details about the project can be found in the project website[1].

3. Project Work Packages

As is typical in large European projects, the research and development required was broken down into a series of work packages (WP) covering three main areas: material development and characterization, process development, and matrix tissue interaction and tissue development. In total, 12 work packages were established as shown in Table 1. Work packages 1, 11 and 12, which are italicized, were largely concerned with the scientific coordination, dissemination and management of the project.

Table 1. List of work packages

WP no.	Description of work package
WP1	*Scientific coordination and definition of requirements*
WP2	Material development and characterisation
WP3	Modelling and design
WP4	Process development
WP5	Biofunctionalization
WP6	Matrix-tissue interactions
WP7	Machine prototype development
WP8	Machine demonstration
WP9	Development of a vascularized composite tissue graft
WP10	Validation of a vascularized composite tissue graft
WP11	*Dissemination, training, exploitation and IPR management*
WP12	*Project management*

4. Material Development and Characterization (WPs 2 and 5)

The overall goal of this section was to provide a new tailored material combination that fulfilled the requirements for soft tissue engineering but was also compatible with additive manufacturing (AM) processes, specifically inkjet printing, stereolithography/multiphoton polymerization (MPP) and electrospin-

ning, as well as enabling biofunctionalization. The most important challenge of the material development research was not related to a singular parameter, but rather the combination of all of the desired properties within an appropriate combination of materials. Within this WP, the materials were also evaluated regarding their chemical, physical, thermal and mechanical properties as well as fundamental tests of cytotoxicity.

4.1 Objectives of WP2

The overall goal of WP2 was to provide a new tailored material that fulfilled the requirements for soft tissue engineering whilst also being compatible with the combined AM processes and biofunctionalization.

- To design and synthesize 40 chemical structures for blood vessel materials and supporting scaffold materials for 3D AM processes and fiber materials for electrospinning,
- To characterize materials in terms of their chemical structure, thermal and mechanical properties, viscosity, photo-curing behavior, surface functionality and cytotoxicity,
- To adapt polymers for AM and for the needs of blood vessel systems in regard to demands for permeability, mechanical properties and biocompatibility,
- To modify surfaces of polymers to enable biofunctionalization,
- To analyze long-term (1–6 months) behavior of basic materials for the vascular system.

4.2 Objectives of WP5

The overall objective was the biofunctionalization of the artificial vascular structures and of the surrounding fiber matrix obtained from WPs 2 and 4. The biofunctionalization was specifically aimed for the following:

- To minimize cytotoxicity of the biofunctionalized material,
- To control cell adhesion and migration on material surfaces and to stimulate proliferation by binding functional groups to the surface,
- To stimulate neo-angiogenesis,
- To design a process that can be integrated into the proposed combined AM process.

4.3 Highlights

Materials compatible with inkjet printing, stereolithography/MPP for blood vessel generation were developed to fulfil the main requirements. An elastic, photocurable polymer that is inkjet printable and UV-curable was successfully used to build branched porous blood vessels by stereolithography[2]. However, developing an entirely compatible support material proved challenging and was not achieved during the project. Consequently, as inkjet printing necessitates a removable support material, it was not possible to inkjet print vessel structures as envisaged. Additional research was done on gelatin development for additive manufacturing of vessel substitutes [3,4].

To allow endothelialization of those vessels, an inner-surface functionalization was necessary. The University of Stuttgart developed a procedure for coating these vessels with heparin, which allows homogeneous cell cultivation[5]. For local functionalization of vessel scaffolds and cell guidance of the surrounding scaffold, localized laser functionalization was investigated[6]. Another aspect was the scaffold material for the surrounding fat. For that reason, two kinds of materials are considered. One kind of materials are electrospun fibres as scaffolds while the other kind are hydrogels filling the pores between the fibres and providing growth factors and allow nutrition of embedded cells[7]. Furthermore, a huge number of electrospinnable materials were tested for their biocompatibility and showed very promising results (INNO). Electrospun meshes have been successfully characterized for their use in adipose tissue generation[8–10].

5. Process Development (WPs 3, 4, 7 and 8)

The overall goal of this section was to develop and demonstrate a combined AM process that integrated the three technologies inkjet printing, stereolithography/MPP and electrospinning to build up the vascularized scaffold utilizing the newly developed materials.

The design of the vascular structures is essential to enable them to replicate human tissue performance. The design and modelling tasks involved physiological simulation and testing to define the optimum vessel dimensions and configuration. This was done through theoretical calculations, physical experimentation and Computational Fluid Dynamics (CFD). To enable AM the design phase needed to incorporate the optimized parameters and produce three-dimensional models that would define the structures. The design tasks involved the creation of a bespoke Computer-Aided Design (CAD) application that could take in physiological parameters, number of branches, skin patch size, vessel diameters, etc. and automatically generate the vessel structure as a solid three-dimensional computer model in a format suitable for AM (e.g., STL file). In

order to integrate with the newly developed combined AM process, computer programs were devised that sliced the CAD model and produced appropriate layer data for each aspect of the AM process. This included image data to drive the inkjet printing steps and vector files to control the stereolithography steps.

For the AM process development, the first task was to test the new materials for their suitability for inkjet printing and to define the optimal printing parameters. Secondly, MPP was adapted with regard to the developed material and the desired scaffold structures by developing appropriate beam guidance and optics. Thirdly, the materials were tested for their suitability in the electrospinning process and to define the process parameters. Further work involved the development of a process-strategy and concept for combining inkjet, MPP and electrospinning and then to examine the co-action of all three production technologies. This required a test rig including all three technologies to be produced, as well as the development and generation of the necessary machine control code enabling process-integration and optimization.

5.1 Objectives of WP3

The overall goal was the modelling and design of a vascular system that effectively delivers O_2 and other nutrients from the circulating blood flow to the surrounding tissue. Specific objectives were:

- To investigate the nutrient permeation within the vascular system to the cells,
- To identify the requirements for the blood flow through the system and provide an informed design specification,
- To develop design tools for generating 3D CAD models of optimum vascular systems (see Figure 2)[11,12],
- To translate 3D models into an appropriate data format for the proposed AM process.

5.2 Objectives of WP4

The overall goal was to develop a combined AM process that integrates inkjet printing, MPP and electrospinning to work as one single process. Specific objectives were:

- To deliver machine specification for building a working process module in WP7,
- To iteratively adapt and optimize the process for each process technology in cooperation with material development,
- To develop a strategy for combining these three technologies in one process,
- To build a test rig where the combination of the technologies can be examined and developed further.

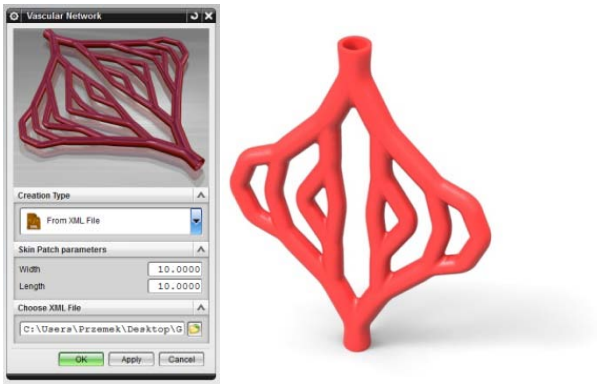

Figure 2. The user interface for the automated generation of vessel designs.

5.3 Objectives of WP7

The overall goal was to develop the integrated machine prototype encompassing the developed processes through a set of pre- and post-processing steps. Specific objectives were:

- To establish the machine prototype specifications for the machine demonstrator,
- To develop prototype solutions for the production module, combining inkjet printing, MPP and electrospinning and modules for necessary pre- and post-processing steps,
- To manufacture and implement the integrated machine prototype,
- To set the prototype into service, commissioning, parameters tuning and equipment adjustment.

5.4 Objectives of WP8

The overall goal was to demonstrate and test the prototype process and equipment resulting from WP7. Specific objectives were:

- To demonstrate the fulfilment of requirements for the scaffold generation,
- To make fully functional scaffolds for analysis,
- To produce scaffolds for biological applications.

5.5 Highlights

The three AM processes have been installed and extensively characterized. By using UV-curing it could be demonstrated that vessels with different geometries and sizes could be generated either by MPP with dimen-

sions in the micron range or by stereolithography with dimensions in the mm to cm range (see Figure 3)[2,13].

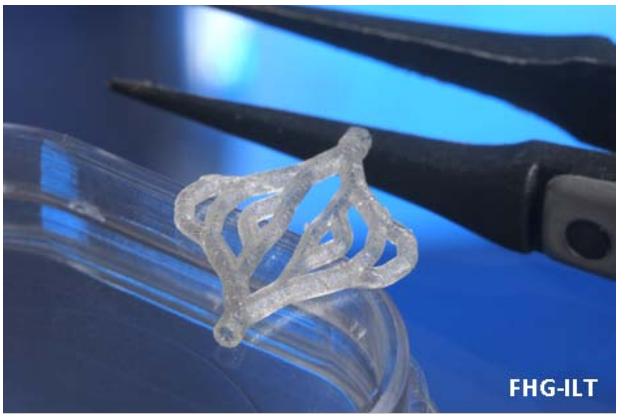

Figure 3. Vessel structure created using stereolithography.

Material development for inkjet printing proved to be very challenging. It was possible to demonstrate the printing of flat structures successfully. However, the development of a support material necessary for multi-layered structures that was water-soluble and yet did not mix with build material proved impossible during the project.

The goal of process combination was realized within a manufacturing chain containing inkjet printing units, stereolithography or MPP-module and UV-curing unit working under inert gas atmosphere (see Figure 4). Electrospinning was not integrated into this machine but a separate electrospinning module exists (INNO, UNISA) and it can be combined by using a container transport system.

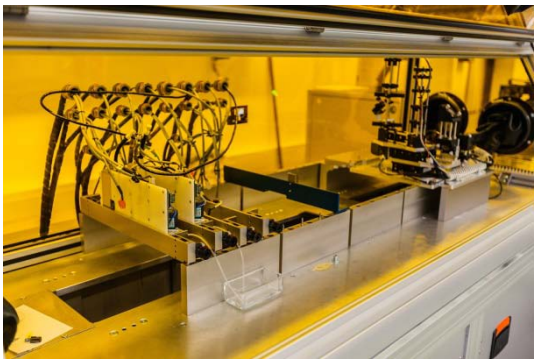

Figure 4. Prototype modular production unit (Fh-IPA).

6. Matrix Tissue Interaction and Tissue Development (WPs 6, 9, 10)

The overall objective of this WP was to achieve a detailed understanding of the characteristics and functions of vascular cells in contact with novel materials to optimize the establishment of composite vascular systems. This included the interaction of perivascular cells, with endothelial cells and the underlying extracellular matrix (ECM). Additionally the interaction between adipocytes and electrospun or biological matrices will be investigated.

The vasculature is characterized by a composite structure of functionally distinct cells like pericytes (PC) and endothelial cells (EC) in the vessel wall, specialized ECM layers (vascular basement membrane, interstitial matrix) and contacts with surrounding tissues. This WP defined the effects of novel materials on the phenotype, behavior and receptor-mediated signaling of vascular cells with a focus on perivascular and endothelial cells to improve maturation and stability of engineered vascular structures. In parallel adipocyte interactions with electrospun and biological scaffold materials was analyzed.

6.1 Objectives for WP6

The main objective was to achieve a detailed understanding of the characteristics and functions of vascular cells in contact with novel materials to optimize the establishment of composite vascular systems. This included perivascular cells, essential for the mutual interactions of endothelial cells to the underlying ECM and surrounding tissues. Additionally, the interaction between adipocytes and electrospun or biological matrices was investigated. Specific objectives were:

- To define and modify the effects of novel materials and specific ligands regarding to adhesion, proliferation and differentiation on individual vascular cells with a focus on pericytes, endothelial cells and adipocytes,
- To realize the efficient endothelialization of the artificial vascular systems,
- To evaluate the interaction of adipocytes with electrospun or biological matrices,
- To transfer the knowledge from the murine system to human systems.

6.2 Objectives for WP9

The overall objective of WP9 was the development of a vascularized composite graft using the example of vascularized skin by the achievement of the following specific objectives:

- To develop *in vitro* fatty tissues and compare them to non-scaffold and scaffold-based models,
- To combine this fat layer with a dermal and

epidermal layer,
- To integrate the artificial vascular system produced in WP6 in the fatty tissue,
- To build up a vascularized composite tissue graft, including a fat, dermal and epidermal layer,
- To characterize and evaluate cell and tissue properties considering in particular morphology, viability, cell proliferation and the expression of specific markers.

6.3 Objectives for WP10

The overall aim of this work package was to validate the biofunctionality of the delivered scaffolds and composite grafts. Specific objectives were:
- To evaluate the biocompatibility of electro-spun scaffolds and artificial vascularized raw material,
- To validate the functionality of cell seeded composites and their combination,
- To validate the usability of the artificial vascularized skin as a pharmaceutical test system,
- To validate the usability of the artificial vascularized skin as a tissue graft.

6.4 Highlights

A three-layered vascularized skin will consist of at least four or five different kinds of cells in co-cultivation. All those cells will interact. Therefore, mechanisms and interaction effects have to be studied. Additionally, all cells must be available from the same species, in this case from human. However, until the beginning of this project some cells e.g. pericytes had only been characterized from mice. Therefore, scientists had to establish protocols for the isolation of human pericytes. They characterized human pericytes in comparison to mouse pericytes[14]. In the end, they achieved stable human pericyte populations. Co-cultivation of pericytes and endothelial cells was analyzed as well. A cultivation medium that supports both cells was found.

The second aspect was the build-up of fatty tissue. After development of isolation and cultivation protocols, the optimized surrounding material was tested. Scientists chose a hydrogel from hyaluronic acid and gelatin for the cultivation of adipocytes (see Figure 5)[15–19].

The integration of the vascular system into the fatty tissue is the last challenge in the project. The first experiments in the newly developed bioreactors are ongoing and results are expected in October 2015.

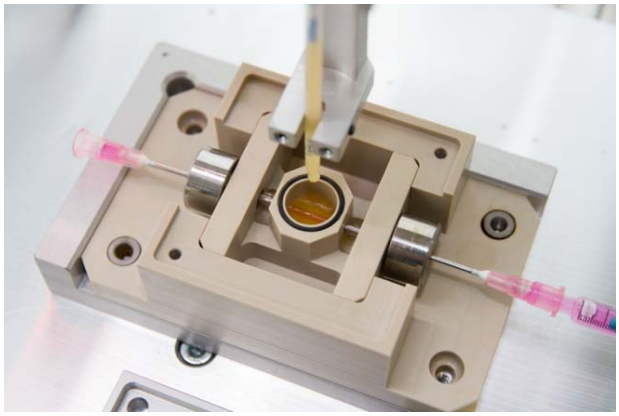

Figure 5. Newly developed bioreactor for vascularized fat cultivation (Fh-IGB, Unitechnologies).

7. Overall Results

In order to achieve the desired properties, the scientists in this project combined the freeform AM methods of inkjet printing and stereolithography (or MPP). With these combined processes, the researchers were able to achieve a very fine resolution for the construction of branched, porous blood vessels with layer thicknesses of about 20 microns. The researchers used mathematical simulations to develop data for the construction of branched structures. This data should create the conditions so that branched structures can be generated which allow uniform blood supply to a given size of skin patch. The use of the acrylate-based synthetic polymer developed in the project permits the scientists to construct these optimized vessels with a pore diameter in the order of hundreds of microns. Compared to conventional methods, the ArtiVasc 3D process provides the general conditions to produce branched and biocompatible vessels in this size range for the first time.

The development of an artificial, three-layered perfused skin model was ambitious and pioneering but this project has developed a 3D Printing process for the production of artificial blood vessels using innovative materials. The project has laid the foundation to cultivate a full-thickness skin model to a much greater layer thickness than previously possible.

One of the biggest challenges the project ArtiVasc 3D faced was to develop the right material for the production of artificial blood vessels. For them to be used in the human body, these vessels must have the correct mechanical properties and biocompatibility as well as full processability. Indeed, endothelial cells and pericytes must be able to colonize the artificial blood vessels.

At the time of writing, the project has generated 26 conference presentations (2 pending), 15 journal publications (with 5 in press or under review) and a PhD thesis. Many more are currently in progress.

8. Discussion

The results of ArtiVasc 3D are shaping the future. A toolbox has been developed that can respond flexibly to diverse materials, shapes and sizes. These results can be viewed as a precursor to a fully automated process chain for the production of artificial blood vessels that can be integrated into existing lines. Another highlight of the project is the successful breeding of adipose tissue in a novel bioreactor. The combination of the fatty tissue with an existing skin model allowed the production of a full-thickness skin model that has a thickness of up to 12 millimeters.

Throughout the four years of research, the researchers have faced many challenges that were not expected in the beginning. At the beginning, researchers defined specifications that were to be met at the end of the project. Those specifications ranged from material properties for processability, such as viscosity and material interaction, to the biological requirements, such as biocompatibility and elasticity. The material scientists met 9 out of 10 of those requirements. Nevertheless, the development of two biocompatible materials able to print next to each other and to dissolve one of these materials afterwards (i.e., a support material) was unfortunately not possible within the timeframe. This influences the build-up of blood vessels within the combined automated process. Nevertheless, researchers found alternative routes to generate porous branched vessel structures by using stereolithography and produce linear porous vessels by using electrospinning or dip coating. Thus, new technologies have been established to achieve the final goal of porous vessels.

While engineers worked on vessel generation, another group of chemists and biologists worked on the endothelialization of those vessels. It took a lot of effort, a huge number of materials and protocols to define the best protocol for endothelialization.

In parallel, biologists and chemists broke new ground in the field of fat tissue generation. The biggest, and up until now unavailable, third layer of the three-layered skin model. They developed protocols for isolating cells and gained knowledge in handling of adipose tissue derived stem cells and mature adipocytes. In the end, they could successfully demonstrate cells growing in hydrogels developed within the ArtiVasc 3D Project. It is still challenging to find the right cultivation media allowing not only adipocytes but also pericytes and endothelia cells to grow under co-culture conditions. Biologists together with engineers developed a bioreactor that can be perfused with media to provide nutrition to all cultivated cells.

Since not only fatty tissue was the goal of the project but also three-layered skin, the biologists tried to develop a dermal and epidermal tissue from existing protocols on top of the adipose tissue. In stainings, they were able to show the formation of all three layers. Analysis of the expression of typical tissue marker is still under investigation.

The final aim to build up a genuinely vascularized artificial skin remains a big challenge. Due to unforeseen challenges coming from the material and process development and a tight project plan, some steps towards the vascularized tissue are still open. Up to now, we have demonstrated the three-layered skin without vessels. By using stereolithography as the build-up strategy, branched porous vessels are available today. The integration and function of these available endothelialized vessels has to be demonstrated. We expect neo-angiogenesis from those porous blood vessels containing endothelial cells and pericytes, which would be a real benefit for the nutrition of the thick fatty tissue because more natural and reliable processes are expected. However, this will most probably be a challenge for future research projects. The original plan in ArtiVasc 3D foresaw the generation of an elastic, branched blood vessel system, to provide a scaffold for endothelial cell and pericyte organization. Since we found that just a hollow channel in the middle of a hydrogel could be used as a supply channel, we could imagine different strategies for nutrition supply and vessel organization without having a static scaffold wall. By just using functionalized hydrogels that contain growth factors, those factors could be released by time dependent or by photo-induced degradation of the hydrogel. This would add the fourth dimension (time or 4D) to the 3D printing technology and could induce cell organization and blood vessel formation with time[20]. Nevertheless, the generation of a branched blood vessel scaffold is necessary for other applications such as blood vessel replacement. The other reason for such a scaffold is the connectivity to the natural tissue in case of implantation in the future. This will not be possible with those self-organized vessel systems.

The successful conquest of the third dimension need not be confined to the skin, however. The ArtiVasc 3D project has also laid the foundations for future developments in three-dimensional tissue engineering. By using the principle of blood circulation with artificial blood vessels, medical engineers will be able to build larger structures such as whole organs in the future. For full skin cultured *in vitro*, there are a variety of applications: quick assistance for large-area skin injuries such as burns or after tumor resection as well as a replacement model that would make animal testing in the pharmaceutical industry unnecessary.

Whilst some of the objectives were not fully achieved, the project has produced a significant number of scientific findings and technical innovations. It is our view that these achievements could not have been made by the individual partners working in isolation. This kind of large, multidisciplinary, multi-institution project poses some practical, logistical and managerial challenges. Some of the pros and cons are summarized in Table 2. However, the authors hope that the achievements of the project illustrate that it was productive and successful and forms a valuable and significant contribution to the research in tissue engineering and bioprinting. We encourage other researchers in the international community to develop multidisciplinary and multi-institutional projects where the combination of expertise and facilities can achieve more than the sum of the parts.

9. The ArtiVasc 3D Project Partners

1. Aalto University, Finland
2. Albert-Ludwig University of Freiburg, Germany
3. AO Research Institute, Davos, Switzerland
4. International Management Services ARTTIC, Germany
5. Beiersdorf AG, Germany
6. Berufsgenossenschaftliche Kliniken Bergmannsheil [Bergmannsheil Hospital of the Ruhr-Universität Bochum], Germany
7. Fraunhofer Institute for Applied Polymer Research IAP, Germany
8. Fraunhofer Institute for Interfacial Engineering and Biotechnology IGB, Germany
9. Fraunhofer Institute for Laser Technology ILT, Germany
10. Fraunhofer Institute for Production Technology and Automation IPA, Germany
11. Fraunhofer Institute for Mechanics of Materials IWM, Germany
12. INNOVENT e.V. Technology Development Jena, Germany
13. KMS Automation GmbH, Germany
14. Medical University of Vienna, Austria
15. Unitechnologies SA, Switzerland
16. University of East Anglia, UK
17. Loughborough University, UK
18. Institute for Interfacial Engineering and Plasma Technology IGVP, University of Stuttgart, Germany
19. University of Salerno, Department of Industrial Engineering, Italy
20. Vimecon GmbH, Germany

Table 2. Pros and cons of large, multidisciplinary, multi-partner projects

Pros Positive features and opportunities	Cons Negative features and challenges
• Enables multidisciplinary working • Well planned projects • Clear aims and objectives • Inclusive approach • Shared resources • Intellectual stimulation from wide variety of colleagues • Academic rigour (debate, consensus and internal peer review) • Mutual, cross-disciplinary learning • Training and researcher development • Forming new collaborations and future projects • Co-authoring papers • Wider international dissemination of results (in more languages) • Cultural exchange and learning	• Challenging to set up the consortium and attract all the right partners • Have to develop the proposal with little or no funding • Securing competitive funding • Communication difficulties — language barriers and translation issues • Time and cost associated with travel • Logistical challenges (e.g. moving materials or equipment around partners) • Tight plans and limited resources • Time and cost of legal agreements • Administrative burden of strictly controlled financial reporting and record keeping • Unforeseen changes (people leaving, companies coming or going)

10. Summary of Conference Presentations

The project outcomes have been presented in 28 presentations including Tissue Engineering and Regenerative Medicine International Society — EU Meeting, Genova, Italy, 2014 (3 presentations); EuroBioMat 2015 (4 presentations) and 2013 (2 presentations); 26th European Conference on Biomaterials, Liverpool, UK, 2014 (3 presentations); Euronanoforum, Dublin, Ireland, 2013 (3 presentations); DGBM conference, Erlangen, Germany, 2013 (2 presentations)

Conflict of Interest and Funding

No conflict of interest was reported by all authors. The project was funded by the European Union 7th Framework Programme (FP7-NMP-2010-Large-4, GA no: 236416). Update ArtiVasc3D-Generation of a 3D vascularized skin substitute; Keck M, Gugerell A, Kober J, Engelhart S, Gillner A, Nottrodt N; GA no: 263416; revised (2014), http://www.artivasc.eu

Acknowledgements

This extremely ambitious challenge could only be achieved in an interdisciplinary network. All over Europe, twenty partners from the fields of biomaterial development, tissue engineering, freeform methods, automation and simulation have joined forces under the leadership of Fraunhofer ILT.

References

1. *ArtiVasc 3D*, n.d., viewed August 30, 2015, <http://www.artivasc.eu/>
2. Engelhardt S, Wehner M and Refle O, 2012, Method for the fabrication of macroscopic high resolution scaffolds by the combination of inkjet printing and laser initiated polymerization. *Journal of Tissue Engineering and Regenerative Medicine*, vol.6: 299–300. http://dx.doi.org/10.1002/term.1586
3. Hoch J, Tovar G and Borchers K, 2014, Photopolymerizable and non-gelling gelatin for the preparation of tissue substitutes by additive manufacturing techniques. *Journal of Tissue Engineering and Regenerative Medicine*, vol.8: 446. http://dx.doi.org/10.1002/term.1932
4. Hoch E, Tovar G and Borchers K, 2014, Bioprinting of artificial blood vessels — current approaches towards a demanding goal. *European Journal of Cardiothoracic Surgery*, vol.46(5): 767–778. http://dx.doi.org/10.1093/ejcts/ezu242
5. Hoch E, Hirth T, Tovar G, *et al*., 2013, Chemical tailoring of gelatin to adjust its chemical and physical properties for functional bioprinting. *Journal of Materials Chemistry B*, vol.1: 5675–5685. http://dx.doi.org/10.1039/C3TB20745E
6. Seiler N, Bremus-Köbberling E, Leonhäuser D, *et al*., 2012, Gradients for cell guidance — functionalization by UV-laser-irradiation. *Journal of Tissue Engineering and Regenerative Medicine*, vol.6: 373–374. http://dx.doi.org/10.1002/term.1586
7. Kessler L, Huber B, Hoch E, *et al*., 2014, Cross-linked hydrogels as a potential tool for soft tissue engineering. *Journal of Tissue Engineering and Regenerative Medicine*, vol.8: 353. http://dx.doi.org/10.1002/term.1932
8. Gugerell A, Kober J, Laube T, *et al*., 2014, Electrospun poly(ester-urethane) and poly(ester-urethane-urea) fleeces as promising tissue engineering scaffolds for adipose-derived stem cells. *PLOS ONE*, vol.9(3): e90676. http://dx.doi.org/10.1371/journal.pone.0090676
9. Gugerell A, Neumann A, Kober J, *et al*., 2014, Adipose derived stem cells cultivated on electrospun L-lactide/glycolide copolymer fleeces and gelatine hydrogels under flow conditions — aiming physiological reality in hypodermis tissue engineering. *Burns*, vol.41(1): 163–171. http://dx.doi.org/10.1016/j.burns.2014.06.010
10. Tammaro L, Vittoria V, Wyrwa R, *et al*., 2014, Fabrication and characterization of electrospun polylactide/β-tricalcium phosphate hybrid meshes for potential applications in hard tissue repair. *BioNanoMaterials*, vol.15: 9–20. http://dx.doi.org/10.1515/bnm-2014-0001
11. Han X, Bibb R and Harris R, 2015, A junction rounding method for the efficient design of bifurcation vascular vessels in skin tissue engineering for additive manufacturing. *Journal of Visual Languages and Computing*, vol.28: 238–249. http://dx.doi.org/10.1016/j.jvlc.2014.12.005
12. Han X, Bibb R and Harris R, 2015, *Artificial Vascular Bifurcations — Design and Modelling*, Procedia CIRP, in press.
13. Engelhardt S, Tempeler J and Wehner M, 2015, The voxel onset time as an *in situ* method to evaluate focal position effects on two-photon-induced lithography. *Applied Physics A*, vol.121(2): 513–519. http://dx.doi.org/10.1007/s00339-015-9449-9
14. Huber B, Klechowitz N, Borchers K, *et al*., 2012, Isolation and culture of primary human subcutaneous adipocytes and construction of a fatty tissue equivalent. *BioNanoMaterials*, vol.13(1–4): 195. http://dx.doi.org/10.1515/bnm-2012-0015

15. Huber B, Borchers K, Tovar G E M, *et al*., 2016, Methacrylated gelatin and mature adipocytes are promising components for adipose tissue engineering. *Journal of Biomaterials Applications*, vol.30(6): 699–710. http://dx.doi.org/10.1177/0885328215587450
16. Keck M, Kober J, Schnabelrauch M, *et al*., 2014, Generation of the hypodermis in a vascularized three layered skin substitute. *Journal of Tissue Engineering and Regenerative Medicine*, vol.8: 99. http://dx.doi.org/10.1002/term.1931
17. Kluger P, Huber B, Hoch E, *et al*., 2014, Development of soft tissue equivalents — build up with mature adipocytes in a gelatin hydrogel. *BioNanoMaterials*, vol.15(S1): 42. http://dx.doi.org/10.1515/bnm-2014-9006
18. Kober J, 2015, Adipose tissue stem cells and secretomes for advanced skin tissue engineering, doctoral thesis, Medical University of Vienna, viewed June 30, 2015, <http://permalink.obvsg.at/AC10777441>
19. Huber B, Volz A C and Kluger P J, 2015, How do culture media influence *in vitro* perivascular cell behavior? *Cell Biology International*, vol.39(12): 1395–1407. http://dx.doi.org/10.1002/cbin.10515
20. Khoo Z X, Teoh J E M, Liu Y, *et al*., 2015, 3D printing of smart materials: A review on recent progresses in 4D printing. *Virtual and Physical Prototyping*, vol.1(3): 103–122. http://dx.doi.org/10.1080/17452759.2015.1097054

INTERNATIONAL JOURNAL OF BIOPRINTING

ISSN (print): 2424-7723

ABOUT THE JOURNAL

International Journal of Bioprinting is a biannual, double-blind peer-reviewed, open access journal. This journal focuses on the use of 3D printing technology with materials that incorporate viable living cells or biological elements to produce tissue or biotechnological products. Further discourses and technological advancements in bioprinting are the goals behind acceptance of high-quality basic and applied research: from concept creation to fabrication of the bioprinting process, associated clinical applications as well as social implications.

Whioce Publishing, official publisher for the journal welcomes researchers to submit their papers relevant to bioprinting for consideration via **http://ijb.whioce.com/** For general enquiries and order for prints and reprints, please write in to **IJB@whioce.com** for a fast response.

SUBMIT YOUR PAPERS HERE

WHIOCE
PUBLISHING PTE. LTD.

ABOUT THE PUBLISHER

Whioce Publishing in Singapore is a registered publisher of excellent quality academic journals for an international readership. We deliver exceptional editorial support for the advancement and dissemination of scientific research by linking readers and researchers with networks and industries. We have ambitions to get our journals indexed in prominent databases such as EI, SCI, SSCI and AHCI, thereby aiming to be a first-class knowledge platform for researchers worldwide.

Whioce Publishing also engages in publishing e-books, organizing academic conferences and educational trainings, and providing translational services.

International Journal of Bioprinting is an
independent open access journal published
by Whioce Publishing Pte.Ltd.

WHIOCE PUBLISHING PTE. LTD.
PROVIDING
FIRST-CLASS SCIENTIFIC INFORMATION
FOR TOP SCHOLARS

Whioce Publishing Pte.Ltd.
7030 Ang Mo Kio Avenue 5
#04-15 Northstar@AMK
Singapore 569880
Tel: +65 65702707/65702718
Fax: +65 65702803